A Synthetic Biology Approach to Engineering Protein Assemblies for use in Vaccine Design.

A thesis submitted to the University of Manchester for the degree of Doctor of Philosophy in Biochemistry in the Faculty of Biology, Medicine and Health.

2020

Freya King

School of Biological sciences

Division of Infection, Immunity and Respiratory Medicine

Table of Contents

Word Count: 51,291

List of Figures

List of Tables

Abbreviations

2D	2- dimensional	KDPG	2-dehydro-3-deoxy-phosphogluconate
3D	3- dimensional	LB	Luria broth
Å	Angstrom	LOS	lipooligosaccharide
A_{260}	absorbance$_{260}$	LPS	lipopolysaccharide
A_{280}	absorbance$_{280}$	MACS	magnetic activated cell sorting
A_{600}	absorbance$_{600}$	MERS	Middle East Respiratory Syndrome
A_{630}	absorbance$_{630}$	MenB	Meningitis group B vaccine
AIDS	acquired immune deficiency syndrome	MHC	major histocompatibility complex
ANOVA	analysis of variance	Mins	minutes
APC	antigen presenting cells	MIR	major immunodominant region
BATF-3	basic leucine zipper transcriptional factor ATF-like 3	MGL	macrophage galactose-type lectin
BIL	bio-layer interferometry	MW	molecular weight
BLAST	basic local alignment search tool	MWCO	molecular weight cut off
BMDC	bone marrow derived cell	NadA	Neisseria adhesin A
BSA	bovine serum albumin	NHBA	Neisseria heparin-binding antigen
BST2	bone marrow stromal antigen 2	NMS	normal mouse serum
CALB	*Candida antarctica* lipase B	OD	optical density
CD	cluster of differentiation	OMP	outer Membrane Protein
cDC	classical dendritic cell	OMV	outer Membrane Vesicle
CFSE	carboxyfluorescein succinimidyl ester	OVA	ovalbumin
CPG	5'—C—phosphate—G—3	PAMP	pathogen-associated molecular pattern
CTF	contrast transfer function	PBS	phosphate buffered saline
CTLA-4	cytotoxic T-lymphocyte-associated protein 4	PCR	polymerase chain reaction
Da	Dalton	PBD	protein data base
°C	Degrees	pDC	Plasmacytoid dendritic cell
DLS	dynamic light scatting	Pen/strep	penicillin/streptomycin
DNA	deoxyribose nucleic acid	PFA	paraformaldehyde
dNTPs	deoxyribonucleotide triphosphate	PI	isoelectric point
e	extinction co-efficient	PMA	phorbol 12-myristate-13 acetate

EDTA	ethylenediaminetetraacetic acid	PRR	pattern recognition receptor
ELISA	enzyme-linked immunosorbent assay	RAG	recombination activating gene
EU	endotoxin unit	RBC	red blood cells
FACS	fluorescent activating cell sorting	RMSD	root mean square deviation
FBS	fetal bovine serum	RNA	ribose nucleic acid
Fc	fragment crystallisable	RPMI	Roswell park memorial institute
FcyR	fragment crystallisable y receptor	RORyt	retinoic acid-related orphan receptor y t
FDA	food and drug administration	RSV	Respiratory syncytial virus
FITC	fluorescein isothiocyanate	SAPN	self-assembling protein nanoparticle
fhbp	factor h binding protein	SARS	Severe acute respiratory syndrome
FMO	fluorescence minus one	SBA	serum bactericidal assay
FPLC	fast protein liquid chromatography	SDM	site directed mutagenesis
FOXP3	forkhead Box P3	SDS	sodium dodecyl sulphate
GFP	green fluorescent protein	SDS-PAGE	SDS- polyacrylamide gel electrophoresis
GM-CSF	granulocyte-macrophage colony-stimulating factor	SEM	standard error of the mean
GMFI	geometric mean fluorescence intensity	SEC	size exclusion chromatography
GNA	genome-derived Neisseria antigen	s	seconds
HBc	hepatitis B virus core antigen	SOC	super optimal broth
HBcAg	hepatitis B virus core antigen	Strep HRP	streptavidin horse radish peroxidase
HBsAg	hepatitis B virus surface antigen	TAE	tris acetate buffer
HBSS	Hanks bank salt solution	T-bet	T box transcription factor
HEK	human embryonic kidney cells	TCR-b	T cell receptor beta
HEPES	4-(2-hydroxyethyl)-1-piperazineethanesulfonic acid	T_{CM}	central memory T cells
HIV	human immunodeficiency virus	T_{EM}	effector memory T cells
HPB	hepatitis B virus	Th	helper T cells

HPV	human papillomavirus	TGF-β	tumour growth factor
HRP	horse radish peroxidase	Th	helper T cells
hr	hour	TIM	triose phosphate isomerase
IEDB-AR	immune epitope database and analysis resource	TBS	tris buffered saline
IFN-y	interferon- y	TLR	toll-like receptor
IgA	Immunoglobulin A	TMB	3,3',5,5'-tetramethylbenzidine
IgE	immunoglobulin E	TNF-α	tumour necrosis factorα
IgG	immunoglobulin G	TNF-β	tumour necrosis factor β
IL	interleukin	TNFR	tumour necrosis factor receptor
IPTG	isopropyl β- d-1-thiogalactopyranoside	Treg	regulatory T cells
IRF8	Interferon regulatory factor 8	UA	uranyl acetate
K_D	dissociation constant	UV	ultraviolet
k_{off}	dissociation rate	VLP	virus-like particle
k_{on}	association rate		

Abstract

Technological advancements have allowed the field of vaccine design to develop rapidly to meet the on-going need to protect against infectious disease. Protein-based formulations are currently at the forefront of vaccine-based research and several virus-like particle (VLP)-based vaccines have entered clinical trials. VLPs are self-assembling structures that form the viral capsid but do not contain nucleic acids, hence are non-infectious. These structures are established antigen presentation platforms with the ability to display a range of antigens to the host immune system to protect against a range of pathogens. Here we investigate a synthetic platform, I3-01, for use as a self-assembling antigen presenting platform. I3-01 was engineered to form a cage-like structure with similar dimensions to a VLP, comprising 20 trimers of the thermostable enzyme 4-hydroxy-2-oxoglutarate aldolase from *Thermotoga maritima.* The I3-01 platform was purified and the structure was determined to 8Å resolution by cryoelectron microscopy; the structure confirmed it matched the designed model within the limits of experimental error. The potential of I3-01 as a vaccine platform was tested by assessing the ability of the assembly to present antigens from *N. meningitidis*. The antigens, adhesin NadA and the heparin binding protein NHBA, were selected because they are included in the licensed meningococcal 4CMenB vaccine. The relevant antigen domains were fused by genetic means to I3-01 but the products failed to assemble correctly. A novel fusion technology, exploiting the ability of Protein A to bind to the Fc portion of antibodies, was designed to overcome this problem. Protein A was fused to the C-terminus of I3-01; the fusion protein was expressed in *E. coli* and electron microscopy was used to confirm that the purified assembly formed a homogeneous population of particles which closely resembled the unmodified I3-01. In order to test that the I3-01-ProteinA (I3-01-PA) assembly was able to bind Fc fusion proteins, a fusion protein consisting of ovalbumin (OVA) fused to the Fc fragment of mouse IgG2A was generated. A bio-layer interferometry assay confirmed that the I3-01-PA construct bound to the Fc-OVA protein with high affinity. *In vitro* studies compared the use of I3-01-PA as an antigen presentation platform to a VLP assembly- Hepatitis B core protein- also fused to Protein A (HBc-PA) VLP. Analysis of the uptake into THP-1 derived macrophages showed that neither platform increase uptake, compared to Fc-OVA alone. A similar observation was made using mouse bone marrow-derived dendritic cells; there was also no increase in the expression of CD40, CD80, CD86 and MHC-II following antigen uptake. This suggested that these cells were not more activated by either platform. The I3-01-PA assembly stimulated a significant increase in IL-10 and TNF- α secretion when in complex with Fc-OVA compared to Fc-OVA alone, showing an effect of the I3-01-PA assembly. However, this effect was significantly less

than when the Fc-OVA antigen was in complex with the HBc-PA VLP. In order to assess the CD4 T cell response following antigen uptake, $CD4^+$ OT-II OVA specific T cells were co-cultured with dendritic cells which had been stimulated by Fc-OVA antigen presented on both platforms. Both the I3-01-PA assembly and the HBc-PA VLP significantly increased the ability of the Fc-OVA antigen to stimulate a specific T cell proliferation, compared to Fc-OVA alone ($p<0.0001$). The presence of either platform also increased the activation status of these T cells, measured through the increase in the CD25 and CD69 markers. Based on the cytokine profiles, initial studies indicated that a Th1 skewing of the T cell response is induced with the presence of both platforms. These initial findings offer a novel method of attaching diverse complex antigens to the thermally stable I3-01 assembly providing the prospect of a unique vaccine technology.

Declaration

No portion of the work referred to in the thesis has been submitted in support of an application for another degree or qualification of this or any other university or other institute of learning.

Copyright Statement

I would like to dedicate my PhD thesis
to my parents
for their endless encouragement
and support

Acknowledgements

I would like to take this opportunity to thank the people who supported me throughout this period of study. I would like to express my sincere gratitude to Professor Jeremy Derrick for providing me with the wonderful opportunity to conduct this research and for sharing his wealth of knowledge, experience and enthusiasm, which were invaluable. The rest of my supervisory team; Dr Alan Roseman, Dr Jim Warwicker and Dr Anil Day were very supportive and I thank them for their insightful advice. I am very grateful for the Macdonald lab, specially Dr Helen Parker, for her expertise and support in the latter stages of my research.

I have really enjoyed working as part of the Derrick lab and the other members, past and present, were incredibly welcoming and have made my time here very enjoyable. I would like to give specific thanks to; Ms Angela Thistlethwaite, Dr Tim Eyes, Dr James Austerberry, Dr John Edwards, Dr Sebastian Aston-Deaville, Dr Ayat Zawawi, Dr Murtala Jibril, Dr Mohd Zulkifli Bin Salleh, Dr Smruti Rashmi, Dr Lenka Stejskal, Mr Francesco Castagna, Mr Fidel Ramirez Bencomo and Ms Leonor De Braganca. I would also like to thank Dr Alan Roseman, Dr Richard Collins and Mrs Samantha Forbes for their expertise in the electron microscopy facility.

I am extremely grateful to the BBSRC for funding this project and for their support and additional training provided during my period of study.

Finally, I would like to thank my husband, family and friends for their constant support, patience and encouragement throughout the past four years.

Chapter 1

Introduction

Chapter 1 - Introduction

This thesis is related to a novel vaccine technology so it is important to begin by reviewing the history and principles of vaccines and their design. This aims to cover the field from the first vaccine for smallpox to the most recent novel technologies, with a specific focus on bacterial meningitis.

1.1 A History of Vaccine Design

It could be argued that the introduction of vaccines has been one of the biggest breakthroughs in the history of human health. On average 2-3 million deaths are prevented each year across the world due to the use of vaccines according the World Health Organisation and this number would be higher if cooperation with the available programmes improved [1]. So far, two diseases have been removed from the world- smallpox and Rinderpest-and many more are not far off extinction, such as polio. There has been much development in the design approach since the introduction of the first vaccine against smallpox in the 18th century and the methodologies used plus examples of these are discussed below, Figure 1. Increased knowledge of immunology, microbiology and molecular biology has recently bettered our understanding of the human immune system and its interactions with pathogens. Vaccines are designed based on the methods the specific pathogen uses to evade the host immune system to produce potent and protective immune responses [2].

Smallpox has been completely eliminated from the world through vaccination, the idea of this preventative treatment was introduced by Edward Jenner through his observation of milkmaids [3]. He noticed that any maid infected with cowpox did not contract smallpox and therefore was “immune” and so a heterologous vaccine, using a similar organism to prevent a disease, was born. It was approved for use in the UK 60 years later as the only real manner to test the effectiveness was to correlate the location of deaths from smallpox in comparison to the vaccination areas over time [3]. This was the world’s first vaccine and despite the side effects caused due to being infected with cowpox, it was still successful.

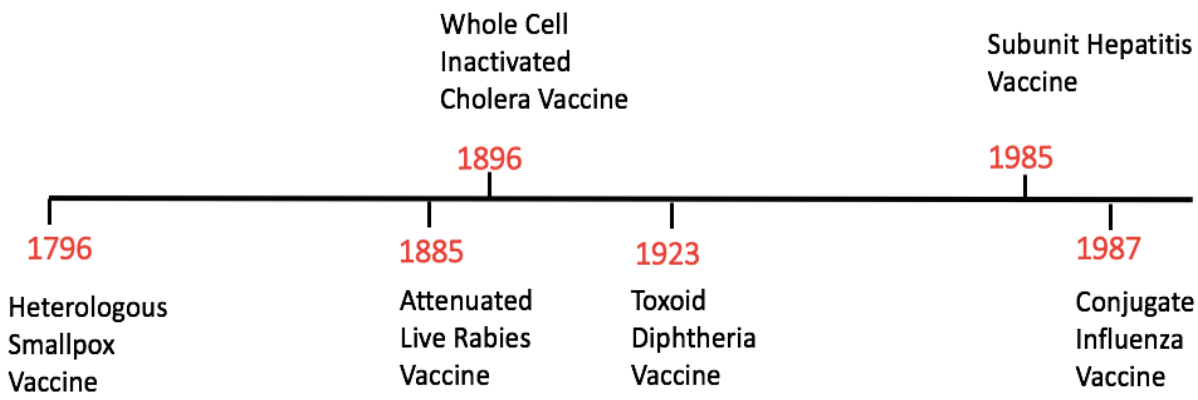

Figure 1-1. Timeline of Vaccine development. The first vaccine was developed in 1796 and was used to successfully eradicate Smallpox. Since then, there has been a shift to different types of vaccines which have been used to protect against various diseases with different success rates. (modified from: Karch and Burkhard, 2016).

Following the description of Germ Theory in 1861, Louis Pasteur discovered that he could weaken infectious bacteria following exposure to adverse conditions. In 1885 a weakened, or attenuated, Rabies virus was used to prevent the onset of Rabies in a young boy bitten by a rabid dog [3, 4]. This represents an advance in the evolution of vaccine design as Rabies is being protected against using the virus itself rather than a similar microbe. However ethical questions, safety and side effects were still clear issues.

Previous work was built upon using a bacterium that has been killed, not just attenuated, to vaccinate against cholera for the first time in 1896 [3]. The basis of this vaccine is currently the only preventative therapy licensed for cholera in the US. The bacterium is inactivated using the organic toxic compound phenol but this is thought to only be around 50% effective in the immediate months following vaccination [5]. This vaccine is now only used in the case of epidemics due to its high risk of side effects and limited ability to protect against the disease [5].

Efforts then progressed to using immunogens produced by the bacterium, such as toxins, rather than the whole cell approach which is known for increased adverse reactions. Specifically, it was noted that Diphtheria produces a toxin as part of its mechanism of pathogenesis. This toxin was purified and in sub-lethal doses was found to produce what we now know as an antibody response in animals. This was a step in producing effective immunogenic vaccines without the toxicity and side reactions associated previously [3]. Diphtheria is still protected against in this way today in a multicomponent vaccine, DTaP. This contains the Diphtheria and Tetanus toxoids along with acellular *pertussis* and has been licensed in the US for a four dose course. It is a safe and successfully immunogenic method of protecting against this disease [6].

By the 1980s the knowledge of biology had expanded; there was much more information and tools to progress in the vaccine design field. The biggest problem with whole cell inoculations is the concern over reactivation and the use of only specific antigens in vaccines rather than whole cells would reduce this [3]. The disadvantage of this is that removing the remainder of the cell leads to a general loss in immunogenicity of the subunit of choice. To overcome this, adjuvants such as aluminium salts have been added to the various subunits to attract innate immune cells to the antigen, enabling a strong immune response [3]. For a Hepatitis vaccine the surface antigen (HBsAg) was selected and was produced in *Escherichia coli* but this proved not to be immunogenic [7]. Vealenzula et al went on to successfully produce HBsAg in a yeast cell line and this was shown to be safe and immunogenic in 1985 [8, 9]. This was then approved the following year and remains the current Hepatitis B vaccine used under many trade names including; Recombivax HB and Engerix-B manufactured by Merck and GSK respectively [10] [11].

A conjugate vaccine is formed when a polysaccharide antigen that is weakly immunogenic alone is attached to a much more immunogenic protein [3]. It has been known for 70 years that this enhances the immunogenicity of a polysaccharide and provides opportunity for vaccine design [12]. During the production of the Haemophilus type B vaccine many toxoids were trialled including from Tetanus and Diphtheria [12]. However, despite the original excitement at the production of T cell dependent memory, the long term protection offered is poor [12]. By the

millennium there was still a need for many vaccines and so the development of new methodology was required to reach these goals, overcoming logistical and economic problems [12].

1.2 The Adaptive Immune Response

The immune system is a complex web of processes which can be categorised into two arms, the adaptive and the innate responses [13]. Together these responses have the joint aim of removing any infectious agent and providing long lasting immunity. Innate immunity acts as the first line of defence and contains physical barriers including: skin, mucosal membranes and phagocytes. Examples of phagocytic cells are natural killer cells, macrophages and dendritic cells [13]. These cells have pattern recognition receptors (PRRs) that recognise highly conserved molecular structures, pathogen associated molecular pattern (PAMPs) [14]. The purpose of the innate arm of the immune system is to eliminate antigen immediately but this isn't always successful and, at this stage, the adaptive immune system is required [13]. This involves cells such as lymphocytes and antibodies which have receptors specifically tailored to antigens and engagement with these leads to cytokine production [13] [14]. Antigen presenting cells (APCs) are a class of cells which bridge the gap between the innate and adaptive immune response and these include macrophages and dendritic cells [15]. The latter are known as the most important APCs and are involved in the antigen uptake and presentation to the adaptive immune system in the context of Major Histocompatibility Complex (MHC). Through antigen presentation, the dendritic cells prime naive T cells to engage the adaptive immune response. This in turn leads to the proliferation of the lymphocytes which stimulates cytokine production from CD4 T cells and cytotoxic activity of CD8 T cells. Circulating naïve T cells are stimulated to become differentiated into their various subtypes. This is initially determined by the context in which the antigen is presented, producing either a CD4 or CD8 T cell response. CD8 cells are also known as cytotoxic T cells and have the main role of eliminating infected cells. The second class, the CD4 T cells, have a more complex function in producing a range of cytokines and chemokines which activate neighbouring cells [16]. The proliferation and activation of this class of T cells has been studied *in vitro* using the well-established OT-II transgenic mouse cell line. This produces

T cells with receptors specific for the chicken ovalbumin epitope from residues 323.339 and allows an analysis of ovalbumin antigen specific CD4 T cells [17]. CD4 cells can be divided into further subtypes defined on their cytokine profile and these include Th1, Th2, Th17 and T regulatory (Tregs) cells which are discuss further below [16].

Th1 were the first class of Th cells to be discovered; they are required for cell-mediated inflammatory responses and to produce interferon-γ (IFN-γ) and tumour necrosis factor-β (TNF-β) [18]. The presence of IFN-γ, produced by the Th1 cells themselves stimulates the differentiation of this subtype of CD4 T cells along with IL-12 which is secreted by dendritic cells in response to antigen uptake [19]. T box expressed in T-cells (T-bet) is a transcription factor involved specifically in the differentiation of Th cells into Th1 cells and is therefore an intracellular marker of this subclass [20, 21]. There is evidence to suggest that the Th1 subclass of CD4 T cell population mediates a range of autoimmune diseases such as Rheumatoid arthritis, Insulin-dependent diabetes mellitus and inflammatory bowel disease [22].

The second class of CD4 T cells to be classified was Th2; these are associated with parasitic helminth infections and tissue repair of damaged tissue. The characteristic cytokines of a Th2 response include IL-4, IL-5, IL-9 and IL-13 [23]. IL-4 is the distinguishing cytokine involved in both the differentiation and proliferation of the Th2 subtype [24]. In terms of the balance of the Th1/Th2 response, IL-4 production works to dampen the Th1, cell mediated reaction [25]. The downstream effects of a Th2 T cell response include the production of class specific IgE antibodies from of B cells, eosinophil activation and mucous production. This explains the role of these responses in allergic reactions and asthma, and why this type of T cell response is not the desired to be produced by potential vaccine candidates [26].

Th17 cells are a more recently defined class of CD4 T cells which are characterised by their production of the cytokine IL-17. The inflammatory cytokines IL-21 and IL-22 are also produced in in this response which may lead to the progression of autoimmune diseases. The transcription factor Retinoid related orphan receptor γ t (RORγt) is the main regulator for the production of this T cell subtype [27]. The influx of these pro-inflammatory cytokines leads to a

promotion of tissue inflammation which is the cause of the associated autoimmune disease [28]. Specifically, the IL-17 cytokine has been associated with the increase in cartilage and bone damage that occurs in Rheumatoid arthritis [27]. Other diseases associated with this CD4 response include autoimmune encephalomyelitis and chronic inflammatory bowel disease [29] [30].

Tregs are the final subclass of CD4 T cells to discuss and the function of these cells is to oppose the autoimmune effects produced by the Th17 cells. They are proliferated through stimulation of a large concentration of tumour growth factor-β (TGF-β) and also have the ability to supress the function of other innate and adaptive immune cells. Transcriptional control of this subtype of T cells is maintained by Forkhead box protein P3 (FoxP3), ensuring 10% of the CD4 T cells population were comprised of these cells [27]. There is suggestion Tregs can be used in the treatment of human diseases such as graft v host disease, graft rejection and autoimmune disease [31-33].

It is clear that for a vaccine to trigger a full and protective immune response there is need for the early steps of APC antigen uptake and processing to be effective. The creation of any novel vaccine candidates produced in this new era of design need to take this into consideration. These processes are heavily affected by the properties of the antigen including the size, shape, charge, hydrophobicity and potential receptor interactions [34]. It is a fruitful line of research to compare these process when antigens are presented to APCs by different methods. Common examples of antigen presentation platforms investigated to display antigens to APCs can be categorised into three groups; virus-like particles (VLPs), bacterial scaffolds and most recently the used of synthetically designed assemblies.

1.3 VLP Assemblies in Vaccine Design

To date, the most potent vaccines have been of a whole cell nature due to the strong immunogenic response produced by B cells to these natural repeated antigen arrays [35]. Using VLPs would provide this strength of response without the safety worry of whole cell inoculations as they contain no viral DNA [35]. These VLPs can be utilised in two different ways to achieve this result. Firstly, the VLP is that of the virus used in the vaccine, or secondly, that the VLP acts as an antigen scaffold for a vaccine against a different virus to the one the particle used originates from [36]. This method was first initiated in trials for a Human Papilloma Virus (HPV) vaccine using a HPV VLP and also for a Hepatitis C vaccine using a Hepatitis B surface antigen VLP [35, 37]. HPV and Hepatitis are just a couple of examples of the diseases being targeted with this type of preventative therapy and in the following section I will describe the use of this technology further.

1.3.1 Hepatitis B Surface Antigen

In 1982, the Hepatitis B surface antigen (HbsAg) was expressed in yeast, purified and was shown to produce anti-HBsAg antibodies, reflecting their immunogenicity (Table 1) [8]. It is now known HBsAgs self-assembles into a VLP and so this ability has been exploited in vaccine trials [37]. HBsAgs was found to be exceedingly good at delivering foreign sequences to give an immune response. For example, when a Hepatitis C epitope, HVR1, was displayed on the HBsAg VLP an anti-Hepatitis C response was induced. This shows the potential this type of vaccine has to produce a strong immune response against multiple viruses [37].

1.3.2 Hepatitis B Core Antigen

The Hepatitis B core antigen (HBcAg) was identified as a vaccine candidate following expression and the definition of insertion sites in preparation for trials [38]. Specific epitopes were added for malaria antigens and these provoke an immune response in rodent experiments, providing evidence for a possible vaccine candidate [39]. In 2004 this vaccine, HBcAg plus *Plasmodium*

falciparum CS protein, was examined in a phase 1 trial [40]. It was discovered that this recombinant protein self-assembled into a VLP that was extremely immunogenic. Following a single 50μg dose, malaria-specific T cells were generated which secreted gamma interferon and also specific antibodies. This suggests a possible use of this core particle as a vaccine platform and as a preventative measure against malaria. The next step was further testing to achieve long term responses and with stronger adjuvants [40]. Influenza was a second virus targeted for vaccine design using this scaffold; in this instance 4 copies of the M2e protein were fused to HBcAg and again memory T cells and antibodies were produced [41]. It is also important that VLPs are optimised for their job as vaccine platforms, i.e. that they are soluble and stable. The fact that modifications of HBcAg did not affect the assembly of the VLP but can enhance the solubility and immunogenicity is important [42]. This can be done through the addition of disulphide bonds and the transplantation of a common spike structure respectively [42].

1.3.3 Hepatitis E

Hepatitis E VLP was used in the design of a vaccine against this disease and a Phase 3 trial took place in China in 2010 [43]. This was established to be both safe and effective in men and women aged between 16-65. The focus then moved to ensuring the safety in younger, older and pregnant potential recipients of the vaccine [43]. The long term protection of the trial in China has been evaluated and there is evidence that the Hepatitis E vaccine induced antibodies and provides protection for at least 5 years [44]. Since then, to aid the mass production of these VLPs, a method of manufacturing them from insect cells has been successfully defined [45]. This is an important consideration throughout vaccine development, keeping production efficient and affordable.

1.3.4 Human Papilloma Virus

Self-assembling VLPs from HPV L1 protein can be effectively used as an antigen delivery system for at least 2 epitopes [46]. This was the first suggestion that these VLPs could be used as vaccines against HPV and other viruses. A large advantage is that HPV6b L1 VLPs are

immunogenic without adjuvant which makes them ideal vaccine candidates [47]. There is also evidence VLPs can work as both a preventative and therapeutic measure: warts formed by the virus seemed to regress following post-infection vaccination [47]. As no adjuvant is needed and multiple epitopes can be displayed the HPV VLPs make perfect vaccine candidates for inducing HPV and other forms of immunity [47]. A quadrivalent HPV inoculation against strains 6, 11, 16 and 18 entered phase 3 trials and was found to significantly lower the incidence of HPV disease presence in young women [48]. The VLP structure has also been analysed to try to understand why the immunogenicity may vary, which is obviously a key desirable feature in vaccine design. One possible reason for this is loop fluctuation on the surface of the VLP, this is important to consider in the generation of future HPV VLP vaccines [49].

1.3.5 Influenza Virus Hemagglutinin

With the development of VLP vaccines, one virus which has had many immunisation struggles is influenza. The safety, effectiveness and ease of delivery makes VLPs attractive candidates for use [50]. These particles can act as multiple epitope displays would enable the production of multivalent hemagglutinin inoculations [50]. VLPs were generated and it was established they induce the production of a T cell response and neutralising antibodies against both heterologous and homologous strains within a particular subtype [51]. An added bonus was that, when immunised and then inoculated with the virus, immune cells rapidly built up further and successfully inhibited viral replication [51]. To further test the theory that VLPs could be immunogenic to multiple strains of influenza, a trial was run to test for the production of specific antibodies to specific subtypes of influenza virus in ferrets [52]. As this was discovered to be the case it was proposed that each year a trivalent vaccine designed towards the strains predicted for that season could be created [52]. A recently troublesome pandemic strain, H7N9, had caused many cases of influenza in China and therefore a vaccine to limit global spread was of prime importance [53]. The candidate vaccine reduced influenza symptoms, such as weight-loss and fever, and protected against tracheal and lung infection in a ferret model. The H7N9 VLP could also be weakened using either the matrix 1 or ISCOmatrix protein which further enhanced the natural immunogenicity of the scaffold. This gives an exciting potential for a safe

and effective vaccine against this particular strain of influenza [53]. Finally, more recent attempts at achieving a universal influenza inoculation targeting all the major strains in one, has been advanced with a novel cocktail design [54]. In this method many VLPs are mixed each encoding a different hemagglutinin epitope, for example H1, H3, H5 and H7. This was trialled in a mouse model and gave the first real prospect for a universal influenza vaccine offering significant protection was detected [54].

1.3.6 Bacteriophage Qβ

In 1993, it was established that bacteriophage Qβ has a coat protein which can self-assemble and act as an epitope carrier [55]. However, this work was done in *E. coli* and for this platform to have any use in vaccine design it would be preferable if it was expressed in a eukaryote such as yeast to avoid potential endotoxin contamination. Successful, yet lower expression yields, have been achieved in two yeast species but the immunogenicity of the VLP products were very similar [55]. Since this time work has been carried out to manipulate Qβ VLPs to increase their immunogenicity by the addition of proteins and small molecules [56]. The stability of the VLPs can also be modified through design and it is now possible to control the stability of a Qβ VLP over at least a 40^0C temperature range [57]. This work points to the likelihood that these structures are applicable for use in vaccines; trials carried out using them will now be discussed. In 2008, an efficacy and safety trial of a Qβ VLP based vaccine targeting high blood pressure took place [58]. Specifically targeted angiotensin 11, a 300μg dose reduced daytime blood pressures of patients with hypotension and caused no serious side effects [58]. A second trial for Qβ VLP's was in a vaccination against rhinoconjunctivitis, an allergic response and, without being clear on the mode of action, over a period of 2 months it was found to reduce allergic responses [59]. It is important that a vaccine can provoke both an effector and memory T cell response, especially against diseases in which relapse is common, for example, melanoma [60]. Finally, a disease which is environmentally stimulated, type 11 diabetes, could also be prevented using a Qβ VLP vaccine [61]. A VLP particle which had IL-1β covalently attached improved glucose tolerance and showed no obvious immunosuppression in a mouse

experiment with diet induced diabetes [61]. This shows the possibility that this scaffold has to be a vaccine against a range of different diseases.

1.3.7 Bacteriophage MS2

Similarly to Bacteriophage Qβ, MS2 VLPs are also capable of displaying a wide range of epitope and proteins or small molecules can be added to the scaffolds to increase the immune response stimulated by them [56, 62]. The MS2 VLPs have some stability problems but it is possible to control this parameter through mutations in the loop structures after the antigen has been added to the particle. This is due to the assembly as a whole only being able to resist temperatures of up to 50^0C [63, 64]. In terms of use in vaccine design, this platform has been mainly used to target malaria. An MS2 VLP was created with epitopes displayed that prevented red blood cell invasion by parasites and had strong immunogenicity which may be developed further into a vaccine candidate [65]. Most recently, a trial in mice was undertaken using VLPs presenting AMA1, a blood stage antigen in malaria [66]. This did produce anti-sera which cross reacted with the protein; nevertheless the response was not strong enough to give protection and so further work must be undertaken [66]. A separate bacteriophage, AP205, was used as a platform for multiple malarial antigens and this provoked a strong antibody response after just one dose without need for adjuvant [67]. This suggests this bacteriophage may be a better option for malarial vaccine design.

1.3.8 Bacteriophage PP7

A third bacteriophage, PP7, can self-assemble into VLPs and have a significant benefit over the MS2 bacteriophage in terms of their potential applications. This is due to the presence of increased disulphide bonds making it a much more stable platform [64]. This scaffold has been utilised in a creation for a HPV vaccine displaying L2 peptides and has been discovered to induce highly immunogenic antibody responses which remain high for at least 12 months [68]. Due to PP7 VLPs natural stability and the fact there is the ability to add aluminium hydroxide as an adjuvant provides the possibility for a vaccine which induces long term strong immunity for use

in the developing world [68]. These scaffolds were used as targets in contraceptive and cancer treatment in targeting human chronic gonadotrophin [69]. This structure provoked an inhibitory hCG response through the production of antibodies suggesting a second role for the platform [69].

1.3.9 Norovirus

There is currently no Norovirus vaccine and so a weakened norovirus VLP was produced in a bid to offer protection against a homologous disease, Norwalk virus [70]. A two dose course of this preventative medicine did indeed protect against gastroenteritis and Norwalk virus, highlighting a potential for a norovirus vaccine [70]. Further support as to the effectiveness of this scaffold is held in the fact both cross reactive antibody and T cell responses are induced by these VLPs [71]. As mentioned previously, the ability to express VLPs in eukaryotic systems is preferable and so the capacity to express self-assembling norovirus VLP in *Pichia pastoris*, a yeast strain is a large advantage to this VLP in vaccine design [72]. Finally, the ability to modulate this platform extremely easily by removing and replacing conjugated molecules to display a range of epitopes makes it a very good candidate for prophylactic treatment [73].

1.3.10 Parvovirus

In 1994, Brown et al provided the first evidence that the capsid protein VP2 from Parvovirus can display antigens [74]. This work was built upon by using this VLP as a platform for Dengue virus 2 antigen presentation which was found to induce humoral although not T cell immunity, which would perhaps require an adjuvant [75]. It has been shown that Parvovirus VLPs are very temperature stable and can withstand 80^0C heat for at least 30 minutes despite ideally requiring 37^0C, this makes them ideal for vaccine design [76]. However as with the Dengue virus trial there have been problems using these platforms to get a strong enough immune response without being reactogenic. Expressing the structures in yeast helped reduce the reactogenicity but in turn limited the immunogenicity produced, emphasising that there is still much work to be done if Parvovirus VLPs are to be used as vaccines scaffolds [77].

1.3.11 Rabbit Haemorrhagic Disease

VLPs have been expressed in insect cells in a bid to vaccinate against rabbit haemorrhagic disease and this was successful in producing antibodies in rabbits which fully protected them from a virulent dose of the virus [78]. These structures have also been designed as an immunotherapy in cancer patients infected with HPV virus. Survival is prolonged when a VLP with HPV peptides attached and an adjuvant are given to mice with tumours, promoting an anti-tumour response [79]. This virus therefore produces VLPs with therapeutic potential.

1.3.12 Other VLP Vaccine Platforms

There are a few other viruses which have displayed the possibility to have their VLPs used in vaccines. Cowpea Chlorotic Mosaic Virus was the first virus to be re-assembled of icosahedral structure and has since been shown to be manipulated to encapsulate cargo [80, 81]. This suggests these VLPs could be used in vaccine design if the exterior could be modified to act as an epitope display platform [81]. Secondly, Cowpea Mosaic virus VLPs also have the ability to be modified on a nanometre scale suggesting the applicability for use in vaccines [82]. Finally, Flockhouse virus has been used to design a new strategy of therapeutic production using VLPs with the addition of whole proteins to induce a potent immune response with appropriate adjuvant added [83]. Overall it is clear VLP's have been very well exploited in the production of vaccines and many successful immunisations have been produced in this way.

Platform	Symmetry	Characteristic feature	Expression System	Current Status	Immunogenicity	Refs
HBcAg	Two forms; 240nm subunits 34nm (T=4) & 180 subunits, 30nm (T=3) Icosahedral 21kDa	Efficient scaffolds for the presentation of heterologous epitopes as vaccine antigens and maintains structural stability	Bacteria Yeast Mammalian insect, plant frog oocytes	Pre-clinical /phase 1	Highly immunogenic- induces both humoral immunity and cellular immunity	[38-42]
HBsAg	Icosahedral symmetry, 17-25nm	Efficient scaffolds for the presentation of heterologous epitopes	Yeast Mammalian cells	Several licenses	Highly immunogenic (humoral and cellular)	[7-9] [37]
HEV Hepatitis E virus	Icosahedral symmetry, 20nm diameter	Efficient for presentation of multiple epitopes	Bacteria Baculovirus	Phase IV	High immunogenicity	[43-45]
HPV L1 Human Papilloma Virus	Icosahedral 50nm in diameter	Efficient platform for delivery of multiple epitopes	Yeast Insect cells	Several licences	Induce potent T cell and B cell responses	[35] [46-49]
Hemagglutinin (influenza virus)	Spherical, 80-120nm in diameter	Efficient platform for multiple epitope delivery	Insect cells	Several licences	Increase in cross protective immunity	[50-54]
Bacteriophage Qß	T=3, icosahedral 25nm in diameter	Easily purified displays multiple epitope	Bacteria + chemical conjugation	Phase I/II	Highly immunogenic	[55-61]
Bacteriophage MS2	Icosahedral, T=3, 27nm diameter	Engineered to display specific peptides	*E. coli*	Pre-clinical	Highly Immunogenic	[52] [62-66]
Parvovirus B19 capsid proteins	Icosahedral VP1, 84kDA VP2= 55kDa	Multiple epitope presentation	Insect cells	Phase I	Strong humoral immune response	[74-77]
Bacteriophage PP7	Icosahedral	More stable than MS2 epitope display platform	*E. coli*	Pre-clinical	Produce neutralising antibodies	[64] [68] [69]
Bacteriophage AP205	Icosahedral	Display multiple a range of antigens	*E. coli*	Pre-clinical	Antibody response without adjuvant, after only a single dose	[67]
Flockhouse virus	Icosahedral	Efficient protein display- multiple copies, high yields, genetically simple and stable	*E.coli*	Pre-clinical	No igG specific antibody responses without adjuvant	[83]
Rabbit Haemorrhagic virus	Icosahedral 35-37nm diameter 60kDa	Multiple epitope display	Bacuolvirus system	Pre-clinical	Produces fully protective antibodies immunotherapy in tumours	[77-78]

Table 1-1. A Summary of VLPs used in vaccine design. (Unpublished, Smruti Rashmi- modifications have been made to the tables based on updated information)

1.4 Assemblies from Bacterial Sources used in Vaccine Design

1.4.1 Ferritin

Ferritin is a 450KDa iron storage protein which contains 24 chains that self-assemble into a hollow shell and the x-ray structure was solved in 1991 [84, 85]. These 24 subunits form a spherical assembly which is stable over a large pH range of 2.2-10 and under neutral conditions has a diameter and volume of 9.8nm and 142nm^2 respectively [86]. Ferritin was found, through the co-expression of different fusion proteins, to be able to present multiple epitopes [87]. This gives the potential for a vaccine as it would allow multiple antibodies to be stimulated simultaneously [87]. To further this point, the nanoparticles formed are able to induce a proliferation of both $CD4^+$ and $CD8^+$ T cells in vitro and in vivo, following them presenting antigens effectively to host dendritic cells [88]. Ferritin cages have most commonly been used in the design of influenza vaccines. In the first case, hemagglutinin was attached and the cage formed contained 8 hemagglutinin trimer spikes which gave a 10 times greater antibody response than the current inoculation Figure 2A [89]. This makes way for a broad influenza vaccine targeting multiple strains which is much needed [89]. The addition of hemagglutinin stem only on to the nanoparticle was another method attempted and again produced broad cross reactive antibodies in mice trials [90]. When the mice were infected with the virus the vaccine protected them successfully, again suggesting a possibility of protection against multiple strains [90]. Other epitopes for other diseases such as Epstein Barr virus and Hepatitis C have also been discovered to have potent neutralising activity when displayed by a ferritin nanoparticle [91, 92].

1.4.2 Lumazine Synthase

When isolated from *Bacillus subtilis*, lumazine synthase is icosahedral in symmetry and contains 60β subunits with 3α core subunits [93]. The potential for use as a vaccine scaffold was introduced when it was proven that the cage structures can deliver antigens to dendritic cells and provoke specific proliferation of T cells [94]. In terms of a specific example, lumazine

synthase has been used to display a known antibody neutralising epitope gp120 for HIV [95]. As there is a great need for a protective HIV vaccine that fact that the breadth and potency of immune response was increased by displaying the epitope in this way was a breakthrough [95].

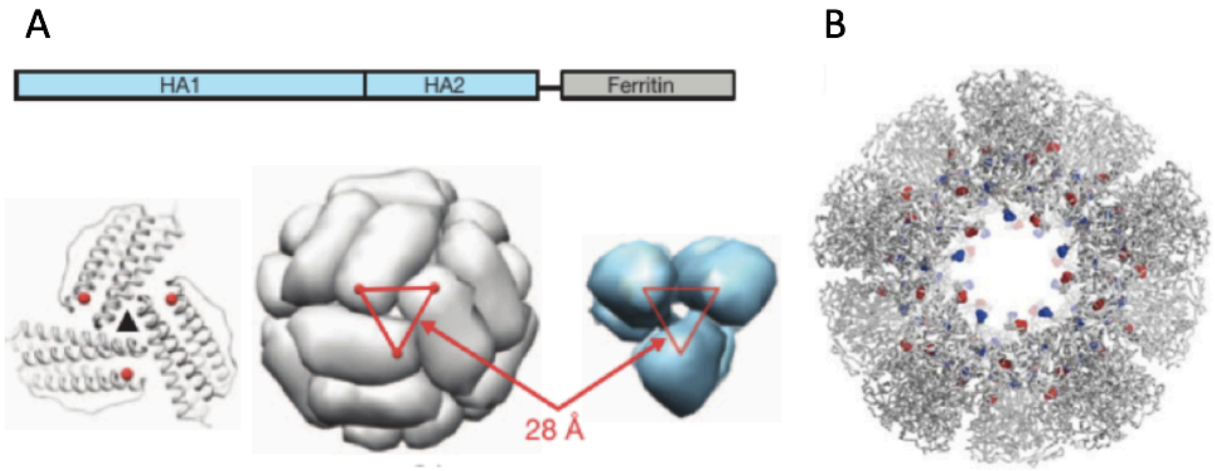

Figure 1-2. Bacterially-sourced scaffolds in vaccine design. (A) The primary sequence of two hemagglutinin proteins attached to ferritin along with the three-fold axis of the assembly followed by the 24 subunit ferritin assembly with the hemagglutinin proteins displayed. This highlights that bacterial ferritin is a potential vaccine scaffold. (B) Encapsulin self-assembles from 60 subunits and mutation sites are highlighted in which the thermostability of the particle can be increased. (modified from: Kanekiyo, M. et al, 2013 and Dalmau, M. et al. 2008).

1.4.3 Heat Shock Proteins

The crystal structure of a heat shock protein from *Methanococcus jannachii* was solved in 1998 and was of octahedral symmetry, with a diameter of 120A that contained 24 beta sandwich monomers [96]. These proteins can be split into 5 groups and function to help a host survive in conditions of extreme heat, having a molecular weight of between 15-30kDa [97]. The proteins self-assemble to form symmetrical particles which can be manipulated to bind multiple substrates; this ability could be utilised to display epitopes in vaccine design [98]. Heat shock protein 16,5 was isolated from the thermophile *M. jannachii* and was found to form a cage which was most stable at high temperatures, rather than at 37^0C which suggests modification

to improve this parameter is needed for vaccine production [99]. Research has included using heat shock proteins to prime dendritic cells to expand their ability to present antigens and generate a T cell response [100]. With this knowledge, a cage derived from *M. jannaschi* was modified by the addition of a peptide which targets tumour vasculature which was shown to bind $CD4^+$ T cells as a successful immunotargetting therapy [101]. A second vaccine which induced anti-infectious and anti-tumour immunity in vivo by increasing a $CD8^+$ T cells response through in particular stimulating MHC-I antigen cross presentation was also produced [102]. This nanocage had the addition of gp96-Ig which suggests a new approach to vaccine design [102].

1.4.4 Encapsulin

Large structures which are formed from the self-assembly of conserved bacterial proteins are known as encapsulins [103]. An example is an icosahedral particle made of 60 monomers and of 240A diameter isolated from *Thermatoga maritima*. Their function is to encapsulate and carry bacterial cell machinery such as enzymes, but as they self-assemble they are interesting from a vaccine research point of view [103]. A recombinant protein of encapsulin and peroxidase from *Rhodococcus jostii* is also capable of self-assembling into these structures, Figure 2B [104]. Encapsulins have been used as the basis of a vaccine to provide protection against Epstein Barr virus, displaying the antigen gp350 [92]. This induced an antibody response which was very potent in trials on non-human primates and mice. Ferritin was established to be a more immunogenic scaffold in comparison to encapsulin, however this highlights the potential of using this platform in vaccine design [92].

1.4.5 E2, Pyruvate Dehydrogenase

The E2 protein from pyruvate dehydrogenase is capable of self-assembling into a thermostable dodecahedron [105]. An important feature is that following up to 120 mutations, which may be required for antigen presentation in vaccine design, there was no loss of stability [105]. This scaffold was used with the addition of CpG and peptide epitopes to demonstrate the ability of

stimulating $CD8^+$ T cell responses stressing the potential anti-viral/anti-cancer uses [106]. An important feature of this cage is its ability to be used to generate immunogenicity without adjuvants which have previously shown to cause unwanted reactogenicty [106].

1.4.6 Vault Proteins

Vault proteins are the largest ribonucleoprotein known at 13MDa in size and have shown to be unstable above 60^0C and below pH5 [107]. In terms of vaccine design, they have been used as a platform against mucosal diseases and were discovered to induce T cell responses at the site of infection whilst escaping unwanted reactions such as inflammation [108]. Finally, an interesting feature of vault protein cages are that the antibody type against the proteins can be switched in vivo which leads to a combination of alternative T and B cell responses which are unique [109]. This idea is being followed up as a future vaccine design method against diseases which are difficult to protect against. A summary of the bacterial platforms used in vaccine design can be found in Table 2.

Protein	Source & Function	Symmetry	Characteristic functions	Expression system	Current status	Immunogenicity	Ref
Ferritin	*H. pylori* Iron homeostasis	24 subunits 450kDa octahedral diameter: outer-12nm inner- 8nm	High stability Versatility for genetic and chemical modifications of both the interiors and exteriors Good scaffold for presentation of heterologous protein	Mammalian Fungus E.coli	Pre-clinical	Increase in antigen specific CD8+ and CD4+ T cells both *in vitro* and in *vivo* Induces cross protective immunity	[84-92]
Encapsulin	*Thermotoga marutuma* Iron storage	60 subunits icosahedral diameter: inner-20nm outer-24nm	Maintain their structure at high temperature No studies for presentation of heterologous antigen	Mammalian cells	Pre-clinical	Increase in immune response	[92] [103] [104]

Lumazine synthase	*Aquifex aeolicus* Involved in the last step of riboflavin biosynthesis	60 subunits icosahedral diameter: inner-9nm outer 15nm	Novel antigen delivery system Antigenic peptide insertion did not cause any significant conformational changes Extremely thermostable Can display multiple antigen copies Specific cell targeting capacity	Mammalian cells	Pre-clinical	Induces proliferation of OT-I specific CD8 T cells and OT-II specific CD4 T cells both *in vitro* and *in vivo*	[93-95]
Small heat shock proteins	*Methanococcus jannaschii* Facilitate the synthesis and folding of proteins	24 subunits 16.5kda spherical diameter: outer 2nm inner 8nm	Stable of up to 70 High porosity specific cell targeting capacity	Mammalian cells	Phase I	Induces antigen specific immunity (IgA, IgG responses)	[96-102]
Vault proteins	Found in all eukaryotes Fibro-nucleoprotein	Barrel shaped 40 x 70nm 12mDa	Involved in cell physiology and gene expression Engineered to elicit desired immune response Can modify antibody isotypes in vivo	Baculovirus	Pre-clinical	CD8/CD4 T cell memory and antibody response Protective immunity at mucosal surfaces	[107-109]

Table 1-2. A summary of bacterial scaffolds used in vaccine design. (Unpublished, Smruti Rashmi- modifications have been made to the tables based on updated information)

1.5 Synthetic Protein Assemblies in Vaccine Design

1.5.1 Use of Coiled-coil Structures

In 1993, a crystal structure was determined of a coiled-coil containing three alpha helices which determined hydrophobic interactions as the main driving force of stability [110]. These motifs contain a heptad repeat of a, b, c, d, e, f, g with a and d representing the positions which are occupied exclusively by hydrophobic residues [111]. Sites b and c are also important in stability and the introduction of charged lysine and glutamate residues here as ion pairs increase this parameter further [112]. Addition of ionic interactions such as salt bridges have also been proven to make these structures more stable [113]. Coiled coils are widespread throughout nature and despite appearing simple they are a very versatile fold with a range of assemblies having a differing stabilities [114]. Coiled-coil motifs can self-assemble into nanoparticles which are known as self-assembling protein nanoparticles (SAPN) and the parameters for formation have been defined [115].

For example, under physiological conditions the particles are spherical and 27nm in diameter and this increases with increase in salt concentration [116]. The optimal pH for formation between 7.5 and 8.5 and a 5% v/v of glycerol is also required [116]. It has been verified that these cages can be used as a vaccine platform as their metabolism shows there are no risk of long term side effects [117].

1.5.2 Examples of coiled-coil SAPN in vaccine design

SAPN was first used in a vaccine against severe acute respiratory syndrome (SARS) as it displayed a B cell epitope, Figure 3 [115]. No adjuvant was needed to induce the production of antibodies which were protective, showing this platform could be used to protect against diseases characterised by surface of B cells [115]. Over the last couple of years this methodology has been used to design other vaccines such as avian influenza [118]. The SAPN presented the M2e epitope and was given to chickens who after a period of time were inoculated with a strain of avian influenza virus which was of low pathogenicity. The immune response was increased

in terms of specific IgG production but was most efficient with the addition of an adjuvant. However, as the viral load was significantly reduced this is a possible vaccine candidate against avian influenza [118]. This method was first used to target a human pathogen in 2011 and specific humoral responses were produced without the need for adjuvants in small animals, suggesting this approach is viable for human inoculations [119]. In the case of HIV, the epitopes 4E10 and 2FE were displayed on a SAPN and this induced a high level of antibodies without adjuvant [120]. The antibodies were found to be poorly neutralising and so different epitopes must be tried to improve this [120]. Research has been done towards designing a vaccine against malaria and a protein from *Plasmodium falciparum*, CSP, has been used to generate B and T cell antigen binding surfaces for a potential malaria inoculation [121]. When these and a CD4 epitope PADRE are added to a SAPN, a long term T and B cell response was induced. This was established to be protective in mice against a pathogenic *Plasmodium* species [121]. The vaccine candidate was discovered to inhibit parasites entering human liver cells and is now said to give immune responses against parasitic infection of malaria which is long term [122, 123]. Finally, as the current immunisation against *Streptococcus pneumonia* is by a polysaccharide based inoculation it was tested to see if using a cage structure with attached antigen binding surface provided a better alternative [124]. The epitopes attached were for PspA and this elicited a strong immune response that was humoral in nature [124].

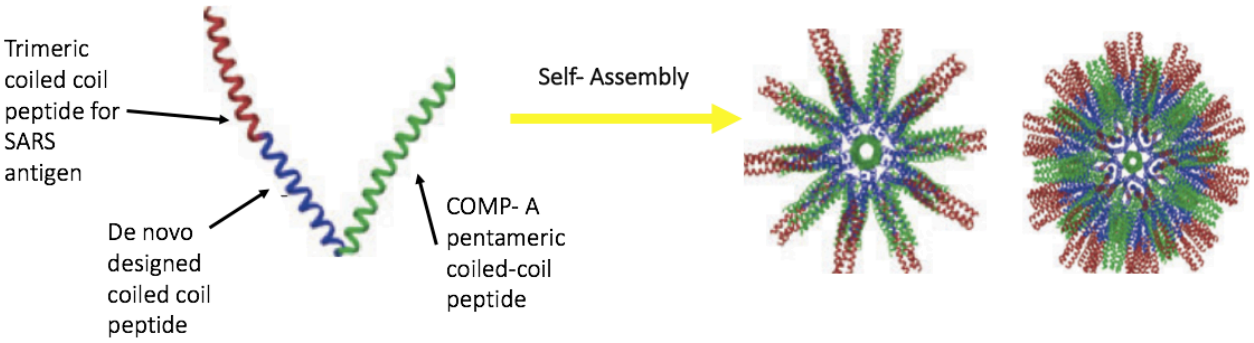

Figure 1-3. The design of a self-assembling protein nanoparticle made from coiled coil domains with appropriate antigen attached. In this example HRC-1 antigen from SARS virus which then spontaneously assemble. The representations for the first and third axis of symmetry are shown. (modified from Pimentel, T.A. et al, 2009).

1.5.3 β-Sheet Forming Fibres Vaccine Design Approach

As revealed in the self-assembly section, β- sheet pairing rules can be manipulated with computer design to successfully manufacture self-assembling peptides of this formation [125]. Q11, an example of a self-assembling β-sheet peptide, has been used in the generation of a malaria vaccine with the addition of the *Plasmodium falciparum* CS protein epitope [126]. This inoculation was found to provoke antibody responses which were long lived as when a mouse was inoculated with this parasitic infection specific antibodies were boosted in them for at least 40 weeks. β-sheet fibre platforms have also showed potential to induce an immune response without adjuvant when two different epitopes are combined on it, showing the possibility for its use as a vaccine displaying multiple antigen binding sites [126].

1.5.4 Layer by Layer Vaccine Design Approach

The final approach to vaccine design using novel assemblies is by a layer by layer method which allows formation of a biofilm which can act as a scaffold [127]. Layers are formed when a $CaCO_3$ core acts as a base for which polypeptides of opposite charge are accumulated. Without the need for adjuvants these assemblies are capable of being taken up by dendritic cells and the production of potent T cells responses in vivo [127]. This technique was used in the formation of a vaccine candidate against malaria, fusing the *Plasmodium falciparum* CS protein epitope. A similar immune response was provoked as when this protein epitope was fused to a SAPN. If anything, this method perhaps had slightly increased potency, showing potential as a viable vaccine candidate [128]. A second example is for use as a preventative treatment for Respiratory Syncytial Virus (RSV) using a specific G protein binding motif, CX3CR1, which prevents G protein binding through the production of blocking antibodies [129]. This has been demonstrated in mice to be both a safe and effective intervention in this disease [129]. A summary of the synthetic platforms used in vaccine design can be found in Table 3.

Platform	Symmetry	Characterisation	Expression system	Status	Immunogenicity	refs
Coiled coil SANP	Icosahedral, T=1/ T=3 Diameter- 27nm	Repetitive antigen display Amenable to engineering	*E. coli*	Pre-clinical	Strong humoral responses Highly immunogenic Long lasting antibody and cellular immune responses which are epitope specific	[115] [118-124]
Layer by layer biofilm	7.8 layer biofilm	Multiple epitope display	N/A	Pre-clinical	Cross presentation of CD8 + T cells More efficient presentation of CD4 T cells Potent T cell and antibody response No production of cytokines No need for adjuvant	[127-129]
ß-sheet forming fibres	Fibrous ß-sheet	Natural adjuvants Multiple epitope display	*E. coli*	Pre-clinical	Long lived antibody responses No need for frequent boosters Antibody responses last for at least 40 weeks in a mouse model	[125-126]

Table 1-3. A summary of synthetic scaffolds used in vaccine design. (Unpublished, Smruti Rashmi- modifications have been made to the tables based on updated information)

1.6 Assemblies Generated by Computational Design

With recent advances in computational design, King et al defined a method for creating high order symmetrical structures involving computational docking and protein interface design stages [130]. A natural building block was used that had a matching symmetry to that predicted for the overall structure. Two assemblies were produced, one octahedral (using 8 trimers) and one tetrahedral (using 4 trimers) which were both stable and had diameters of 14.6nm and

11nm respectively. The crystal structures were determined of both assemblies and in comparison to the computation predictions they have root mean square deviation (RMSD) values between 0.62Å-1.07Å. There is the potential to build on this by moving to designing novel building blocks and creating larger, more complex, structures [130] .

Later in the same year another tetrahedral structure was manufactured that was made from 12 identical large molecules. The diameter was as predicted, 16nm, and the crystal structure is available of the assembly produced [131]. However, unlike previously, atomic level accuracy was not achieved and on average the structure deviated from the model by a RMSD value of 8Å [131]. This group did successfully gain atomic level accuracy of 1.2Å of an octahedral cube structure two years later which was made up of 24 monomers and was 22.5nm in diameter, Figure 4 [132]. Not only was this the largest synthetically designed structure to date it also had the largest pore at 10nm, making it unique.

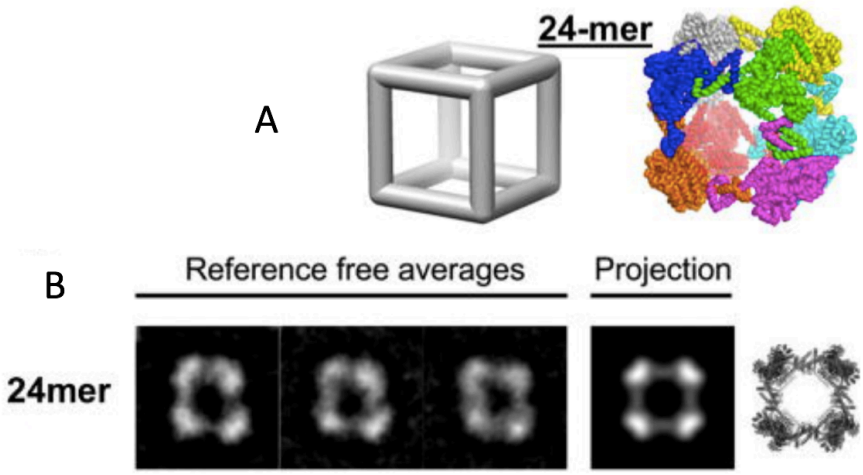

Figure 1-4. A novel octahedral cube. (A) Hypothetical model of the cube, the intended computational design. (B) 2D class averages obtained following aligning and averaging similar particle images. (modified from Lai, Y.T. et al, 2014)

1.7 The I3-01 Assembly

It is important to understand that if a protein assembles but has a fundamental characteristic missing, for example its solubility, this could be amended and the assembly re-designed to meet these specificities required for the designed function. An example of this is a tetrahedral scaffold that was manufactured from four trimers that was very insoluble [133]. Mutations to the protein interface enabled the driving force behind the assembly to be unaffected and the solubility of the complex to be improved, an important advance to note [134]. In 2016 a structure with dodecahedral symmetry, I3-01, was produced with the largest internal volume of any protein assembly designed to date [134]. I3-01 is comprised of 20 trimers of the thermostable enzyme 4-hydroxy-2-oxoglutarate aldolase isolated from *Thermotoga maritima.* These assemblies have been generated through the introduction of novel symmetry axes to folded domains of known structure, by specifically optimising a dimer interface using computational-driven mutagenesis. This produces particles with icosahedral point group symmetry containing two-, three- and five-fold axes of rotation. An initial analysis of the size and stability of the particle was performed by the designers. Cryoelectron microscopy confirmed the structure matched the designed model with 0.92 correlation against an electron density map determined at a resolution of 20Å, Figure 5. In terms of size, the dodecahedra have an internal volume of 3,000nm^3 and a diameter of 25nm, a similar size to a small virus capsid. DLS showed a monodisperse particle population with a hydrodynamic radius of 14nm. The distinctive feature of I3-01, beyond its complex symmetry, is its stability due to its origins from a thermophilic bacterium. Both the trimer and assembly remained intact at 80°C and in 6.7M guanidine hydrochloride, suggesting the protein particles are extremely robust. The ability to withstand genetic fusion was demonstrated by the insertion of green fluorescent protein (GFP) at either terminus, or both termini simultaneously whilst maintaining assembly [134].

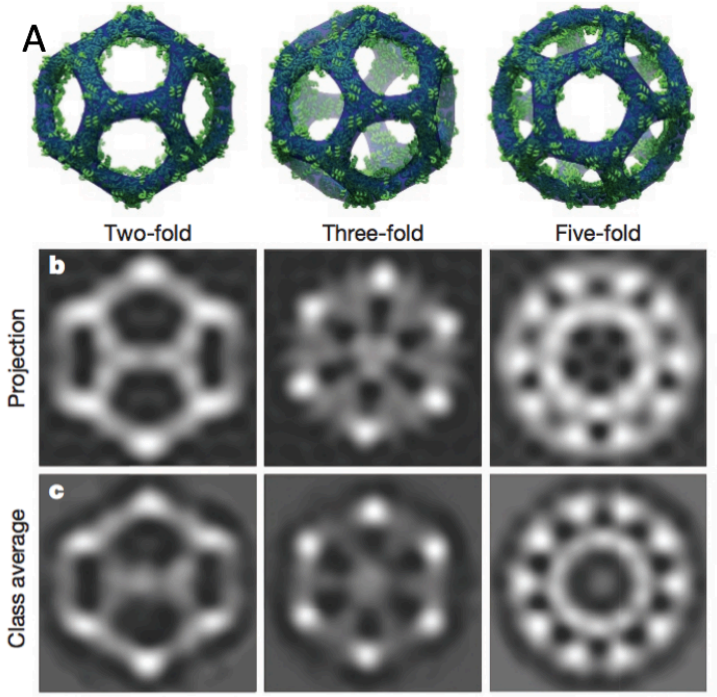

Figure 1-5. The I3-01 Assembly. (A) The calculated unrefined density mapped to the designed model. (B) Back projections of I3-01 from the design model. (C) Cryo-EM class averages match the design projections of the two-fold, three-fold and five-fold axes of symmetry.

Since its design, the I3-01 assembly has been modified to test if it was able to take on virus-like properties by encapsulating a viral genome [135]. This was achieved through the mutation of the interior residues to change the charge of the interior surfaces and to allow the packing of RNA. These assemblies were found to be stable in the blood and have an increase in circulation time *in vivo* in comparison to the empty capsule [135]. A second example of the use of I3-01 is in the form of a Nano reactor to increase the bio catalysis of enzymes such as lactamase. I3-01 was found to protect the enzyme, without affecting its efficiency, whilst increasing its thermostability [136]. The potential to use this assembly as an antigen presentation platform has been explored with a couple of different techniques. Firstly, the assembly was used to present the gp140 HIV-1 antigen using a helper T cell epitope as a linker [137]. This yielded a highly pure population of assembled particles that elicited a strong broadly neutralising antibody binding profile. Displaying the antigen on I3-01 was found to be more effective at

producing a neutralising antibody response in mice and rabbits in comparison to when the antigen is displayed alone [137].

1.8 Methods of Attaching Antigens to Assemblies

A number of methods have been used to attach antigens to a range of assemblies to generate vaccine candidates. The first example is through chemical conjugation either through the use of strong CPG linkers to join the antigen with the nanoparticles following assembly or by utilising azide alykine click chemistry [138] [56]. The latter works by attaching molecules such as granulocyte-macrophage colony-stimulating factor (GM-CSF) to VLPs including bacteriophage Qß [56]. A main drawback to this method is that a homogenous population of particles is unlikely to be formed due to different levels of particle coverage [139]. One way to overcome this problem is to genetically fuse the antigens of interest to the particles before they assemble [140] [141]. This is generally successful with small antigens but there are multiple examples of more complex antigens misfolding upon incorporation with an assembly [142-144]. As maintaining antigen conformation is so crucial this is a clear limitation of this method. More recently there has been the development of Spycatcher technology which has been used as a new technology to decorate VLPs in antigens [67]. This works by relying on the spontaneous isopeptide bond formation between a Spycatcher fused to a VLP and a Spytag fused to an antigen of choice. This was performed using the bacteriophage AP205 VLP and a malaria antigen. A strong antibody response was produced following a single immunisation, suggesting this has provided a successful method for the design of vaccine candidates [67]. This technology has been used in a further malaria vaccine candidate which was found to elicit a robust, functional, antibody response [145] . The method has also been used in the development of anti-cancer vaccine candidates and when the commonly expressed breast cancer protein, HER2, was displayed on the VLP there was inhibited tumour growth in transgenic mice [146].

The Spycatcher technology has also been used with a mutated version of I3-01 which was modified to have improved stability [147]. A malaria antigen was fused to the modified I3-01 in this way and an increased antibody response was observed *In vivo* compared to when the

soluble antigen was administered alone [147]. Finally this same modified I3-01 Spycatcher approach was used in a prime boost vaccine strategy against Middle Eastern Respiratory Syndrome (MERS) [148]. The prime element of the vaccine used a luminase synthase VLP fused to the Spycatcher which was bound to the MERS-COV spike protein. The boost vaccination used the modified I3-01 Spycatcher as the assembly to reduce the anti-scaffold responses produced. Trials in rabbits showed this was a robust strategy with limited anti-scaffold responses being elicited.

This summarizes the assemblies now available for use as vaccine candidates and the types of methods that have been used to fuse antigens to their surfaces. These technologies could be applied to develop vaccines for a whole range of current and emerging diseases.

1.9 Meningitis: The Disease, Symptoms and Transmission

N. meningitidis is the primary causative agent of meningitis and related sepsis complications, colonizing the human upper respiratory tract [149, 150]. This disease is transmitted through respiratory secretions that are spread from infected, not necessarily symptomatic, individuals to uninfected persons [151]. Following exposure to these secretions disease will occur within 14 days, however it is thought around 5-10% of adults carry *N. meningitidis* but are asymptomatic [152, 153]. The number of individuals thought to be carrying the bacterium varies dramatically in different age groups, for example up to 27% of 19 year olds may be infected compared to just 7.8% in 50 year olds[153]. Symptoms of *N. meningitidis* infections also differ greatly with age of the infected patients; common ones in children are vomiting, fever, headaches and photophobia [153]. A stiff neck is a usual symptom in adolescents but occurs sparsely in young children [153]. Meningitis infection can sometimes develop into meningococcal septicaemia and it is reported that this happens in up to 1 in 5 cases [152]. This is a very serious condition in infants as organ failure and ultimately death follows in less than 24 hours, highlighting the speed at which this disease can work at [153]. Symptoms of sepsis include acute fever, haemorrhagic rash, hypotension, leg pain, abnormal skin colour and cold hands and feet [152, 153]. Surviving a symptomatic meningitis infection can often lead to long

term complications, this is especially common following a childhood bout of the disease [153]. These problems include, loss of limbs, hearing or visual impairment and motor or cognitive deficit, emphasizing the seriousness of meningitis [149].

Epidemiology

1.2 million cases of Meningitis are reported each year which lead to 135,000 related deaths [149]. Of the 13 described serogroups of Meningitis, 6 are known to cause disease, A, B, C, W-135, X and Y [153]. The epidemiology of these cases can be discussed in terms of both high risk age groups and geographical locations. The general factors which lead to increased chance of becoming infected with *N. meningitidis* are malnutrition, poverty, poor sanitation, living on school/university campuses and immunodeficiency [152] [153]. The highest incidence age groups are children of less than 12 months old and young adults and in general men are more prone to suffering from the disease but women have a higher mortality rate [149, 152]. A group of 25 countries located in Africa contain the highest rates of meningitis reported which are known collectively as the Meningitis belt [149]. The majority of these cases are caused by the serogroup A, but an affordable MenA vaccine has helped to restrict the number of cases in this area [149]. In Europe, serogroup A is less of a problem and it is serogroup B which causes the majority of cases followed by serogroups C and to a lesser extent serogroup Y [149]. In the Americas, Uruguay was the only country with concerning disease levels of serogroup B, however introduction of the outer membrane vesicle (OMV) MenB vaccine has reduced the number of cases found here. Serogroup Y outbreaks seem to be restricted to Canada and the USA whereas sporadic worldwide outbreaks of serogroup W-135 have been reported, Figure 6 [154] .

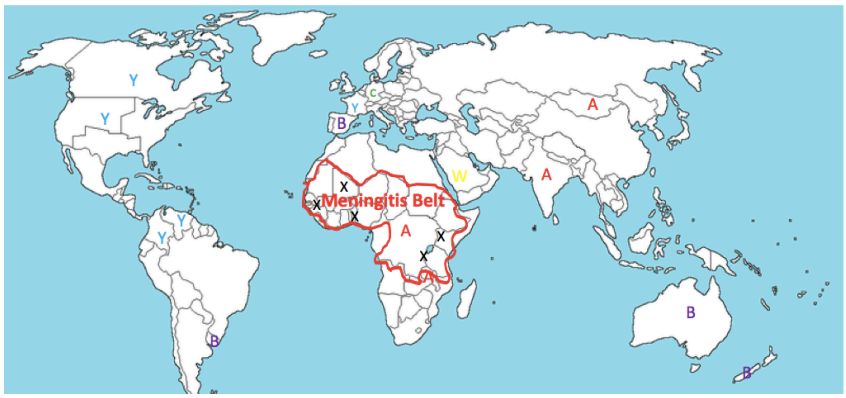

Figure 1-6. The epidemiology of the meningitis subgroups. Most countries have a main serotype dominating, however Europe has three serotypes circulating and the amount each one counts towards total disease is reflected in the size of the letter represented on the map. (modified from Jafri, R.Z. et al, 2013).

1.9.1 Neisseria meningitidis

N. meningitidis is a Gram negative, aerobic, β-class proteobacterium [152, 155]. Key features of these bacteria are that they have an average diameter between 0.6 and 1µm, are diplococcus in shape and may be capsulated or not capsulated [152, 155]. *N. meningitidis* cannot survive on non-living surfaces and have been grown in the laboratory on media such as tryptic soy agar and blood agar, requiring between 3-10% CO_2 and 35-37^{0}C to grow [152, 155]. In terms of metabolism, this microbe relies on a sole carbon source for growth which may be in the form of lactate, glucose or pyruvate as well as a reduced sulphur source, for example thiosulfate [155]. Unlike many bacterial species, antibiotic resistance has not occurred commonly in *N. meningitidis*, although in recent years an increase in cases of penicillin, ciproflaxin, rifampicin and quinolone resistance have been reported [152, 155]. This is surprising as a closely related species, *Neisseria gonorrhoeae*, has been difficult to treat for a long time due to multiple resistance problems [155]. As mentioned above, Meningococcal strains can be divided into serogroups based on their capsular polysaccharide [155]. However further classifications can be made dependent on different structural features, a strain's serosubtype is defined based on

its PorA structure, serotype by its PorB structure or immunotype on its lipooligosaccahride (LOS) structure. More recently, typing has been introduced as a method of classifying strains of meningitis on sequence types which may place strains outside the original 13 serogroups. An example of a common approach to typing is multi-locus sequence typing, which is based on the polymorphisms found within the major house-keeping genes [155].

1.9.2 Neisseria meningitidis Virulence Factors

Genetics

N. meningitidis has a genome which contains around 2000 genes and is between 2 and 2.2 Mbs in length, with 70% of these genes encoding essential proteins such as those with biosynthetic and metabolic functions. The genome of the genus *Neisseria* has as much as 90% homology within the species of *N. gonorrhoeae*, *N. lactamica* and *N. meningitidis* [155].

Capsule

The presence of a capsule surrounding a *N. meningitidis* strain effectively confirms its pathogenicity [156]. Capsules can act as a virulence factors and can evade the immune response in two main ways through; molecular mimicry and capsule switching [154]. Sialic acid is the sugar that makes up the capsule of serogroups B, C, W, and Y, whereas N-acetyl-D-mannosamine-1-phosphate is the main building block of the serogroup A capsule [154, 156]. For the sialic acid based strains, the capsular genes are located on the *cps* locus making serogroups B, C, Y and W genetically similar. Molecular mimicry occurs as sialic acid is found on many host cell surfaces and so the immune system struggles to identify a sialic acid capsulated pathogen as foreign. A specific example is with the serogroup B capsule as the structure of this is identical to a central nervous system polysaccharide involved in neural cell adhesion [154]. Perhaps the most worrying feature of the capsule as a virulence factor is the evidence of capsule switching. It is thought that, as serogroups B, C, W and Y are so genetically similar, horizontal genetic exchange can occur to allow capsule switching during co-infection with strains of these

serogroups [154]. Examples of this have occurred between serogroup B to C in the US and W to C during Hajj in Mecca [156]. This is a huge concern for the effectiveness of vaccines, especially the current serogroup specific

Lipopolysaccharide

The envelope of *N. meningitidis* contains three elements, a cytoplasmic membrane, a peptidoglycan layer and an outer membrane [155]. An outer membrane contains mostly Lipopolysaccharide (LPS), phospholipids such as phophatidylethanolamine [155]. The *N. meningitidis* LPS consists of lipid A, and an oligosaccharide core split into an inner and outer region [154]. This cellular component is responsible for stimulating the host immune response by encouraging the production of pro-inflammatory cytokines [150]. The LPS structures expressed are specifically designed to permit lower adherence but allow greater entry into the bloodstream, which is crucial as a virulence factor [150]. 12 immunotypes of LPS in *N. meningitidis* have been described, the key structures being L3, L7 and L9 [157]. The two main ways the LPS enables evasion from the immune response is through molecular mimicry and antigenic variation [154]. Molecular mimicry occurs in a similar way as in the capsule, a gene, LNnt, which is found exclusively in virulent meningitis strains encodes a protein which acts as a docking site for sialic acid. Depending on the serogroup these sugars can be added either endogenously or exogenously to mimic host cells. Secondly, phase variation of a core biosynthesis enzyme encoding genes provides the antigen variation required to enable evasion of the host immune response by displaying a repertoire of a different LPS structures at the same time [154].

Adhesins

Adhesins are proteins which are produced to enable pathogenic bacteria to specifically bind to host cells [154]. In *N. meningitidis* these factors can be defined as major or minor, the former includes outer membrane proteins (OMP) and pili. The pili are 6nm in diameter and form bundles to aid their role in motility, DNA uptake and can be modified, post translationally, to

influence the host cell interactions to help the bacteria overcome the host immune response. This can be done through glycosylation to promote specific locational immune evasion such as antimicrobial peptide resistance. OMPs, Opa/Opc, are between 27-31kDa in size and form beta barrel structures from 8/10 transmembrane segments. Opa can aid evasion of the immune response through phase variation of the *opa* genes, similarly to the LPS, whereas Opc forms a trimolecular complex which permits human endothelial cell invasion. Finally, NadA is an example of a minor adhesin and was found to be expressed in over 50% of disease isolates, confirming its role as a virulence factor [154].

Metal Acquisition

It is essential pathogenic bacteria contain nutrient acquisition machinery to allow them to survive and multiply in the host. *N. meningitidis* acquires its iron through a transferrin receptor, which consists of two proteins TbpA and TbpB. TbpA is essential for iron uptake whereas TbpB is not, however both proteins have been proven to be essential for *N. meningitidis* to be virulent [158]. Zinc is also a metal essential to the growth and survival of *N. meningitidis* but it is understood levels of available zinc in the respiratory tract, where *N. meningitidis* resides, are low [159]. An uptake system is present as part of the cells' machinery to achieve sufficient levels of intracellular zinc. Asymptomatic carriers have been established to have ZnuD, a component of this uptake system, antibodies. The protein ZnuD is highly conserved across pathogenic *N. meningitidis* strains so may prove a worthwhile vaccine component to consider [159].

Secreted Proteins

The longest known secreted protein from this genus of bacteria is IgA protease, a serine protease [157]. This protein is important in the virulence of this bacterium as it is not present in avirulent *Neisseria* strains. Two known cleavage sites are present for this protease, mucosal IgA1 and lysosome associated membrane protein 1. The combination of cleaving both these sites not only prolongs the extracellular mucosal survival but also the intracellular survival of *Neisseria* species [157]. *N. meningitidis* secretes two iron regulated proteins named FrpA and

FrpC through a type 1 secretion system. The genes encoding these proteins are expressed during infection but are not understood to be essential to the virulence of the bacterium, although they may be a contributing factor. These proteins are homologous to proteases yet do not appear to have this function; why this is the case remains unclear [157].

1.10 History of Meningitis Vaccines

1.10.1 Polysaccharide Vaccines

Vaccines that contain high molecular weight purified meningococcal capsular polysaccharides have been around for 50 years and were first used to target serogroups A and C [160]. There are multiple combinations of the polysaccharide vaccine available such as; bivalent for serogroups A and C, trivalent for serogroups, A, C and W-135 and tetravalent for A, C, W-135 and Y, known as Menomune [156, 160]. All of these vaccines are safe with rare side reactions and are immunogenic exclusively in older children and adults which is a problem as one of the main age groups which suffer from bacterial Meningitis are infants [156, 160]. Limitations such as a short term protection and restricted herd immunity being induced in adult populations were also evident [153, 156]. For these reasons polysaccharide vaccines are not used in global immunisation programmes and are only administered during epidemics or to specific high risk groups [160]. The high risk groups include people without a spleen, with complement deficiency or microbiologists and a repeat dose of this is required every 5 years due to its lack of ability to produce a memory response [152]. An identical approach was attempted with serogroup B. A very poor immune response was provoked and this was later discovered to be due to the fact the capsule of this strain is almost identical to a host neural cell adhesion molecule. This made using this method of design impossible for this serogroup due to this and the risk of autoimmunity [160].

1.10.2 Conjugate Vaccines

In the late 1990s a meningitis vaccine was manufactured which had an improved immunological response in comparison to the polysaccharide based inoculation that had come before [156].

Carriers used in the design of these vaccines included the diphtheria and tetanus toxin; this enabled a safe and effective responses to be produced [153, 160]. The UK was the first country to roll out a national immunisation programme against meningitis using a conjugate vaccine to Serogroup C, targeting the two main risk age groups, 15-17 year olds and infants [160]. This programme had impressive results as infants were protected with the highest incidence and within 2 years there was an 89% reduction of cases of meningitis C in the UK [156, 160]. The second success of this initiative was that herd immunity was created which was not seen previously, the carriage of meningitis C in adolescents in the UK had reduced by 75% following the introduction of the vaccination [151]. Following this, other countries such as Australia and Canada began using conjugate meningitis C vaccines and had similar results [160]. MenAfrivac is a conjugate inoculation against serogroup A which is currently being used to combat the epidemics of this serogroup found in the meningitis belt region of Africa as described above [160]. This vaccine has been used since 2010 and is very cost effective, a single dose is priced at $0.40, making it ideal for use in developing countries where some are simply not affordable [151]. The quadravalent conjugate vaccine gives protection against the same serogroups as the previous polysaccharide injection, and has been licensed in the US since 2005 [160, 161]. It is clear that this approach to vaccine design has much more successfully brought cases of certain serogroups of meningitis under some sort of control. It is important to consider thus far no vaccine against serogroup B has been discussed.

1.10.3 Protein-Based Vaccine Design

In developed countries there is a high incidence of meningitis serogroup B and previous attempts at vaccine design are not applicable to strains derived from this serogroup [153]. In the 1970s whilst researching the potential of outer membrane proteins (OMPs) in vaccine strategy it was revealed outer membrane vesicles (OMVs) are released during *N. meningitidis* growth [160]. These vesicles were shown to be able to display proteins to stimulate a strong immune response. Trials of serogroup B OMV vaccines took place during an epidemic of disease in areas such as Cuba, Brazil and Norway during the late 1970s and 1980s. However, protection rates, specifically in children under the age of 2, were found to be disappointingly low. More

recently an epidemic in New Zealand was brought under control using a OMV vaccine- it was established to be 80% effective in children aged between 6 months and 5 years following a 4 dose course. Disappointingly, this was limited to use against this strain of serogroup B due to the specificity of antibodies against PorA; worldwide vaccine would need to be polyvalent [156, 160]. Firstly, a nonavalent vaccine was designed with 9 PorA variants to try to capture as many strains as possible which was discovered to be immunogenic against 80% of disease across Europe when tested in mice [160]. In 2013 the first multicomponent vaccine, Bexsero, was licensed for use in Europe in infants over 2 years of age. This included the antigens; Neisseria adhesin A (NadA), Neisseria heparin-binding antigen (NHBA) and Factor H binding protein (Fhbp) [153, 162]. Fhbp is known to inhibit factor H in complement killing and this vaccine generates bactericidal antibodies across all age groups [160]. Antigens such as Fhbp were selected for use in these vaccines through a process known as reverse vaccinology, a method of screening the meningitis genome [160]. It is calculated that in Europe this protects against 66-68% of strains circulating and is licensed in Europe, Canada, and Australia for 10-25 year olds as a 2 dose course [151, 153]. The most recent vaccine is a combination of an OMV serogroup B licensed inoculation with the current conjugate polysaccharide quadravlent ACYW combination to produce a MenABCWY vaccine. It is hoped this will be approved for use in the next 12 months [153]. A summary of vaccines used to prevent Meningitis currently are summarised in Table 2.

1.10.4 VLPs in Meningitis Vaccine Design

More recently, the method of using VLPs as antigen scaffolds has been used to research a potential vaccine for serogroup B meningitis [163]. The commonly used HBc VLP was engineered to incorporate antigen domains derived from Fhbp and NadA, two components of the Bexsero vaccine. Three constructs were designed each containing either, the extracellular domain of NadA at the major immune dominant region (MIR), the C-terminal of Fhbp at the C-terminus or finally a construct containing both antigens. All the constructs were found to be assembled correctly and immunisations in mice showed that reactive IgG1, IgG2a and IgG2b antibodies were produced against the antigens. However, only the VLP containing the NadA

insert was found to elicit antibodies with serum bactericidal activity. This suggests that the 3D conformation of the Fhbp was altered when it was inserted into the VLP. Future work must ensure the correct conformation of an antigen is displayed to get a protective immune response when using this type of vaccine design technology [163].

1.11 Challenges in meningococcal vaccine development

The clear necessity is to broaden the coverage of the current serogroup B vaccines, to provoke a strong, long lasting immune response [160]. There is also no current inoculation against *N. meningitidis* serogroup X, which is causing the disease across the Meningitis belt in Africa, the most likely candidate would be a conjugate polysaccharide vaccine [164]. An ideal vaccine contender would provide immunity against all the main strains of bacterial meningitis [153]. The problem comes in doing this, using novel approaches and latest technologies but in an affordable way so that it can reach developing countries [151, 156].

Name	Type	Strain	License	Location	When used	Advantages	Disadvantages	Ref
Menomune	Poly-saccharide: Bi/tri/tetra valent	A C W-135 Y	1970s	Worldwide	During epidemics To high risk groups Travel	Safe Rare Side effects	Poor immunogenicity in infants No herd immunity	[152] [153] [157] [161]
MenAfrivac	Conjugate	A	2010	Africa India	Mass vaccination programmes	Persistent response Safe Cheap	Unsure if herd immunity was induced	[161] [151]
MenC	Conjugate	C	1999	UK Europe Australia Canada	Infant and adolescent vaccination programmes	Induced herd immunity	Requires a booster	[151] [157] [161]
Menveo	Conjugate	A C W-135 Y	2010	Worldwide	European vaccination programmes	Safe Induces herd immunity		[161] [162]

Bexosero	OMV	B	2013	Europe	Vaccination programme in infants 2+ years of age	Co-administration doesn't affect immunogeni-city	Some systematic side effects when co-administered	[151] [153] [157] [161] [163]

Table 1-4. A summary of current meningitis vaccines.

1.12 Aims and Objectives

The overall aim of this project is to examine the potential of the dodecahedral self-assembly I3-01 to act as a scaffold for vaccine antigen presentation, using meningococcal vaccine development as an example. It has been shown that displaying meningococcal antigens on VLPs leads to a robust immune response through the production of antibodies with serum bactericidal activity [163]. I3-01 is an extremely stable platform and this work looks to compare the I3-01 platform with the HBc VLP, in terms of its ability to incorporate antigens and the responses produced [134].

The objectives set to achieve this aim are:

- To purify assembled I3-01 in ClearColi^{TM}, an endotoxin free cell line and to fully characterise the I3-01 structure [165]. This will be done using Cryo-EM to verify that the structure closely matches the designed model, in higher resolution than previously [134]. The thermal stability and homogeneity of the population of particles will also be tested, providing a point for comparison with any fusion constructs.

- To design and purify meningococcal antigen fusions with I3-01 and to analyse their assembly and properties in comparison to the I3-01 assembly.

- To design, produce and characterise an assembled construct with Protein A and show it binds antibody, offering a novel fusion technology. Protein A is a small stable protein that should be incorporated into the assembly successfully. As it binds antibodies

readily, it will provide a covalent attachment point for any Fc-fusion antigen of choice-post assembly.

- Compare the ability of the I3-01-PA fusion and the HBc-PA VLP fusion to present antigen to human macrophages derived from a THP-1 cell line, using a fluorescently labelled Fc fusion model antigen, Fc-OVA. The ability to boost the level of uptake over a certain time period using antibody targeting to the macrophages will also be tested. This will indicate that it is possible to target antigens to specific receptors on APCs

- Investigate antigen presentation in mouse bone marrow derived dendritic cells. A comparison of the responses will be analysed depending on whether the Fc-OVA antigen is presented alone, with the HBc VLP or I3-01 platform. The responses evaluated will include the level of antigen uptake, the activation of the dendritic cells in terms of expression of activation markers and the production of cytokines. The level of T cell proliferation stimulated and cytokine profiles produced will also be evaluated to test if the method of presentation skews the T cell response. This will allow an evaluation into how the initial antigen presentation to APCs can affect the adaptive immune response.

Chapter 2

Materials and Methods

Chapter 2 - Material and Methods

2.1 Materials

2.1.1 Bacterial Strains

Strain	Genotype	Source
XL1-Blue Supercompetent	recA1 endA1 gyrA96 thi-1 hsdR17 supE44 relA1 lac [F´ proAB $lacI^qZ\Delta M15$ Tn10 (Tet^r)]	Stratagene
XL10-Gold® Ultracompetent	Tet^rD(mcrA)183 D(mcrCB-hsdSMR-mrr)173 endA1 supE44 thi-1 recA1 gyrA96 relA1 lac Hte [F´ proAB $lacI^qZ\Delta M15$ Tn10 (Tet^r) Amy Cam^r]	Stratagene
T7 Express	fhuA2 lacZ::T7 gene1 [lon] ompT gal sulA11 R(mcr-73::miniTn10--Tet^S)2 [dcm] R(zgb-210::Tn10--Tet^S) endA1 Δ(mcrC-mrr)114::IS10	New England Biolabs
ClearColi^{TM} BL21 (DE3) Electrocompetent Cells	F^- ompT hsdSB ($r_B^-m_b^-$) gal dcm lon ʎ (DE3 [lacl lacUV5-T7 gene 1 ind1 sam7 nin5]) msbA148 ΔgutQ ΔkdsD ΔlpxL ΔlpxM ΔpagP ΔlpxP ΔeptA	Lucigen
Human Embryonic Kidney (HEK)-Blue™-4 Cells	Engineered HEK293 endotoxin sensor cells. These cells stably express TLR4 and also co-express an NF-κB-inducible secreted embryonic alkaline phosphatase reporter gene.	Invivogen
Lemo21 (DE3) Competent *E. coli*	fhuA2 [lon] ompT gal (λ DE3) [dcm] ΔhsdS/ pLemo(CamR) λ DE3 = λ sBamHIo ΔEcoRI-B int::(lacI::PlacUV5::T7 gene1) i21 Δnin5 pLemo = pACYC184-PrhaBAD-lysY	New England Biolabs

Table 2-1. A summary of the bacterial strains used.

2.1.2 Cell Lines

Cell Line	Additional Information
THP-1	Human acute monocytic leukemia cell line [166]

Table 2-2. The cell lines used.

2.1.3 Primary Cells

Mouse Strain	Use of Cells
C57BL/6	Bone marrow derived dendritic cell (BMDC) culture
Transgenic OT-11 x Recombinant Activating Gene $(RAG)^{-}/^{-}$	OT11 Spleenocytes

Table 2-3. A summary of the primary cells used.

WT C57BL/6 and Transgenic OT-11 x RAG$^{-/-}$ mice were maintained under pathogen-free conditions in the Biological Unit Services Unit at the University of Manchester. They were used at 6-12 weeks old and all procedures were performed in accordance with the Home Office Scientific Procedures Act (1986) and under the Department for Environment, Food and Rural Affairs (DERFA) license.

2.1.4 Constructs

Key: His-tag Linkers Insertions/modifications

Protein	Protein Sequence
I3-01 Molecular Weight (MW) = 23.8kDa (Dalton) 224 residues Extinction co-efficient (e)= 7240 Isoelectric point (PI)= 8.29	HHHHHHGGSGGSGGSGGSMK^{1}MEELFKKHKIVAVLRANSVEEAKKKALAVFLGGVHLIEITFTVPDADTVIKELSFLKEMGAIIGAGTVTSVEQCRKAVESGAEFIVSPHLDEEISQFCKEKGVFYMPGVMTPTELVKAMKLGHTILKLFPGEVVGPQFVKAMKGPFPNVKFVPTGGVNLDNVCEWFKAGVLAVGVGSALVKGTPVEVAEKAKAFVEKIRGCTE^{201}
I3-01-T40S MW= 23.8kDa 224 residues E= 7240 PI= 8.29	MHHHHHHGGSGGSGGSGGMK^{1}MEELFKKHKIVAVLRANSVEEAKKKALAVFLGGVHLIEI^{40}SFTVPDADTVIKELSFLKEMGAIIGAGTVTSVEQCRKAVESGAEFIVSPHLDEEISQFCKEKGVFYMPGVMTPTELVKAMKLGHTILKLFPGEVVGPQFVKAMKGPFPNVKFVPTGGVNLDNVCEWFKAGVLAVGVGSALVKGTPVEVAEKAKAFVEKIRGCT E^{201}
I3-01-OVA1 MW= 27.4kDa 795 residues E= 7240 PI= 7.21	MMHHHHHHGGSGGSGGSGGSMK^{1}MEELFKKHKIVAVLRANSVEEAKKKALAVFLGGVHLIEITFTVPDADTVIKELSFLKEMGAIIGAGTVTSVEQCRKAVESGAEFIVSPHLDEEISQFCKEKGVFYMPGVMTPTELVKAMKLGHTILKLFPGEVVGPQFVKAMKGPFP^{147}GGGGSGGGGSSLKISQAVHAAHAEINEAGREVEFGGGSGGGGNKVPTGGVNLDNVCEWFKAGVLAVGVGSALVKGTPVEVAEKAKAFVEKIRGCTE^{243}
I3-01-OVA11 MW= 26.7kDa 768 residues E= 7240 PI= 6.8	MMHHHHHHGGSGGSGGSGGSMK^{1}MEELFKKHKIVAVLRANSVEEAKKKALAVFLGGVHLIEITFTVPDADTVIKELSFLKEMGIIGAGTVTSVEQCRKAVESGAEFIVSPHLDEEISQFCKEKGVFYMPGVMTPTELVKAMKLGHTILKLFPGEVVGPQFVKAMKGPFP^{147}GGGGSGGGGSQLESIINFEKLTEEFGGGGSGGGGNVKFVPTGGVNLDNVCEWFKAGVAVGVGS LVKGTPVEVAEKAKAFVEKIRGCTE^{235}
I3-01-CP-G60 MW= 25.1kDa 239 residues E= 7240 PI= 7.74	MMHHHHHHGGSGGSGGSGGS^{1}MAIIGAGTVTSVEQCRKAVESGAEFIVSPHLDEEISQFCKEKGVFYMPGVMTPTELVKAMKLGHTILKLFPGEVVGPQFVKAMKGPFPNVKFVPTGGVNLDNVCEWFKAGVLAVGVGSALVKGTPVEVAEKAKAFVEKIRGCTEGGSGGSGGSGGSGGSMKMEELFKKHKIVAVLRANSVEEAKKKALAVFLGGVHLIEITFTVPDADTVIKELSFLKEMLE^{213}
I3-01-CP-N148 MW= 24.6kDa 235 residues E= 7240 PI= 8.29	MMHHHHHHGGSGGSGGSGGS^{1}MVKFVPTGGVNLDNVCEWFKAGVLAVGVGSALVKGTPVEVAEKAKAFVEKIRGCTEGGSGGSGGSGGSGGSMKMEELFKKHKIVAVLRANSVEEAKKKALAVFLGGVHLIEITFTVPDADTVIKELSLKEMGAIIGAGTVTSVEQCRKAVESGAEFIVSPHLDEEISQFCKEKGVFYMPGVMTPTELVKAMKLGHTILKLFPGEVVGPQFVKAMKGPF^{215}

I3-01-PA MW= 31kDa 287 residues E= 8730 PI=7.18	MMHHHHHHGGSGGSGGSGGS MK[1]MEELFKKHKIVAVLRANSVEEAKKKALAVFLGG VHLIEITFTVPDADTVIKELSFLKEMGAIIGAGTVTSVEQCRKAVESGAEFIVSPHLDEEIS QFCKEKGVFYMPGVMTPTELVKAMKLGHTILKLFPGEVVGPQFVKAMKGPFPNVKFV PTGGVNLDNVCEWFKAGVLAVGVGSALVKGTPVEVAEKAKAFVEKIRGCT[201]EGGSM ADNKFNKEQQNAFYEILHLPNLTEEQRNGFIQSLKDDPSVSKEILAEAKKLNDAQAP[263] K
NadA MW= 17kDa 163 residues E= 2980 PI=4.73	MHHHHHHGGSGGSGGSGGS[1]MATSDDDVKKAATVAIVAAYNNGQEINGFKAGETIY DIGEDGTITQKDATAADVEADDFKGLGLKKVVTNLTKTVNENKQNVDAKVKAAESEIE KLTTKLADTDAALADTDAALDETTNALNKLGENITTFAEETKTNIVKID[144]E
I3-01- CP-NHBA MW= 38.5kDa 372 residues E= 20190 PI= 7.22	MMMHHHHHHGGSGGSGGSGGS[1]MVKFVPTGGVNLDNVCEWFKAGVLAVGVGSA LVKGTPVEVAEKAKAFVEKIRGCTEGGSGGSGGSGGSMKMEELFKKHKIVAVLRANSV EEAKKKALAVFLGGVHLIEITFTVPDADTVIKELSFLKEMGAIIGAGTVTSVEQCRKAVES GAEFIVSPHLDEEISQFCKEKGVFYMPGVMTPTELVKAMKLGHTILKLFPGEVVGPQFV KAMKGPFPGSMGGGGSGGGGSGGGGSMLAGAAVYNGEVLHFHTENGRPYPTRGRF AAKVDFGSKSVDGIIDSGDDLHMGTQKFKAAIDGNGFKGTWTENGSGDVSGKFYGPA GEEVAGKYSYRPTDAEKGGFGVFAGKKEQ[351]D
Ovalbumin MW= 42.9kDa 386 residues E= 21775 PI= 5.19	[1]MGSIGAASMEFCFDVFKELKVHHANENIFYCPIAIMSALAMVYLGAKDSTRTQINKVV RFDKLPGFGDSIEAQCGTSVNVHSSLRDILNQITKPNDVYSFSLASRLYAEERYPILPEYLQ CVKELYRGGLEPINFQTAADQARELINSWVESQTNGIIRNVLQPSSVDSQTAMVLVNAI VFKGLWEKAFKDEDTQAMPFRVTEQESKPVQMMYQIGLFRVASMASEMKILELPFAS GTMSMLVLLPDEVSGLEQLESIINFEKLTEWTSSNVMEERKIKVYLPRMKMEEKYNLTS VLMAMGITDVFSSSANLSGISSAESLKISQAVHAAHAEINEAGREVVGSAEAGVDAASVS EEFRADHPFLFCIKHIATNAVLFFGRCS[386]P
NadA-I3-01 MW= 54.2kDa 514 residues E= 11710 PI= 5.26	HMMHHHHHHGGSGGSGGSGGS[1]MATSDDDVKKAATVAIVAAYNNGQEINGFKAG ETIYDIGEDGTITQKDATAADVEADDFKGLGLKKVVTNLTKTVNENKQNVDAKVKAAE SEIEKLTTKLADTDAALADTDAALDETTNALNKLGENITTFAEETKTNIVKIDEKLEAVAD TVDKHAEAFNDIADSLDETNTKADEAVKTANEAKQTAEETKQNVDAKVKAAETAAGK AEAAAGTANTAADKAEAVAAKVTDIKADIATNKADIAKNSARIDSLDKNVANLRKETR QGLAEQAALSGLFQPYNVGGGSMEELFKKHKIVAVLRANSVEEAKKKALAVFLGGVHLI EITFTVPDADTVIKELSFLKEMGAIIGAGTVTSVEQCRKAVESGAEFIVSPHLDEEISQFCK EKGVFYMPGVMTPTELVKAMKLGHTILKLFPGEVVGPQFVKAMKGPFPNVKFVPTGG VNLDNVCEWFKAGVLAVGVGSALVKGTPVEVAEKAKAFVEKIRGCT[491]E
I3-01- NadA MW= 53.8kDa 511 residues E= 11710 PI= 5.23	MHHHHHHGGSGGSGGSGGSMK[1]MEELFKKHKIVAVLRANSVEEAKKKALAVFLGGVH LIEITFTVPDADTVIKELSFLKEMGAIIGAGTVTSVEQCRKAVESGAEFIVSPHLDEEISQFC KEKGVFYMPGVMTPTELVKAMKLGHTILKLFPGEVVGPQFVKAMKGPFPNVKFVPTG GVNLDNVCEWFKAGVLAVGVGSALVKGTPVEVAEKAKAFVEKIRGCT[201]EGGSMATS DDDVKKAATVAIVAAYNNGQEINGFKAGETIYDIGEDGTITQKDATAADVEADDFKGL GLKKVVTNLTKTVNENKQNVDAKVKAAESEIEKLTTKLADTDAALADTDAALDETTNAL NKLGENITTFAEETKTNIVKIDEKLEAVADTVDKHAEAFNDIADSLDETNTKADEAVKTA NEAKQTAEETKQNVDAKVKAAETAAGKAEAAAGTANTAADKAEAVAAKVTDIKADIA TNKADIAKNSARIDSLDKNVANLRKETRQGLAEQAALSGLFQPYNV[494]G
NadA-I3-01-CP MW= 40.8kDa 394 residues E= 10220 PI=5.58	MHHHHHHGGSGGSGGSGGS[1]MATSDDDVKKAATVAIVAAYNNGQEINGFKAGETIY DIGEDGTITQKDATAADVEADDFKGLGLKKVVTNLTKTVNENKQNVDAKVKAAESEIE KLTTKLADTDAALADTDAALDETTNALNKLGENITTFAEETKTNIVKIDEKGGGGSGGG GSGGGGSMVKFVPTGGVNLDNVCEWFKAGVLAVGVGSALVKGTPVEVAEKAKAFVE KIRGCTEGGSGGSGGSGGSGGSMKMEELFKKHKIVAVLRANSVEEAKKKALAVFLGGVHLIE ITFTVPDADTVIKELSLKEMGAIIGAGTVTSVEQCRKAVESGAEFIVSPHLDEEISQFCKEK GVFYMPGVMTPTELVKAMKLGHTILKLFPGEVVGPQFVKAMKGP[375]F
Mouse IgG Fc MW= 24.8kDa 218 residues E=32680 PI=6.19	[1]MPAPNLLGGPSVFIFPPKIKDVLMISLSPIVTCVVVDVSEDDPDVQISWFVNNVEVHT AQTQTHREDYNSTLRVVSALPIQHQDWMSGKEFKCKVNNKDLPAPIERTISKPKGSVR APQVYVLPPPEEEMTKKQVTLTCMVTDFMPEDIYVEWTNNGKTELNYKNTEPVLDSD GSYFMYSKLRVEKKNWVERNSYSCSVVHEGLHNHHTTKSFSRTPG[220]K

Fc- OVA MW= 68kDa 611 residues E= 64455 PI=5.52	GSIGAAS[1]MEFCFDVFKELKVHHANENIFYCPIAIMSALAMVYLGAKDSTRTQINKVVRF DKLPGFGDSIEAQCGTSVNVHSSLRDILNQITKPNDVYSFSLASRLYAEERYPILPEYLQC VKELYRGGLEPINFQTAADQARELINSWVESQTNGIIRNVLQPSSVDSQTAMVLVNAIV FKGLWEKAFKDEDTQAMPFRVTEQESKPVQMMYQIGLFRVASMASEKMKILELPFAS GTMSMLVLLPDEVSGLEQLESIINFEKLTEWTSSNVMEERKIKVYLPRMKMEEKYNLTS VLMAMGITDVFSSSANLSGISSAESLKISQAVHAAHAEINEAGREVVGSAEAGVDAASV SEEFRADHPFLFCIKHIATNAVLFFGRCVSPGGSGGGSGPAPNLLGGPSVFIFPPKIKDVL MISLSPIVTCVVVDVSEDDPDVQISWFVNNVEVHTAQTQTHREDYNSTLRVVSALPIQ HQDWMSGKEFKCKVNNKDLPAPIERTISKPKGSVRAPQVYVLPPPEEEMTKKQVTLTC MVTDFMPEDIYVEWTNNGKTELNYKNTEPVLDSDGSYFMYSKLRVEKKNWVERNSYS CSVVHEGLHNHHTTKSFSRTPG[604]K
HBc WT MW= 20kDa 190 residues E= 35075 PI=5.13	[1]MDIDPYKEFGATVELLSFLPSDFFPSVRDLLDTASALYREALESPEHCSPHHTALRQAILC WGELMTLATWVGNNLEDGGGGSGGGGSPAEFGGGGSGGGGSRDLVVNYVNTNM GLKIRQLLWFHISCLTFGRETVLEYLVSFGVWIRTPPAYRPPNAPILSTLPETTVVGSGGG TGKLGGGWSHPQFE[190]K
HBc-PA MW= 36kDa 340 residues E= 39545 PI=5.16	M[1]MDIDPYKEFGATVELLSFLPSDFFPSVRDLLDTASALYREALESPEHCSPHHTALRQAI LCWGELMTLATWVGNNLEDGGGGSGGGGSGGGGSGGGGSMADNKFNKEQQNAF YEILHLPNLTEEQRNGFIQSLKDDPSVSKEILAEAKKLNDAQAPKGGGSGGGGSHMKFN KEQQNAFYEILHLPNLNEEQRNAFIQSLKDDPSQSANLLAEAKKLNEQQAAFYEILSLGG GGSGGGGSEFGGGGSGGGGSRDLVVNYVNTNMGLKIRQLLWFHISCLTFGRETVLEY LVSFGVWIRTPPAYRPPNAPILSTLPETTVVGSGGGTGKLGGGWSHPQFE[339]K

Table 2-4. A summary of protein constructs used.

2.1.5 Vectors

The vector used was pET-29a from Novagen®.

2.1.6 Primers

The following table details the primers used. All of the sequences were ordered as unmodified deoxyribose nucleic acid (DNA) oligos from Eurofins Genomics. These were then solubilised in Milli-Q water to a concentration of 100μM.

Primer	Sequence	Annealing Temperature
T40S Forward	GTTCATCTGATTGAAATCTCCTTTACCGTTCCGGATG	69.5°C
T40S Reverse	CATCCGGAACGGTAAAGGAGATTTCAATCAGATGAAC	69.5°C

Table 2-5. Table 2.5 The primers used.

2.1.7 Restriction Enzymes

The restriction enzymes have 100% activity in CutSmart® buffer at 37°C.

Restriction Enzyme	Description	Source
BamHI-HF®	Recognition site: G/GATCC Inactivation temperature; NO	New England Biolabs
NdeI	Recognition site: CA/TATG Inactivation temperature; 65°C	New England Biolabs
XhoI	Recognition site: C/TCGAG Inactivation temperature; 65°C	New England Biolabs

Table 2-6. The restriction enzymes used

.

2.1.8 Chemical Product and Supply List

Chemical/Reagent	Supplier	Chemical/ Reagent	Supplier
5x Loading Buffer	Bioline	Live Dead eFlour450 Macrophage Stain	Invitrogen
Acetic Acid	Fisher Chemicals	Lipopolysacchardide (LPS) from *E. coli* O111:B4	Sigma Aldrich
Accutase	Invitrogen	Luria Broth (LB) Agar	Merck
Agar	Sigma Aldrich	LB Media	Sigma Aldrich
Agarose	Lonza	Na_2HPO_4	Fisher Chemicals
Ampicillin (Sodium Salt)	Sigma Aldrich	NaCl	Fisher Chemicals
2- mercaptoethanol	Sigma Aldrich	NaOH	Fisher Chemicals
BamHI	New England Biolabs	NdeI	New England Biolabs
BD Pharm Lyse™	BD Biosciences	Ni-NTA- Nanogold ® 5nm	Nanoprobes
Betaine	Sigma Aldrich	$NiSO_4$	Sigma
Biotin	Sigma Aldrich	Normal Mouse Serum (NMS)	Sigma
Bovine Serum Albumin (BSA)	Sigma Aldrich	NuPAGE ® Sodium Dodecyl Sulphate (SDS) Running Buffer	Life Technologies
Bradford Reagent (5x concentrate)	Sigma Aldrich	NuPAGE bis-tris pre-cast	Life Technologies
Bromophenol Blue	Sigma Aldrich	OneComp eBeads™ Compensation Beads	Thermofisher
Carbon Film on Copper 400 Mesh Electron Microscopy Grids	EM Resolutions	Orange G	Sigma Aldrich
CellMask™ Deep Red Plasma Membrane Stain	Thermofisher	Ovalbumin protein (EndoFit)	Invivogen

Chemical/Reagent	Supplier	Chemical/ Reagent	Supplier
Carboxyfluorescein Succinimidyl Ester (CFSE)	Thermofisher	Penicillin/Streptomycin (Pen/strep)	Sigma Aldrich
CD4 (cluster of differentiation) (L3T4) MicroBeads, Mouse	Miltenyl Biotec	Paraformaldehyde (PFA)	Sigma Aldrich
Chloramphenicol	Sigma Aldrich	Phorbol 12- Myristat 13-Acetate (PMA)	Sigma Aldrich
cOmplete™ Protease Inhibitor Cocktail Tablets	Roche	Phusion ® High Fidelity DNA Polymerase	New England Biolabs
CutSmart® Buffer	New England Biolabs	Precision Plus Protein Standard Dual Colour	Bio-Rad
DNA Hyperladder	Bioline	Precision Plus Protein Standard Unstained	Bio-Rad
DNAse	Sigma Aldrich	Proteinase K	Thermofisher
Deoxyribonucleotide Triphosphate (dNTPs)	Bioline	QIAprep Gel Extraction Kit	QIAgen
DpnI	New England Biolabs	QIAprep Spin Miniprep Kit	QIAgen
Ebio Permeability Buffer	Thermofisher Scientific	QIAquick Polymerase Chain Reaction (PCR) Purification Kit	QIAgen
Ethylenediaminetetraacetic acid (EDTA)	Fisher Chemical	Quantifoil R1.2/1.3 400 Mesh Gold Cryo-Electron Microscopy Grids	EM Resolutions
Endotrap ® HD- High Definition Endotoxin Removal Column	Hyglos	Rapid Ligation Kit	Roche
Fetal Bovine Serum (FBS) Heat Inactivated	Sigma Aldrich	Recombinant Human Granulocyte-Macrophage Colony-Stimulating Factor (GM-CSF)	Abcam
Fragment crystallisable (Fc) Block (Purified anti-mouse CD16/32)	Biolegend	Roswell Park Memorial Institute (RPMI) 1640 Media	Sigma Aldrich
Foxp3 Transcription Factor Fixation/Permeabilization buffer	Thermofisher Scientific	SIGMAFAST™ 3,3'-Diaminobenzidine Tablets	Sigma Aldrich
GenePulser 0.1cm Electroporation Cuvettes	Bio-Rad	Sodium Azide	VWR Chemicals
Glycerol	Fisher Chemicals	SDS	Fisher Chemicals
Glycine	Fisher Chemicals	Stericup- GP 0.22µm Polyethersulfone 500ml	Millipore
H_2SO_4	Fisher Chemicals	Streptavidin-horseradish peroxidase (Strep-HRP)	R & D Systems

Chemical/Reagent	Supplier	Chemical/ Reagent	Supplier
H_2SO_4	Fisher Chemicals	Streptavidin-horseradish peroxidase (Strep-HRP)	R & D Systems
Hanks' Balanced Salt Solution	Sigma Aldrich	Streptrap HP 5ml	GE Healthcare
HCl	Fisher Chemicals	Super Ni-NTA Agarose Resin	Generon
HEK-Blue™-4 Cells	Invivogen	Superose 6 10/300 GL Column	GE Healthcare
HEK-Blue™-4 Cell Growth Medium	Invivogen	SYPRO Orange	Sigma Aldrich
HEK-Blue™-4 Cell Detection Medium	Invivogen	Taq DNA Polymerase	New England Biolabs
4-(2-hydroxyethyl)-1-piperazineethanesulfonic acid (HEPES)	Sigma	Taq Reaction Buffer (10x)	New England Biolabs
HiLoad Superdex 200 pg 120ml Column	GE Healthcare	3,3',5,5'-Tetramethylbenzidine (TMB) High sensitivity	ThermoFisher
HisTrap HP 5ml Column	GE Healthcare	Tris-base	Fisher Chemicals
HiTrap Streptavidin HP 5ml Column	GE Healthcare	Tryphan Blue	Sigma Aldrich
Human Serum immunoglobulin G (IgG)	Sigma Aldrich	Tween-20	Sigma Aldrich
IgG Sepharose 6 Fast Flow Affinity resin	GE Healthcare	Uranyl Acetate (UA)	Agar Scientific
Imidazole	Sigma Aldrich	Ultracomp eBeads	Invitrogen
Instant Blue Protein Stain	Expedeon	VivaSpin 20 100,000 molecular weight cut-off (MWCO)	Sartorius Stedium
Isopropyl 1-thio-B-D galactopyranoside (IPTG)	Generon	VivaSpin 6 100,000 MWCO	Sartorius Stedium
L- glutamine	Sigma Aldrich	XhoI	New England Biolabs
Lemo21 (DE3) Competent *E. coli*	New England Biolabs	XL1-blue Supercompetent cells	Aglient Technologies
Lightning-link Fluorescein Conjugation Kit	Expedeon	Zombie Ultraviolet™ (UV) Live Dead dendritic cell stain	Biolegend
Live Dead compensation arc reactive beads	Invitrogen		

Table 2-7. A summary of the chemicals and their suppliers used.

2.1.9 Standard Buffer Composition

Buffer	Composition
Blocking Buffer	1x Phosphate Buffered Saline (PBS) + 1% BSA
Ebio Permeability buffer	Ebio Permeability Buffer + dH_2O (1:3)
Fluorescence-activated cell sorting (FACS) Buffer	PBS, 1% BSA, 0,05% Sodium Azide
Fc Block	FACS Buffer, 5% NMS, 1% Human IgG
Foxp3 Transcription Factor Fixation/Permeabilization for T cell Intracellular staining	Foxp3 Transcription Factor Fixation/Permeabilization diluted 10x with Permeabilization Buffer
Lysis Buffer	50mM Tris pH 8 500mM NaCl
Lysis Buffer NadA Only	50mM Tris pH 7.5 50mM HEPES, 200mM NaCl
Magnetic Activated Cell Sorting (MACS) Buffer	PBS, 2% FBS, 2mM EDTA
Red Blood Cell (RBC) Lyse	10x dilution BD Pharm Lyse in H_20
PBS	No Calcium, No Magnesium pH 7.4
PBS- 0.05% Tween (PBS-T)	No Calcium, No Magnesium pH 7.4, 1L + 0.5ml Tween
PFA	Diluted to 1% and 4% in PBS
Protein A Elution Buffer	100mM Glycine pH 2.8
Protein A Neutralisation Buffer	1M Tris pH 9.0
Protein A Regeneration Buffers	25mM Tris pH 7.4, 1M NaCl, 25mM Tris pH 7.4, 25mM NaCl
Protein A Wash Buffers	100mM Tris pH 8.0, 10mM Tris pH 8.0
10x SDS Gel Running Buffer	25mM Tris, 192mM Glycine, 0.1% SDS
4x SDS Loading Buffer	250mM Tris pH6.8, 40% (v/v) Glycerol, 20% (v/v) 2-Mercaptoethanol, 8% (w/v) SDS, 0.04% (w/v) Bromophenol Blue
Small Scale Expression Lysis Buffer	50mM Tris + 500mM NaCl + 60µl 0.5M EDTA
Streptavadin Tag Lysis Buffer	100mM Tris pH 7.5, 50mM NaCl, 1mM EDTA
Streptavadin Tag Lysis Elution Buffer	100mM Tris pH 7.5, 50mM NaCl, 1mM EDTA + 2.5mM Desthiobiotin
Stripping Buffer for HisTrap columns	4% 0.5M Na_2HPO_4, 37.5% 4M NaCl, 10% of 0.5M EDTA
Super Optimal Broth (SOC) Buffer	20g/L Tryptone, 5g/L Yeast Extract, 4.8g/L $MgSO_4$, 3.603g/L Dextrose, 0.5g/L NaCl, 0.186g/L KCl
10 x Tris Base, Acetic acid, EDTA (TAE)	2M Tris pH 8.6, 1M Acetic Acid, 50mM EDTA
10x Tris Buffered Saline (TBS)	0.2M Tris pH 8, 1.5M NaCl
2% UA	5% UA diluted to 2%
Western Blot Transfer Buffer	25mM Tris, 192mM Glycine, pH 8.3 - 20% Methanol (vol/vol)

Table 2-8. A summary of the standard buffers used.

2.1.10 Antibiotics

Antibiotic	Concentration for Use
Ampicillin	100mg/ml
Kanamycin	50mg/ml
Chloramphenicol	25mg/ml
Pen/Strep	5000U/ml

Table 2-9. A summary of antibiotics used.

2.1.11 Antibodies

Use	Antibody	Fluorochrome	Clone	Supplier
Macrophage	anti-Human CD11b	Fluorescein isothiocyanate (FITC)	ICRF44	Biolegend
Macrophage	anti-Human CD13	APC- Cy7	WM15	Biolegend
Macrophage	anti-Human CD205	APC	HD30	Biolegend
Macrophage	anti-Human CD209	APC	DCS-8C1	Biolegend
Macrophage	anti-Human CLEC10A	PE	H037G3	Biolegend
Macrophage	anti-Human CD13	Unconjugated	WM15	Abcam
Dendritic Cell	anti-Mouse Major Histocompatibility Complex (MHC)-I	APC	AF6-88.5.5.3	Invitrogen
Dendritic Cell	anti-Mouse MHC-II	AF700	M5/114.15.2	Biolegend
Dendritic Cell	anti-Mouse CD11c	APC/eFluor780	N418	eBioscience
Dendritic Cell	anti-Mouse CD80	BV605	16-10A1	Biolegend
Dendritic Cell	anti-Mouse CD86	BV650	GL-1	Biolegend
Dendritic Cell	anti-Mouse CD83	PE/Cy7	Michel-19	Biolegend
Dendritic Cell	anti-Mouse CD40	PE	2/23	Biolegend
T Cell Extracellular	anti-Mouse CD4	APC	RM4-5	Biolegend
T Cell Extracellular	anti-Mouse TCRß	APC/eFluor780	H57-597	Invitrogen
T Cell Extracellular	anti-Mouse CD62L	BV605	MEL-14	Biolegend
T Cell Extracellular	anti-Mouse CD25	BV650	PC61	Biolegend
T Cell Extracellular	anti-Mouse CD69	BV711	H1-2F3	Biolegend
T Cell Extracellular	anti-Mouse CD44	BV785	IM7	Biolegend
T Cell Extracellular	anti-Mouse CD8a	PE/Cy7	53-6.7	Biolegend
T cell Intracellular	anti-Mouse Tbet	PerCP/eF710	4B10	Biolegend
T Cell Intracellular	anti-Mouse Foxp3	e450	FJK-16s	Invitrogen
T Cell Intracellular	anti-Mouse Retinoic Acid-related Orphan Receptor yt (RORyt)	PE	AFKJS-9	eBioscience
Western Blot Primary Antibody	Tetra His Antibody, BSA-free	Unconjugated	Mouse monoclonal	Qiagen
Western Blot Secondary Antibody	Goat anti-mouse igG (whole molecule)- Alkaline Phosphatase	Unconjugated	Polyclonal	Sigma
Bio-Layer Interferometry (BLI) Assay	anti-Human CLEC9A	Unconjugated		Biolegend
BLI Assay	anti-Mouse CD40	Unconjugated		Biolegend

Table 2-10. The flow cytometry antibodies used with their associated fluorochromes.

2.1.12 Cytokines

Cell Type	Cytokine	Coating Antibody	Detection Antibody	Recombinant Protein Standard
Dendritic Cell	Interleukin-6 (IL-6)	Biolegend	Biolegend	Peprotech
Dendritic Cell	IL-10	Biolegend	Biolegend	Peprotech
Dendritic Cell	IL-12P40	Biolegend	Biolegend	Peprotech
Dendritic Cell	IL-12P70	Biolegend	Biolegend	Peprotech
Dendritic Cell	Tumour Necrosis Factor-α (TNF-α)	R & D Systems	R & D Systems	R & D Systems
T Cell	IL-4	Biolegend	Biolegend	Peprotech
T Cell	Interferon-y (IFN-y)	In House	Biolegend	BD Biosciences
T Cell	IL-10	Biolegend	Biolegend	Peprotech
T Cell	IL-17a	Biolegend	Biolegend	Peprotech
T Cell	IL-2	BD Pharmingen	Biolegend	Peprotech
T Cell	Granzyme B	R & D Systems	R & D Systems	R & D Systems

Table 2-11. The cytokines used with their suppliers

2.2 Computational Methods

2.2.1 Predicting Stabilising Mutations in Rosetta3.5

A protein database (PDB) file for one of the 60 monomers of I3-01 was prepared in UCSF Chimera and this was run in Rosetta3.5 according to the 'Idealize' protocol in order to provide a structure to analyse further [167] [168]. The lowest energy structure was run through a 'Relax' protocol to discover the structure with the lowest energy based on relaxing the molecular interactions. This structure was put through a 'Point Mutation Scan' protocol to identify single stabilising mutations [169]. This script was adapted, adding "-double_mutant_scan", to search for stabilising double mutations by the same method. The resulting PDBs produced for the mutants of interest were put through a 'Relax' protocol to give an idea of the overall stability of the potential mutants. A list of mutants to be produced was decided upon based on the combined effects the predicted stability of the overall structure, and the location of the sites within the structure. All protocols can be found in appendix 2.

2.3 Cloning Methods

2.3.1 Construct Design

Gene design was performed in a word processor, based on the sequence published by the designers [134]. Restriction sites were added manually and the GeneArt Gene Synthesis service was used to generate the DNA before it was cloned into the pET-29a(+) expression vector.

2.3.2 Transformation into Competent Cells 2.3.3 Plasmid Amplification in XL1-Blue *E.coli* Cells

XL1-Blue Supercompetent cells and DNA were thawed on ice. DNA (100ng) was added to 25µl of cells which were incubated on ice for 30 minutes (mins). A heat shock stage was then performed for 1 min at 42°C, followed by incubation on ice for 2 mins. Under sterile conditions, 300µl SOC buffer was added to the cells and these were grown at 37°C for 1 hour (hr). Following this, 200µl of the cells were spread onto an agar plate containing appropriate antibiotic and plates were incubated at 37°C for 16-20 hrs.

2.3.3 Plasmid Amplification in XL1-Blue *E.coli* Cells

A single colony was added to a sterile flask containing 40ml Lysogeny Broth (LB) and 40µl antibiotic. The culture was grown at 37°C for 16 hrs before the cells were centrifuged at 3500rpm for 10 mins and the resulting supernatant was discarded. The extraction of the DNA was carried out using a QIAquick® MiniPrep Kit. Briefly, buffer P1 was used to re-suspend the pellet and this solution was split between four Eppendorf tubes. Buffer P2 (250µl) was added to each sample and all of the tubes were mixed by inverting. This step was repeated using 350µl of buffer N3. The samples were centrifuged for 10 mins at 13000rpm, the supernatant was applied to the respective spin columns and centrifuged for 1 min, the flow-through was discarded. Buffer PE (750µl) was added, the columns were centrifuged for 1 min, the flow-through was discarded and the columns were centrifuged again for 1 min. The spin columns were placed into 1.5ml Eppendorf tubes and 30µl sterile water was added to the centre of the

columns. The samples were incubated at room temperature for 4 mins and then centrifuged for 1 min. The DNA was stored at -20°C.

2.3.4 Agarose gel Electrophoresis

A 1% gel was made using 40ml 1x TAE buffer and 0.4g of Agarose with the addition of 6µl of Safeview™ DNA stain once cooled. The gel was set in a holder then placed in a gel tank filled with 1% TAE buffer. The gel was then loaded and was run at 100V for 30-40 mins.

2.3.5 DNA Digestion and Purification by Gel Extraction

A 40µl reaction mix containing 1µg DNA, 2µl of each restriction enzyme, 4µl of CutSmart® buffer and sterile water was incubated for 3 hrs at 37°C. The products of the digestion were run on a 1% Agarose gel, the relevant bands were cut under UV light and were placed in separate tubes. The QIAquick® Gel Extraction kit was used and three times the volume of the gel of buffer QG was added before a 10 min incubation period at 50°C. Once dissolved, 1 gel volume of Isopropanol was added to each sample and the samples were centrifuged at 13000rpm for 1 min. Buffer PE (750µl) was added, the samples were centrifuged for 1 min at 13000rpm, the supernatant was removed and the samples were centrifuged again. The columns were then moved to clean Eppendorf tubes and 38µl of sterile water was added to each. The columns were incubated for 4 mins and then centrifuged for 1 min at 13,000rpm. The final samples were run on a 1% Agarose gel to check for the presence of purified products.

2.3.6 Ligation

The Roche™ Rapid Ligation kit was used to perform the ligation reaction. To a 0.5ml Eppendorf, 1µl of purified digested vector, 7µl of purified digested insert and 2µl of the five times concentrated Ligation buffer were added. This solution was mixed gently before the addition of 10µl of the two times concentrated Ligation buffer and 1µl T4 Ligase. This final ligation mixture was incubated at room temperature for 1 hr. XL10-Gold® cells were prepared by thawing 50µl on ice. Once thawed, 2µl of 2-mercaptoethanol was added, the cells were incubated on ice for

10 mins and swirled every 2 mins. The ligation mix (5µl) was added to the prepared competent cells and this transformation reaction was incubated on ice for 30 mins. A heat shock step was performed for 1 min at 42°C, and then the cells were returned to ice for 2 mins. A sterile 300µl of SOC solution was added and cells were grown at 37°C for 2 hrs. Finally, this solution was plated aseptically onto an antibiotic plate and incubated for 16 hrs at 37°C.

3.3.7 Conformation of Cloning by Gel Electrophoresis

Single colonies were selected from the plate and were grown in 12ml LB with 12µl antibiotic for 16 hrs at 37°C. These samples were then centrifuged at 3500rpm for 10 mins and the supernatant was removed. The DNA extraction protocol was followed using the QIAquick® MiniPrep Kit. A 10µl digestion reaction of 0.5µg of each sample was set up with 1µl of CutSmart® buffer, 1µl of each restriction enzyme and sterile water. Following a 1 hr incubation at 37°C, these samples were run on a 1% Agarose gel to check for the presence of bands at the correct size for the insert in each lane.

2.3.8 DNA Sequencing

All sequencing was carried out by GATC-Biotech using the Sanger Supreme run service and their primers. Products to be analysed were shipped at a concentration of 3ng/µl in 20µl (made up with sterile water) and the results were provided in a .fasta format. The results were analysed using the ExPASy Translate and the Basic Local Alignment Search Tool (BLAST) to compare the DNA sequences of the clones to the original constructs design [170] [171].

2.3.9 Site Directed Mutagenesis

A master mix was made up for the number of reactions taking place. A single reaction mixture would contain; 27µl dH_2O, 5µl Phusion reaction buffer, 1µl dNTPs, 10µl Betaine, 1.5µl DNA and 1µl Phusion Polymerase. This was multiplied up depending on the number of reactions taking place. Once this had been split into separate reactions, 5µl of each of the related primer pair (F and R) were added. The PCR was run according to: 95°C initial denaturation for 1 min then 18

cycles of, 95°C denaturation for 50 seconds (s), 60°C annealing for 50s, and 68°C extension for 6 mins. A 7-min final extension took place at 68°C and samples were held at 10°C. Samples were transferred to sterile tubes and 1µl DpnI was added to each sample, followed by a 2 hr incubation at 37°C. Each reaction (5µl) was transformed into XL10-Gold® cells as previously. DNA extraction was performed using the QIAquick® MiniPrep Kit and the DNA was sent for sequencing to confirm the mutation was successful.

2.4 Protein Expression Methods

2.4.1 Expression in *E. coli* T7 Express Cells/ Lemo21 (DE3) Competent Cells

The transformation to competent cells protocol in section 2.3.2 was followed using T7 Express cells. A single colony and 60µl of antibiotic were added to 6 LB flasks each containing 60mls LB media. The cells were grown for 16 hrs at 200rpm and 37°C. The optical density (OD) at 600nm of the overnight culture was measured and a volume of overnight culture was added to each 450ml LB containing 450µl antibiotic, to give an OD_{600nm} of 0.15. The cultures were grown at 37°C and 200rpm until the OD_{600nm} reached 0.8. The cells were immediately induced using 0.4mM IPTG and were grown at 37°C for a further 3 hrs. Harvesting was carried out by centrifugation at 6000g for 20 mins at 4°C, and the pellets frozen on liquid nitrogen and were stored at -80°C.

2.4.2 Transformation into Clearcoli™ BL21 (DE3) Electrocompetent Cells

Recovery medium was stored alongside a GenePulser 0.1cm electroporation cuvette with a 0.1cm gap and a microfuge tube on ice. Clearcoli™ cells purchased from Lucigen were thawed and 25µl was added to a microfuge tube with 100ng of DNA. The mixture was pipetted into a cuvette without introducing bubbles, and the cuvette was tapped to ensure all cells were in the bottom of the well. Electroporation took place at 10µF, 600Ohms and 1.8kV for 3.5ms. The recovery media (975µl) was immediately added to the cuvette and the mixture was pipetted to re-suspend the cells before they were transferred to a round-bottomed tube. The tube was placed in the shaker at 37°C at 250rpm for 1 hr. A plate with appropriate antibiotic was inoculated with 100µl of cells and was incubated at 37°C for 16-30 hrs.

2.4.3 Expression in *E.coli* ClearColi^{TM} Cells

A single colony and 60µl of antibiotic were added to 6 LB flasks each containing 60mls LB media. The cells were grown for 16 hrs at 200rpm and 37°C. The OD_{600nm} of the overnight culture was measured and a volume of overnight culture was added to each 650ml LB containing 650µl antibiotic, to give an OD_{600nm} of 0.15. The cultures were grown at 37°C and 200rpm until the OD_{600nm} reached 0.8. The cells were immediately induced using 0.4mM IPTG and were grown at 37°C for a further 3 hrs. For the expression of some proteins, the cells were allowed to cool at 4°C for 4 hrs before induction and cells were grown at 16°C for 16 hrs. Harvesting was carried out by centrifugation at 6000g for 20 mins at 4°C, and the pellets frozen on liquid nitrogen and were stored at -80°C.

2.4.4 insect Secreted Batch Purification Method

A 1 litre of Hi-5 cell culture at $2.5x10^6$ cells/ml was infected with Protein P2 virus. The media, containing 0.05% sodium azide was harvested post-infection (Eddie Mckenzie, Institute of Biotechnology carried out this work and provided the media for the purification which took place in our lab).

2.4.5 Small Scale Expression Test for Solubility

DNA was transformed into T7 Express competent cells as previously. A single colony was added to 6ml sterile LB and 6µl of appropriate antibiotic. The cells were grown for 16 hrs at 37°C. A 50ml flask of LB was inoculated with between 0.15-0.20 OD_{600nm} overnight culture, and was grown shaking at 37°C until the OD_{600nm} reached 0.8. Once the OD_{600nm} was reached, a 1ml sample was taken, centrifuged at 13000rpm for 5 mins and the supernatant was removed. This pellet was frozen with liquid nitrogen and stored as the pre-induction (-IPTG) sample at -20°C. To the remaining flask, 0.4mM IPTG was added and the cells were grown at 37°C for a further 3 hrs. A 3 hr (+ IPTG) sample was taken and treated in the same way as previously. Both samples were defrosted on ice, 500µl of small scale lysis buffer was added to both pellets and was mixed gently on ice. Three tubes for each sample (+/- IPTG), total cell, lysate and insoluble were

labelled. The -/+ IPTG samples were sonicated on ice for 2 mins each, 5s on/10s off at an outage wattage of #6. A 10µl sample was removed into the total cell tube and the remaining sample was centrifuged at 16500g for 10 mins. The lysate supernatant was removed into a new tube, the pellets were re-suspended in 200µl lysis buffer and 3µl of loading buffer was added to each sample. Samples were analysed by 10% Sodium dodecyl sulphate polyacrylamide gel electrophoresis (SDS-PAGE) and if most of the protein was in the soluble fraction, large scale expression was carried out as above.

2.4.6 Making a Glycerol Stock

A 1.4ml sample of overnight Clearcoli™ culture was added to 600µl 80% sterile Glycerol and was frozen at -80°C. This was thawed on ice, streaked onto a plate with appropriate antibiotic and then incubated at 37°C for 16-30 hrs as needed.

2.5 Protein Purification Methods

2.5.1 5ml Nickel HisTrap Purification

Cell pellets were defrosted in five times volume of lysis buffer, one times volume of DNase and a cOmplete™ Protease Inhibitor Cocktail Tablet. The cells were sonicated on ice for 8 mins; 5s on/10s off at a wattage amplitude of 30%. Centrifugation was carried out at 4°C, 16000g for 40 mins and the cell lysate was filtered through a 0.22µm filter. The Nickel chelate column was equilibrated in 30mls sterile Milli-Q water and 30mls lysis buffer at 3mls/min. The cell lysate was applied to the column at 1ml/min and the flow-through was collected. The column was washed with 20mls lysis buffer, 20mls lysis buffer 10mM imidazole pH 8.0, 20mls lysis buffer 30mM imidazole pH 8.0, 10mls lysis buffer 50mM imidazole pH 8.0, 10mls lysis buffer 100mM imidazole pH 8.0, 10ml lysis buffer 150mM imidazole pH 8.0 and all washes were collected. Protein was eluted using two volumes of 10ml lysis buffer 200mM imidazole pH 8.0 and four volumes of 10ml lysis buffer 500mM imidazole pH 8.0. The column and pump were washed with 25mls sterile Milli-Q water at a flow rate of 3mls/min, and the column was stored in 20mls of 20% ethanol. The presence and purity of the protein eluted was analysed by 12% SDS-PAGE.

2.5.2 Streptavidin Tag Purification

Cell lysate was prepared in the same way as for the nickel purification. This was applied to a 5ml Streptavidin column equilibrated in Milli-Q water and lysis buffer. The column was washed with 50mls lysis buffer at 3mls/min and five volumes of 10ml fractions were collected. Protein was eluted using 25mls lysis buffer + 2.5mM Desthiobiotin at 1ml/min and 5ml fractions were collected. The column was cleaned at 5mls/min with 15mls Milli-Q water, 15mls 0.5M NaOH, 15mls Milli-Q water and 25mls 20% ethanol. The presence and purity of the protein eluted was analysed by 12% SDS-PAGE.

2.5.3 Protein A Purification

A 5ml Protein A column was washed in 30mls sterile water and 30mls 100mM Tris pH 8.0 at 3mls/min. The media was filtered through a 0.22µm filter, was applied to the Protein A column at 2mls/min and the flow-through was collected. The column was washed in 30mls 100mM Tris pH 8.0 followed by 20mls 10mM Tris pH 8.0 and the fractions were collected. Protein was eluted using 20mls 100mM Glycine pH 2.8 and was neutralised using 1M Tris pH 9.0. The column was cleaned with 30mls 25mM Tris pH 8.0 2M NaCl, 30mls 25mM Tris pH 8.0 25mM NaCl, 30mls sterile water and was stored in 20mls 20% ethanol. The presence and purity of the protein eluted was analysed by 12% SDS-PAGE.

2.5.4 Protein Concentration

A volume up to 15mls of lysis buffer was added into a concentrator (molecular weight cut-off dependent on the specific protein). The concentrator was centrifuged (speed dependent on concentrator being used) for 10 mins. The lysis buffer was replaced with 15ml of protein and was centrifuged until the protein volume decreased to the required volume.

2.5.5 Superose 6 10/300 GL Column Size Exclusion Chromatography

A Superose 6 column was attached to the ÄKTA fast protein liquid chromatography (FPLC) purchased from GE healthcare, and the column were washed in 50mls of Milli-Q water at

0.4ml/min. The pumps and column were then equilibrated in buffer in the same way. The 2ml loop was attached and was washed with 4mls of PBS. Pure protein was concentrated from the previous purification step to 1.8mls and was filtered before being applied to the column. Gel filtration was selected and the parameters set at; flow rate 0.4mls/min, pressure 1.1MPa, fraction size 1ml, injection volume 1ml and elution volume 25mls. The presence and purity of the protein eluted in the peak was analysed by 12% SDS-PAGE.

2.5.6 HiLoad 16/600 Superdex 200 Size Exclusion Chromatography

A Superdex 200 column was attached to the ÄKTA prime and the columns were washed in 200mls Milli-Q water at 1ml/min. The pumps and column were then equilibrated in buffer using the same method as above. The 5ml loop was attached and was washed with 10mls of PBS. Pure protein was concentrated from the previous purification step to 4.8mls and was filtered before being applied to the column. Gel filtration was selected and the parameters set at; flow rate 1ml/min, pressure 0.8Mpa, fraction size 1.5ml, injection volume 8mls and elution volume 120mls. The presence and purity of the protein eluted in the peak was analysed by 12% SDS-PAGE.

2.6 Further Purification Methods

2.6.1 Cleaning and Recharging a 5ml Nickel Column

The column was washed in: 25mls of sterile Milli-Q water at 3mls/min, 10mls 0.5M NaOH at 1ml/min, 20mls Milli-Q water at 3mls/min, 25mls of stripping buffer at 3mls/min, 25mls sterile Milli-Q water at 3mls/min, 2.5mls of 0.1M Nickel Sulphate at 1ml/min, 25mls of 20mM Na_2HPO_4 at 3mls/min, 25mls of Milli-Q sterile water at 3mls/min and was stored in 10-25mls of 20% ethanol.

2.6.2 Cleaning AKTA Prime/FPLC systems

With the column detached, a pump wash was performed in Milli-Q water followed by a pump wash in 1M NaOH. The system was washed in 50mls 1M NaOH at 5mls/min and the loop was

washed with 10mls. The pumps were returned to Milli-Q water before the pump wash, system wash and loop wash was repeated.

2.6.3 Cleaning Superose 6 10/300 GL and HiLoad 16/600 Superdex 200 Columns

Once the column was attached to a clean system, a pump wash in Milli-Q water followed by a column wash in 200mls Milli-Q water at 1ml/min were performed. A pump wash in 0.5M NaOH was completed before the column was washed in 1 column volume 0.5M NaOH at 0.5mls/min. The column was then immediately washed in 2 column volumes of Milli-Q water at 1ml/min.

2.6.4 Protein Dialysis

Depending on the volume and size of protein to dialyze, an appropriate length of tubing or a tube was equilibrated in Milli-Q water before appropriate buffer. The protein was added, placed in a beaker of dialysis buffer (volume depending on volume of protein to dialyse) and was left stirring for 20 hrs at 4°C.

2.7 Electron Microscopy

2.7.1 Negative Stain Method

A carbon coated 400 mesh copper grid was prepared by placing it on a slide with the carbon side face up. The slide was then vacuum discharged for 2 mins at 25mA and the grid removed from the slide. A 3µl drop of protein (0.1mg/ml) was placed on the grid and left for 30s before 60µl UA (2% solution) was added in a drop on drop off method. Excess stain was blotted off and grids were allowed to dry.

2.7.2 Electron Microscope Data Collection

An FEI TECnai 12 BioTwin was used to acquire over 100 images of each sample at 23,000x magnification. Single particle averaging was performed using the RELION-1.3 software which was used to generate a 3-Dimensional (3D) model [172].

2.7.3 Cryoelectron Microscopy Grid Preparation

Quantifoil R1.2/1.3 400 mesh copper grids were glow discharged at 25mA for 2 mins. 3µl of protein was diluted to 0.1mg/ml in 25mM Tris pH 8.0, 150mM NaCl was applied to the grids using a Vitrobot to freeze in liquid ethane with a 1.5s blotting time.

2.7.4 Cryoelectron Microscopy Data Collection

An FEI Technai G Polara was used to acquire over 1000 images of each sample using serial electron microscopy autoimaging at 23,000x magnification. The micrographs were converted to .mrc file format and were imported to RELION-1.3. Following the RELION-1.3 tutorial, these files were first motion corrected and the CTF (contrast transfer function) estimation was carried out [172]. The tutorial was followed for the whole processing procedure. Particle picking was performed manually and the extraction was to a box size of 256 pixels which was immediately shrunk to 128 pixels. 2- dimensional (2D) classification then placed the particles into multiple classes, a number of classes were selected and this process was repeated several times. These particles were selected to produce an initial model. 3D classification was used to split the particles into 2 classes, these classes were used to refine the initial model before it was masked and post processed.

2.7.5 Gold Labelling for Negative Stain Electron Microscopy

Proteins were dialysed to 50mM Tris pH 8.0 500mM NaCl for 48 hrs at 4°C and was then diluted to 0.05mg/ml. A number of ratios of diluted protein and antibody were set up. These were incubated at 4°C for 2 hrs, the negative stain grid preparation protocol was then followed (2.7.1) and the data collection was carried out using the FEI TECnai 12 BioTwin.

2:8 Protein Analysis

2.8.1 Estimation of DNA/Protein Concentration by UV absorption

Assessment of DNA and protein concentrations in low volume samples was carried out using the NanoDrop spectrometer. Briefly, the spectrophotometer was blanked against sample buffer

before conducting an absorption scan of 2µl of the sample. It automatically calculated DNA concentration (at 260nm), the protein concentrations (at 280nm) if the predicted absorption co-efficient and molecular weight were provided.

2.8.2 SDS-PAGE

A 12% NuPAGE Bis-Tris gel was placed in a tank with SDS running buffer and the wells were washed. Samples were prepared with the addition of 2µl 5x loading buffer to each 10µl sample and were heated to 90°C for 5 mins. Samples were briefly centrifuged at 13000rpm and loaded onto the gel which was run at 160V for 1 hr. The gels were stained in Instant Blue for 1 hr and then de-stained in sterile water.

2.8.3 Dynamic Light Scattering

Proteins were prepared in phosphate buffered saline (PBS) at 0.25mg/ml and were centrifuged at 16000g for 30 mins at 4°C. The samples were added in a volume of 100µl to a cuvette and placed in a Zetasizer DLS (dynamic light scattering) machine. Triplicate runs were performed on each sample at 25°C following a 2 min equilibration phase. An average of the Z-average diameter and polydispersity of the 3 runs was calculated.

2.8.4 Temperature Ramp Thermal Shift Assay

Proteins to be analysed were added to a 96 well plate (15µg/well) and 2µl of SYPRO orange (50x working solution) was mixed with each sample. The final volumes were made up to 22µl using 1x PBS. Controls of 15µg ovalbumin and PBS were also prepared. All samples were run in triplicate. The plate was sealed and centrifuged at 1000g for 1 min before being placed in the PCR StepOnePlus machine. The assay was run on a continuous setting that produced a melt curve between the temperatures of 25°C to 99°C, and at a ramp rate of 1%. The resulting data was analysed through the generation of graphs of the derivative data in GraphPad Prism Version 7 [173].

2.8.5 Western Blot

A 10% SDS-PAGE was run, the gel was soaked in Transfer buffer and was stacked from cathode to anode with pre-soaked sponges below it. Whatman Protan 0.2µm nitrocellulose paper and sponge were stacked above it. The whole stack was squeezed to remove any water and was placed in a gel tank containing Transfer Buffer, which was then placed on ice. The SDS-PAGE was run at 30V for 1 hr, the nitrocellulose paper was carefully removed and placed in a box containing 3% BSA-PBS-T shaking for 1 hr at room temperature. The primary antibody was diluted 1:2000µl in a total volume for 4mls PBS-T. The nitrocellulose paper was placed in a plastic cover, was sealed following the addition of the primary antibody and was incubated at 4°C shaking for 16 hrs. The nitrocellulose paper was washed in PBS-T 3 times following incubation. The secondary antibody was diluted 1:5000µl in a volume of 5mls PBS-T and was added to the nitrocellulose for 1 hr, shaking at room temperature. A further 3 washes in PBS-T were completed before the nitrocellulose paper was developed in the dark using a SIGMAFAST^{TM} tablet diluted Milli-Q water before Milli-Q water was used to end the reaction.

2.8.6 Mass Spectrometry

Protein samples were separated by SDS-PAGE and the gel was stained before being handed over in this format to the Biological Mass Spectrometry Core Research Facility at the University of Manchester. The bands were excised from the gel and were solubilised before Trypsin digestion. The resulting fragments were then identified by Tandem Mass Spectrometry. The library generated was then searched against the protein sequence of the designed synthetic proteins.

2.8.7 Assessment of binding to IgG Resin

A 2ml volume of IgG Sepharose resin was washed twice for 1 min at 6000rpm in 1ml of water and then in 1ml PBS. The prepared resin was incubated with 3ml I3-01/I3-01-PA at 0.2mg/ml for 1 hr at 4°C, rotating. The resin was added to a 5ml plastic column purchased from Thermofisher, and the flow-through was collected. A total of four PBS washes were performed and the flow-through was collected. I3-01-PA was eluted in four 2ml fractions in 100mM citric

acid (pH 3.5) following 2 mins of mixing. The protein fractions were pH adjusted to pH 8 using 1M Tris (pH 9). The wash and elution fractions were collected separately. The sample, flow-through, wash and elution fractions were analysed by 10% SDS-PAGE.

2.8.8 BLI Assay

The ForteBio Octet Red96 system was used to conduct this assay in conditions of 37°C and a plate shake speed of 1000rpm. The antibodies to be tested were biotinylated and loaded onto biosensors coated with streptavidin. These were dipped into a Kinetic buffer (ForteBio pH 7.4) to establish an initial baseline. The protein was then loaded onto the sensors at a range of concentrations for 10 mins, before dipping the sensors back in buffer to measure the association and dissociation rates respectively. The data was analysed by the ForteBIO Octet RED96 software version 11.1 to obtain the determination of association (k_{on}), determination of dissociation (k_{off}) and the equilibrium dissociation constant (K_d) values.

2.8.9 FITC Labelling of Proteins

Proteins at 1mg/ml were labelled in 200µl aliquots using the Lightning-Link® conjugation kit. To each protein, 25µl of Rapid Modifier was added and the sample was gently mixed. The sample to be labelled was then added to a vial containing FITC and 100µl sterile PBS. This dilution was re-suspended and incubated at room temperature for at least 15 mins in the dark. Following incubation, 27.5µl of Quencher was added and mixed. Labelled proteins were stored covered at -20°C, with a final protein concentration of 0.66mg/ml. 2.9.1 THP-1 Cell Culture

2.9 Cell Culture

2.9.1 THP-1 Cell Culture

2.9.1.1 Defrosting THP-1 Cell Culture

THP-1 Cells were thawed at 37°C in a water bath. RPMI 1640 media was prepared with 10% FBS, 1% Pen/Strep, 1% Glutamine, 1% HEPES and was warmed to 37°C. The cells were then added to 2mls RPMI 1640 media, mixed by pipetting and were centrifuged at 4°C, 1000rpm for 3 mins.

The supernatant was discarded and pellet re-suspended in 5ml of RPMI 1640 media in a culture flask which was incubated at 37°C, 5% CO_2, for 48 hrs. A further 5ml RPMI 1640 media was added following this and cells were incubated for 48 hrs. The 10mls of cell culture was centrifuged, the supernatant was removed and 20ml RPMI 1640 media was used to re-suspend the cells before incubation at 37°C, 5% CO_2, for 72 hrs. Cells were centrifuged, re-suspended in 10mls RPMI 1640 media, and added to haemocytometer to count cells. RPMI 1640 media was added to give between 1-2.5x10^5/ml in 20mls in a flask, and these were then incubated at 37°C, 5% CO_2, for 72 hrs.

2.9.1.2 Cell Counting

A well-mixed sample of cells was diluted 100x in Trypan Blue dye and 10µl was viewed under a light microscope on a haemocytometer. The total number of cells in the grid were counted (N). This value was subbed into the below equation:

N/4 x dilution factor x10^4 = number of cells/ml

2.9.1.3 Macrophage Differentiation

Cells were centrifuged and re-suspended in RPMI 1640 media to give a concentration of 1million/ml. PMA was added to the cells at 200nM, they were seeded into 12 well plates and then incubated at 37°C, 5% CO_2, for 72 hrs. RPMI 1640 media was removed from all wells and was replaced with 2mls of PBS. The plates were gently shaken and the PBS was then removed. Each well then had 2mls RPMI 1640 media added and cells were incubated at 37°C, 5% CO_2, for 24 hrs.

2.9.1.4 Preparation of Protein for BMDC and Macrophage Cell Stimulation

Proteins were prepared at 1mg/ml and were centrifuged at 16000g for 10 mins to remove any aggregates. The incubations required for all cell experiments were prepared 24 hrs in advance and following mixing, were stored at 4°C.

2.9.1.5 Addition of Proteins to Macrophages

The protein conditions and incubations were diluted in 1ml RPMI 1640 media following 24 hrs of incubation at 4°C. These were added to 1ml of cells in 12 well plates and were incubated for 5 hrs at 37°C.

2.9.1.6 Staining and Flow Cytometry

The RPMI 1640 media was removed from the cells, was replaced with 2ml warm PBS; and the plates were incubated for 5 mins at room temperature. The PBS was removed, 3mls of Accutase supplied by Invitrogen was added to each well and the cells were incubated for 20 mins at 37°C, 5% CO_2. The cells were scraped and re-suspended in each well before being collected into a Falcon tube. The Falcon tubes were made up to 50mls using warm RPMI 1640 media, were centrifuged at 300g for 5 mins at 4°C and the supernatant was discarded. The cells were washed twice more in PBS before being re-suspended in enough PBS to give 200µl for every condition in the 96 well plates. To prepare the live/dead cell sample, 100µl was taken from the live/dead cell well and was heated to 65°C for 7 mins. This was then cooled on ice for 2 mins before being added back to the remaining 100µl live/dead cell well in the plate. The plate was centrifuged at 300g for 5 mins at 4°C, the supernatant was removed and plate was vortexed. The viability dye was made up (1:1000 dilution), 200µl was added to each well and the plate was incubated, covered, on ice for 30 mins. The plate was centrifuged and washed twice in PBS. Fc Block was prepared, 50µl was added to each well and the plate was incubated on ice for 20-30 mins. Each antibody was then added directly (2µl/well) and the incubation period continued for a further 30 mins. The plate was washed 3 times in PBS, the cells were added to FACS tube with the addition of 350µl PBS and was then stored on ice. OneComp eBeads™ compensation beads were prepared by adding 1 drop of beads and 2mls PBS to a FACS tube for every antibody used. The beads were centrifuged, supernatant was discarded and the correct antibody was added to each tube. The beads were then washed in PBS twice and then re-suspended in 350µl PBS. The flow cytometry was carried out by Michael Jackson in the Flow Cytometry Facility using a BD LSRFortessa™ instrument, and the data was analysed using the FlowJo software version 10 [174].

2.9.2 BMDC Culture

2.9.2.1 Cell Culture

Mice were euthanized, sprayed with 70% ethanol and the hind limbs were removed with any muscle cut away from the femur. The knee was dislocated and any remaining tissue was removed from the femur without damaging the integrity of the bone. All of the bones were placed in a Petri dish with 70% ethanol and were washed for 2-3 mins. The bones were then transferred to a second Petri dish containing PBS, washed 3 times and this was repeated. Each bone was cut at both ends, a needle and syringe were used to flush out the bone marrow into the PBS where it was gently re-suspended with a syringe. The cells were counted and a suspension of 10mls was made up at 2 $x10^5$ cells/ml using RPMI 1640 media (supplemented with 5% Pen/Strep 5000U/ml, 10% FBS, 1% Glutamine and 20ng/ml GM-CSF). The BMDCs (2.5mls/dish) were seeded dropwise in the centre of sterile untreated Petri dishes and incubated at 37°C 5% CO_2 for 72 hrs. Following 72 hrs, 2.5mls of dendritic cell RPMI 1640 medium supplemented with 20ng/ml GM-CSF was added to each plate. The RPMI 1640 media supplemented with 20ng/ml GM-CSF was renewed to each plate 2-3 times a week.

2.9.2.2 Stimulation of BMDCs with Protein

The dendritic cells were harvested through gentle washes in RPMI 1640 media and collection from the dishes followed by centrifugation at 500g for 5 mins at room temperature. The cells were counted following resuspension in 10ml of RPMI 1640 media supplemented with 10ng/ml GM-CSF and were diluted to a concentration of $4x10^6$/ml. A volume of 500µl was seeded into 24 well plates and the cells were incubated at 37°C whilst the proteins were prepared. The protein incubations labelled with FITC (preparation in section 2.9.3) in different conditions were diluted in 500µl RPMI 1640 media and were added to the 24 well plates, which were then incubated for 5 hrs at 37°C.

2.9.2.3 Staining BMDCs and Flow Cytometry

The cells were stained to allow analysis of uptake of FITC labelled proteins and marker expression (CD40, CD80, CD83, CD86, MHC-I and MHC-II) by flow cytometry. Each well was washed and the cells were collected into 1.5ml Eppendorf tubes which were centrifuged at 500g for 10 mins at room temperature. The supernatants were removed and stored in 1.5ml Eppendorf's at -20°C for later cytokine analysis. The cell pellets were re-suspended in 200µl PBS and were added to 96 V bottom plates. These plates were centrifuged at 500g for 3 mins at 4°C, the supernatant was discarded and this was repeated. The cells were re-suspended in 10µl Live/Dead stain (diluted 1:1000). The plate was then vortexed and incubated in the dark for 15 mins. The Fc Block stain was diluted (1:100) and 50µl was added directly on top of the Live/Dead stain, the plate was vortexed and was incubated at 4°C for a further 10 mins. The plate was centrifuged at 500g for 3 mins and the supernatant was discarded. A cocktail was made up in FACS buffer using antibodies against the markers selected (enough for 50µl/well per desired concentration, MHC-I, MHC-II, CD40, CD80, CD83 and CD86, Section 2.1.11). This cocktail was added to all wells except the control well which has CD11c only antibody added (50µl). The plate was vortexed incubated for 30 mins in the dark at 4°C. The plate was then washed twice in FACS buffer and the cells were fixed in 50µl 1% PFA for 10 mins at room temperature in the dark. The cells were washed, re-suspended in 200µl FACS buffer and were added to FACS tubes for flow cytometry acquisition. Compensation Beads were prepared as in section 2.9.1.6 and the flow cytometry was carried out by Dr Helen Parker on a Fortessa instrument, and the data was analysed using version 10 of the FlowJo software [175].

2.9.2.4 Cytokine Assay

To coat 96 well enzyme-linked immunosorbent assay (ELISA) plates, 50µl of non-biotinylated antibodies, TNFα, IL-6, IL-10, IL-12p40, IL-12p-70 were applied at 4000pg/ml, 50ng/ml, 100ng/ml, 100ng/ml and 50ng/ml respectively. The plates were sealed to prevent evaporation and were stored at 37°C for 2 hrs. The cytokines were discarded and were washed in PBS-T twice before being blotted dry. To prevent non-specific binding, 200µl of Blocking buffer (1x PBS + 1% BSA) was added and the plates were covered at room temperatures for 1 hr. The

plates were washed again in PBS-T twice and standards for each of the cytokines were added in duplicate. The standards were prepared in RPMI 1640 media in 2x serial dilutions from 100,000, 50,000, 50,000, 50,000 and 2000pg/ml for IL-10, IL-6, IL-12p40, IL-12p70 and TNFα respectively. The samples were added to the plate in 50µl duplicate samples, the plates were covered and incubated at 4°C overnight. The plates were washed twice in PBS-T, the 50µl of each detection antibody diluted in PBS were added and the plates were incubated at room temperature for 2 hrs. The plates were washed in PBS-T twice before the addition of 50µl Strep-HRP (1:40 dilution) to each well which was incubated for 30 mins at room temperature. The plates were washed twice in PBS-T, were blotted dry and 50µl TMB was added. The plates were left to develop, H_2SO_4 (50µl) was used to stop the reaction and the OD_{450nm} of the plates was read. The data were analysed using the GraphPad Prism version 7 software [176]. A non-linear plot was produced for each of the standards. These plots were transformed so the recorded sample data could be extrapolated from it to reveal the cytokine concentrations produced from each sample.

2.9.3 CD4 T Cell Culture

2.9.3.1 T Cell Isolation

The mice were euthanized, the spleens were removed and placed in 6mls Hanks' Balanced Salt solution (HBSs). The spleens were placed in a sieve and were ground between 2 pieces of gauze into a Petri dish. The splenocytes were re-suspended in RPMI 1640 media in the well using a Pasteur pipette and all of the cells were centrifuged at 500g for 5 mins at 4°C. The pellet was re-suspended in 2ml red RBC lyse, was incubated on ice for 8 mins and RPMI 1640 media was added to quench the lysis. The cells were counted and centrifuged at 500g for 5 mins. The pellet was re-suspended well in RPMI 1640 media and the $CD4^+$ beads were vortexed before being added (90µl RPMI 1640 media and 10µl beads/ 10^7 cells). The beads and cells were incubated on ice for 20 mins. The column was equilibrated by adding it to the magnetic stand and washing with RPMI 1640 media. The cells and bead mixture was made up to 9mls with RPMI, was centrifuged and the supernatant was discarded. The cells and beads were re-suspended in 2ml RPMI 1640 media, any clumps were removed before it was added to the column with a Pasteur

pipette and the flow-through was collected. The column was washed with 9ml ice cold RPMI 1640 media. The column was removed from the stand whilst holding it over a 15ml Falcon tube. The cells were eluted with the addition of 3mls FBS free RPMI 1640 media and the $CD4^+$ T cells were collected.

2.9.3.2 CFSE Labelling of T Cells

The $CD4^+$ T cells were centrifuged for 5 mins at 500g and cells were re-suspended in CFSE (5µM, 1% Pen/Strep) made up to 1ml RPMI 1640 medium. The cells were incubated at 37°C for 6 mins and then 1ml RPMI 1640 media was added to quench the reaction. The cells were up made up to a 15mls volume with RPMI 1640 media, were centrifuged at 400g for 5 mins and the wash was repeated. The cells were counted and re-suspended to give 100,000 $CD4^+$ T cells/50µl.

2.9.3.3 Dendritic and T Cell Co-Culture

The proteins were prepared and incubated with dendritic cells for 5 hrs as in method 2.9.6.3. Following the incubation, the cells were removed from the plate, washed twice, were collected and counted. The cells were centrifuged for 5 mins at 500g and each sample was re-suspended to give 10^6 cells/ml. In a round bottomed 96 well plate, 50µl dendritic cells (50,000 cells) were added to 50µl $CD4^+$ T cells (100,000 cells) and the cells were incubated at 37°C 5% CO_2 for 3 days.

2.9.3.4 T Cell Staining

The cells were centrifuged at 500g for 5 mins at 4°C, the supernatants were collected into a fresh 96 well plate and were stored at -80°C for cytokine analysis later. The cells were re-suspended in 200µl of PBS and were transferred to a V-bottom plate purchased from Sigma Aldrich. The plate was centrifuged at 500g for 5 mins and the supernatant was discarded. The dendritic cell staining protocol 2.9.6.3 was followed (extracellular stain to include antibodies to the markers; CD4, TCRß, CD62L, CD25, CD69, CD44, CD8a). Following fixation, the plate was centrifuged at 500g for 3 mins and the cells were re-suspended in FACS buffer before being centrifuged again for 3 mins at 500g. A 90µl volume of eBioscience Foxp3

Fixation/Permeabilization buffer was added to the cells (diluted 1:3, Table 2.1.9) which were then vortexed and incubated for 30 mins at 4°C. Samples were centrifuged at 500g for 3 mins following addition of 100µl Ebio Permeability buffer (diluted 1:10) and the supernatant was discarded. This was repeated with 150µl Ebio Permeability buffer. The intracellular stain was then added using antibodies to the markers; Tbet, FoxP3 and RORyt (50µl/sample; Tbet) to all cells except the control (50µl of CD4) and the cells were incubated for 1 hr at 4°C. Cells were centrifuged in 150µl Ebio Permeability Buffer for at 500g for 3 mins. The cells were re-suspended in 400µl FACS buffer and added to FACS tubes for flow cytometry acquisition. Compensation beads were prepared as in section 2.9.1.6, the flow cytometry was carried out by Dr Helen Parker on a Fortessa instrument and the data was analysed using version 10 of the FlowJo software [177].

2.9.3.5 Sandwich ELISA for T cell Cytokine Production

To assay for T cell cytokine production, 96 well plates were coated with 50µl each cytokine (8-0.5ng/ml IL-4, IL-10, IL-2, IL-17α, IFN-y and Granzyme B). The plates were covered at 37°C for 2 hrs before 2 washes with PBS-T. A volume of 200µl Blocking buffer (1xPBS + 1%BSA) was added to all well and the plates were incubated at room temperature for 1 hr. The plates were washed twice in PBS-T and 50µl of the prepared standards were added in duplicate in 1:2 dilutions. The samples were also added to the plates (50µl to each to two of the plates first, then the following day they were transferred from these plates to plates coated with 2 new cytokines), the plates were covered and stored at 4°C overnight. Detection antibodies were prepared at 0.5ng/ml for all cytokines except anti-Granzyme B which was at 0.05ng/ml. The plates were washed twice in PBS-T and 50µl detection antibody was added to each plate. The plates were stored at room temperature for 2 hrs. The plates were washed twice in PBS-T before the addition of 50µl Strep-HRP to every well and the plates were incubated for 30 mins. The plates were washed again twice in PBS-T before the addition of 50µl TMB to develop and the reaction was stopped with 50µl H_2SO_4. The plates were read at OD_{450nm} and the analysis was performed in the GraphPad Prism software version 7 as in section 2.9.2.4 [176].

2.9.4 Endotoxin Assay using HEK-BlueTM-4 Cells

2.9.4.1 Thawing of Frozen HEK-Blue™-4 Cells

The HEK-Blue™ -4 cells vial was thawed by gentle agitation in a 37°C water bath keeping the O-ring and cap out of the water for 2 mins. The contents of the vial were transferred to a sterile tube containing 15mls of growth medium and were centrifuged at 1500rpm for 5 mins. The supernatant containing the cryoprotective agent was removed and the cells were re-suspended with 1ml of the HEK-Blue™ -4 cells growth medium. Re-suspended cells were transferred to a 25cm^2 tissue culture flask containing 5ml of growth medium. The flask was incubated at 37°C in a 5% CO_2 incubator for 20 hrs. When 50-80% confluency was reached, the cells were grown in growth medium supplemented with 1x HEK-Blue™ Selection Reagent.

2.9.4.2 HEK-Blue^{TM} -4 Cell Maintenance

HEK-Blue™ -4 cells were maintained and sub-cultured in growth medium supplemented with 1x HEK-Blue™ Selection Medium. The medium was renewed every 2 days and the cells were either used or passaged when 60-80% confluency was reached. Cells were never grown to 100% confluency.

2.9.4.3 Sample Preparation

The samples were prepared in triplicate at 0.2mg/ml in PBS. All samples were digested with Proteinase K at a concentration of 400µg/ml for 16 hrs at 37°C and digestion was confirmed by SDS-PAGE. Triplicate samples of sterile water and Proteinase K were used as negative controls. Dilutions of LPS between 0-3ng/ml were prepared for the calibration curve. A sterile 96 well plate was labelled and 20µl of each sample was added in triplicate to each well.

2.9.4.4 Addition of HEK-Blue^{TM}-4 Cells and Assay Measurement

Once the HEK-Blue™-4 cells were 70-80% confluent, they were removed from the incubator and the medium was discarded. The cells were gently rinsed with 5-10mls PBS followed by an additional 2-5mls PBS before returning to 37°C for 1-2 mins. The cells were then detached by tapping and gentle re-suspension. HEK-blue^{TM} Detection Media was prepared using 50ml of

sterile endotoxin-free water. The solution was swirled before heating to 37°C for 1 hr and filtering through a 0.2µm membrane. Cells were counted and diluted with pre-warmed Detection Medium to 140,000/ml in enough volume to provide each sample with 180µl (28,000 cells/well). The cells in Detection Medium were added to each well and the plate was immediately incubated at 37°C, 5% CO_2 for 6 hrs. The plate was read at OD_{630}nm following incubation and graphs were produced in GraphPad Version 7 [173].

2.10 Confocal Microscopy

2.10.1 Confocal Labelling

Macrophages were differentiated from THP-1 cells as previously, at a concentration of 90,000 cells/ml in a 300µl volume in 10 well slides (Section 2.9.2). The proteins were prepared and the cells were stimulated in parallel with any FACS samples (Section 2.9.3/2.9.4). Following incubation, the RPMI 1640 media was removed from each well and cells were washed twice in 200µl PBS. For fixation, 100µl of 4% PFA was added to each well and cells were incubated at 37°C for 15 mins. The PFA was removed from each well and the cells were washed in PBS three times. The PBS was removed and 200µl CellMask^{TM} Deep Red Plasma Membrane stain 1µl diluted in 2mls RPMI 1640 media) was added to each well. The cells were incubated for 10 mins at 37°C. The CellMask^{TM} was removed from each well and the cells were washed three times in PBS.

2.10.2 Confocal imaging

The Confocal Leica SP8 inverted microscope is in the Bioimaging Facility in Michael Smith Building at the University of Manchester. The microscope setup was carried out by Roger Meadows using the lasers at 660nm/495nm for the cell mask and FITC labelled proteins respectively. The images were captured as Z-stack images for each sample in the chamber slide; the images were analysed by myself, combining the two channels to create composite images of each condition using the ImageJ 1.x software [178].

2.11 Statistics

Statistical analyses were performed using GraphPad Prism software, version 7.00. Statistical difference was determined using a one-way analysis of variance (ANOVA) (Tukey's multiple comparison test). NS $p > 0.05$, * $p \leq 0.05$, ** $p \leq 0.01$, *** $p \leq 0.001$, ****$p \leq 0.0001$ [179].

Chapter 3

Characterisation of native and engineered forms of I3-01

Chapter 3 - Characterisation of native and engineered forms of I3-01

3.1 Introduction

To date, the most effective vaccines have been of a whole cell nature due, in part, to the strong immunogenic responses produced by B cells to these natural repeated antigen arrays [180]. In this new era of vaccine design, developments have included using virus-like particles (VLPs). VLPs are diverse nanoparticles ranging between 20-100nm in size, which are non-infectious due to their lack of genetic material, but resemble viruses in terms of their structure [181, 182]. Using VLPs in vaccine formulations provides a strong and rapid immune response, as our immune system recognises these structures as foreign and processes them quickly [183]. VLPs can be utilised as effective vaccines in two different ways. Firstly, the VLP is derived from the infecting virus, or secondly, the VLP acts as an antigen scaffold to support antigens derived from a different virus [184]. These methods were implemented in trials for a Human Papilloma virus (HPV) vaccine using a HPV VLP, and also for a Hepatitis C vaccine using a Hepatitis B surface antigen VLP [180, 185].

One of the first reported VLPs used in vaccine design was Hepatitis B virus core antigen (HBc). This system has been used to deliver foreign epitopes from viruses such as malaria and influenza with positive results in clinical trials [41, 186, 187]. Structurally, HBc is comprised of two symmetrical dimers which self-assemble to form an icosahedral VLP with a diameter of 35nm [188, 189]. Different sites have been selected for foreign epitope insertion including the N-terminal and C-terminal regions [190]. The major insertion region (MIR) is a third, most preferred site to attach epitopes. This is located between residues 78-82 and is the most protruding point of the VLP spike [188, 190, 191].

Recent work has inserted meningococcal antigens into the HBc VLP to test if larger entities can be incorporated into this structure [163]. The initial antigen selected was Factor H binding protein (fHbp), which is a purified component of the current MenB vaccine 4CMenB [192]. The HBc antigen fusion assembled following incorporation of fHbp at the C-terminal of the protein, but the melting temperature of this new construct dropped by 20°C compared to the native

HBc VLP. A second antigen, Neisseria adhesin A (NadA), was inserted into the MIR and this particle was correctly folded as shown by cryoelectron microscopy; however, the melting temperature of this construct decreased by 30°C compared to the empty VLP. A key finding with the VLP-NadA fusion was that it was found to yield antibodies capable of bactericidal activity by serial bactericidal assay (SBA) [163]. This work revealed that the HBc VLP is a promising scaffold candidate in meningococcal vaccine design, but it does have its limitations in terms of which antigens can be inserted whilst maintaining assembly and the associated decrease in melting temperature.

Recent increases in computational power have enabled the design of protein assemblies with tetrahedral and octahedral symmetries [193, 194]. I3-01 is a symmetrically complex structure with the largest internal volume of any protein assembly designed to date [134]. This assembly is a similar size to the HBc VLP and also shares the same icosahedral point group symmetry. An analysis of this assembly's ability to support antigen insertion and maintain stability in comparison to a known vaccine platform, such as the HBc VLP, is yet to be completed. The focus of this chapter was to further characterise I3-01 and to test its ability to support incorporated epitopes and larger antigens. This will help to gain an understanding as to whether this synthetically designed particle could be used to form a suitable vaccine candidate, much like the HBc VLP.

3.2 Production of I3-01

3.2.1 Expression and purification of I3-01

To enable characterisation of I3-01 to begin, the first step was to clone a synthetic DNA coding sequence into a suitable vector to allow expression of the protein. The process of cloning, expression and purification was the same for all of the constructs used in this project (Figure 3.1). Briefly, the coding sequence for I3-01 was supplied with the NdeI and XhoI restriction sites inserted at the N- and C-termini respectively. The gene was ligated into pET29A (+), supplied by Novagen®, using the cloning method in section 2.3.

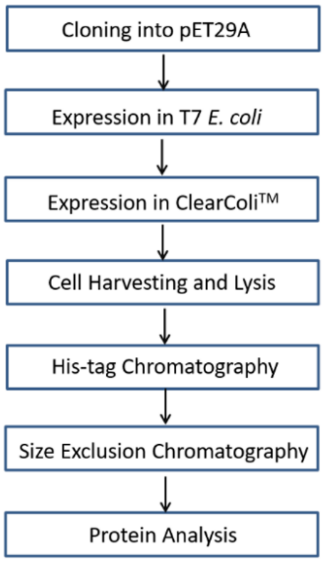

Figure 3-1. The I3-01 construct production process. I3-01 and all designed constructs were purified following this procedure.

Following cloning, the I3-01 constructs were initially expressed in the T7 *E.coli* expression strain to test that soluble protein was produced. Small scale expression trials were performed using the method in section 2.4.1. Since all of the proteins purified in this project had the potential to be used as vaccine candidates, it was important that they were also well expressed in a bacterial cell line with low endotoxin. The cell line of choice was ClearColi™, an *E.coli* strain which has modified endotoxin that does not bind innate toll-like receptors (TLRs) and so does not trigger an innate immune response [165]. The I3-01 DNA was transformed to ClearColi™ cells by electroporation and the overexpression was carried out for 3 hrs at 37°C. His-tag purification, followed by size exclusion chromatography (SEC) was used to purify the I3-01 protein from the

cell pellet following the methods in sections 2.5.1 and 2.6.3. The size exclusion trace revealed that the sample was pure and the peak was in the void volume, suggesting large assembled particles had been eluted (Figure. 3.2A). SDS-PAGE analysis confirmed the purity of the sample and that the protein was the correct size (I3-01 monomer MW= 23.8kDa) (Figure 3.2B).

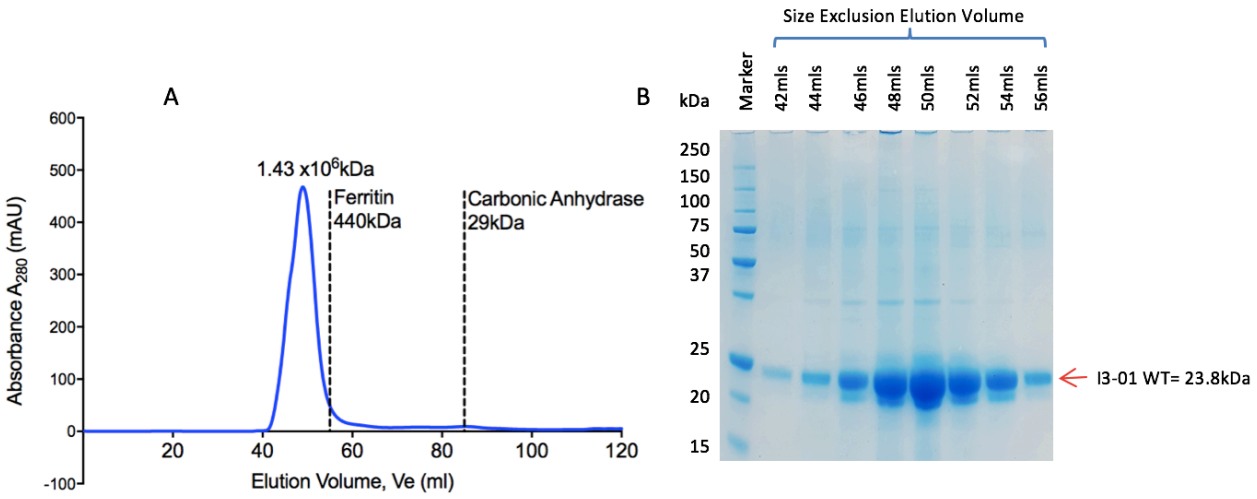

Figure 3-2. SEC purification of I3-01 from ClearColi^{TM}. (A) UV absorption profile of I3-01 eluting from a SEC column. I3-01 cell pellets were purified using a 5ml HisTrap column and rising concentrations of imidazole in lysis buffer containing 50mM Tris-HCl pH 8.0 and 500mM NaCl. Elution fractions containing 500mM imidazole were concentrated to a 5ml loading volume and were run on a Sepharose 200 column at 1ml/min. Fractions of volume 1.5mls were collected for further analysis. (B) SDS-PAGE analysis of I3-01 eluted from a SEC column. A volume of 10µl of each of the protein fractions purified by SEC (between the elution volumes of 42-56mls) was analysed on a 10% SDS-PAGE gel; the MW of the I3-01 monomer is 23.8kDa.

3.2.2 Negative stain electron microscopy analysis of I3-01

It was important to verify the assembly status of I3-01 before introducing antigens as incorrect folding of the protein at this point would likely hinder successful antigen display by this particle. A sample of I3-01 purified from ClearColi^{TM} cells was viewed by electron microscopy. It was clear a uniform population of assembled proteins had been purified when I3-01 was expressed in

ClearColi^{TM} (Figure 3.3). Analysis of the negative stain electron microscopy verified that I3-01 was assembled, but revealed little detail of the overall structure.

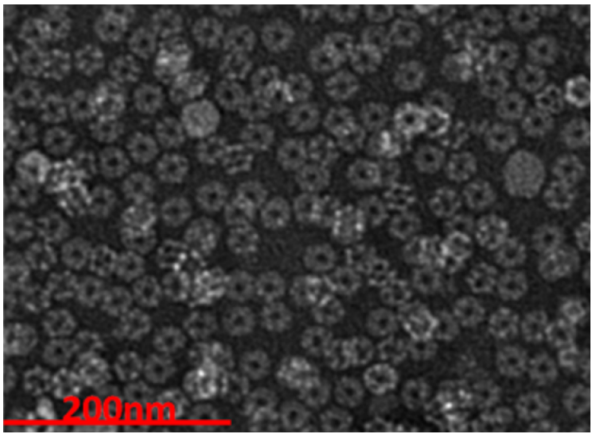

Figure 3-3. Negative stain electron mircoscopy analysis of purified I3-01. *I3-01 at 0.3mg/ml in 50mM Tris, 500mM NaCl pH 8.0 was negatively stained with 2% UA. The samples were viewed on an FEI Tecnai 12 Biotwin microscope at 23,000x magnification.*

3.2.3 DLS analysis of I3-01

DLS was carried out to confirm the diameter of the native particles and to determine the homogeneity of the I3-01 preparation. It was important to establish these parameters in the native particles so any changes upon modification could be evaluated. The diameter was recorded as 35.3nm which was larger than the previously reported value 28nm (Figure 3.4) [134]. This could be explained by the increased concentration of I3-01 used here and the change in buffer conditions (1mg/ml in PBS compared to 0.5mg/ml in 50mM Tris, 500mM NaCl pH 8.0). In terms of homogeneity, the polydispersity index was measured at 0.125, suggesting a uniform population was present when this assembly was purified in PBS.

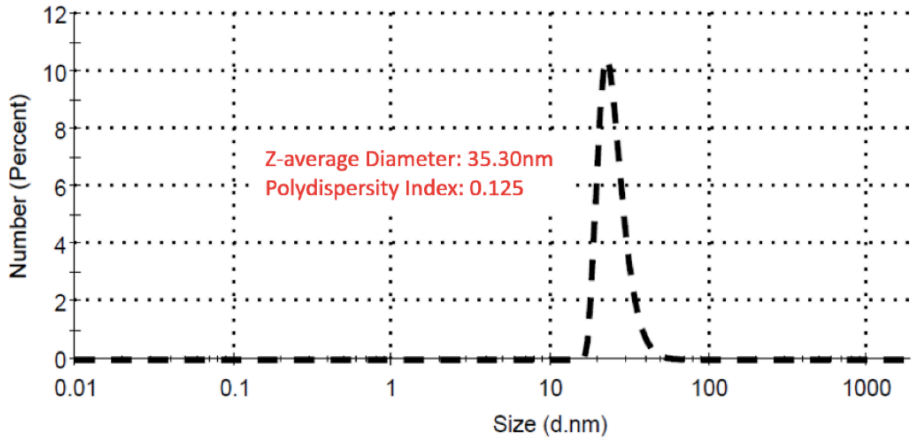

Figure 3-4. DLS analysis of I3-01 constructs. Samples of 100µl volume of I3-01 at a concentration of 1mg/ml in PBS were centrifuged at 16,000 xg for 30 mins directly prior to adding to a cuvette in a Zetasizer DLS machine. A series of three measurements were taken of each parameter; Z-average diameter and polydispersity index, which indicate the particles size and populations homogeneity respectively.

3.2.4 Cryoelectron microscopy analysis of I3-01

Cryoelectron microscopy was used to analyse and verify the structural model proposed by the original designers of the assembly [134]. This would provide more information on the structure of the assembly and confirm it matched the designed model. Samples of I3-01 were frozen in liquid ethane on to Quantifoil gold grids and serial electron microscopy imaging was performed on the Polara FEI Technai G microscope. The micrographs were imported into RELION-1.3, and 2956 particles were picked manually [172]. A specific workflow was applied following data collection to allow a model to be produced (Figure 3.5).

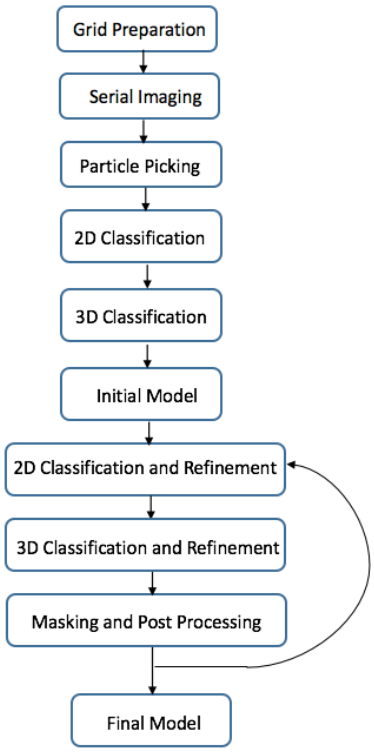

Figure 3-5. The process of model generation. The I3-01 structure was solved following this workflow. After the first masking and post processing step, all of the particles that were initially selected were brought back into the classification process and were refined against the best current map. This was repeated twice before the production of the final reconstruction.

Multiple rounds of 2D classification placed the selected particles into 3 classes (Figure 3.6B). 3D classification was used to split these particles into 2 classes which were used to refine an initial reconstruction to 9.04Å resolution (Figure 3.6C). In order to try to improve the map further, this process was repeated and the particles were refined against the 9.04Å map already generated. Following masking and post processing, a reconstruction with a resolution of 8.54Å was produced (Figure 3.6D). This process was repeated a final time and both of the 3D classes formed were refined against the 8.54Å reconstruction which gave a final structure, following masking and post processing, with 8Å resolution (Figure 3.6E).

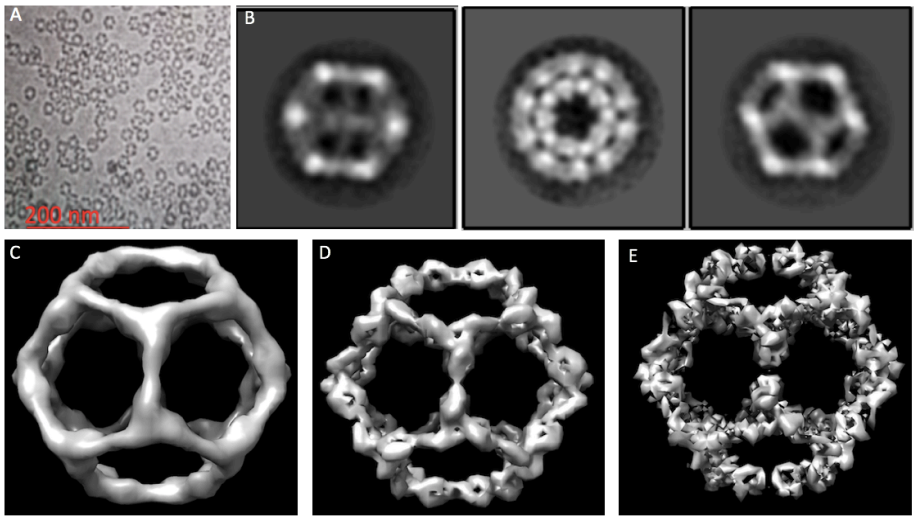

Figure 3-6. The cryoelectron microscopy reconstruction process. I3-01 was prepared in 25mM Tris pH 8.0, 150mM NaCl, diluted to 0.3mg/ml, and 3µl of protein was added to Quantifoil R1.2/1.3 400 mesh gold grids. The Vitrobot was used to freeze the grids in liquid ethane with a 1.5s blotting time. Serial electron microscopy auto-imaging was performed on the FEI Tecnai G Polara microscope. (A) A cryoelectron micrograph, demonstrating a homogenous sample of I3-01. (B) The 2D class averages highlighting the 2, 3 and 5-fold axis of symmetry present in I3-01. (C-E) Maps of I3-01 produced to 9.04Å, 8.54Å and 8Å resolution respectively.

The final cryoelectron microscopy map from the original authors was at 20Å resolution; the structural analysis here has provided a higher resolution map than previously created (8Å) and the designed structure mapped on it with a correlation coefficient of 0.92 (Figure 3.7) [134].

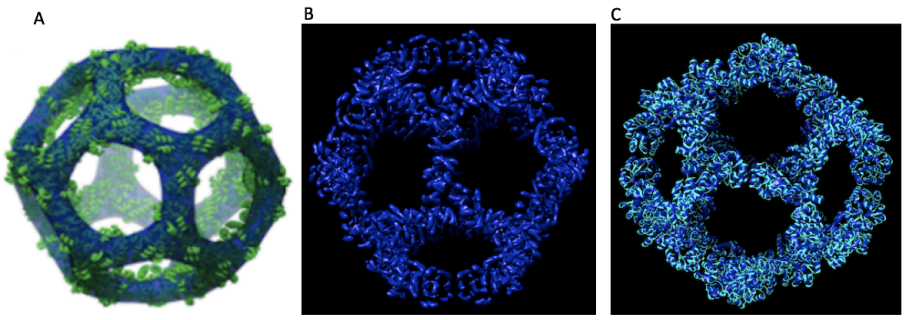

Figure 3-7. Mapping I3-01 to the published PDB. (A) The cryoelectron microscopy structure published previously mapped to the designed model to 20Å resolution [134] . (B) The I3-01 reconstruction to 8Å resolution. (C) The I3-01 density map was fitted to the published PDB with 0.92 correlation.

The original authors modelled this construct based on a trimer of known structure and they computationally designed a dimer interface to allow the trimers to assemble spontaneously. To enable an evaluation of how the cryoelectron microscopy data presented here agreed with the original design, a RMSD (root mean square deviation) calculation was performed. This allowed a comparison to be made of the dimer interface from our data fitted to the original PDB compared the original design (Figure 3.8). The RMSD was calculated at 1.1Å which verified that the I3-01 protein assembly forms a structure which was very similar to the designed model.

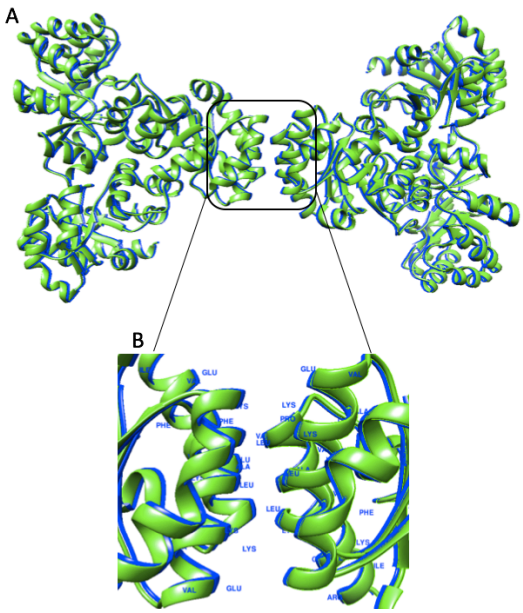

Figure 3-8. A comparison of I3-01 cryoelectron microscopy data with the original assembly design. (A) The cryoelectron microscopy map produced here (Figure 3.7B) was fitted to the original PDB and this modified PDB (blue) was matched to the original PDB (green). (B) As the dimer interface was the computationally designed element of the assembly, this was specifically analysed and the RMSD between the two structures was calculated. This interface contained many hydrophobic residues and also some positively charged residues, suggesting the interactions were mainly polar but that salt bridges were also formed.

3.2.5 Analysis of the thermal stability of I3-01

A thermal shift assay was run to examine the stability of the I3-01 assembly; the I3-01 construct designers previously found it to be stable up to at least 80°C [134]. This would provide a baseline for comparison of any changes to this parameter with the insertion of any epitopes/antigens. The assay measured the melting temperature of I3-01 following the addition of SYPRO orange dye over a temperature range of 25°C-99°C. A denaturation curve was produced; the ovalbumin control had a melting temperature of 73.6°C, which was slightly lower than the previously reported value of 77.3°C [195]. The trace plotted for I3-01 shows that no denaturation transition occurred up to 99°C (Figure 3.9). This highlighted the stability of the native assembly when purified in PBS.

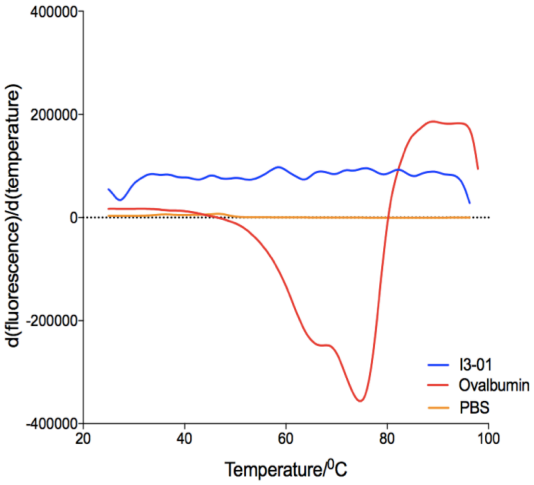

Figure 3-9. Measurement of I3-01 denaturation by Thermofluor assay. A thermal stability assay was performed in triplicate using 15µg samples of I3-01, and a melt curve was produced at a 1% ramp rate between the temperatures of 25°C-99°C. Ovalbumin and PBS were run as positive and negative controls respectively.

3.2.6 Measurement of I3-01 endotoxin contamination

Although I3-01 had been purified from a ClearColi^{TM} strain of *E.coli*, it was important to confirm there was no contamination with endotoxin. A colorimetric cell-based assay was performed using HEK-Blue cells to detect biological active endotoxin. I3-01 was digested with proteinase K for 16 hrs at 37°C and SDS-PAGE analysis confirmed successful digestion. HEK-Blue cells were incubated with each sample at 37°C for 21 hrs and a reading of the OD was taken at OD_{630}. An endotoxin level of 20 EU/ml (endotoxin units) is acceptable for use in vaccine design which equates to 2ng/ml [196]. The I3-01 sample had an average absorbance under the threshold equating to 2ng/ml. It can be concluded that purification of I3-01 constructs from ClearColi^{TM} cells produces protein that has limited endotoxin contamination and could be used in our studies.

3.3 Purification of I3-01 antigen fusions

The purpose of this section was to investigate the potential modification sites within I3-01. This includes, the selection of: T cell epitopes to mutate, sites of circular permutation; and locations for epitope and antigen insertion. This was important as the chosen locations should be those which would least likely affect the ability of I3-01 to assemble, so it was worth careful consideration. The aim of this was to select the optimal sites for these mutations and insertions to give the best chance of them being incorporated successfully.

3.3.1 Examination of potential sites for antigen insertion

To design the fusion constructs two factors had to be considered. The first is the nature of the specific modification or insertion selected, and the second is the site of this within the I3-01 assembly. The location of the modification sites required careful attention as it was important to try to maintain assembly. The I3-01 monomer has a triose phosphate isomerase (TIM) barrel fold and was studied carefully before sites for modifications were selected; sites were nominated based on the prediction that insertion at these points would result in surface exposure of the antigen. The longest two surface exposed loops were examined and the two residues were selected as potential insertion points: G-60; and N-148 (Figure 3.10B). The termini were also surface exposed, suggesting these are also sensible candidate sites for modification (Figure 3.10C).

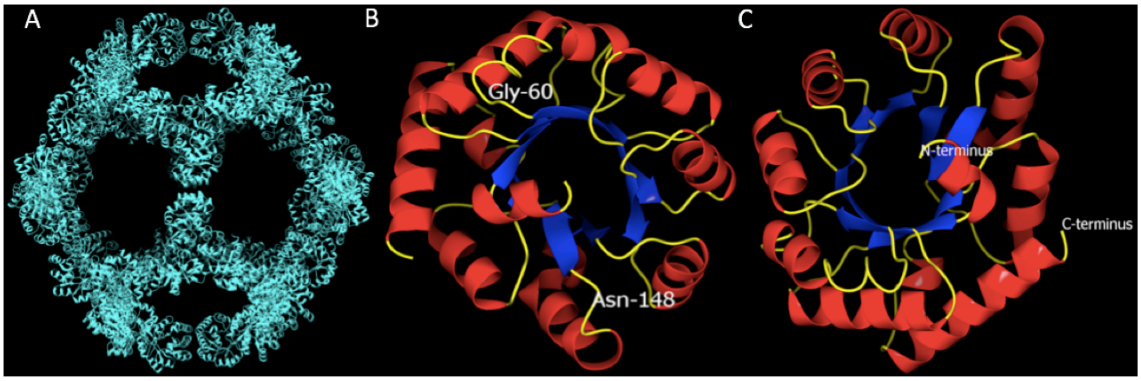

Figure 3-10. The identification of the I3-01 modification sites. (A) The I3-01 assembly. The particle was designed to form a dodecahedron protein cage with icosahedral symmetry using 60 subunits of the naturally trimer-forming enzyme KDPG (2-dehydro-3-deoxy-phosphogluconate) aldolase [134]. (B) The I3-01 monomer. KDPG aldolase has a TIM barrel fold, containing eight α-helices (red) and eight β-strands (blue) and the N- and C-termini are in close proximity. (C) The I3-01 monomer has multiple surface exposed loops. Upon examination, the surface exposed loops (yellow) were examined for areas of stability for possible antigen insertion. Two residues; G-60 and N-148 were selected as potential modification sites.

3.3.2 Identifying and mutating T cell epitopes within the I3-01 assembly

To enable the production of engineered I3-01 with modified human or mouse T cell epitopes, the sequence was analysed using the IEDB-AR (Immune epitope database and analysis resource) (www.iedb.org). The MHC-II T cell epitope consensus method was used to identify potential human T cell epitopes, whereas the search for any mouse T cell epitopes was performed using the H2-IAb allele. There were five epitopes identified; the highest scoring ran from residues 31-55, with a binding affinity score of 0.08 on the HLADRB1*03:01 allele (Figure 3.10). A low score indicates a high binding affinity and a score <1 is considered as high [197, 198].

The most potent epitope predicted was analysed to identify possible mutation sites. As loop regions are the most flexible section of proteins, the residues from this T cell epitope located in a loop were analysed using molecular graphics (UCSF Chimera) [167]. Residues T-40, F-41, T-42, V-43, P-44 and D-45 were selected as possible mutation sites (Figure 3.11). These target

residues were mutated, *in silico*, to every other amino acid and the changed sequence was then analysed using the IEDB-AR. Multiple mutation possibilities were found that would weaken this T cell epitope (data not shown). It was important to assess, computationally, which of these mutations would have a stabilising effect on the assembly as any mutation made could destabilise the assembly. Using methods in ROSETTA-3.5, multiple mutations were selected which would both weaken the T cell epitope and be stabilising (methods in section 2.5) [168, 169]. The threonine at position 40 was successfully mutated to serine using site directed mutagenesis (SDM), a modification which would reduce the predicted T cell epitope potency and have a stabilising effect on the structure (Figure 3.11).

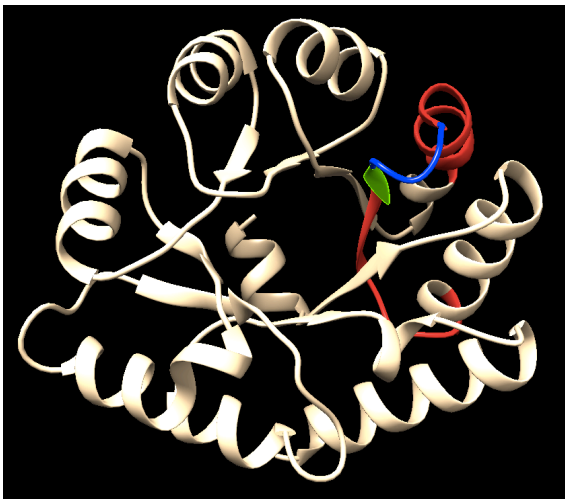

Figure 3-11. Identification and mutation of a predicted T cell epitope in I3-01. The IEDB MHC-II consensus method identified residues 31-55 as a T cell epitope (red). The residues in the loop region of the epitope (blue) were mutated in silico and ROSETTA-3.5 predicted the mutation of threonine residue at position 40 to serine (green) was the most stabilising mutation, and so this was carried out by SDM.

3.3.3 Design of circular permuted I3-01

The second modification selected was circular permutation, a method by which the current N- and C-termini of a protein are joined by a linker and a section of polypeptide chain is broken to give new termini. This engineering offered an opportunity to form an assembly more suitable

for antigen insertion, whilst also probing the robustness of the structure. It was performed to move the termini to within a surface exposed loop which would provide a more optimal, exposed, site for antigen display. This is illustrated in Figure 3.10: the original position of the termini and the proposed new sites of the termini are shown in Figure 3.10C and 3.10B respectively.

There were two main features to consider in the design of the circular permutation; the length of the loop and the sites of the new termini. The locations of the new termini were decided based on a range of factors. Firstly, the loop regions within I3-01 were selected manually using interactive molecular graphics. It was determined whether they were surface exposed and if they were involved in interface binding. Once the surface exposed loops were selected, a number of criteria were used to finalise the best loop to break; these included the B factor and the level of conservation of the sequences. A high B factor and a low level of sequence conservation are the desirable features of sites which would increase the chance of maintaining assembly following modification. The two residues selected to form a new N- terminal in two separate constructs were G-60 and N-148 (Figure 3.10B). To design a loop region that would join the current N- and C-termini, the distance between them was calculated to be 23Å (Figure 3.10C). A $(GGS)_4$ linker was determined to be long enough to join the N and C-termini. The complete protein sequences were designed starting with the original histidine tag and linker followed by the new N-terminal sequence through to the original C-terminal end, followed by the designed linker $(GGS)_4$. The previous N-terminal methionine came directly after the linker and the sequences continued through to the residue prior to the selected break site which is now the new C-terminus. The considerations taken here were to ensure these modifications maintained the structure of the I3-01 trimer-forming unit as a TIM barrel structure, allowing I3-01 to assemble correctly whilst providing new sites for antigen insertion.

3.3.4 Insertion of ovalbumin epitopes

The second modification was the insertion of short ovalbumin epitopes. Ovalbumin was selected as the first antigen to incorporate into I3-01 as it has been used multiple times as a

model antigen in various vaccine design technologies [199]. The availability of transgenic mice with T cell receptors that specifically recognised one of two short ovalbumin epitopes (between 8 and 18 residues in length) provided a relatively simple first engineering opportunity [200, 201]. These small sequences ($OVA_{257-265}$ and $OVA_{323-339}$) were incorporated into I3-01, giving the potential to evaluate the T cell proliferation when the ovalbumin epitopes were presented to cells by these assemblies. The first step was to decide where the insertion site should be located. The N-148 site was selected for inserting the ovalbumin epitopes based on the fact that it was part of the least conserved surface exposed loop in the I3-01 monomer (Figure 3.10B).

3.3.5 Insertion of the trimeric bacterial antigen NadA into I3-01

The first meningococcal antigen to be inserted was NadA, an antigen that is a component of 4CMenB, the current licensed MenB vaccine [192]. NadA has previously been engineered into the HBc VLP, suggesting its structure is amenable to being displayed on an engineered particle in a repetitive pattern (Dr Murtala Jibril- unpublished work). Three different constructs were designed, inserting NadA at both termini of I3-01 and also incorporating a truncated form of NadA into the N-terminal region of I3-01-CP-N148 (Figure 3.12A). NadA is a trimer that forms a coiled-coli formation; it was important to consider how this would assemble when attached to I3-01.

3.3.6 Insertion of the bacterial antigen NHBA into I3-01

A second antigen, Neisseria heparin-binding antigen (NHBA), was selected to be inserted into I3-01. NHBA is also a component of 4CMenB so was a good candidate antigen to insert as it has been approved for use in a current licenced vaccine [202]. Since NHBA has a β-barrel structure, this may be incorporated more easily into I3-01 than NadA which forms a coiled-coil trimer. The I3-01-CP-N148 construct had termini which were more surface exposed than I3-01, so this was the scaffold selected and specifically the N-terminus was the site for insertion (Figure 3.12B).

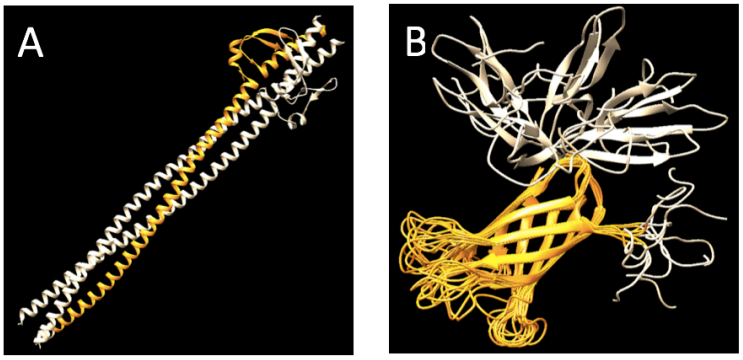

Figure 3-12. Structures of the antigens inserted into I3-01. (A) NadA was inserted into I3-01. The truncated version of trimer forming NadA was inserted to form NadA-I3-01-CP. The yellow colour highlights the specific section inserted (6eun.PDB) (B) NHBA was inserted into I3-01. The ß-barrel section of NHBA was inserted into I3-01 (NHBA in yellow), the sequence was designed, inserting only the region encoding the ß-barrel section of the antigen (2lfu.PDB).

3.4 Expression and purification of engineered I3-01

In total, nine constructs were designed, cloned, expressed and purified following the same methodology as I3-01 (Figure 3.13). These can be split into two groups; scaffold adaptions including I3-01 T40S, I3-01-CP-G60 and I3-01-CP-N148 constructs (Table 3.1 rows 3-5) and scaffold insertions including ovalbumin, NadA and NHBA (Table 3.1, rows 6-11). I3-01-T40S, I3-01-CP-N-148, both I3-01-Ovalbumin (OVA) constructs and I3-01-NadA performed during expression and purification as I3-01 (Table 3.1). Following expression in Clearcoli^{TM} at 37°C, they were all purified as the native I3-01 construct. These proteins will be analysed further in section 3.5. The remaining constructs of I3-01-CP-G60, NadA-I3-01, NadA-I3-01-CP and I3-01-CP-NHBA did not express and purify as the native I3-01 protein. This was either due to low expression in Clearcoli^{TM} or that, when purified, a homogeneous population of assembled particles was not formed. The aim of this section is to discuss these constructs further to give a clearer understanding into the modifications that cannot be supported by I3-01.

Construct Name	Construct Design
I3-01	
I3-01-T40S	
I3-01-CP-G60	
I3-01-CP-N148	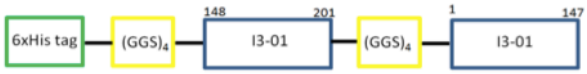
I3-01-OVA1 I3-01-OVA11	
NadA- I3-01	
I3-01-NadA	
NadA- I3-01-CP (Truncated NadA)	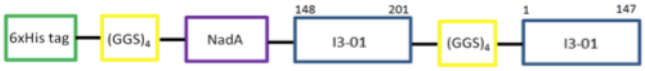
I3-01-CP-NHBA	

Figure 3-13. Schematic illustrations of engineered I3-01 assemblies.

Construct	Cloned?	Expression in T7?	Expression in ClearColi™?	Purified?
I3-01	Yes	Yes	Yes	Yes
I3-01-T40S	Yes	Yes	-	Yes
I3-01-CP-G60	Yes	Yes	No	No
I3-01-CP- N148	Yes	No	Yes	Yes
I3-01-OVA1	Yes	Yes	Yes	Yes
I3-01-OVA2	Yes	Yes	Yes	Yes
NadA-I3-01	Yes	Yes	No	No
I3-01-NadA	Yes	Yes	Yes	Yes
NadA-I3-01-CP (Truncated NadA)	Yes	Yes	Yes	Yes
I3-01-CP-NHBA	Yes	Yes	Yes	Yes

Table 3-1. Summary of the expression and purification of I3-01 assemblies. A total of 9 constructs were designed, only I3-01-CP-N148 could not be expressed in T7 *E.coli* and only I3-01-CP-G60 and NadA-I3-01 could not be expressed in ClearColi™. Of the proteins successfully expressed, all were purified following the method used for the native I3-01 construct.

3.4.1 Constructs with low Clearcoli™ expression: I3-01-CP-G60 and NadA-I3-01

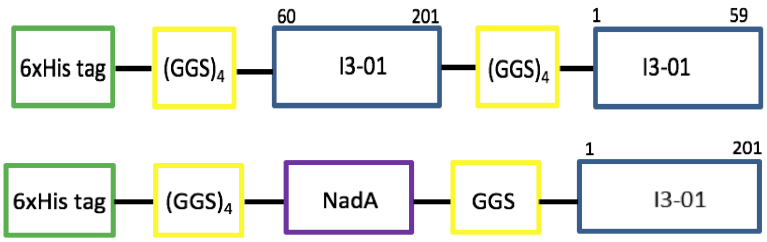

Protein overexpression from I3-01-CP-G-60 and NadA-I3-01 was tested on a small scale in two different cell lines, T7 express competent *E.coli* and ClearColi™. Expression trials were run and the supernatants (soluble fraction of protein expression) were analysed by SDS-PAGE. It was clear that there was soluble protein produced when I3-01-CP-G-60 was overexpressed in T7 express competent *E. coli,* but that in ClearColi™ there was only a small amount of soluble protein overexpressed (Figure 14A). As the ClearColi™ cell line is the more important and expression appeared to be poor, the I3-01-CP-G60 construct was not selected as the construct

of choice for the circular permutation modification. The NadA-I3-01 construct was overexpressed in T7 express competent *E. coli* cells but not in the ClearColi^{TM} cell line, therefore the focus moved towards the alternative NadA fusions (Figure 3.14B).

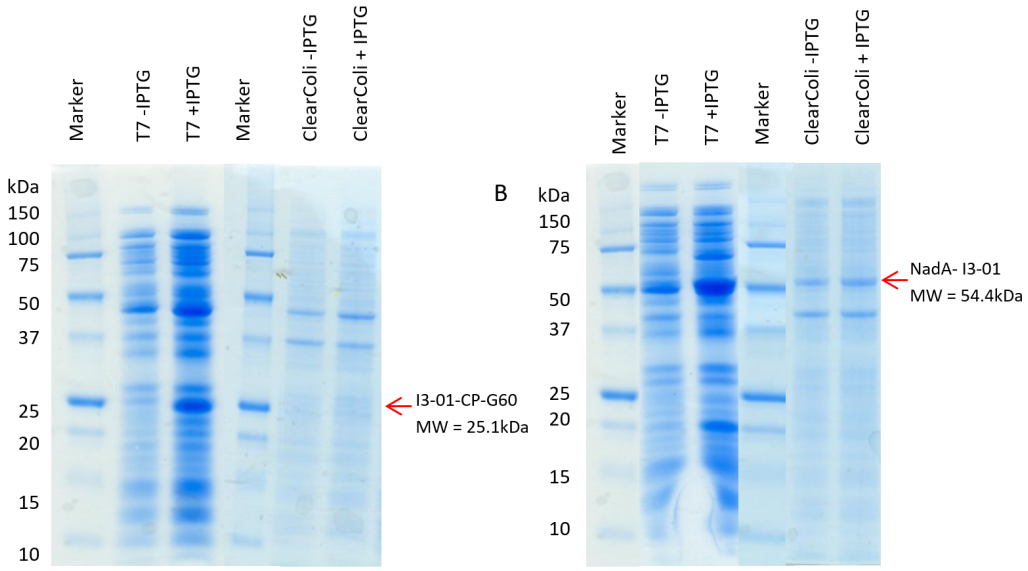

Figure 3-14. SDS PAGE of small scale overexpression trials of I3-01 constructs with low Clearcoli^{TM} expression. (A) Small scale overexpression analysis of I3-01-CP-G60. (B) Small scale overexpression analysis of NadA-I3-01. Small scale overexpression trials which ran for 3 hrs at 37°C following induction with 0.4mM IPTG were carried out in both the T7 express competent *E.coli* and ClearColi^{TM} cell lines. Samples before and after IPTG induction were analysed by SDS-PAGE. I3-01-CP-G60 MW= 25.1kDa and NadA-I3-01 Mw= 54.4kDa.

3.4.2 NadA-I3-01-CP

In the NadA-I3-01-CP construct the I3-01-CP-N148 protein was used as the scaffold and a truncated form of NadA encoding only the coiled-coil portion of the antigen was inserted. The N-terminal region was the location selected to try to ensure surface exposure and ensure that the NadA antigen was presented in the correct orientation. NadA-I3-01-CP was cloned into pET29A (+) and soluble protein overexpression was induced in the T7 express competent *E.coli* and ClearColi^{TM} cell lines. Following expression and purification, the SEC revealed that the protein eluted in the void volume (Figure 3.15A). However, the SDS-PAGE run of the peak

samples showed the protein in the peak was not a single monomer of NadA-I3-01-CP (MW= 41kDa) (Figure 3.15B). There were two further bands, one of which appeared to be the same size as the I3-01 native monomer (23.8kDa) and another which seemed to fall in the middle as an intermediate species (30kDa) [203]. This suggested there was some degradation of the protein assembly and only a fraction was assembled with NadA attached (~30%). In an attempt to increase the amount of NadA-I3-01-CP purified, the protein was expressed for 16 hrs at 16°C but this reduced the amount of soluble protein produced and was not a good expression method for this construct.

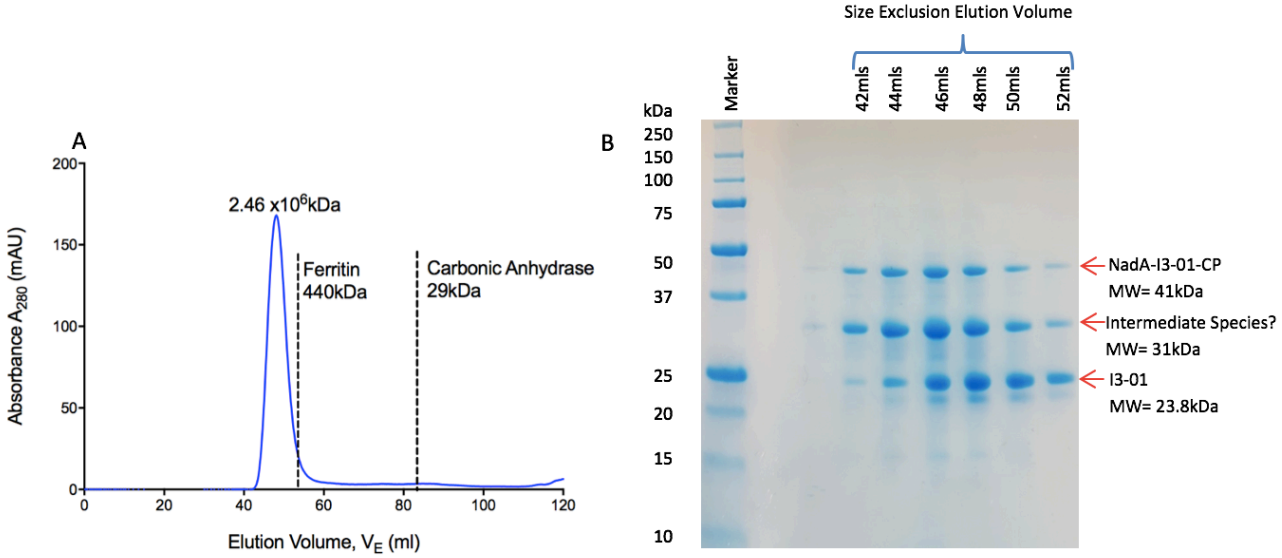

Figure 3-15. SEC purification of NadA- I3-01-CP from ClearColi^{TM} cells. (A) UV absorption profile of NadA-I3-01-CP eluting from a SEC column. NadA-I3-01-CP cell pellets were purified using a 5ml HisTrap column and rising concentrations of imidazole in lysis buffer containing 50mM Tris-HCl pH 8.0 and 500mM NaCl. Fractions containing 500mM imidazole were concentrated to a 5ml loading volume and were run on a Sepharose 200 column at 1ml/min. (B) SDS-PAGE analysis of NadA-I3-01-CP eluted from a SEC column. A volume of 10µl of each of the protein fractions purified by SEC (between the elution volumes of 45-55mls) were run on a 10% SDS-PAGE, the MW of the NadA-I3-01-CP monomer is 41kDa.

As the overexpression at 37°C gave three protein bands in the SEC peak an effort was made to identify the component proteins. A Western blot was performed which showed two His-tagged bands at 41kDa and 31kDa, suggesting that the full length NadA-I3-01-CP and some form of intermediate of NadA-I3-01-CP were the species eluted rather than contaminants (Figure 3.16). Mass spectrometry was also used to identify the peptides and this confirmed all three bands were fragments of NadA-I3-01-CP.

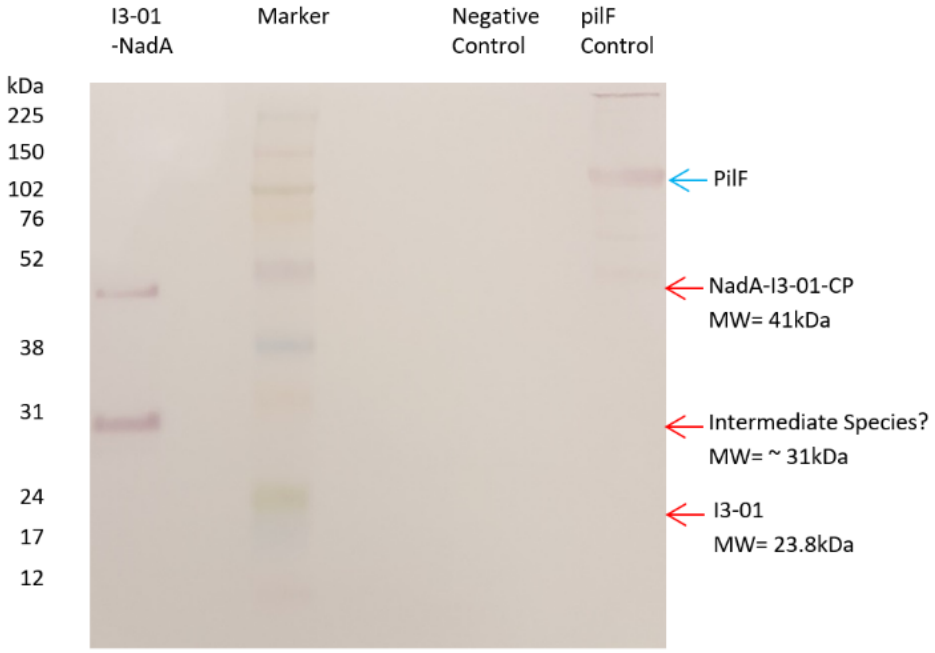

Figure 3-16. Western blot analysis of NadA-I3-01-CP. NadA-I3-01-CP was overexpressed at 37°C for 3 hrs following induction with 0.4mM IPTG, and was purified using a 5ml HisTrap HP column followed by SEC (Figure 3.15). Western blot analysis using a 10µl sample of NadA-I3-01-CP 1mg/ml, a non-His tagged protein and His-tagged PilF was carried out. NadA-I3-01-CP, NadA-I3-01-CP intermediate species and I3-01 monomer MWs are 41kDa, 31kDa, 23.8kDa respectively. PilF was run as a positive control and has a MW of 132kDa.

As the His-tag was linked to the NadA section of the protein, an anti-His-tag antibody that was gold labelled was incubated with NadA-I3-01-CP. The purpose of this was to label any assemblies which had NadA attached and to highlight the position of the attachment, which could then be visualised by electron microscopy. It was clear some particles were assembled

with 1 or 2 copies of NadA attached (Figure 3.17). However, there are also many assemblies with no gold label, suggesting they were assembled but the NadA portion had been cleaved. It was concluded that NadA was so sporadically inserted into assembled I3-01 that this construct could not be used further as a vaccine candidate.

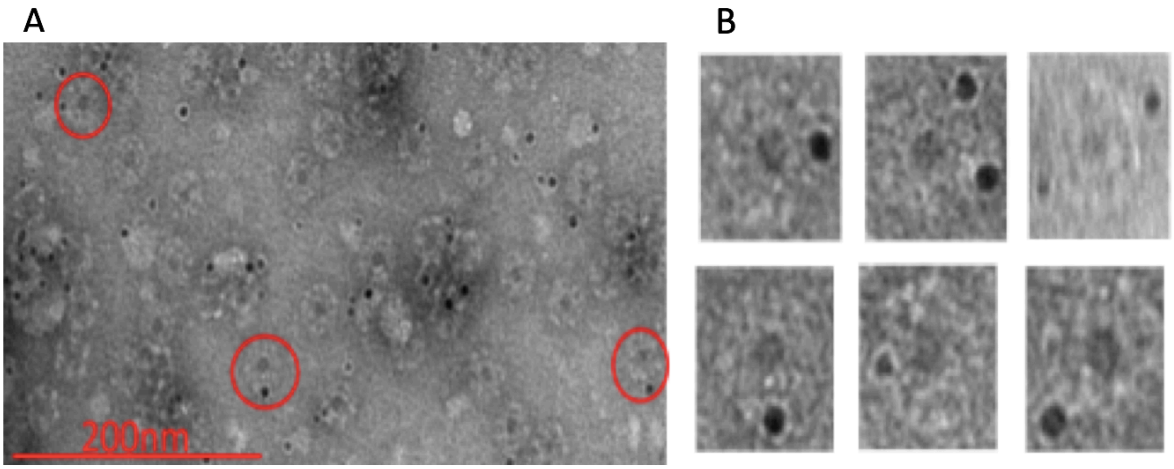

Figure 3-17. Negative stain electron microscopy analysis of NadA-I3-01-CP. (A) A sample of NadA-I3-01-CP was dialysed to 50mM Tris 500mM NaCl pH 8 and was diluted to 0.05mg/ml. The protein was incubated with a 5nm Ni-NTA-Nanogold® label for 2 hrs at 4°C. This was applied to a carbon coated grid following the negative stain protocol and was viewed on the FEI Technai microscope at 23000x magnification. (B) Individual gold labelled NadA-I3-01-CP particles were visualised to assess the orientation of the attached gold labels.

3.4.3 I3-01-CP-NHBA

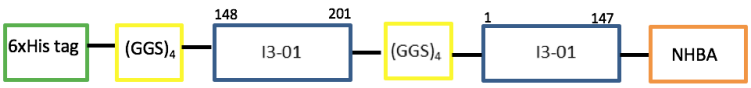

Following cloning into pET29A (+), the overexpression of I3-01-CP-NHBA was tested on a small scale in T7 express competent *E.coli* and ClearColi™ cells. The soluble fragment of protein overexpression was analysed by SDS-PAGE, I3-01-CP-NHBA was expressed in the soluble protein fragment when expressed in both cell lines. The overexpression was scaled up and the protein was purified but there were two bands present in the elution samples. One corresponded to the I3-01-CP-NHBA monomer and the other to the I3-01 native monomer. This suggested a

similar degradation effect occurred with this construct when it was expressed at 37°C as was seen with the NadA fusion construct.

In an attempt to stop this degradation, the ClearColi^{TM} expression was repeated for 16 hrs at 16°C. The protein was purified and the trace produced two small peaks. The larger peak was at the expected elution volume (30-40mls) and so these fractions were analysed by SDS-PAGE (Figure 3.18). This peak contained a low concentration of pure protein that was the correct size of the I3-01-CP-NHBA monomer (38.5kDa). This suggested that expressing under these conditions limited the degradation that was seen previously. Negative stain electron microscopy was used to examine the assembly status of I3-01-CP-NHBA following overexpression at 16°C. This revealed there were no assembled particles present and suggested the I3-01-CP-NHBA protein was not appropriate for use as a vaccine candidate (data not shown).

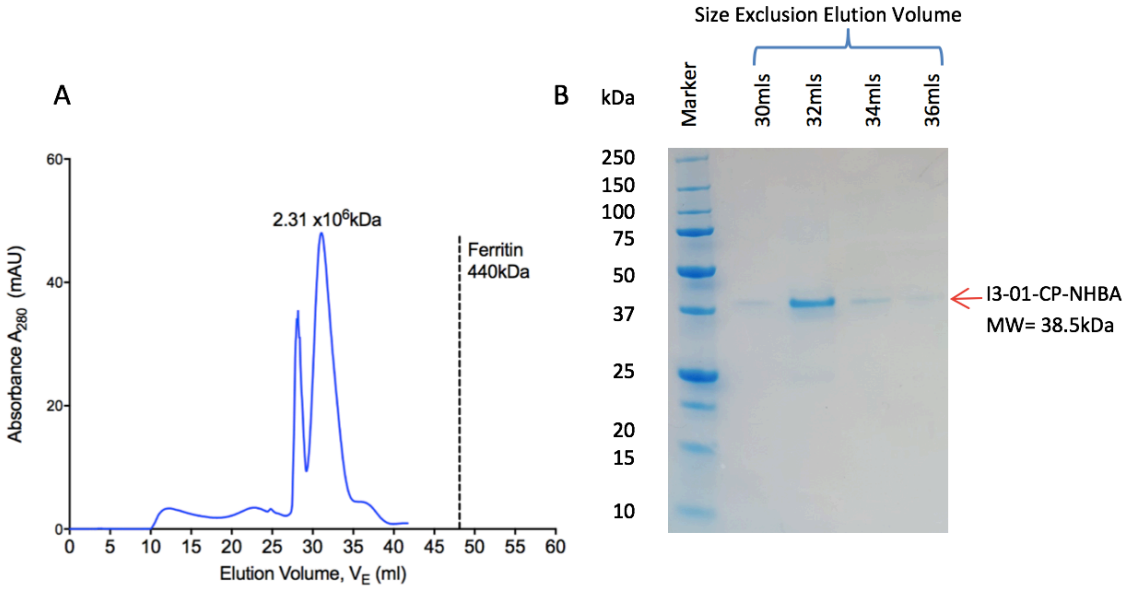

Figure 3-18. SEC purification of I3-01-CP-NHBA following overexpression in ClearColi^{TM} cells at 16°C. (A) UV absorption profile of I3-01-CP-NHBA eluting from a SEC column. Overexpression of I3-01-CP-NHBA was carried out at 16°C for 16 hrs following induction with 0.4mM IPTG and the cells were harvested. HisTrap purification was performed and the 10ml fractions containing 500mM imidazole were concentrated and run on SEC (B) SDS-PAGE analysis of I3-01-CP-NHBA eluted from a SEC column. Samples of 10µl volume of the SEC peak between 30-36ml elution volumes were analysed by SDS-PAGE. I3-01-CP-NHBA monomer has a MW of 38kDa

3.5 Characterisation of the purified engineered I3-01 forms

Five constructs were successfully expressed and purified in Clearcoli^{TM} (I3-01-T40S, I3-01-CP-N148, I3-01-OVA1, I3-01-OVA11 and I3-01-NadA); they were analysed for their homogeneity and stability in comparison to I3-01. All five constructs were originally analysed to confirm they had assembled correctly by negative stain EM (section 3.5.2) and if a homogenous population was not clear then DLS was used (section 3.5.3) to confirm if the constructs could be taken forward. Finally, the assembled constructs that were taken forwards were analysed for thermal stability in comparison to I3-01.

3.5.1 Analysis of I3-01 constructs by negative stain electron microscopy

I3-0-1-CP-N148

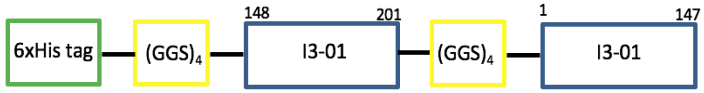

I3-01-OVA1/11

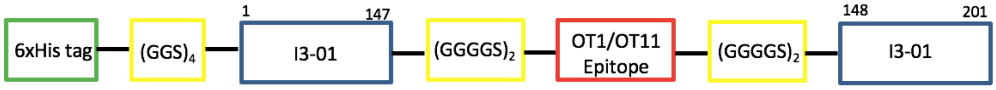

I3-01-NadA

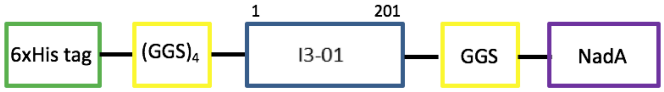

I3-01-T40S and I3-01-CP-N148 was studied in the same way as I3-01 and the particles in both samples appeared the same size as I3-01 and formed homogeneous populations (Figure 3.19A & B). This shows I3-01 is robust to those modifications. It was important that proteins with inserts were fully assembled following purification so that the epitopes were displayed on the surface exposed loops, according to the construct design. The I3-01-OVA constructs were analysed and it was clear that a population of assembled particles containing the ovalbumin epitopes had been purified (Figure 3.19C). This was the first demonstration that I3-01 could be

engineered to display an antigen epitope and still maintain its assembled state. Finally, I3-01-NadA was assessed to test if the purified I3-01-NadA protein was homogenous and correctly assembled. This showed a population that contained some assembled particles but also many aggregates and mis-assemblies; therefore, this construct was further analysed by DLS before a decision was made on its use in future experiments (Figure 3.19D).

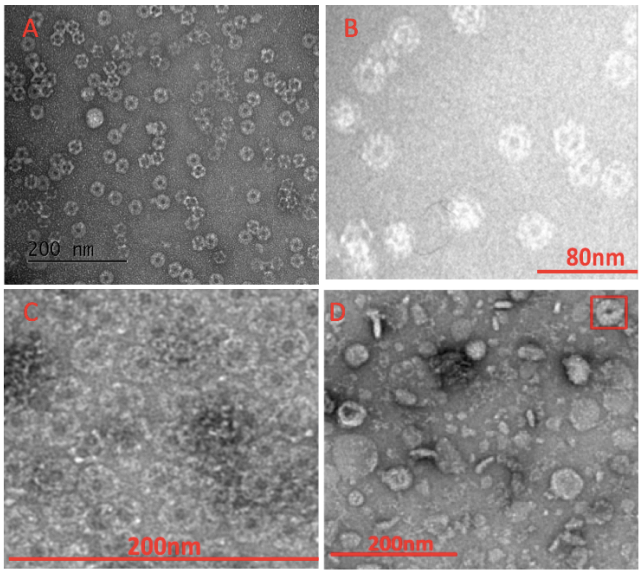

Figure 3-19. Negative Stain electron microscopy analysis of purified constructs. (A) I3-01-T40S at 0.3mg/ml, (B) I3-01-CP-N148 at 0.1mg/ml, (C) I3-01-OVA1 at 1mg/ml, (D) and I3-01-NadA at 0.3mg/ml in 50mM Tris, 500mM NaCl pH 8.0 were negatively stained with 2% UA. The samples were viewed on an FEI Tecnai 12 Biotwin microscope at either 23,000x (A and D) or 30,000x (B and C), magnifications respectively.

3.5.2 Analysis of I3-01 constructs by DLS

I3-01

I3-01-NadA

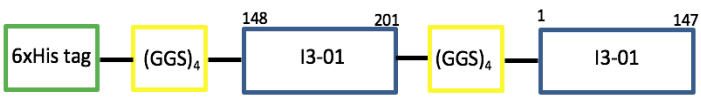

DLS was a second method used to assess the homogeneity of the I3-01-NadA sample, which by electron microscopy looked to be a mixed population of particles, to enable further clarification on its assembly status. The I3-01-NadA construct was analysed and the three separate runs each gave very different results, making an accurate Z-average diameter hard to interpret (Figure 3.20). This suggested that the sample had aggregated- in agreement with the electron microscopy data (Figure 3.19D). The most important parameter in terms of the whole population was the average polydispersity index and this was extremely large- 0.863. It was clear that insertion of NadA into the C-terminus of I3-01 led to the formation of heterogeneous samples and so this construct was not developed further.

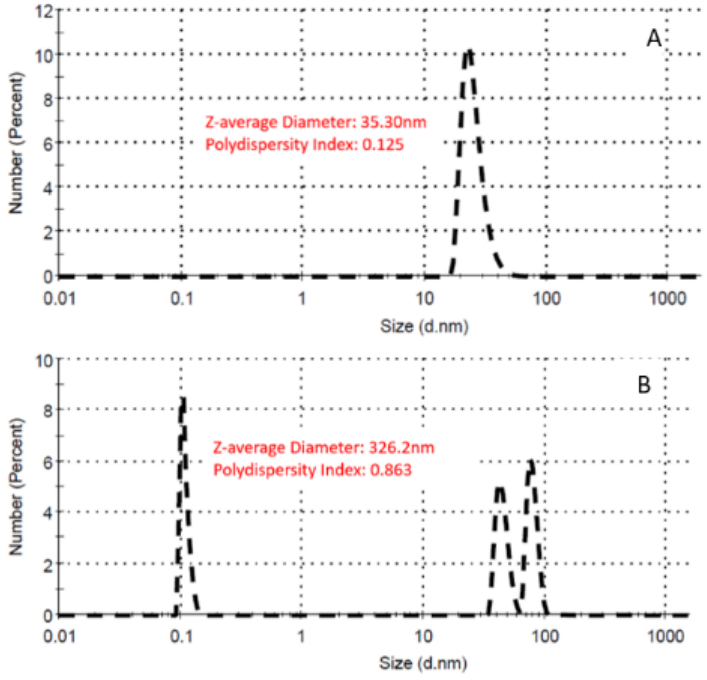

Figure 3-20. DLS analysis of I3-01 constructs. Samples of 100µl volume of (A) I3-01 (for comparison) and (B) I3-01-NadA at a concentration of 1mg/ml in PBS were centrifuged at 16,000 xg for 30 mins directly prior to adding to a cuvette in a Zetasizer DLS machine. A series of three measurements were taken and the average of each parameter; Z-average diameter and polydispersity index, was calculated.

3.5.3 Analysis of the thermal stability of I3-01 constructs

I3-01

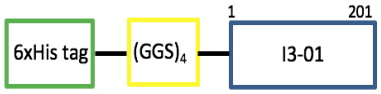

I3-01-T40S

I3-01-CP-N148

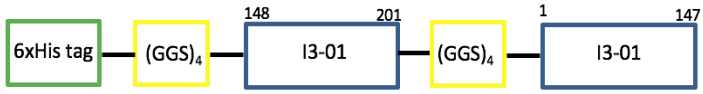

I3-01-OVA1/11

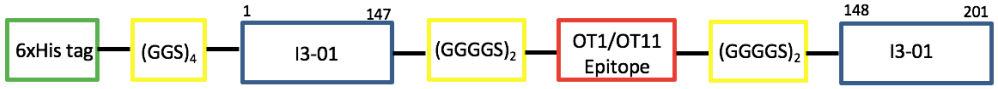

The thermal stability assay measured the melting temperature of the constructs following the addition of SYPRO orange dye over a temperature range of 25°C-99°C. As previously discussed, I3-01 had no detectable melting point, even at 99°C, indicating high thermal stability. It has been shown that the I3-01-T40S and I3-01-CP-N-148 constructs were assembled in ambient conditions, so the thermal stability assay was repeated in order to determine the melting temperature in these newly designed assemblies. The two assemblies were analysed and it was verified that much like I3-01, neither construct had a detectable transition point in this temperature range (Figure 3.20). Finally, the I3-01-OVA constructs were analysed to evaluate how the stability changed following epitope insertion. In this case, the melting temperatures were found to be 84.05°C and 86.45°C for the I3-01-OVA1 and I3-01-OVA11 constructs respectively (Figure 3.21). This observation indicated that the addition of ovalbumin epitopes did slightly reduce the stability of the I3-01 assembly, and that introducing a longer epitope decreased the stability by 2.4°C further than the smaller epitope. However, despite this, the melting temperature of both particles remained over 80°C.

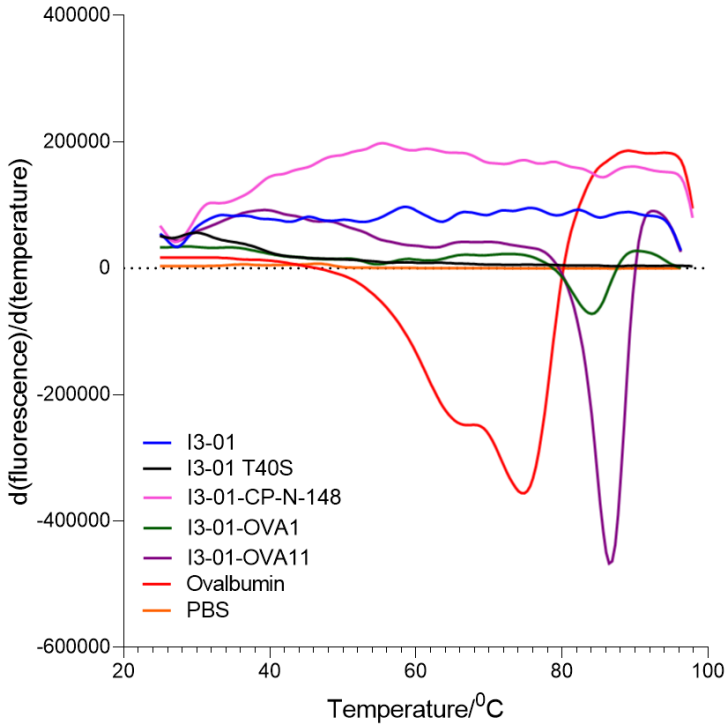

Figure 3-21. Thermal stability analysis of I3-01 constructs. A thermal stability assay was performed in triplicate using 15µg samples of I3-01, I3-01-T40S, I3-01-CP-N148, I3-01-OVA1 and I3-01-OVA11 and the melt curves were produced at a 1% ramp rate between the temperatures of 25°C-99°C. Ovalbumin and PBS were run as positive and negative controls respectively.

The endotoxin assay was repeated with the I3-01-OVA constructs and these were found to have endotoxin contamination under the 2ng/ml threshold [196]. It can be concluded that purification of I3-01-OVA constructs from ClearColi^{TM} cells produces protein which was not contaminated with endotoxin and could be used in our studies.

3.6 Discussion

The aim of this chapter was to characterise a range of modified I3-01 assemblies and therefore to establish to what extent this platform is amenable to engineering. These modifications range from simple single residue mutations to whole antigen insertions. I3-01 was selected to be examined as a potential vaccine scaffold in this project for two main reasons. Firstly; this platform was designed to form a 25nm particle with icosahedral symmetry which is the most complex structure produced to date [134]. This symmetry and size mimics a natural immunogenic virus structure, much like VLPs, which are currently used as antigen presentation platforms [188, 204]. Secondly, I3-01 has been designed using trimers of the thermostable enzyme 4-hydroxy-2-oxoglutarate aldolase isolated from *Thermotoga maritima.* The potential of I3-01 to be used as a therapeutic is enhanced by the reported stability of the assembly at high temperatures (up to 80°C) which may overcome possible cold chain issues that commonly arise in vaccine distribution [134].

It is important to evaluate I3-01 as a potential vaccine platform based on the new knowledge gained in this chapter in terms of its structure, characteristics and ability to present antigens. Whilst considering this, it is also crucial to evaluate the methods used to produce these fusions for use as vaccine candidates.

3.6.1 I3-01 as a potential therapeutic

The designers of the I3-01 assembly performed some initial analysis of the proteins structure and stability. However, it was important to verify and even improve on these details before any modifications were designed. The cryoelectron microscopy structure produced by the designers was restricted to 20Å resolution- an attempt was made to improve on this and to confirm the protein produced closely matched the calculated model [134]. The cryoelectron microscopy structure presented in this work was at 7.68Å with 0.97 correlation when mapped to the designed model. This revealed that when I3-01 was produced in Clearcoli^{TM}, it assembled according to the construct design. DLS was used to enable quantification of the particles size and homogeneity, in order to provide additional details of native I3-01 for comparison with future genetic fusions. The results indicated an extremely homogenous I3-01 sample. The

homogeneity of a vaccine formulation is essential to ensure each dose contains an equal amount of the active ingredient. This feature of the I3-01 assembly was measured in all of the fusion constructs to ensure this characteristic was maintained.

The thermal stability of I3-01 was an important property feature of this protein scaffold; this property therefore needed validation following the verification of assembly when expressed in Clearcoli^{TM}. The measurement also provided a baseline for the level of thermal stability against which the fusion constructs could be measured. A thermal shift assay with SYPRO Orange was used to measure the melting temperature of I3-01. This assay was used as it is a high-throughput, low cost, established method for detecting the melting points of proteins [205]. No melting point was found for I3-01, supporting the claim made by the designers that the assembly was stable to at least 80°C.

Finally, as this protein assembly is not natural, it was imperative to test if it contained any predicted human or mouse T cell epitopes. This would help to gain an understanding of the immunogenicity of I3-01 before any antigen was added. The IEDB-AR was used to predict epitopes from the I3-01 sequence. This database represents the adaptive immune responses to epitopes from around 1.6 million experiments and is updated every two weeks so is a reliable and up to date source [206]. In order to decide what threshold would define a sequence as being a potential epitope, the HBc VLP sequence was entered. The HBc-VLP is currently in clinical use so the most potent epitope predicted from the sequence, the MIR, was used as the threshold for defining what would be considered a particularly powerful epitope in I3-01 [207]. Five possible epitopes were discovered but only one was significantly stronger than any sequence found in the HBc VLP. This sequence was found to interact with the human HLA-DRB3 allele with a binding score of 0.08. An effort was made to mutate the residues from within this epitope to reduce its potency and one mutation generated soluble protein. This alteration lowered the strength of the T-cell epitope (from 0.08 to 0.14); the assembly status and thermal stability of I3-01 was maintained, as verified by negative stain electron microscopy and a thermal shift assay.

3.6.2 I3-01 as an antigen scaffold

Having confirmed I3-01 could be used as a potential therapeutic in terms of its inherent properties, an evaluation of the ability of this assembly to support mutations and antigen insertions was conducted.

Circular permutation

Circular permutation is a phenomenon that occurs as a process of directed evolution: this method has recently been exploited by protein engineers to manipulate a protein's structure and function. The procedure involves breaking a peptide sequence to form new N and C-termini and joining the former termini with a linker. This method does not necessarily involve any amino acid substitutions but works purely on the basis of re-organisation of the native peptide chain. Circular permutation has direct effects on a protein's structure and function. The overall protein structure is often unaffected by circular permutation but this largely depends on the site chosen to insert the new termini and the design of the linker [208]. Structural integrity has also been found to be more likely to be maintained if the original termini are in close proximity [209].

An example of circular permutation is the engineering of the Candida antarctica lipase B (CALB) enzyme, a Lipase B from *Candida antarctica*. A total of 63 variants were produced through circular permutation and many of these had sustained or improved ability to catalyse a range of substrates over the wild type or mutants. The circular permutation was thought to make the active site of Lipase B more accessible, which either improves the turnover of the enzyme or the degree of local backbone flexibility to achieve the same effect [210].

A second example lies in the multiple attempts to introduce a circular permutation in Xylanase from *Bacillus circulans.* The N and C-termini were naturally in very close proximity and so only a couple of glycine residues were needed to join them together. The sites selected to form the new termini were, as for other examples, in the surface exposed loops. However, only a few successful sites were found in β-sheet regions of the protein's secondary structure. Surprisingly, in this example, catalytic residues were selected to act as the new termini and the deleterious effects on the enzyme activity were minimal. In some cases, even improved catalytic ability was

observed. Local changes to mobility of the protein in the linker and termini regions were noted, but the overall global protein changes were minimal. One major change observed was a decrease in thermal stability of the protein following circular permutation compared to the monomer [211].

These examples provided useful information to guide the process of the circular permutated I3-01 construct design. The TIM-barrel fold of I3-01 is a structure known to be robust to circular permutation, and has even be found to be a naturally occurring process in these structures [212]. Based on the evidence presented thus far, the surface exposed loops were an optimal location to insert the new termini. The literature here also supports the fact that the circular permutation is most likely to least affect the overall structure of a protein if the termini were in close proximity, which was the case for I3-01. This gave reason to believe I3-01-CP-N148 would be successful. Circular permutation of I3-01 at residue N-148 yielded soluble protein which assembled into particles in a homogenous population. This demonstrates that circular permutation of I3-01 produce new termini which were more surface exposed and therefore enable the display of various antigens. Thermal stability was also maintained and this provided further support as to the I3-01-CP-N148 constructs applicability to form the basis of a vaccine candidate.

Ovalbumin epitope insertion

Ovalbumin epitopes have been inserted into many self-assembling proteins previously to allow the assessment of T cell responses. A range of self-assembling proteins have been utilised in this way and the first example of this is the use of VLPs from the Hepatitis B virus surface antigen (not the Hepatitis B virus core antigen VLP previously discussed). The ovalbumin epitopes that stimulate OT-I and OT-II responses were inserted into the C-terminus of the VLP of the Hepatitis B virus surface antigen. The assembly status of these particles was not confirmed but the large cytotoxic T lymphocyte responses measured suggested the epitopes were successfully displayed [213]. A similar result of successful display of ovalbumin epitopes was confirmed when the OT-I epitope, SIINFEKL, was inserted into murine polyomavirus VLPs. Protective

responses were produced following display by this method [214]. Finally, VLPs from the rabbit haemorrhagic disease virus were used to display the OT-I epitope SIINFEKL to assess the responses produced. Assembly of the particles with these epitopes inserted was established using negative stain electron microscopy. No difference between the native VLPs and the constructs with either ovalbumin epitope inserted was observed [215].

The literature suggests that these epitopes can be inserted into self-assembling structures to assess T cell responses. The results presented here confirmed that I3-01 is able to display these epitopes and maintain assembly and homogeneity across the population. A further point to note in this case, is that thermal stability only reduces slightly following the insertions (melting temperatures remain over 84°C), a factor not measured in previous studies. This was important to consider as thermal stability was a key design feature of this synthetic self-assembling protein.

Meningococcal antigen insertion

The process of fusing larger antigens to I3-01 proved to be more problematic. Insertion of NadA into the N-termini appeared to yield soluble protein in T7 express competent *E.coli,* but when overexpression was carried out in the ClearColi^{TM} strain this was not the case. This was the strain of choice as vaccine candidates produced in a bacterial cell line must be endotoxin free, a feature found in this strain of *E.coli*. It appeared the NadA-I3-01 fusion protein was most likely insoluble due to incorrect folding when expressed by this method in this bacterial system, leading to an alternative site for insertion being selected.

Both the N and C-termini of I3-01 have been used successfully as insertion sites for GFP with verification of assembly following this engineering by electron microscopy [134]. Given this was the case, the next insertion site selected for NadA was the C-terminus of the protein. Unfortunately, electron microscopy analysis showed an aggregated population of particles, with only a couple of individual assemblies being visualised. DLS confirmed a heterogeneous

population of I3-01-NadA. This location of the insertion of the NadA antigen had clearly led to protein aggregation; this construct was taken no further as a possible vaccine candidate.

A truncated version of NadA was incorporated (removing 140 residues from the C-terminus of the previous NadA sequence used), to leave only the trimer-forming coiled-coli section of the protein. The rationale behind this was to try to encourage assembly formation through inserting a trimer-forming structure onto an assembly which was also built from trimers. The expressed and purified assembly was found to incorporate NadA, but is then subjected to posttranslational proteolysis. The lack of uniformity to this construct, in terms of I3-01's ability to incorporate NadA, renders it inappropriate for further vaccine development.

A second meningococcal antigen, NHBA, also in the current 4CMenB vaccine formulation, was fused to I3-01 to further probe I3-01's ability to perform as an antigen presenting platform. This antigen was selected as it had a very different structure to NadA so may have overcome any potential steric clashes that had hindered previous antigen incorporations into I3-01. However, upon scaling up and purifying I3-01-CP-NHBA, the same degradation and aggregation effects were seen as with the I3-01-NadA construct, even upon altering the expression conditions. This was a second example of I3-01 not being able to present antigens effectively when incorporated through a genetic fusion.

3.6.3 Summary

In summary, I3-01 is amenable to circular permutation and the insertion of small epitopes but has thus far been unable to incorporate whole antigen domains. The HBc VLP has been shown to display the same ovalbumin epitopes and maintain assembly, but it is unclear if it is as stable as I3-01 [213]. Previous members of this group have successfully inserted NadA into the HBc VLP and this has not been possible with I3-01 [163]. The inability to present whole antigens is a major limitation of I3-01 in comparison to the HBc VLP platform. The reason for this inability is not clear but there are a couple of limiting factors. The site of antigen insertion is important, the MIR region is well defined as an optimal position in the HBc VLP but there isn't such a site

in I3-01 [207] . The structure of I3-01 is very open and it may be that an inserted antigen has fallen inside the cage-like structure and has interfered with the assembly in this way. A summary of each construct is presented in Table 2.

Construct	Cloned?	Expression in T7?	Expression in ClearColi™?	Purified?	Assembled?	Homogenous Population?	Thermally Stable?	Endotoxin Free?
I3-01	Yes	Yes	Yes	Yes	Yes	Yes	Yes	Yes
I3-01 T40S	Yes	Yes	-	Yes	Yes	Yes	Yes	-
I3-01-CP-G60	Yes	Yes	No	-	-	-	-	-
I3-01-CP-N148	Yes	No	Yes	Yes	Yes	Yes	Yes	-
I3-01-OVA1	Yes	Yes	Yes	Yes	Yes	Yes	Yes	Yes
I3-01-OVA2	Yes	Yes	Yes	Yes	Yes	Yes	Yes	Yes
NadA-I3-01	Yes	Yes	No	-	-	-	-	-
I3-01-NadA	Yes	Yes	Yes	Yes	Yes	No	-	-
NadA-I3-01-CP (Truncated NadA)	Yes	Yes	Yes	Yes	Yes	No	-	-
I3-01-CP-NHBA	Yes	yes	yes	yes	No	No	-	-

Table 3-2. Summary of I3-01 constructs. A '– ' in the table indicates this was an undetermined feature of the construct.

3.6.4 Evaluation of the suitability of I3-01 for use as a vaccine scaffold

A key hurdle following the production of a vaccine is delivering them to where they are needed and keeping them at the correct temperature (between 2-8°C). It was found that in shipments alone, up to 35% of vaccines are exposed to freezing [216]. This is clearly a major problem and the thermal stability of I3-01 offers an opportunity to deliver vaccines without the risk of freeze-thaw to the formulations, which may affect their efficiency and therefore the cost effectiveness.

A limitation of many current vaccines is the requirement for repeat doses [217]. The fact that I3-01 spontaneously forms cage-like assemblies allows any antigen inserted to be displayed multiple times on a single particle. This would increase the number of antigens displayed to the immune system at any one time. This multiple antigen array approach of vaccination may perhaps enable the production of a vaccine that requires fewer doses [218]. This would overcome some of the typical practical and economic problems associated with vaccine design.

Another consideration in the design of vaccines is the use of adjuvants. The storage of these as part of a vaccine formulation could lead to problems such as aggregation during freeze thaw, so an ideal vaccine would not need an adjuvant present. The VLP has been described as a natural adjuvant as it is not only a vehicle for antigen display, but also stimulates a strong immune response [219]. Specifically, the HBc VLP has been used in a vaccine formulation against Hepatitis B without an adjuvant and this elicited both neutralising antibodies and potent T cell responses [203]. If this effect can be replicated in the thermostable I3-01 then this could also form the base of a vaccine without the need for adjuvant.

The ClearColi^{TM} bacterial expression system has the advantage of being an *E. coli* cell line which is inexpensive and easy to culture. However, producing therapeutic proteins in a bacterial expression system poses the risk of endotoxin contamination, so LPS removal is an essential process. To overcome this issue whilst still gaining the advantage of using a bacterial expression system, the ClearColi^{TM} strain was used. ClearColi^{TM} contains genetically modified LPS that does not cause an endotoxic response in human cells [165]. In addition to using this expression system, all equipment and materials used in this process were soaked in 1M/0.5M NaOH. This ensured the use of communal equipment did not lead to endotoxin contamination. We have used a HEK-blue cell assay to determine the level of endotoxin contamination in proteins produced in ClearColi^{TM} and this has shown the expression methods used here produces protein that is suitable for vaccine use in terms of its contamination levels. However, purification in this expression system gives poor yields of protein (~2.5mgs/L of cells). In terms of scalability, this is a potential problem and investigation may be needed into more efficient expression systems that still produce endotoxin free protein such as the use of yeast or insect cells.

6.3.5 Summary of I3-01 as a vaccine scaffold for therapeutic use

In summary, I3-01 is a well characterised protein assembly with icosahedral symmetry which is extremely thermostable. The structure has also been found to be amenable to single mutations, circular permutation and ovalbumin epitope display, with limited effects on the overall stability of the construct. However, unlike the HBc VLP. It has so far not been not possible to successfully genetically fuse larger antigens to the surface of the I3-01 assembly. So even though this

construct has the advantage over the VLP of extreme thermal stability, its inability to display antigens is a limiting factor as a vaccine candidate. Therefore, an alternative method of fusing antigens to this scaffold is required to take this protein forward as a potential vaccine.

Chapter 4

Design, purification and functionality of the I3-01 Protein A fusion construct

Chapter 4 - The design, purification and functionality of the I3-01 Protein A fusion construct

4.1 Introduction

The work presented in Chapter 3 demonstrated that genetically fusing whole antigens to I3-01 led to protein aggregation and disruption of the assembly. The focus of this chapter was to explore a different method of attaching antigens to I3-01 following the assembly of the native particles.

Protein A is a 42kDa cell wall component of *Staphylococcus aureus* that comprises 5 homologous domains that are known to bind human IgG [220, 221]. The protein is small and stable and is used in multiple biotechnological processes. These include uses in both antibody production and diagnostic sensors [221]. Structural studies initially revealed that the protein consisted of four Fc-binding regions: A; B; C; and D [222]. In fact, a fifth domain, E, has since been found to also bind human IgG at the Fc region [223]. The crystal structure of the Protein A B domain bound to polyclonal IgG at 2.8Ä resolution was solved in 1981 [224]. The B domain is a stable and compact three helix bundle which folds and unfolds extremely rapidly, making it an ideal candidate for protein engineering [225].

Fc-fusion proteins comprise the Fc domain segment from an immunoglobulin chain bound to a particular protein of interest [226]. The introduction of these proteins as a form of therapy is one of the major breakthroughs in the field of designing novel protein based drugs over the last decade. These therapeutics have been used to successfully treat a range of conditions from organ rejection to Rheumatoid Arthritis [227, 228]. There are two main reasons that make Fc-fusion proteins extremely effective. Firstly, the presence of the Fc domain specifically increases the plasma half-life of the protein, maximising the therapeutic potential of any drug administered [229]. The second reason is that the Fc-domain can be specifically targeted to the Fc-receptors on antigen presenting cells, which is particularly useful in drugs targeted to cancer [230].

Ovalbumin was one of the first proteins to be purified and is the major protein in avian egg-white [231]. As this protein has been widely available for many years, it has classically been used as a model antigen in vaccine design studies. In this new era of vaccine design, ovalbumin has been used in multiple 'proof of principle' vaccine experiments. An example of this is the fusion of ovalbumin to polymers to form a repetitive antigen array; however this was shown to be ineffective without the addition of adjuvant [232]. Secondly fragments of ovalbumin were fused to nanoparticles that self-assemble to form antigen displays. These particles were found to produce an increase in antibody titre when displaying ovalbumin in this way [233]. The availability of transgenic mice with T cell receptors specific for the ovalbumin OT-1 and OT-11 epitopes, enables the levels of antigen specific proliferation of CD4+ and CD8+ T cells to be monitored [200, 201, 234]. This provides a good evidence base for selecting ovalbumin as a model antigen to fuse with I3-01.

In order to continue investigating I3-01 as a vaccine candidate, an alternative method of attaching antigens to the assembled particles was required. It was proposed the strong affinity of Protein A B domain for the Fc-region of IgG could be exploited as a novel form of covalent attachment (Figure 4.1). The antigen selected in this case was ovalbumin. However, in principle, this technology could be applied to attach any antigen to I3-01.

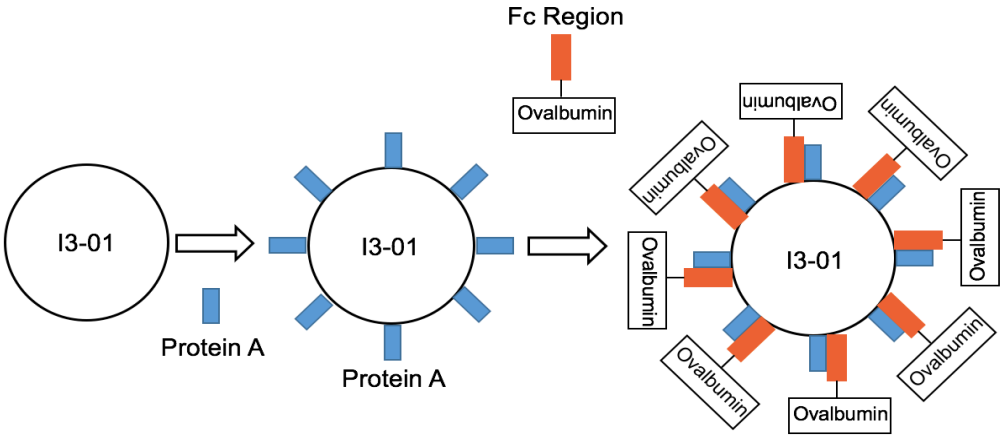

Figure 4-1 Novel Protein A fusion technology. The Protein A B domain could be fused to I3-01 in a surface exposed location and an antigen of choice would be fused to the Fc region of IgG. The free Fc regions would then bind to the Protein A domain fused to I3-01, attaching the antigen to the surface of the assembly**.**

The aim of this chapter was to design and produce an assembled I3-01-PA (Protein A) construct. There was reason to believe this would be successful as the Protein A B domain is small and stable in comparison to the previous larger antigen insertions that were attempted. It was important to characterise I3-01-PA and to establish any effects the insertion of the B domain of Protein A had on the homogeneity and thermal stability of the assembly. Following characterisation, the functionality of the Protein A domain was tested to demonstrate it successfully bound antibodies. The second key element of the work presented here was to produce the Fc-OVA fusion protein and to show this also bound to the I3-01-PA assembly with high affinity.

4.2 Design and purification of the I3-01 Protein A fusion construct

4.2.1 The design of the I3-01 Protein A fusion construct

The original I3-01 structure was used as the basis for the I3-01-Protein A fusion construct (I3-01-PA) as it has been successfully engineered previously to incorporate GFP at the C- and N-termini [134]. Specifically, the C-terminal of the I3-01 sequence was chosen as the insertion site, as this was surface-exposed within the whole assembly and in the individual trimers (Figure 4.2A & 4.2B). The IgG binding B domain of Protein A was selected for insertion as this was small and stable with a high affinity for IgG (Figure 4.2C) [225]. A short GGS linker was used to fuse the C-terminal of I3-01 to the N-terminal of Protein A.

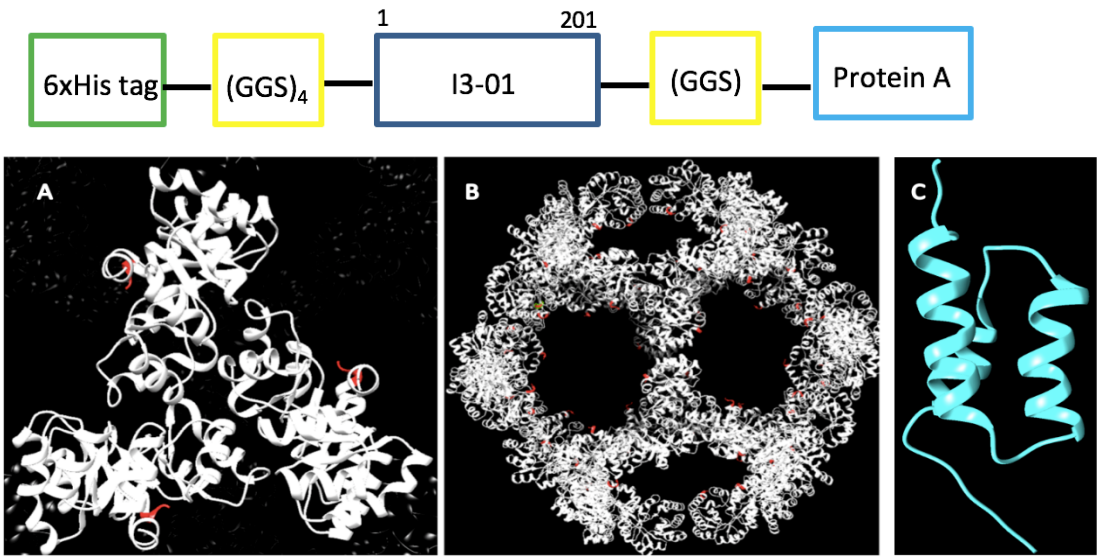

Figure 4-2. The design of I3-01-PA. (A and B) The selection of the insertion site. The C-terminus of the native I3-01 was selected as the insertion point for Protein A B domain due to its surface exposure, highlighted in red in the trimer (A) and whole assembly (B). (C) The structure of the B domain of Protein A. The B domain of Protein A is small containing 3 helices that form a compact bundle.

4.2.2 Expression and purification of I3-01-PA

To enable characterisation of I3-01-PA, the cloning process was carried out using the method in section 2.3 to ligate the DNA into the pET29A(+) vector, supplied by Novagen®. The expression of soluble protein from this construct was tested in the T7 and ClearColi™ *E.coli* cell lines using the method in section 2.4.1. The I3-01-PA protein was overexpressed in the soluble fraction in both cell lines, and the expression scaled up in ClearColi™ for 3 hrs at 37°C. The protein was purified using the same method as the native I3-01 in chapter 3, section 3.2.1. The size exclusion elution profile revealed that the sample was pure and eluted at the same position as the native I3-01 protein, between 40-60mls, in the void volume (Figure 4.3A). This suggested that assembled particles had been eluted. SDS-PAGE analysis confirmed the purity of the sample and that the protein was the correct size of I3-01-PA (monomer MW= 31kDa) (Figure 4.3B).

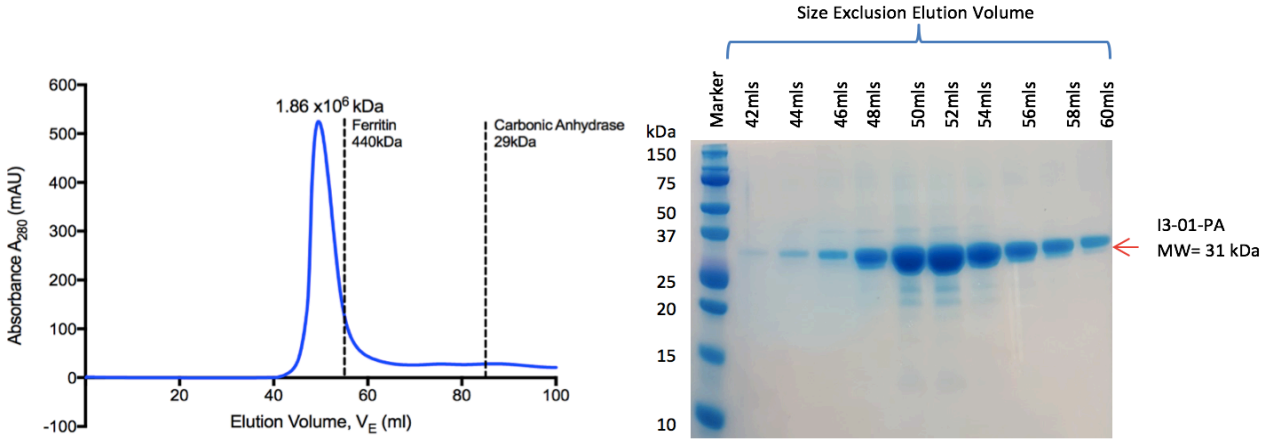

Figure 4-3. SEC purification of I3-01-PA from ClearColi™. (A) UV absorption profile of I3-01-PA eluting from a SEC column. I3-01-PA cell pellets were purified using a 5ml HisTrap column and rising concentrations of imidazole in lysis buffer containing 50mM Tris-HCl pH 8.0 and 500mM NaCl. Fractions containing 500mM imidazole were concentrated to a 5ml loading volume and were run on a Sepharose 200 column at 1ml/min. Fractions of volume 1.5mls were collected for further analysis. (B) SDS-PAGE analysis of I3-01-PA eluted from a SEC column. A volume of 10µl of each of the protein fractions purified by SEC (between the elution volume of 42-60mls) were run on a 10% SDS-PAGE, the MW of the I3-01-PA monomer is 31kDa.

4.3 Characterisation of I3-01-PA

4.3.1 Electron microscopy analysis of I3-01-PA

It was important to verify, following purification, that I3-01-PA correctly assembled to display Protein A on the surface of the particle in order to enable binding to IgG. A sample of I3-01-PA purified from ClearColi^{TM} cells was viewed by electron microscopy. A uniform population of assembled proteins was purified when I3-01-PA was expressed in ClearColi^{TM} (Figure 4.4A). These assemblies appeared to be the same size as native I3-01 proteins, suggesting the assembly was unaffected by the incorporation of the B domain of Protein A (Figure 4.4B).

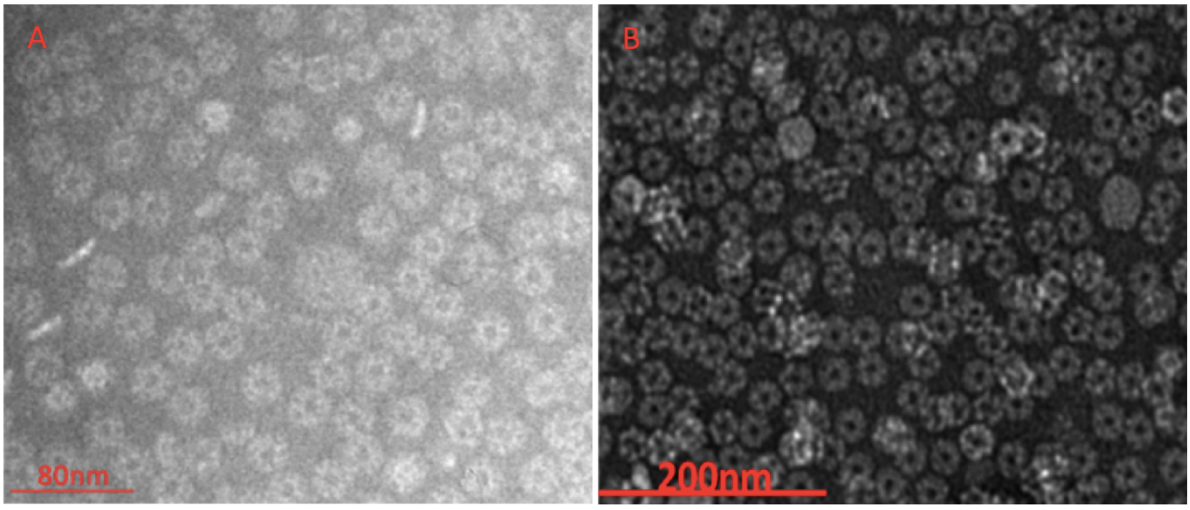

Figure 4-4. Negative stain electron microscopy analysis of I3-01-PA. (A) I3-01 and (B) I3-01-PA at 0.3mg/ml in 50mM Tris, 500mM NaCl pH 8.0 were negatively stained with 2% UA. The samples were viewed on an FEI Tecnai 12 Biotwin microscope at 23,000x magnification.

4.3.2 Analysis of I3-01-PA by DLS

DLS was carried out to measure the diameter of the I3-01-PA particles and to determine the homogeneity of the I3-01-PA preparation. The diameter was recorded as 34.3nm which was slighter smaller than the native particle, 35.3nm (Figure 4.5). This is unsurprising due to the compact nature of the Protein A B domain's structure. In terms of homogeneity, the

polydispersity index was measured at 0.167, which is comparable to the native I3-01 (0.125), suggesting a uniform population was present when this assembly was purified in PBS.

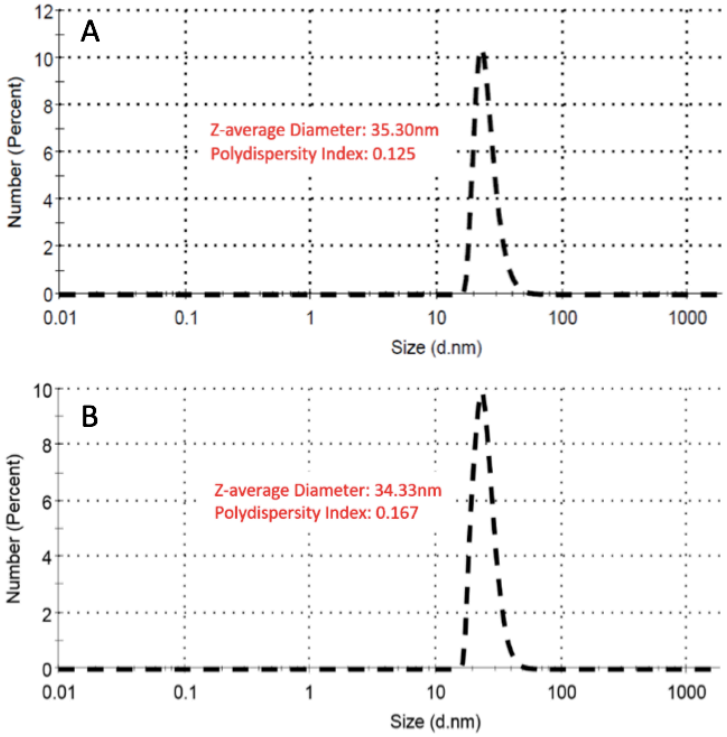

Figure 4-5. DLS analysis of the I3-01-PA construct. Samples of 100µl volume of I3-01 (A) and I3-01-PA (B) at concentrations of 1mg/ml in PBS were centrifuged at 16,000 xg for 30 mins directly prior to adding to a cuvette in a Zetasizer DLS machine. A series of three measurements were taken and the average of each parameter; Z-average diameter and polydispersity index, was calculated.

4.3.3 Analysis of the thermal stability of I3-01-PA

A thermal shift assay was run to further assess the stability of the I3-01-PA assembly, as the native I3-01 construct was previously shown to have no detectable melting point up to 99°C. The assay measured the melting temperature of I3-01-PA following the addition of SYPRO orange dye over a temperature range of 25°C-99°C. A denaturation curve was produced; the ovalbumin control had a melting temperature of 73.6°C, which was slightly lower than the previously reported value of 77.3°C [195]. The trace plotted for I3-01-PA shows no denaturation

transition occurred up to 99°C (Figure 4.6). This highlighted that the stability of the I3-01 native assembly was maintained upon the insertion of the Protein A B domain when purified in PBS.

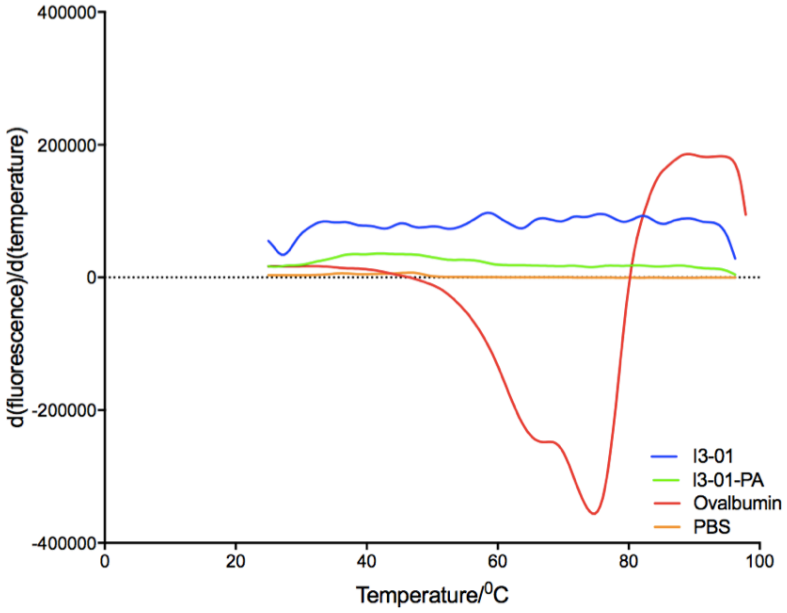

Figure 4-6. Measurement of I3-01-PA denaturation by Thermofluor assay. A thermal stability assay was performed in triplicate using a 15µg samples of I3-01-PA and a denaturation curve was produced at a 1% ramp rate between the temperatures of 25°C-99°C. Ovalbumin and PBS were run as positive and negative controls respectively and I3-01 was run for comparison.

Endotoxin levels of the purified construct were determined (section 3.2.5). An endotoxin level of 20 EU/ml is acceptable for use in vaccine design which equates to 2ng/ml [196]. The I3-01-PA samples had an average absorbance under the threshold equating to 2ng/ml. It can be concluded that purification of the I3-01-PA construct from ClearColi^{TM} cells produces protein that has limited endotoxin contamination and could be used in our studies.

4.4 Binding of I3-01-PA to antibody

4.4.1 The ability of I3-01-PA to bind IgG resin

I3-01-PA is a thermally stable construct which assembles into a homogenous population. However, it was now important to test if the Protein A was functional and could successfully bind to antibody. To test this, a sample of the protein was incubated with IgG Sepharose resin for 1 hr at 4°C. A series of washes and fractions were carried out and the resulting fractions were analysed by SDS-PAGE. This showed that the native I3-01 protein did not bind IgG as when it was applied to the resin, all of the protein was found in the wash fractions. However, I3-01-PA did bind IgG; when the protein was applied to the resin the protein was not present in the wash fractions but could be eluted (Figure 4.7).

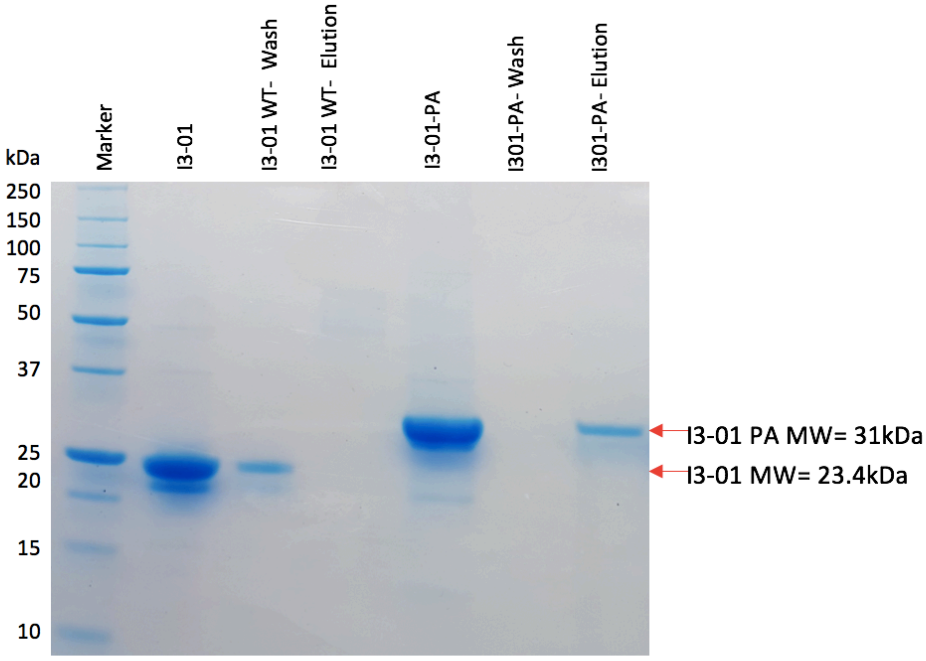

Figure 4-7. SDS-PAGE analysis of I3-01 and I3-01-PA binding IgG Sepharose resin. Native I3-01 and I3-01-PA were diluted to 0.2mg/ml in a 3ml volume and were applied to 2mls of IgG resin prepared in PBS. The samples were mixed for 1 hr at 4°C before a series of 2ml washes in PBS. The resin was then washed with 100mM citric acid pH 3.5 to elute any bound protein. The washes and fractions were then collected and were analysed by SDS-PAGE.

4.4.2 Quantification of the ability of I3-01-PA to bind specific antibodies

The Protein A domain incorporated into I3-01 has been shown to be functional by binding IgG resin. However, a quantitative method which would allow a precise binding affinity of I3-01-PA for specific antibodies was needed to allow the full binding potential of this construct to be realised. Bio-layer interferometry (BLI) is an effective analytical method that allows real-time monitoring of binding events, and has been previously used to determine binding affinities between antibodies and antigens in Ebola and Influenza vaccine research [235]. Two different antibodies were selected to be assessed, anti-CLEC9A, an anti-human antibody (IgG2A) and anti-CD40, an anti-mouse antibody (IgG1), both of mouse origin. BLI was performed to confirm the binding of I3-01-PA to anti-CD40 and anti-CLEC9A monoclonal antibodies; a specific workflow was followed using the ForteBIO Octet RED96 instrument and software version 11.1 (Figure 4.8).

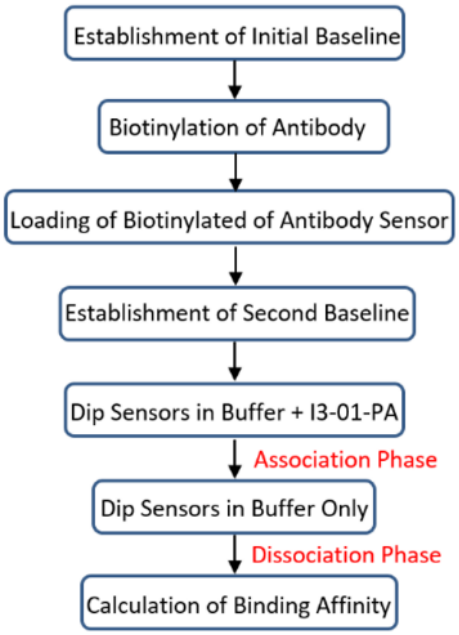

Figure 4-8. The BLI workflow. The process of determining the binding affinity of I3-01-PA for different antibodies and Fc-OVA antigen fusion protein was kept constant.

Each antibody was biotinylated through the coupling of EZ-link-NHS-PEG4-Biotin at room temperature, and any non-biotinylated protein was removed using a spin column. The sensors were first dipped into buffer and a baseline was recorded. The biotinylated antibodies were then loaded at 5µg/ml for 10 mins to establish a binding signal and the sensors were then

washed in buffer for 1 mins to allow a second baseline to be established. The I3-01-PA was then applied in 2-fold dilutions beginning at 20µg/ml and I3-01-PA binding both antibodies was observed. Finally, the sensors were dipped in buffer without the I3-01-PA protein for 10 mins, so the dissociation and therefore the binding affinity could be quantified (Figure 4.9).

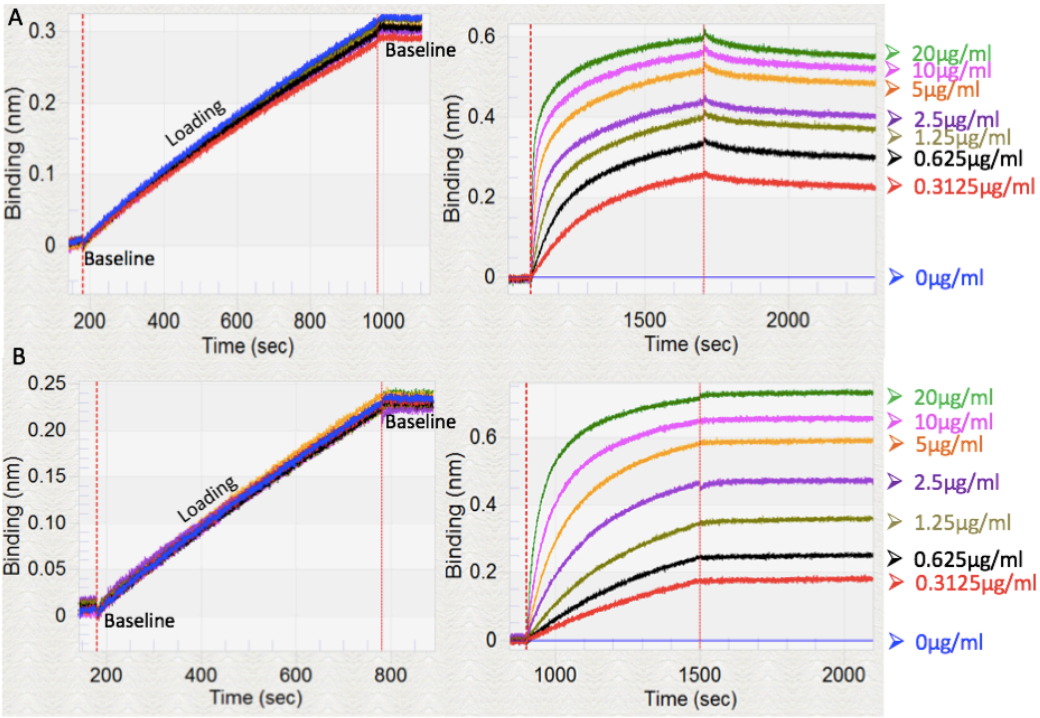

Figure 4-9. Bio layer interferometry analysis of I3-01-PA binding anti-human and anti-mouse antibodies. (A) I3-01-PA binding kinetics with anti-CD40 anti-mouse mouse origin antibody. (B) I3-01-PA binding kinetics anti-CLEC9A anti-human mouse origin antibody. The Octet RED96 instrument was used to perform the BIL. The left hand panels show the loading of the biotinylated antibody onto the sensors before a stable baseline was established. The right hand panels show I3-01-PA was then applied at a range of concentrations, showing varying binding strengths. The I3-01-PA protein was then removed for a 10-min dissociation phase, allowing the binding affinity to be calculated.

The dissociation phase of the analysis demonstrates a very high binding affinity of I3-01-PA for either antibody as very little loss in binding signal was observed. The specific equilibrium binding constants (K_D's) were calculated as $<10^{-12}$M for binding with anti-CLEC9A, and $<8 \times 10^{-12}$M for binding with anti-CD40, indicating strong binding and little dissociation. This forms a second piece of evidence that the Protein A B domain is functional and successfully binds antibody with high affinity when bound to the I3-01 assembly.

4.5 Design and purification of the Fc-OVA construct

4.5.1 The design of Fc-OVA antigen fusion

There were two parts of the fusion to consider in the design process- the Fc-region which would bind the Protein A B domain on I3-01, and the specific antigen that was displayed using this technology. The Fc-region selected was from the mouse IgG2A antibody, which has the highest binding affinity for the B domain of Protein A, giving the best chance of binding the I3-01-PA construct (New England Biolabs) (Figure 4.10A). Ovalbumin was selected to be fused by this technology and a short linker was placed between the two sequences (Figure 4.10B).

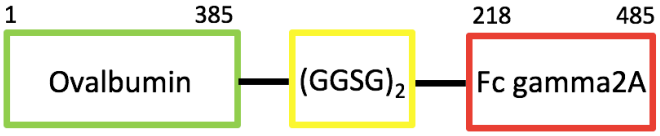

Figure 4-10. Fc-OVA construct.

4.5.2 Expression and purification of Fc-OVA

The expression and purification of Fc-OVA was carried out by Dr Edward McKenzie in the Manchester Institute of Biotechnology. The protein expression facility is well established to produce recombinant protein from insect cells [236]. Briefly, HI-5 insect cells were infected with protein P2 virus and the media was harvested post-infection. The protein was purified on a Protein A column and the elution fractions were neutralised, concentrated and further purified by SEC (Figure 4.11A). This gave single peaks at the correct predicted size for the dimers in each

case suggesting pure protein had been eluted and the peak fractions were confirmed to be Fc-OVA by SDS-PAGE (Fc-OVA monomer MW= 68kDa) (Figure 4.11B).

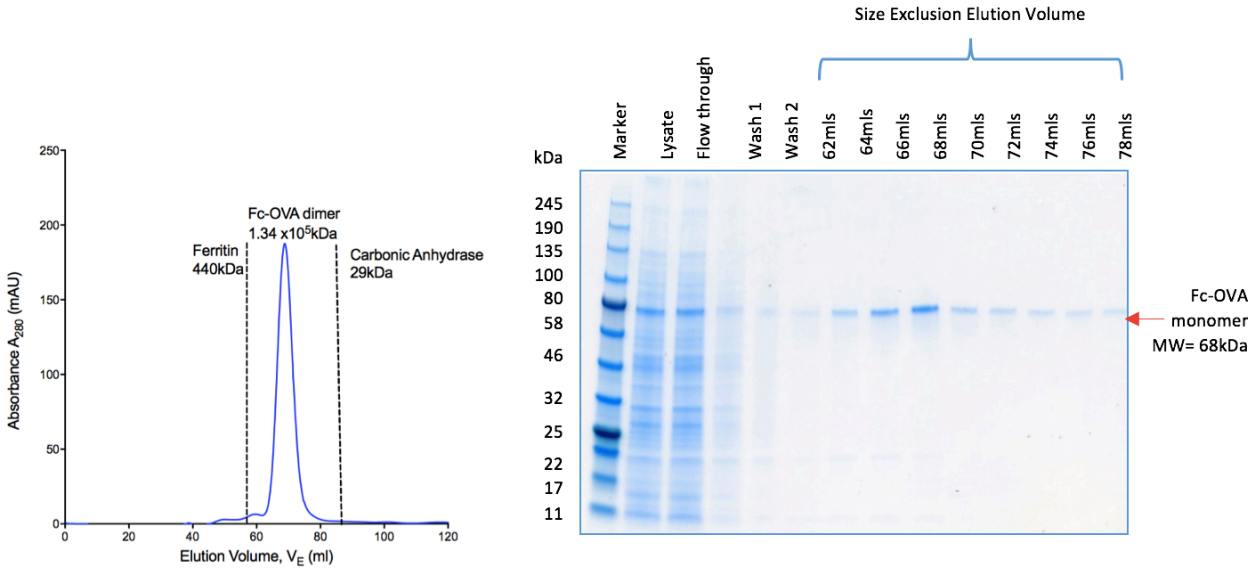

Figure 4-11. SEC purification of Fc-OVA from Hi-5 cells. (A) UV absorption profile of Fc-OVA eluting from a SEC column. Fc-OVA was purified from media post infection with protein P2 virus using 2ml Protein A column and following 20mls of washes, 1ml fractions were eluted containing neutralisation buffer. These fractions were concentrated to a 5ml loading volume and were run on a Sepharose 200 column at 1ml/min. Fractions of volume 1.5mls were collected for further analysis. (B) SDS-PAGE analysis of Fc-OVA eluted from a SEC column. A volume of 10µl of each of the protein fractions purified by SEC (between the elution fractions of 62-80mls) were run on a 10% SDS-PAGE, the MW of the Fc-OVA monomer is 68kDa.

4.6 Analysis of I3-01-PA binding Fc-OVA

4.6.1 Ability of I3-01-PA to bind Fc-OVA

It was important to quantify the ability of I3-01-PA to bind the Fc-OVA antigen to test how effective this coupling technique is. The BLI analysis was carried out at 37°C, as this is the temperature these fusion constructs would be used at in *in-vitro* and *in-vivo* experiments. The procedure was repeated using the Fc-OVA protein as with the anti-CLEC9A and anti-CD40 antibodies (section 4.4.2). Again, much like with the antibodies, very little dissociation was observed, the K_d for the binding affinity between the I3-01-PA platform and Fc-antigen was <1 x10^{-12} M at 37°C (Figure 4.12). The k_{on} rate was 1.18 x$10^{6}$$M^{-1}$ s^{-1} and the k_{off} rate was 1 x10^{-7} M^{-1} s^{-1}, suggesting strong binding and extremely slow dissociation. This demonstrated that binding to the Fc-antigen was just as strong as with the previous antibodies tested. The analysis provided here shows proof of principle that I3-01-PA can be decorated with antigen via an Fc-linkage with high affinity binding at 37°C, as the off rate is negligible.

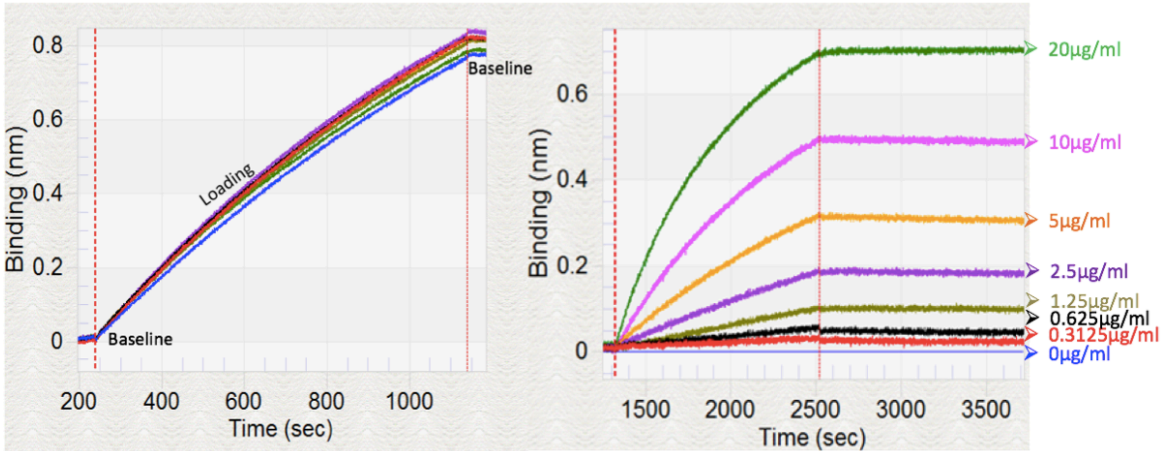

Figure 4-12. Bio layer interferometry analysis of I3-01-PA binding Fc-OVA. The left hand panel shows the loading of the biotinylated Fc-OVA at 3µg/ml for 10 mins onto the sensors before a stable baseline was established. The right hand panels show I3-01-PA was then applied at a range of concentrations, (2-fold dilutions from 20-0.3125µg/ml), showing varying binding strengths. The I3-01-PA protein was then removed for a 10-mins dissociation phase, allowing the binding affinity to be calculated.

4.6.2 Electron Microscopy analysis of I3-01, I3-01-PA and the complex of I3-01 with Fc-OVA

It was important to verify that the I3-01-PA remained correctly assembled following the addition of Fc-OVA to its surface. A sample of I3-01-PA was incubated with Fc-OVA for 16 hrs at 4°C and was viewed by electron microscopy. A uniform population of assembled proteins was present following the addition of Fc-OVA to I3-01-PA (Figure 4.13C). These assemblies appeared very similar to the native I3-01 protein and I3-01-PA protein without the addition of Fc-OVA, suggesting the assembly was unaffected by the addition of the Fc-OVA antigen (Figure 4.13A & 4.B). There also doesn't seem to be an obvious increase in size between the I3-01-PA proteins alone, compared to when they are complexed with FC-OVA. A possible explanation is that the Fc-OVA protein is mobile and so no density could be seen for the attachment.

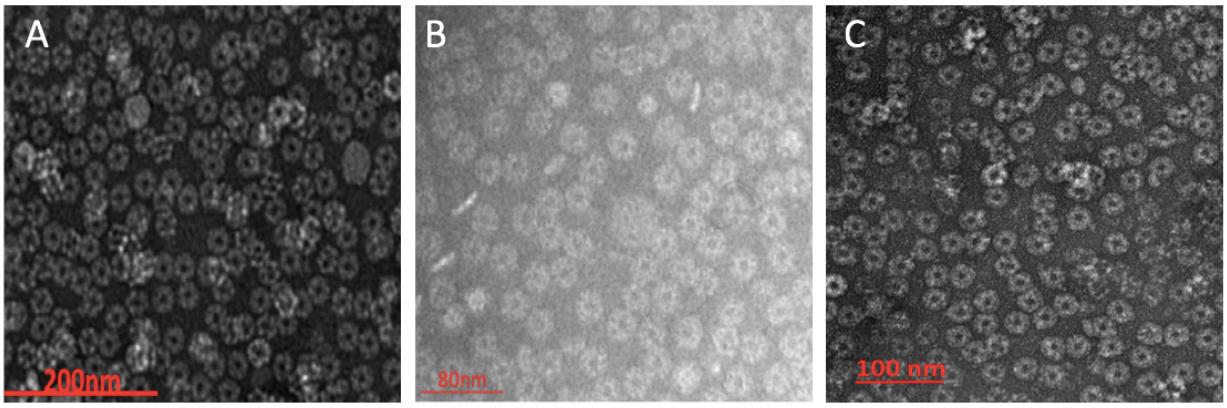

Figure 4-13. Negative stain electron microscopy analysis of I3-01-PA + Fc-OVA. (A) I3-01 at 0.3mg/ml (B) I3-01-PA at 0.3mg/ml C) I3-01-PA at 0.4mg/ml was incubated with Fc-OVA 0.2mg/ml at 4°C for 16 hrs. The samples were negatively stained with 2% UA and viewed on an FEI Tecnai 12 Biotwin microscope at 23,000x magnification.

4.7 Analysis of I3-01-PA binding Fc-NadA

4.7.1 Expression and purification of Fc-NadA

The expression and purification of Fc-NadA was carried out by Dr Edward McKenzie in the Manchester Institute of Biotechnology. The protein expression facility is well established to produce recombinant protein from insect cells [236]. Briefly, HI-5 insect cells were infected with protein P2 virus and the media was harvested post-infection. The protein was purified on a Protein A column and the elution fractions were neutralised, concentrated and were confirmed to be Fc-NadA by SDS-PAGE (Fc-NadA monomer MW= 55kDa) (Figure 4.11B).

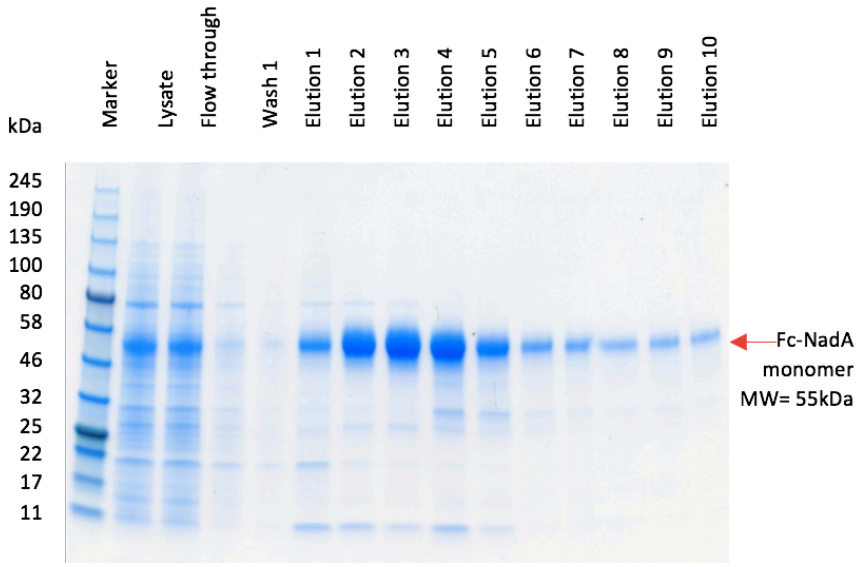

Figure 4-14. SEC purification of Fc-NadA from Hi-5 cells. SDS-PAGE analysis of Fc-NadA eluted from a Protein A column. A volume of 10µl of each of the protein fractions purified were run on a 10% SDS-PAGE, the MW of the Fc-NadA monomer is 55kDa.

4.7.2 Ability of I3-01-PA to bind Fc-NadA

It was important to quantify the ability of I3-01-PA to bind the Fc-NadA antigen to test how effective this coupling technique is, especially as NadA was unable to be attached to I3-01 by genetic fusion. The BLI analysis was carried out at 37°C, as this is the temperature these fusion

constructs would be used at in *in-vitro* and *in-vivo* experiments. The procedure was repeated using the Fc-NadA protein as with the anti-CLEC9A and anti-CD40 antibodies (section 4.4.2). Again, much like with the Fc-OVA fusion, very little dissociation was observed, the K_d for the binding affinity between the I3-01-PA platform and Fc-NadA was <1 x10^{-12} M at 37°C (Figure 4.15). The k_{on} rate was 1.86 x$10^{5}$$M^{-1}$ s^{-1} and the k_{off} rate was 1 x10^{-7} M^{-1} s^{-1}, suggesting strong binding and extremely slow dissociation. This demonstrated that binding to the Fc-NadA was just as strong as with Fc-OVA. The analysis provided further evidence I3-01-PA can be decorated with multiple antigens (OVA and NadA) via an Fc-linkage with high affinity binding at 37°C.

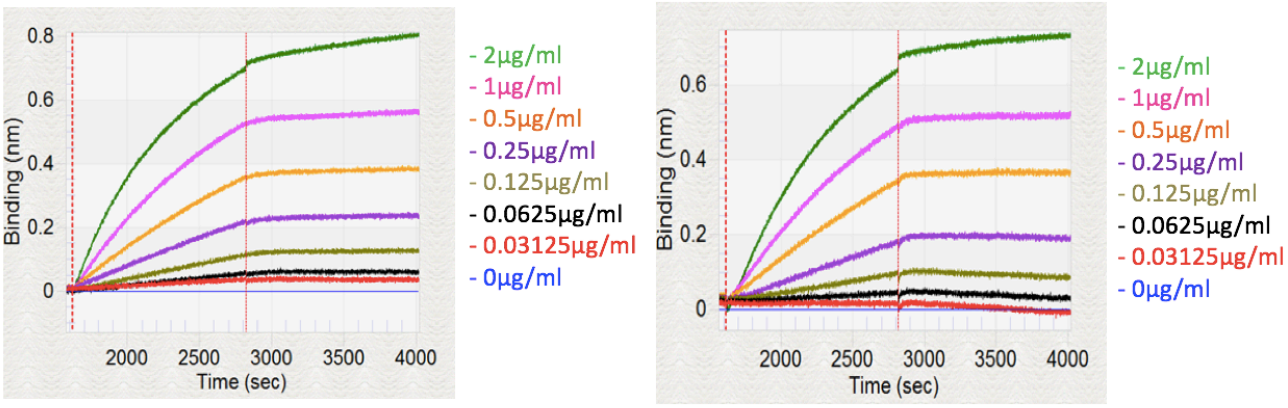

Figure 4-15. Bio layer interferometry analysis of I3-01-PA binding Fc-NadA. The left hand panel shows the loading of the biotinylated Fc-NadA at 3µg/ml for 10 mins onto the sensors before a stable baseline was established. The right hand panels show I3-01-PA was then applied at a range of concentrations, (2-fold dilutions from 20-0.3125µg/ml), showing varying binding strengths. The I3-01-PA protein was then removed for a 10-mins dissociation phase, allowing the binding affinity to be calculated.

4.7 Discussion

The aim of this chapter was to design, produce and characterise an engineered form of I3-01 which was assembled with multiple copies of fused Protein A B domains. This would enable the fusion of Fc-antigens to I3-01, post-assembly, to overcome the problems of antigen fusion discussed in Chapter 3.

It is well known that the B domain of Protein A binds IgG with high affinity [221]. However, there is very little evidence for the exploitation of this interaction in the world of protein engineering, specifically in terms of antigen display. The majority of Protein A engineering in industry has been for the function of optimising the process of antibody purification. One example, is the immobilisation of Protein A onto nanoparticles to enable high efficiency purification of IgG [221]. In this case, silica and graphene oxide nanoparticles were used as the support. This allowed IgG to be purified from human serum with high affinity whilst also, importantly, retaining its functional properties [221]. This confirms the novelty of the engineering work undertaken in this chapter.

The I3-01-PA construct was designed to insert a single B domain of Protein A to the C-terminal of each of the 60 monomers in the I3-01 construct. This site is surface exposed and has been used previously to display GFP whilst assembly was maintained [134]. The cloning, expression and purification from Clearcoli^{TM} cells was performed using the same methods as the native I3-01 assembly; this was successful. A homogenous population of assembled particles was purified and this was verified by both negative stain electron microscopy and DLS, suggesting this insertion did not affect the ability of the construct to assemble correctly. It was clear that the extreme thermal stability exhibited by the native I3-01 construct was maintained upon this insertion. The thermal stability is a key feature of I3-01 so it was important to limit the decrease in the melting temperature following any insertion. The HBc VLP has also had the B domain of Protein A inserted, but this led to a significant decrease in melting temperature despite the protein still assembling correctly (Dr Smruti Rashmi- unpublished work).

Fc-fusion proteins are a widely accepted therapeutic treatment and ten of these had FDA (Food and Drug Administration) approval by the end of 2017 [237]. The majority of the indications these drugs have been approved for are autoimmune conditions. The first FDA approved Fc-fusion drug was Enbrel, which is an effective treatment for Rheumatoid Arthritis and is composed of TNFR (tumor necrosis factor receptor), fused to the Fc of human IgG1 [238]. A

second example is Nulojix, which used the same Fc region as Enbrel but with CTLA-4 (cytotoxic T-lymphocyte-associated protein 4) fused to it [227]. This was approved to successfully target organ rejection. The evidence suggests there is scope for producing Fc-antigens for use as components of future vaccines. The Fc-fusion proteins were designed to include ovalbumin, a commonly used model antigen and NadA, a meningococcal antigen that could not be genetically fused to I3-01 previously. These were successfully expressed and purified from Hi-5 insect cells, avoiding endotoxin contamination.

Having purified and characterised the I3-01-PA and Fc-OVA/Fc-NadA constructs, further work presented here was performed to show that I3-01-PA binds the two Fc proteins with high affinity. According to the literature, a suitable Protein A ligand for purification of IgG should have a $K_d \leq 10^{-6}$M, and the K_d's calculated here was significantly lower $<10^{-12}$M [239]. This indicates that the binding measured is extremely tight. However, the k_{off} rates measured (1×10^{-7} M^{-1} s^{-1}) makes an accurate K_d hard to calculate as the level of dissociation is so low, the system is never truly at equilibrium. However, for the purpose of this work, the fact that there is clear strong binding of Fc-OVA/Fc-NadA with I3-01-PA, with little dissociation at 37°C, provides evidence that the Protein A fusion technology is working. It can be argued having an accurate K_d value is less important. It was also significant to confirm that the assembly of I3-01-PA was maintained following incubation with the Fc-OVA protein. This was to ensure the Fc-OVA protein was displayed on the I3-01-PA assembly surface according to the construct design. Negative stain electron microscopy confirmed that the assembly was unaffected by this addition, and a homogenous assembled population of particles remained which had their surface coated in Fc-OVA. Further work was done to test the binding of Fc-OVA to the HBc VLP following the addition of the B domain Protein A. A very similar K_d value was observed (10^{-12}M), with very little dissociation, whilst maintaining assembly (Dr Smruti Rashmi- unpublished work). This shows that both the I3-01 and VLP platforms can bind the designed Fc-OVA fusion protein with high affinity.

The work described here has established a technology for the display of the ovalbumin antigen on the surface of I3-01, without affecting the construct's assembly or melting point. Crucially, the binding between the Fc-fusion and I3-01-PA construct has been shown to be high affinity, without affecting the assembly. This provides the opportunity to assess the ability of I3-01 to perform as an antigen scaffold, whilst displaying multiple copies of Fc-OVA on its surface. A further point to note is that this technology can be expanded to display any antigen of interest on the surface of I3-01. This provides a new opportunity for the vaccine design field.

Chapter 5

Studies of the *in vitro* uptake of I3-01-PA-Fc-OVA into THP-1 derived macrophages

Chapter 5 - Studies of the *in vitro* uptake of I3-01-PA-Fc-OVA into THP-1 derived macrophages

5.1 Introduction

The THP-1 cell line is a human cell line and was first cultured from the peripheral blood of a one-year-old boy with acute monocytic leukaemia. The initial use suggested for these cells was as an aid to understanding the role of monocytes in studying the human immune response [166]. There are many reasons that support the use of these cells in *in vitro* studies, such as their quick doubling time of 35-50 hrs, so maintenance is relatively easy. They have also been proven to be safe to culture, with no infectious viruses or toxins reported to be present in these cells [240]. However, as the cells are cultured outside their natural environment, they are not representative of macrophages in general. The THP-1 cells can be differentiated into a macrophage phenotype, with evidence of their use as an accurate model to study macrophage function [240]. The best protocol for differentiation of THP-1 cells into macrophages has been debated. The combination of the use of PMA and a 24-48 hr resting period seems to most accurately represent circulating human monocytic macrophages [241]. This method produces the most effective phagocytosing cells as confirmed by both flow cytometry and microscopy. Measurements were quantified in terms of both the number of particles taken up by individual cells, and the percentage of the cell population capable of uptake [241]. THP-1 derived macrophages have previously been used as a model of uptake of diphtheria toxoid loaded onto nanoparticles, with over 50% of cells taking up the antigen when the diameter of the complex was between 200-400nm [242].

Macrophage receptor expression is notoriously hard to characterise as this may vary due to the cells specific environment or activation state [243]. There are four main groups of receptors expressed on macrophage surfaces: toll-like; mannose; scavenger and (Fcγ) receptors. The mannose and fragment crystallisable γ (Fcγ) receptors are thought to be the most important in uptake and are the most rapid at this process [243]. Examples of these receptors, their function and their specific expression on THP-1 derived macrophages are discussed below.

CD205, also known as DEC-205 is a 205kDa C-type lectin molecule which is part of the mannose receptor family [244]. It is important in antigen uptake, and expression of this receptor is found on macrophages, dendritic cells and B cells [245]. Expression was assessed in both THP-1 monocytes and macrophages. The CD205 expression was high in THP-1 monocytes and this level reduces slightly 48 hrs after PMA treatment [246]. Following stimulation with LPS, the expression of CD205 reduces further but is still fairly well expressed. This receptor is of particular interest on dendritic cells as it has been used to target antigen delivery in vaccine design with significant increases in the stimulation of CD8+ T cells measured [247].

CD209 is a type 11 integral membrane protein and is a C-type lectin which, similarly to CD205, is a member of the mannose receptor family [248]. This receptor is known to engulf cargo by phagocytosis which precedes antigen processing [249]. This receptor has been targeted to dendritic cells to increase the uptake of therapeutics, specifically in cancer immunotherapy [250]. CD209 is expressed at very low levels in monocytes and unstimulated differentiated macrophages, which was found to increase following 24-hr stimulation of LPS [246].

The macrophage galactose-type lectin (MGL/CLEC10A) is a type 11 transmembrane receptor [251]. It is a C-type lectin, specifically recognising terminal GalNAc sugars with high affinity [251, 252]. Much like CD205 and CD209, this C-type lectin receptor has been targeted on dendritic cells. This was found to have the effect of an adjuvant, by increasing the activation of dendritic cells in anti-cancer vaccines [253]. MGL is expressed on both THP-1 monocytes and macrophages, with the greater level being found on macrophages, and this effect was further increased by the stimulus of LPS [246].

CD13 is a glycosylated type 11 transmembrane receptor which functions primarily as an ectoenzyme [254]. Other functions of CD13 include cell adhesion, signalling and most importantly endocytosis as a competent phagocytic receptor, mediating the uptake of large molecules [254] [255]. This receptor can mediate different types of internalisation depending

on the size of the particles with comparable rates of uptake to the FcγR1 internalisation receptor [255]. There is evidence to suggest exploitation of CD13 may enhance antigen uptake and presentation by dendritic cells, providing a targeting opportunity [256]. The expression of CD13 is high on THP-1 monocytes but is hugely increased on differentiated macrophages; this level is maintained upon a 24-hr stimulation of LPS [246].

Historically macrophages have been targeted to treat a range of diseases through either directing the killing of cells in cancers or to increase drug uptake in vaccine research [257, 258]. To achieve this, a range of receptors have been targeted including the mannose, scavenger and Fcγ receptor. The mannose receptor has been targeted through the coating of cargo with mannose [257]. Tumour-associated macrophages can be targeted in this way using current treatments such as M-chlorin. There was an increase in apoptosis of the tumour-associated macrophages whilst THP-1 macrophages were unaffected by the treatment [257]. A second example of mannose receptor targeting revealed that nanoparticles coated in mannose were taken up in a mannose-dose dependent manner, offering a novel drug delivery method [259]. Further work has shown an inhibitor drug has been successfully targeted to mannose receptors *in vivo* [260]. A specific scavenger receptor expressed by tumour associated macrophages was targeted using an antibody to induce anti-tumour activity in breast and colon cancers [261]. Finally, the Fcγ receptor was targeted with an antibody to increase antigen phagocytosis and antigen presentation *in vivo*. This showed an increase in specific IgG1, IgG2A and IgG2B antibody titres, suggesting macrophages can be effectively targeted *in vivo* [258]. Taken together, this provides evidence that targeting macrophage receptors has been found to be effective in certain circumstances.

The work in Chapter 4 has characterised the protein assemblies produced, and has shown that I3-01-PA binds Fc-OVA with high affinity. VLPs have been used as platforms for antigen display previously but the key question here is to address if a synthetic protein assembly can be adapted to provide protective responses in the same way [184]. This poses an interesting question and one that has not been investigated previously with the I3-01 assembly. There are

examples of other synthetic proteins being manipulated to display epitopes and antigens in the design of vaccines for Malaria and Respiratory Syncytial virus (RSV), but these have less complex symmetries than I3-01 [126] [129].

A VLP assembly was required to enable a comparison to be made: the HBc VLP has been used in our group as an antigen presenting platform [163]. This VLP has been adapted to incorporate Protein A and was designed in a similar way to I3-01-PA. The major insertion region (MIR) of the HBc VLP was used to insert two domains of Protein A. This protein was expressed and purified in Clearcoli^{TM} and electron microscopy was used to verify the assembly of these particles. This insertion led to a decrease in melting temperature compared to the native VLP, from 77.8°C to 48.49°C. This is a major difference in comparison to the I3-01-PA where thermal stability was maintained over 90°C following the addition of Protein A domains. The Protein A domains on the HBc-PA VLP bound IgG and Fc-OVA with high affinity (K_D <10^{12}M) which is very similar to the I3-01-PA assembly, providing the opportunity to compare the two platforms (Dr Smruti Rashmi- unpublished work).

It was important to demonstrate the I3-01-PA assembly was capable of the same biological function as the HBc-PA VLP- antigen presentation. The use of the THP-1 cell line provided an opportunity to assess the effect of either platform on the uptake of Fc-OVA into human macrophages. The aim of this chapter is to analyse the uptake of the labelled Fc-OVA antigen, either alone or when displayed on either platform into the THP-1 derived macrophages. This was to provide a comparison of the presentation of a common antigen by a VLP and a synthetic platform. Secondly, the ability to increase the levels of uptake through specific receptor targeting using antibodies was evaluated. The effects will be analysed using a combination of flow cytometry and confocal microscopy.

5.2 Uptake of FITC-labelled protein into macrophages derived from THP-1 cells

5.2.1 Determining a macrophage gating strategy

It was important to establish that the THP-1 cells had differentiated into live macrophages and that there was a gating strategy implemented to allow their selection in the flow cytometry experiments conducted. The differentiation method was followed as in section 2.9.1.3, and the cells were washed. The cells were stained to allow identification of the live cells and specifically macrophages using the CD11b marker. The cells were analysed by flow cytometry and were gated following a specific gating strategy to select the live macrophages (Figure 5.1). This showed that the vast majority of cells gated were live macrophages, confirming the differentiation method was successful. The cells were also analysed for any FITC autofluoresnce through the gating of a FITC control to enable the selection of the FITC positive cells in future experiments.

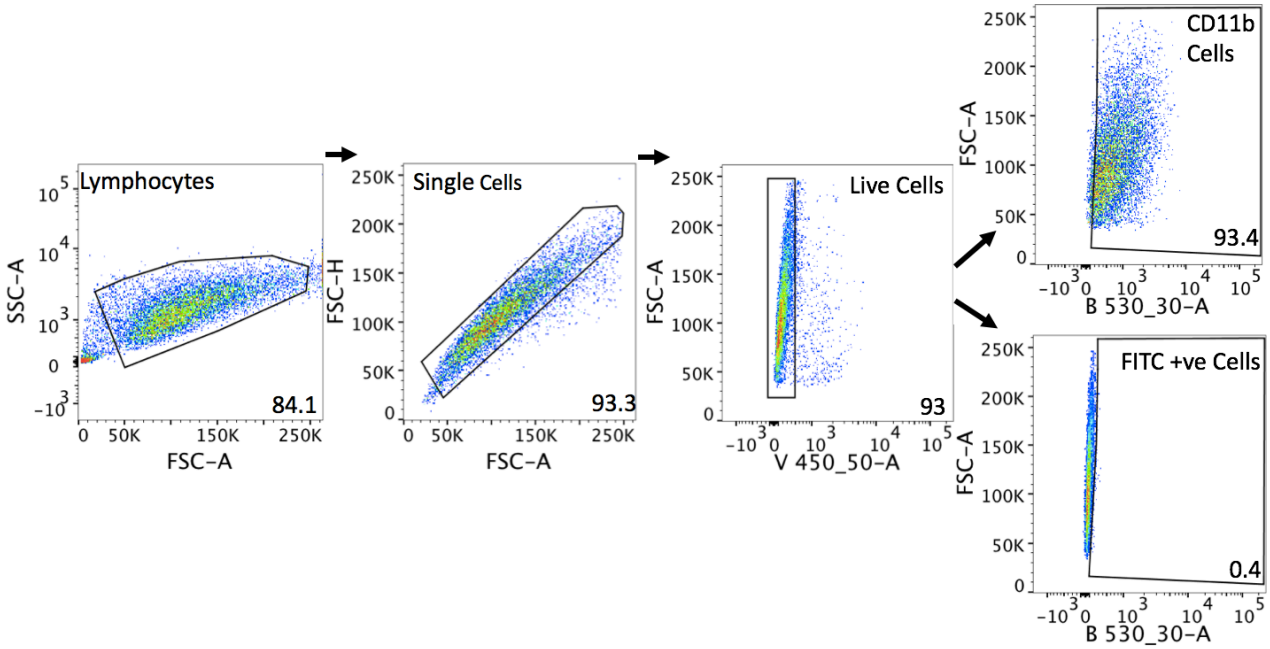

Figure 5-1. THP-1 macrophage flow cytometry gating strategy. The cells were first gated to select the single lymphocytes and the live/dead control was used to focus on the live cells. The macrophages were gated using the CD11b marker and the FITC control was used to select the FITC positive cell population in each sample.

5.2.2 Uptake of FITC-labelled protein into macrophages

The ability of macrophages derived from THP-1 cells to engulf FITC-labelled proteins over a 5 hr time period was assessed. This would aid the establishment of the appropriate conditions for the measurement of *in vitro* protein uptake using macrophages derived from this cell line. The selected proteins were- I3-01-PA, Fc-OVA, ovalbumin and BSA. The latter was used as a positive control. The FITC-labelled proteins (5µg) were added to wells of 300,000 macrophages and the proteins were incubated with the cells for 5 hrs at 37°C. The cells were washed, detached and then stained for FACS following the method in section 2.9.1.6. The FACS was carried out and the cells were gated to establish the percentage of FITC positive cells in each sample. The geometric mean fluorescence intensity (GMFI) from the cells in each sample was also calculated. Both of these measurements were used to compare the uptake at 37^0C in 5 hrs of 5µg of I3-01-PA, Fc-OVA, ovalbumin and BSA. There was a significant increase in the percentage of FITC positive cells when they were stimulated with Fc-OVA, in comparison to both I3-01-PA and ovalbumin (Figure 5.2 A and B). A similar effect was seen in the analysis of geometric mean fluorescence intensity; in the difference in uptake of Fc-OVA in comparison to both the I3-01-PA and ovalbumin conditions with increases measured. (Figure 5.3 C). This data suggested over a 5 hr time period the uptake of this amount of labelled protein is good, and the Fc-OVA antigen has a better uptake than equivalent masses of both I3-01-PA and Ovalbumin. The BSA positive control is very well taken up showing the macrophages, when prepared and stimulated in this way, are effective at uptake over this 5 hr time period.

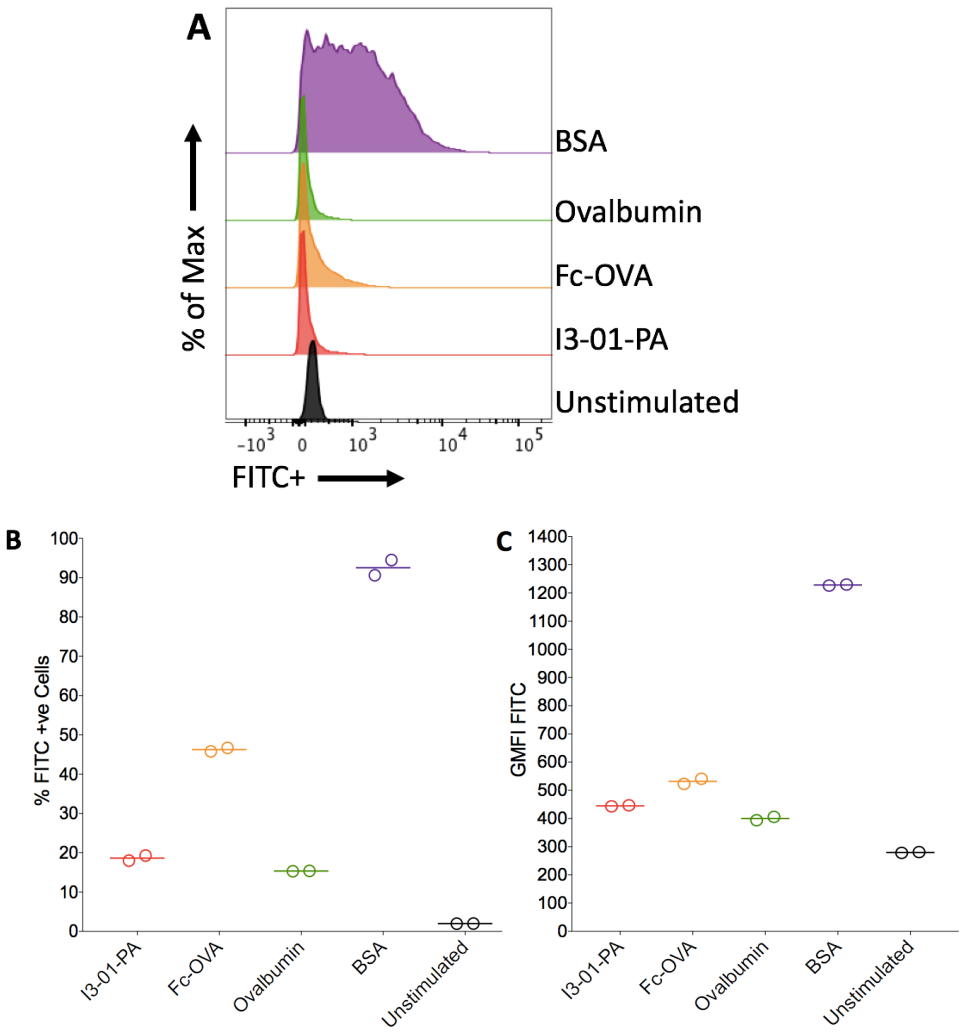

Figure 5-2. In vitro uptake of FITC-labelled proteins analysed by flow cytometry. The FACS was carried out on a BD LSRFortessa™ flow cytometer and both the gating and statistical analyses were performed using FlowJo software version 10. (A) Histogram showing a comparison of the uptake of the different FITC-labelled proteins and unstimulated cells. (B) Comparison of the percentage of FITC positive cells and (C) Comparison of the GMFI of FITC from the FITC positive cells following a 5 hr protein stimulation. For (B) and (C) each condition was run in duplicate in a single experiment, with points for each sample and the respective mean shown. Statistical analysis was performed using a one-way ANOVA with Tukey's multiple comparison tests to calculate statistical significance. P>0.05 defines no significant difference.

5.3 Uptake of FITC-labelled protein conjugates into macrophages derived from THP-1 cells

It was important to evaluate the effect of the method of antigen presentation on uptake of labelled antigen into THP-1 derived macrophages. The uptake of FITC-labelled Fc-OVA was compared when incubated alone, with I3-01-PA, and with the HBc-PA VLP, and BSA was run as a positive control. The amount of Fc-OVA was fixed at 0.053nmol and the amounts of scaffolds used were 0.088nmol and 0.0106nmol respectively for the I3-01-PA, and the HBc-PA VLP. This stoichiometry was selected to ensure a molar excess of the scaffold, and the reduced amount of I3-01-PA reflected the molar difference in Protein A in comparison to the HBc-PA VLP construct. The conjugates were prepared 24 hrs in advance, were mixed and stored at 4^0C.

The protein conjugates were incubated with the macrophages under the same experimental conditions as in section 5.2. The cells were stained for flow cytometry following the method in section 2.9.1.6, and the same gating strategy was used as above (Figure 5.1). There were no significant differences observed between the uptake of the Fc-OVA protein, no matter how it is displayed to the THP-1 derived macrophages (Figure 5.3). The previous experiment showed that, aside from the BSA positive control, Fc-OVA was the protein that was taken up the best, a result also seen here. The fusion of Fc-OVA to both I3-01-PA and HBc-PA VLP actually reduced the amount of uptake of Fc-OVA (Figure 5.3). This could be due to the fact that the Fc region is bound to the Protein A so cannot bind the Fcγ-receptors expressed on the THP-1 derived macrophages. The uptake of the Fc-OVA antigen occurs in less than 15% of the THP-1 derived macrophages, independent of the method of presentation, which is much lower than the BSA positive control. This may be due to either the short time period used in these experiments or a difference in the method of uptake, as BSA is much smaller than the I3-01-PA assembly or HBc-PA VLP.

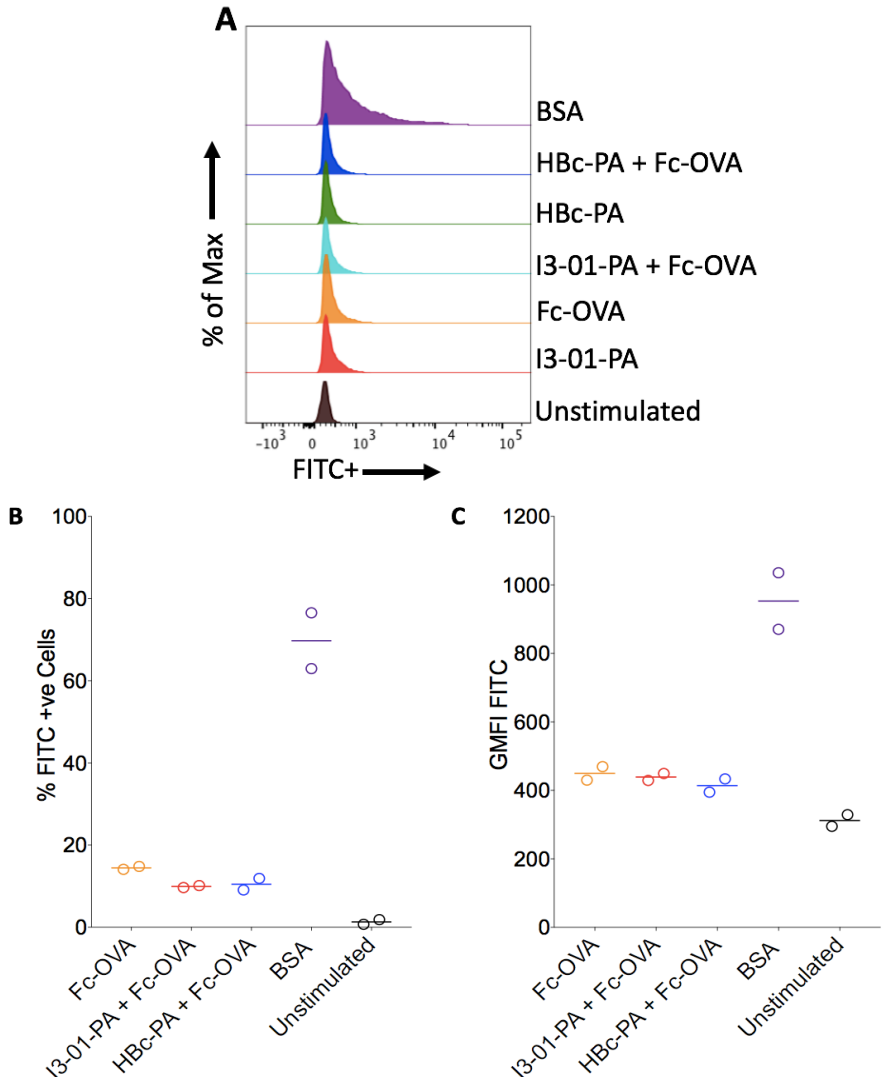

Figure 5-3. In vitro uptake of FITC-labelled Fc-OVA protein conjugates analysed by flow cytometry. (A) Histogram showing a comparison of the uptake of the same amount of different FITC-labelled Fc-OVA protein conjugates and unstimulated cells. (B) Comparison of the percentage of FITC positive cells and (C) Comparison of the GMFI of FITC from the FITC positive cells following a 5 hr stimulation with protein conjugates (5µg Fc-OVA, 8.3µg I3-01-PA and 10µg HBc-PA VLP) to unstimulated cells. For (B) and (C), each point represents the mean of duplicate samples from individual experiments. Statistical analysis was performed using a one-way ANOVA, with Tukey's multiple comparison tests to calculate statistical significance. P>0.05 defines no significant difference.

5.4 Confocal microscopy analysis to confirm uptake into macrophages

The flow cytometry analysis thus far has evaluated the uptake into THP-1 derived macrophages at 37^0C. This assumes that any fluorescence measured is from the inside of the cells themselves rather than just surface binding. To confirm that the measured fluorescence is from uptake and not surface binding, the experiment was repeated with only the labelled Fc-OVA and labelled Fc-OVA + I3-01-PA conditions at both 37^0C and 4^0C. The cells were fixed and were then stained with a plasma membrane mask for confocal microscopy. Images were taken and these clearly show uptake at 37^0C, but only surface binding at 4^0C (Figure 5.4). Much like the flow cytometry analysis, there is generally quite low uptake and there is little obvious difference to the Fc-OVA uptake with or without the I3-01-PA scaffold.

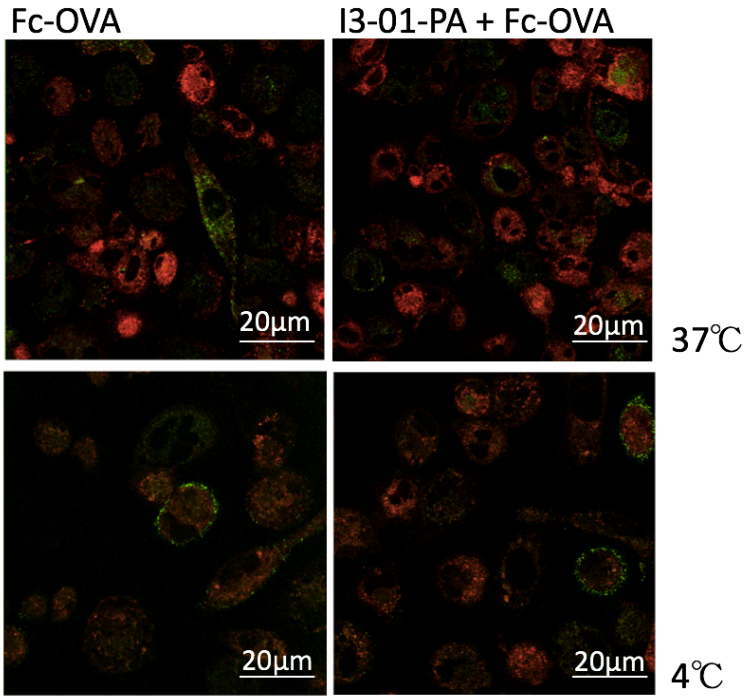

Figure 5-4. Confocal imaging of fixed THP-1 derived macrophages. The cells were fixed in 4% PFA before they were stained with a red cell plasma membrane mask. FITC-labelled Fc-OVA (green) uptake at 37^0C and surface binding at 4^0C is shown in the top and bottom panels respectively.

5.5 Targeting THP-1 derived macrophage receptors to increase uptake of Fc-OVA

The uptake of Fc-OVA into THP-1 derived macrophages appears fairly limited over this 5 hr incubation period. This provided an opportunity to increase the amount of protein uptake over this time period using receptor targeting, and to show this methodology can be successful. Published literature suggests it is possible to target macrophages, mainly in the treatment of cancers but also in developing novel vaccine design technologies [258] [261]. However, the hypothesis presented here is that the Fc-OVA-I3-01-PA construct could be targeted to a specific receptor on macrophages, to enhance uptake into these cells over a 5 hr incubation period.

5.5.1 Selection of a target receptor

The differentiated macrophages were analysed to select a receptor to target which was well expressed. A selection of receptors were chosen based on expression levels previously reported in the literature, CD205, CD206, CLEC10A, CD13 [246]. The THP-1 cells were differentiated and were either stimulated with 5µg Fc-OVA or remained unstimulated. Fc-OVA was chosen to stimulate the cells as this is our target antigen, so will most closely mimic the intended targeting scenario. This allowed an evaluation of the expression of each of the receptor's expression levels in both unstimulated cells and cells stimulated with protein for 5 hrs (Figure 5.5).

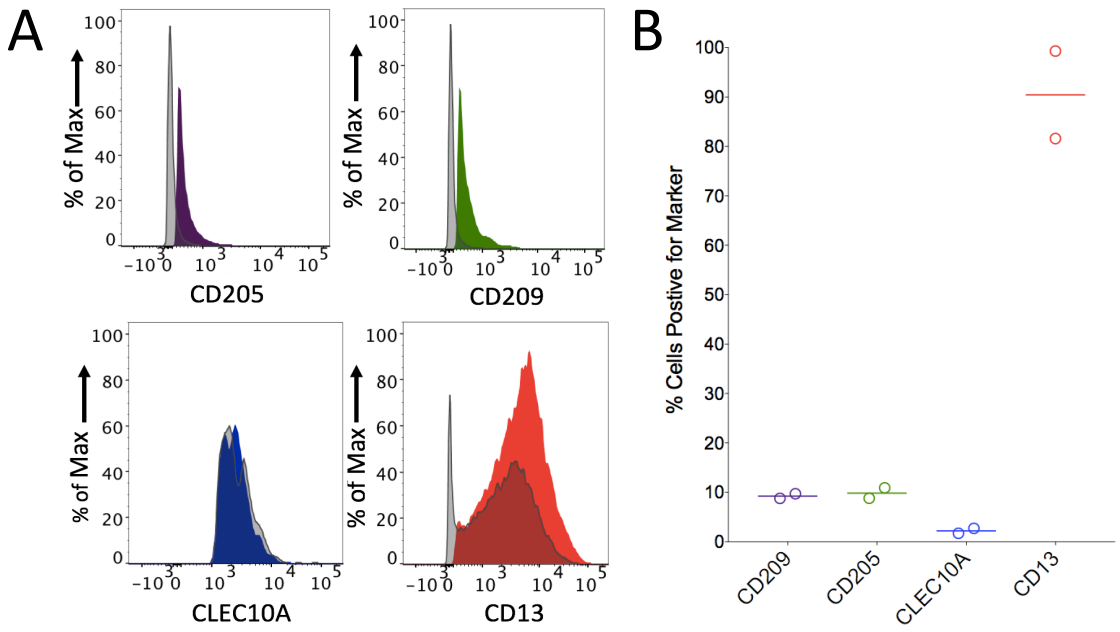

Figure 5-5. Expression of THP-1 derived macrophage receptors. (A) Histogram showing a comparison of cell receptor expression with (coloured) and without (grey) protein stimulation. (B) Comparison of the percentage cells positive for the cell surface receptors following 5 hr stimulation with protein. For (B) Each condition was run in duplicate in a single experiment, with points for each sample and the respective mean shown. Statistical analysis was performed using a one-way ANOVA with Tukey's multiple comparison tests to calculate statistical significance. P>0.05 defines no significant difference.

The expression of all of the cell surface receptors increased with protein stimulation. The CD205, CD209 and CLEC10A receptors were only present in 10% of the THP-1 derived macrophages, which is not high enough to target to stimulate a significant increase in uptake. However, CD13, Aminopeptidase N, is extremely highly expressed with and without protein stimulation, with up to 90% of cells expressing this phagocytic receptor following a 5 hr stimulation with Fc-OVA protein. CD13 is the clear choice of receptor to target in an attempt to increase the level of protein uptake.

5.5.2 Effect of targeting the CD13 receptor on the uptake of Fc-OVA

To analyse the effect of targeting CD13 to increase the uptake of FITC-labelled Fc-OVA, 3 protein conjugations were set up. These were: Fc-OVA + anti-CD13; Fc-OVA + I3-01-PA –anti-CD13; and Fc-OVA + I3-01-PA + anti-CD13, at the ratios of 0.053nmol:0.088nmol:0.053nmol (Fc-OVA, I3-01-PA, anti-CD13). The conjugates were stored at 4^0C and were added to the prepared macrophages for a 5 hr incubation period at 37^0C. The effect of the targeting was first analysed by flow cytometry, looking at both the percentage of FITC positive cells and the GMFI produced (Figure 5.6).

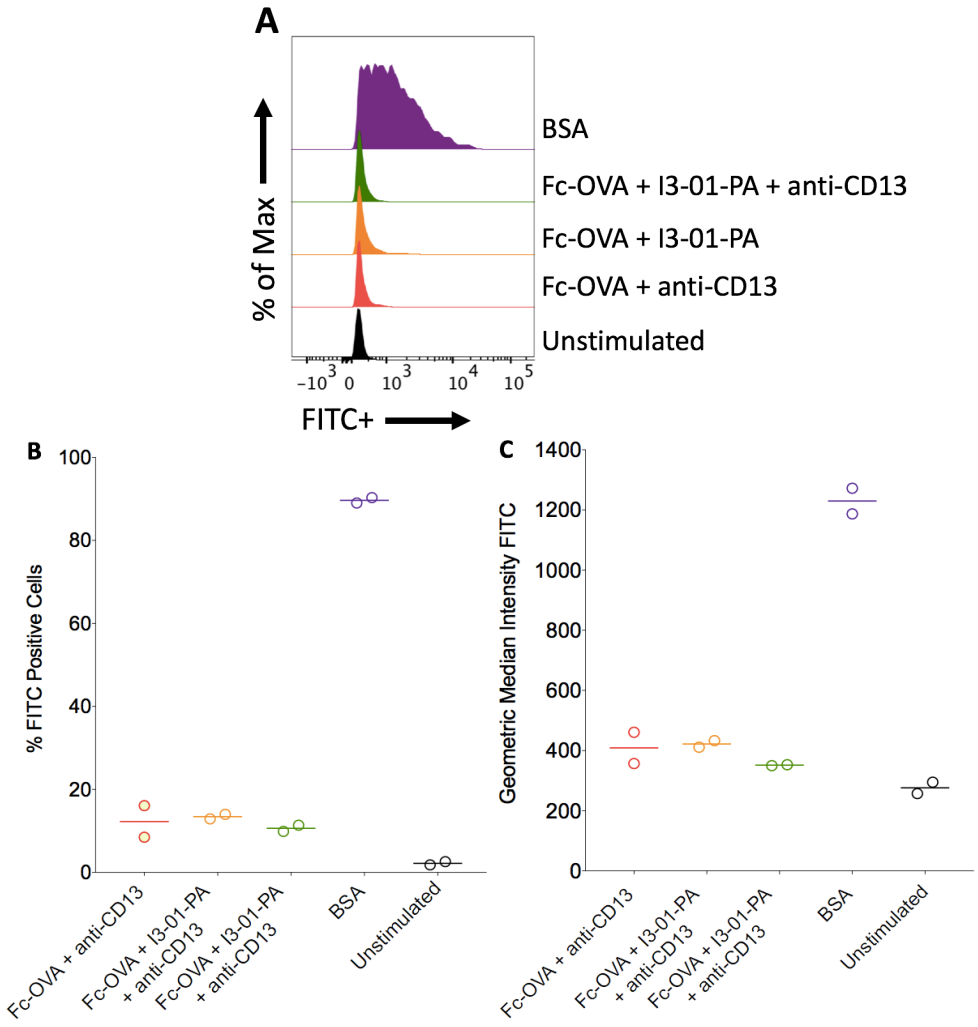

Figure 5-6. In vitro targeting of FITC labelled Fc-OVA protein conjugates to the CD13 receptor

(A) Histogram showing a comparison of the uptake of the same amount of different FITC-labelled Fc-OVA protein conjugates and unstimulated cells. (B) Comparison of the percentage of FITC positive cells and (C) Comparison of the GMFI of FITC from the FITC positive cells following a 5 hr stimulation with protein conjugates (5µg Fc-OVA, 8.3µg I3-01-PA and 5µg anti-CD13) to unstimulated cells. For (B) and (C) each condition was run in duplicate in a single experiment, with points for each sample and the respective mean shown. Statistical analysis was performed using a one-way ANOVA with Tukey's multiple comparison tests to calculate statistical significance. P>0.05 defines no significant difference.

5.6 Confocal microscopy analysis of the effect of CD13 receptor targeting

There is no significant difference in the uptake of FITC-labelled Fc-OVA, whether in combination with I3-01-PA (as seen previously) or when targeted to the macrophages to the CD13 cell receptor. Despite the high expression of this receptor, it is clear that targeting uptake by this method does not lead to an increase in uptake of labelled Fc-OVA. To examine this phenomenon by a different method, the experiment was repeated using 5µg of Fc-OVA in each condition, and the cells were examined by confocal microscopy (Figure 5.7). It was shown that Fc-OVA was taken up by the cells but there was very little difference between the conditions investigated, as the flow cytometry results suggested.

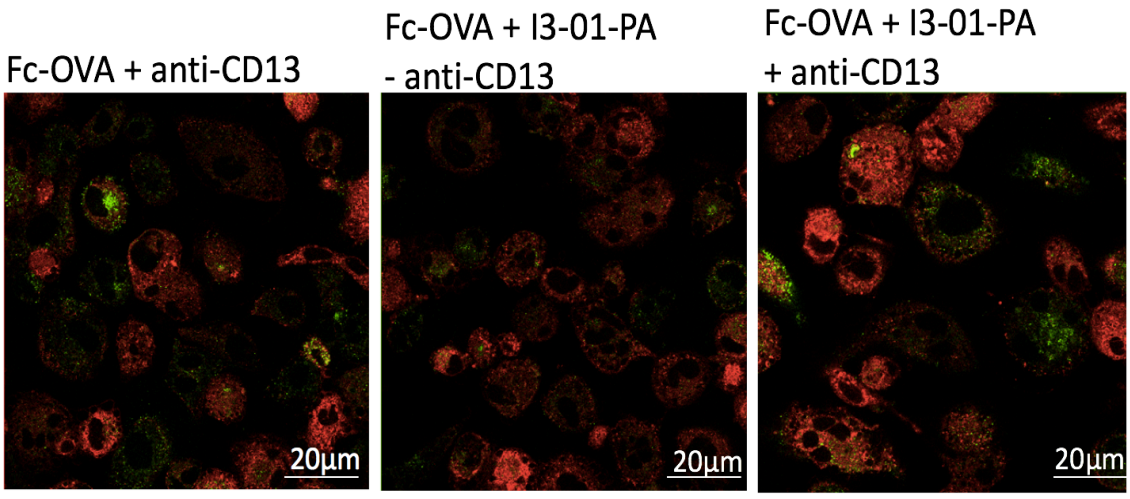

Figure 5-7. Confocal imaging of targeting of THP-1 derived macrophages through the CD13 receptor. The cells were fixed in 4% PFA before they were stained with a red cell plasma membrane mask. FITC-labelled Fc-OVA (green) uptake was examined when incubated with anti-CD13 (left), with I3-01-PA (centre) and with both anti-CD13 + I3-01-PA (right) at 37^0C.

5.7 Discussion

The focus of the chapter was to examine the ability of I3-01-PA to support the uptake of a model antigen, Fc-OVA. This was achieved through evaluating the uptake of Fc-OVA when incubated with THP-1 derived macrophages either; alone, fused to I3-01-PA or fused to the HBc-PA VLP. The THP-1 cell line was selected for this work as it is easy to culture and the method of differentiating the cells into macrophages is well established within our group, limiting the heterogeneity in the population. This meant that the results There was no significant difference between these conditions when the number of FITC positive cells or the GMFI was analysed. This could be due to a number of factors such as the size of the protein conjugations or the 5 hr incubation period. Fc-OVA was found to be taken up the best in comparison to other single proteins and no improvement was seen when it was presented to the cells when attached to either scaffold. This may be due to the fact that THP-1 derived macrophages express two separate Fcγ-receptors (CD32/CD64) which may facilitate this effect [246]. In order to improve the uptake, a receptor expressed on over 90% of the macrophages, CD13, was targeted. However, this didn't appear to work, with very little difference being observed between targeting and no targeting when analysed by both flow cytometry and confocal microscopy. Microscopy was an important technique to use in parallel with flow cytometry, as it clearly showed the difference between binding at 4^0C and uptake into the macrophages at 37^0C. The fact that there is no increase with the addition of CD13 targeting suggests that the THP-1 macrophage uptake is limited by a factor other than the ability of labelled Fc-OVA to reach the THP-1 derived macrophage cell surface. Despite the low uptake of Fc-OVA into the THP-1 derived macrophages, the BSA positive control was consistently extremely well taken up. This shows that the macrophages had the ability to engulf protein rapidly and the lack of uptake was not due to a fault with the cells themselves. There are two reasons for this high uptake, as BSA is taken up by macropinocytosis and it will appear much smaller to the cells than the protein assemblies; this may facilitate easier and more rapid uptake [250]. The second reason is that these THP-1 derived macrophage cells grow in media supplemented in bovine serum so the cells are familiar with the recognition and uptake of this protein.

There is evidence to suggest protein uptake appears to vary in macrophages depending on whether primary cells or a tumour derived cell line is used, and also the relative polarisation towards M2 macrophages [262] [263]. To further investigate the reasons for poor uptake into THP-1-derived macrophages, a number of factors have been considered in the literature: the size of protein, the incubation time period and the presence of serum in the media. The effect of charge of the protein has also been explored but this seems to be less important than the above mentioned factors [264].

The ability of THP-1 derived macrophages to engulf proteins of different sizes has been researched. The uptake of nanoparticles between 30-70nm in diameter was found to be low (comparable to the current work), and there was little difference in the uptake between the different nanoparticle sizes [265]. In another study, the nanoparticles were PEGylated to remove any potential charge repulsion issues and to allow the factor of size to be analysed independently [264]. The uptake of nanoparticles was found to occur in a size-dependent manner, with a decrease in uptake correlating with a decrease in nanoparticle diameter. This was further verified by decreasing the diameter of each particle and comparing the uptake with the original particle [264].

The incubation time period used in the current work was 5 hrs, based on the fact it would provide the clearest differences between the different protein conjugations. The BSA uptake was clear, but there was a requirement for some experimental conditions which provide a low uptake, so a measurable amplitude in uptake could be quantified using the targeting antibody. However, this may have been a fault in the experimental design as the literature seems to imply a longer time period is best for uptake into this THP-1 cell line. For all of the uptake studies reviewed, a 24-hr incubation period is used, suggesting this would be something to consider in a repeat of this work [264-267]. There is evidence that the majority of nanoparticle uptake appears to occur in the first 8 hrs of this time period [268].

In this work, to best mimic *in vivo* conditions, the media used during the incubation periods of the THP-1 cells with protein contained serum. The effect of the presence of this serum in the THP-1 cell medium during protein uptake has been assessed [263-265, 268]. Nanoparticles of various sizes were incubated with and without serum in the media and in all cases the uptake decreased with the presence of serum [265]. The biggest difference was found to be in particles of the same size as the I3-01-PA construct, suggesting that our uptake could be increased if serum was removed from the media [265]. The reason for this effect could be due to the fact the serum may bind the proteins and form a protein corona. This would have a repulsive charge against the cell membrane and reduce the uptake of the protein [269]. A further study also found this was the case as there was a 5-fold decrease in uptake of a 50nm nanoparticle when incubated in media with, compared to without, the presence of serum [268]. This phenomenon is intriguing and could offer a potential explanation as to the low uptake of the proteins into macrophages derived from this cell line.

To summarise, the work in this chapter has provided an insight into the differences in uptake of Fc-OVA when displayed to macrophages *in vitro* by different platforms, showing the I3-01-PA assembly and HBc-PA VLP behave in a similar way. There is clearly uptake into the macrophages, however using the I3-01-PA platform for antigen presentation doesn't appear to increase this level. This informs us that the I3-01-PA platform does not influence antigen uptake. However, this does not necessarily mean that I3-01-PA is not useful as a scaffold for antigen presentation. It is important to remember that antigen uptake is just one measureable factor involved in antigen presentation. The effect that the different methods of antigen presentation had within the cells once the protein had been taken up, remains unclear. Therefore, to further this work, an alternative *in vitro* approach looking at the other aspects of the adaptive immune response is necessary.

Chapter 6

In vitro studies of I3-01-PA-Fc-OVA in bone marrow derived dendritic cells

Chapter 6 -*In vitro* studies of I3-01-PA-Fc-OVA in bone marrow derived dendritic cells

6.1 Introduction

The work in Chapter 5 investigated the uptake of labelled Fc-OVA into THP-1 derived macrophages when presented on different platforms. Here the aim is to build on the conclusions drawn previously, using bone marrow-derived dendritic cells (BMDCs) to further our understanding of the effect the method of Fc-OVA presentation has on antigen uptake and processing by dendritic cells, including the T cell response.

Dendritic cells are professional antigen presenting cells (APCs) that can both process antigens and present them to T and B cells [270]. Their ability to stimulate naïve T cells makes them the most powerful antigen presenting cell. The method for producing dendritic cells from mouse bone marrow *in vitro* was first established in 1992, using granulocyte-macrophage colony-stimulating factor (GM-CSF) as the stimulant [271]. Dendritic cells can be differentiated from mouse bone marrow cells and markers such as CD11c, CD40, CD80, CD86 and Major Histocompatibility Complex (MHC)-I/MHC-II are used to confirm a dendritic cell type [272]. CD11c is a commonly used marker to distinguish dendritic cells both *in vitro* and *in vivo* [273]. A key role of the dendritic cells in the immune response is the presentation of antigen to stimulate the T cells in the context of either MHC-I or MHC-II. Antigen presentation through MHC-I leads to the activation of CD8 cytotoxic T cells whereas with MHC-II, the CD4 T helper (Th) cells are activated. MHC-II is particularly important as it promotes the production of T regulatory and most importantly memory T cells [274]. The use of mouse BMDCs has been commonly used to evaluate protein uptake and dendritic activation and is a step used before moving to *in vivo* methods.

There are a number of processes required to fully activate the immune system through vaccination. These include the delivery of antigen to APCs, the presentation of these antigens to T cells and their stimulation, and the induction of memory. This involves promoting the uptake and presentation of antigens by innate immune cells such as macrophages and dendritic

cells. It is then vital to engage the adaptive arm of the immune response by stimulating circulating naïve T cells to become differentiated into their various subtypes. This is initially determined by the specific MHC class that presents the antigen to T cells, with MHC class I and II producing a CD4 or CD8 T cell response respectively. CD8 cells are also known as cytotoxic T cells and have the main role of eliminating infected cells. The second class, the CD4 T cells, have a more complex function in producing a range of cytokines and chemokines which activate neighbouring cells [16]. The proliferation and activation of this class of T cells has been studied *in vitro* using the well-established OT-II transgenic mouse cell line. This produces T cells with receptors specific for the chicken ovalbumin epitope from residues 323-339 and allows an analysis of ovalbumin antigen specific CD4 T cells [17]. CD4 cells can be divided into further subtypes defined on their cytokine profile and these include Th1, Th2, Th17 and T regulatory (Tregs) cells.

An area of a specific interest is the effect that antigen presentation has on the T cell response. This has been previously studied using nanoparticles to display antigens to APCs. Nanoparticles which were acid degradable were used to deliver ovalbumin to APCs [275]. It was found that there was a production of antigen-specific cytotoxic T lymphocytes and, therefore, the use of this platform to present antigens had the ability to engage the adaptive section of the immune response [275]. A cytotoxic T cell response was also induced when a nanoparticle vehicle was used to deliver antigen to dendritic cells in pulmonary parenchyma [276]. These particles had a specific chemistry allowing optimal release of antigen for antigen cross-presentation to T cells. There was also found to be a CD4 T cell response as there was a localised increase in the Th1 and Th17 cells found in the lung [276]. Th1 cells are required for cell mediated inflammatory responses and to produce Interferon-γ (IFN-γ) and tumour necrosis factor (TNF-β) [18]. Th17 cells are a more recently defined class of CD4 T cells which are characterised by their production of the cytokine IL-17 which may lead to the progression of autoimmune diseases [28]. Taken together, it is suggested that the presentation of antigen in this way stimulated a full T cell response [276]. Nanoparticles have also been decorated to target specific receptors on APCs, such as the mannose receptor on dendritic cells. This has been shown to stimulate the production of both CD4 and CD8 T cells which were ovalbumin specific [277]. Aside from

nanoparticles, liposomes have also been used for vehicles of delivery of antigen to APCs. Specifically, cationic liposomes are very efficiently taken up by dendritic cells and have been show to produce a CD4 and CD8 T cell response and offer long term protection *in vivo* [278].

This chapter looks to investigate the importance of the specific assembly used to present antigen to dendritic cells. This will be evaluated in terms of antigen uptake. the activation of dendritic cells and the stimulation of T cell proliferation. Similarly, to the work in chapter 5, the Fc-OVA antigen will be used and it will be displayed to the cells on either the HBc-PA VLP or the I3-01-PA assembly. It has previously been shown that the HBc-PA VLP is an effective platform at activating dendritic cells *in vitro* and that an ovalbumin specific proliferation in T cells is observed when the Fc-OVA antigen is displayed in this way. The focus of this chapter is to investigate if the novel, I3-01-PA assembly is as successful at producing these responses.

6.2 *In vitro* uptake of the Fc-OVA antigen into BMDCs

6.2.1 Optimisation of the BMDC flow cytometry gating strategy

In these experiments, the BMDCs were cultured for 10 days prior to the addition of the fluorescein isothiocyanate (FITC) labelled proteins which were incubated for 5 hrs at 37°C. The cells were then harvested and stained for flow cytometry. In order to analyse the cells a specific gating strategy was used to identify the live single cells by both forward and side scatter. The dendritic cells were identified using CD11c, a common BMDC selection marker. A FITC only positive control was used to identify the FITC positive population within each dendritic cell sample, identifying the autofluorescence of the BMDCs (Figure 6.1).

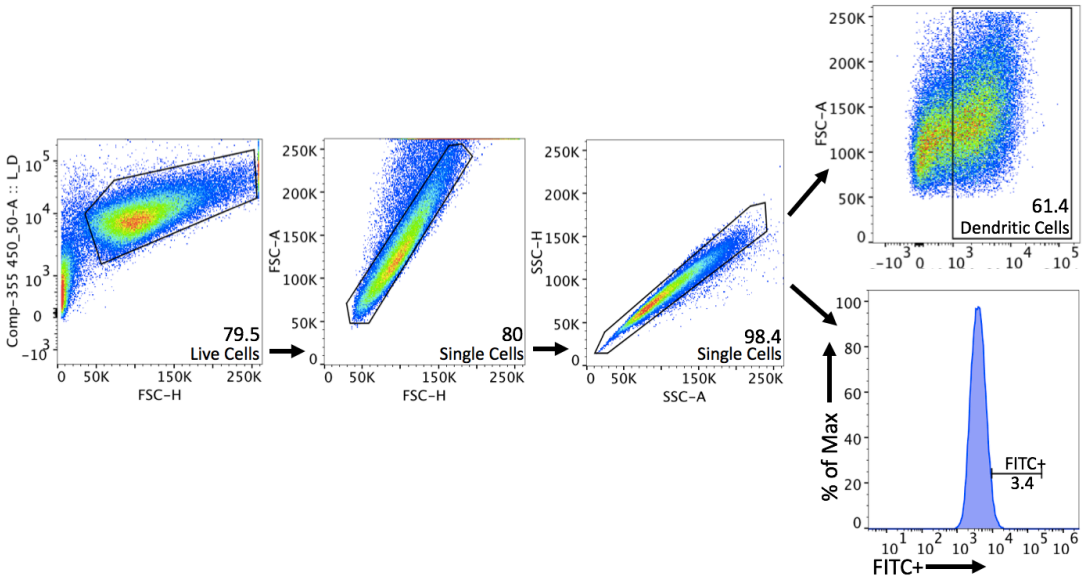

Figure 6-1. BMDC flow cytometry gating strategy. The live cells were first selected followed by the single cells by both forward and side scatter areas. The dendritic cells were gated using the CD11C+ marker and the FITC control was used to select the FITC positive cell population in each sample.

6.2.2 Stimulation of BMDCs with prepared Fc-OVA conjugations

The purpose of this section is to analyse the uptake of Fc-OVA into BMDCs when presented alone, in complex with the HBc-PA VLP or I3-01-PA. This will provide an insight into the role that the method of antigen presentation has in the level of uptake into dendritic cells. The antigen, Fc-OVA was labelled with the FITC fluorophore prior to incubating with the purified assemblies (section 2.8.9). The labelled Fc-OVA was used to prepare three antigen conjugations for the experiments 24 hrs before the stimulation of the BMDCs**.** The amount of Fc-OVA was fixed at 0.053nmol (5µg) and was either incubated alone, with 0.088nmnol I3-01-PA (8.3µg) or with 0.106nmol HBc-PA VLP (10µg). This provided an approximate molar excess of platform to ensure there was no unbound Fc-OVA in the conjugations and that the molar concentrations of Protein A were comparable between the HBc-PA VLP and I3-01-PA platforms. Flow cytometry was carried out using the gating strategy in Figure 6.1. The uptake of FITC-labelled Fc-OVA was analysed from the percentage of FITC positive cells and the geometric mean fluorescent intensity (GMFI) of the cells in each condition. In both measurements, there was no significant

difference in uptake when FITC labelled Fc-OVA was incubated with the dendritic cells alone or presented on either the HBc-PA VLP or I3-01-PA platform (Figure 5.2). Fc-OVA was well taken up when alone, probably due to the presence of the fragment crystallisable γ receptor (Fcγ) receptors on the dendritic cell surface. Neither platform was found to affect the amount of labelled Fc-OVA antigen taken up into the cells over this 5 hr time period.

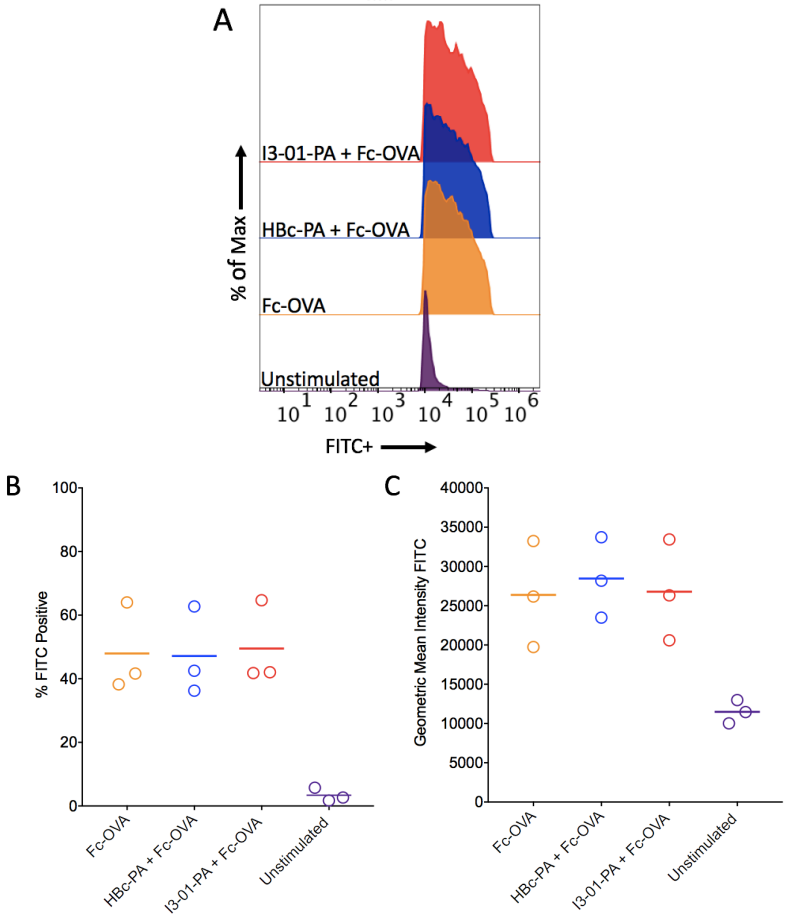

Figure 6-2. Analysis of Fc-OVA uptake by flow cytometry. (A) Comparison of the uptake of the different proteins conjugations and unstimulated cells. (B) Comparison of the percentage of FITC positive cells and (C) Comparison of the GMFI of FITC from the FITC positive cells following a 5 hr protein stimulation. For (B) and (C) Each point represents the mean of duplicate samples for a single experiment, with three experiments shown for each condition. A one-way analysis of variance (ANOVA) with Tukey's multiple comparison tests was used to analyse the statistical significance.

6.2.3 Analysis of BMDC marker expression following stimulation with Fc-OVA conjugations

It was important to investigate the expression level of key dendritic cell activation markers in response to the different Fc-OVA conjugations. The expression of four markers (CD40, CD80, CD86 and MHC-II) was analysed by flow cytometry by both the percentage of positive cells and GMFI from the positive cells (Figure 6.3). There was no significant difference in levels of CD40, CD80, CD86 or MHC-II expression between the three conditions used to stimulate the dendritic cells (Figure 6.2). This suggests that neither the HBc-PA VLP or I3-01-PA platforms are able to boost the Fc-OVA antigen's ability to activate dendritic cells.

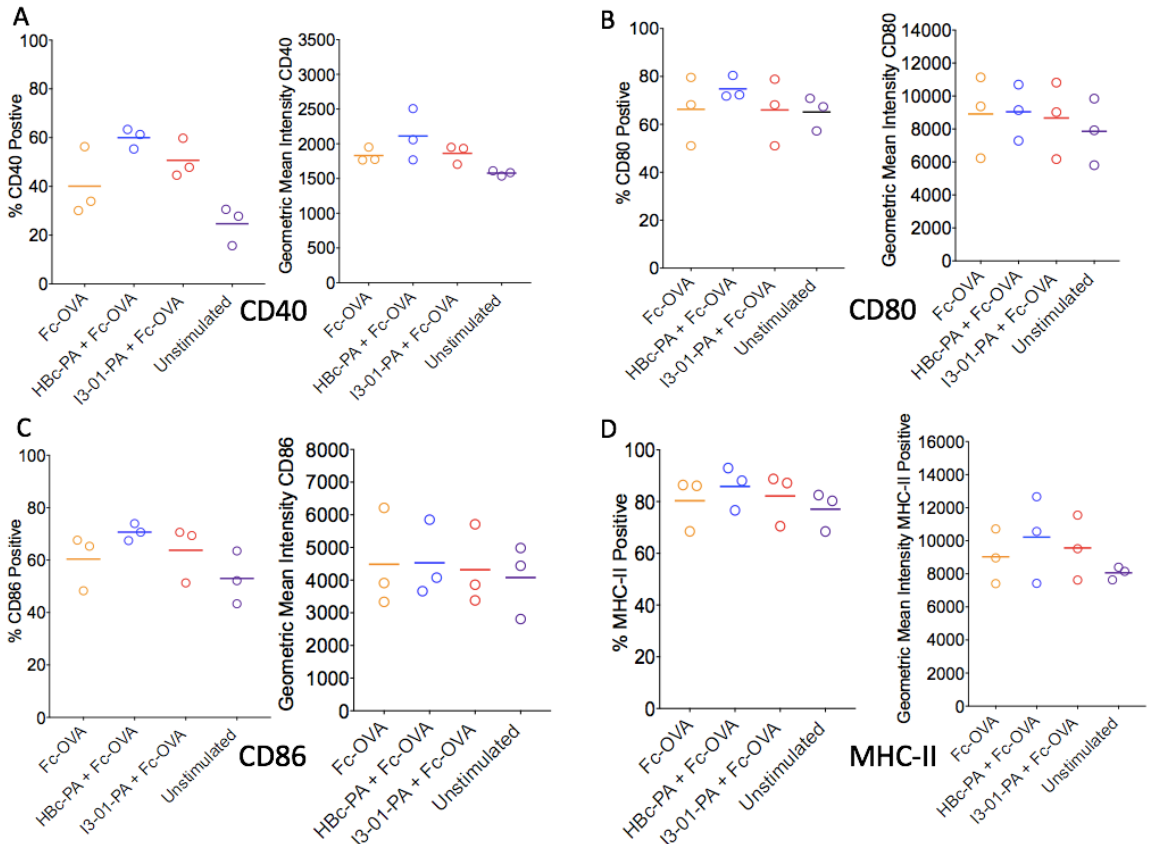

Figure 6-3. Analysis of BMDC marker expression by flow cytometry. (A-D) The expression of CD40 CD80, CD86 and MHC-II was analysed by the percentage of positive cells (left) and the GMFI from the positive cells (right) following a 5 hr protein stimulation. Each point represents the mean of duplicate samples for a single experiment, with three experiments shown for each condition. A one-way ANOVA with Tukey's multiple comparison tests was used to analyse the statistical significance.

6.2.4 Comparison of cytokines expression from dendritic cells were stimulated by Fc-OVA on different platforms

Cytokines are a key component of the immune response, acting as intracellular signals and are produced by activated dendritic cells. The production of cytokines is particularly important in the mediation of co-stimulatory molecules and T-cell differentiation [279]. To investigate whether the cytokine profiles vary depending on the method of Fc-OVA presentation to dendritic cells, the levels of IL-6, tumour necrosis factor α (TNF- α), IL-12p40 and IL-10 produced by the different samples were examined.

IL-6 is a cytokine that stimulates the production of Th17 cells through the upregulation of the transcription factor retinoic acid-related orphan receptor γ t (RORγt) [280]. There was a significant increase in the production of IL-6 when Fc-OVA was coupled to HBc-PA in comparison to presentation alone ($p<0.0001$), an effect that was not replicated when the antigen was coupled to the I3-01-PA platform ($p=0.0630$, Figure 6.4A). There was also a significant difference in the level of IL-6 secretion when Fc-OVA was conjugated to the HBc-PA VLP in comparison to the I3-01-PA assembly ($p=0.0007$), suggesting an increase in the production of this cytokine only occurred in the presence of the HBc-PA VLP.

TNF-α is produced in response to dendritic cell activation and leads to the proliferation of both CD4 and CD8 T cells which in turn are involved in the killing of infected cells [281]. There was a significant increase in the TNF-α production when Fc-OVA was conjugated to both the HBc-PA VLP and I3-01-PA assembly compared to when the Fc-OVA antigen was presented alone ($p<0.0001$ and $p=0.0016$ respectively, Figure 6.4B). However, the increase was significantly larger when the HBc-PA VLP was used as the method of antigen presentation, in comparison to the I3-01-PA assembly ($p<0.0001$). This indicates that there was a significant increase in TNF-α production due to the presence specifically of the HBc-PA VLP. The final pro-inflammatory cytokine analysed was IL-12p40 which is one subunit of the IL-12 cytokine and is produced by activated dendritic cells in response to antigen uptake, stimulating the production of the Th1 subset of CD4 T cells [282]. There was a significant increase in IL-12p40 production when Fc-OVA was conjugated to the HBc-PA VLP but not when it was attached to the I3-01-PA assembly

(p= 0.017 and p= 0.9235 respectively, Figure 6.4C). Finally, there was a significant difference in the production of IL-12p40 when the Fc-OVA antigen was presented on the HBc-PA VLP in comparison to the I3-01-PA assembly (p=0.0046). This, much like the production of IL-6 and TNF-α, suggests a key role of the HBc-PA VLP in the secretion of pro-inflammatory cytokines from stimulated dendritic cells.

IL-10 is an anti-inflammatory cytokine which is produced to dampen the immune response in reaction to a pathogenic challenge [283]. There was a significant increase in the production of IL-10 in response to Fc-OVA when it was conjugated to either the HBc-PA VLP or I3-01-PA assembly in comparison to Fc-OVA alone ($p<0.0003$ and $p=0.0016$ respectively, Figure 6.4D). There was no significant difference between using the HBc-PA or I3-01-PA platform for antigen display, suggesting that presenting Fc-OVA on an assembly stimulates a more potent cytokine response than the antigen alone.

Taken together, cytokine secretion was low when Fc-OVA was presented to dendritic cells alone but higher when conjugated to the HBc-PA VLP. When Fc-OVA was fused to the I3-01-PA assembly, the cytokine production was low except for the anti-inflammatory cytokine IL-10 (Table 6.1). In comparison to the Fc-OVA antigen alone, there was a significant increase in all of the cytokines measured when the antigen was conjugated to the HBc-PA VLP, whereas with I3-01-PA there were only significant differences in IL-10 and TNF-α secretion. Perhaps most importantly, there was a significant increase in all cytokine production when the Fc-OVA antigen was presented on either platform except for IL-10. The anti-inflammatory cytokine was secreted similarly with the presence of either of the two assemblies. It is important to note that neither the HBc-PA VLP or I3-01-PA platform drove the cytokine responses alone (data not shown). The HBc-PA VLP appears to outperform the I3-01-PA assembly in terms of its ability to increase the secretion of the pro-inflammatory cytokines measured; IL-6, TNF-α and IL-12p40. One possible explanation for these differences is the increased number of mouse T cell epitopes present in the HBc-PA VLP in comparison to the I3-01-PA assembly (www.iedb.org). The MHC-II T cell epitope consensus method identified potential mouse T cell epitopes using the H2-IAb allele: there were 7 epitopes found to have predicted stronger binding scores in the HBC-PA VLP than

any epitope predicted in the I3-01-PA assembly [197] [198].

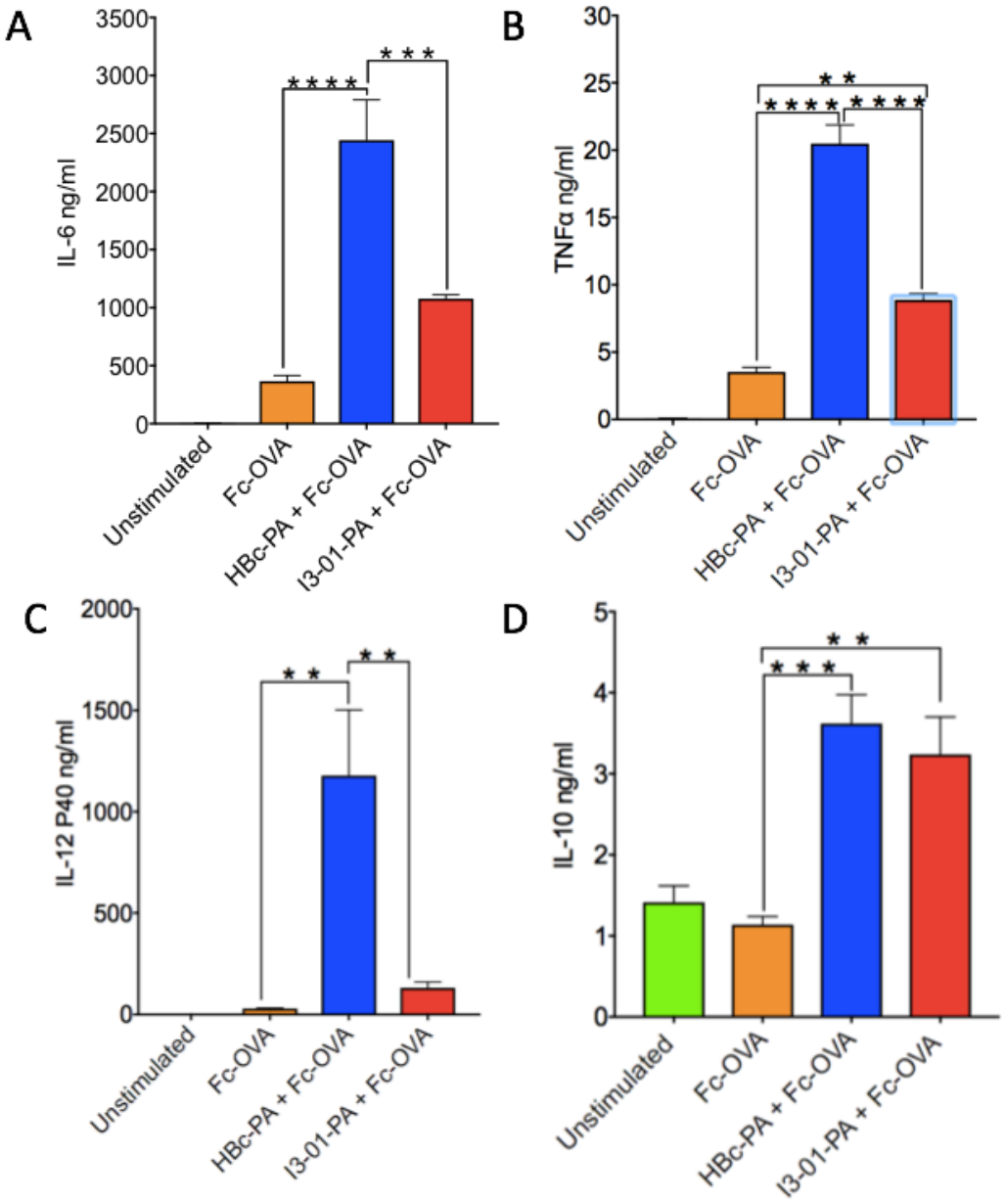

Figure 6-4. Dendritic cell cytokine secretion following stimulation with various Fc-OVA conjugations was detected by enzyme-linked immunosorbent assays (ELISAs). (A-D) The secretion of IL-6, TNF- α, IL-12p40 and IL-10 was analysed following a 5 hr protein stimulation period. Each point represents the mean and standard error of the mean (SEM) of duplicate samples for three separate experiments. A one-way ANOVA with Tukey's multiple comparison tests was used to analyse the statistical significance. ****p<0.0001, ***p<0.001, **p<0.01, *p<0.05.

6.2.5 Summary of dendritic cell uptake and activation

Experiment		Fc-OVA	HBc-PA + Fc-OVA	I3-01-PA + Fc-OVA
Dendritic Cell Uptake	% FITC Positive Cells	High	High	High
	GMFI Positive Cells	High	High	High
Dendritic Cell Activation	CD80, CD86, MHC-II CD40	High	High	High
Dendritic Cell Cytokine Production	IL-6	Low	High	Low
	IL-12-p40	Low	High	Low
	TNF-α	Low	High	Low
	IL-10	Low	High	High

Table 6-1. Summary of the uptake and activation of dendritic cells when stimulated by different Fc-OVA conjugations.

Experiment		Fc-OVA v HBc-PA + Fc-OVA	Fc-OVA v I3-01-PA + Fc-OVA	HBc-PA + Fc-OVA v I3-01-PA + Fc-OVA
Dendritic Cell Uptake	% FITC Positive Cells	NSD	NSD	NSD
	GMFI Positive Cells	NSD	NSD	NSD
Dendritic Cell Activation	CD80, CD86, MHC-II, CD40	NSD	NSD	NSD
Dendritic Cell Cytokine Production	IL-6	$p<0.0001$	NSD	$p=0.0007$
	IL-12-p40	$p<0.0017$	NSD	$p=0.0036$
	TNF-α	$p<0.0001$	$p=0.0016$	$p<0.0001$
	IL-10	$p=0.0003$	$p=0.0016$	NSD

Table 6-2. Comparison of the uptake and activation of dendritic cells when stimulated by different Fc-OVA conjugations. NSD= No significant difference, a one-way analysis of variance (ANOVA) with Tukey's multiple comparison tests was used to analyse the statistical significance. ****$p<0.0001$, ***$p<0.001$, **$p<0.01$, *$p<0.05$.

6.3 *In vitro* analysis of the ovalbumin-specific OT-II T cell response

6.3.1 Stimulation and identification of the CD4 T cell population

Following the uptake of Fc-OVA and activation of dendritic cells, it was important to assess the ability of these cells to stimulate an effector CD4 T cell response. This T cell response is important and carries out multiple functions including the activation of B cells, cytotoxic T cells. It is also clear that CD4 cells are crucial for the suppression of the immune reaction through the stimulation of the production of T regulatory cells [284]. The availability of OT-II transgenic mice provides an opportunity to explore the proliferation of specific ovalbumin CD4 T cells in response to dendritic cell stimulation with the Fc-OVA antigen [201].

The purpose of this section was to establish if the specific CD4 T cell response is dependent on the method of presentation of the Fc-OVA antigen to dendritic cells. To study this, the Fc-OVA conjugations were prepared as in section 6.2.1 (without the FITC labelling step) and were incubated with the dendritic cells for 5 hrs. The CD4 OT-II cells were isolated and purified from the OT-II mouse spleen and lymph nodes before being labelled with carboxyfluorescein succinimidyl ester (CFSE) using methods in section 2.9.3. This allows the T cell proliferation to be measured by flow cytometry. The CD4 T cells were incubated with the dendritic cells following antigen stimulation for 3 days prior to supernatant removal and flow cytometry analysis. This allowed for later cytokine analysis and staining for the detection of specific extracellular and intracellular markers. A gating strategy was used to select the CD4 T cell population and from within this the expression of different populations was selected using their respective controls (Figure 6.5).

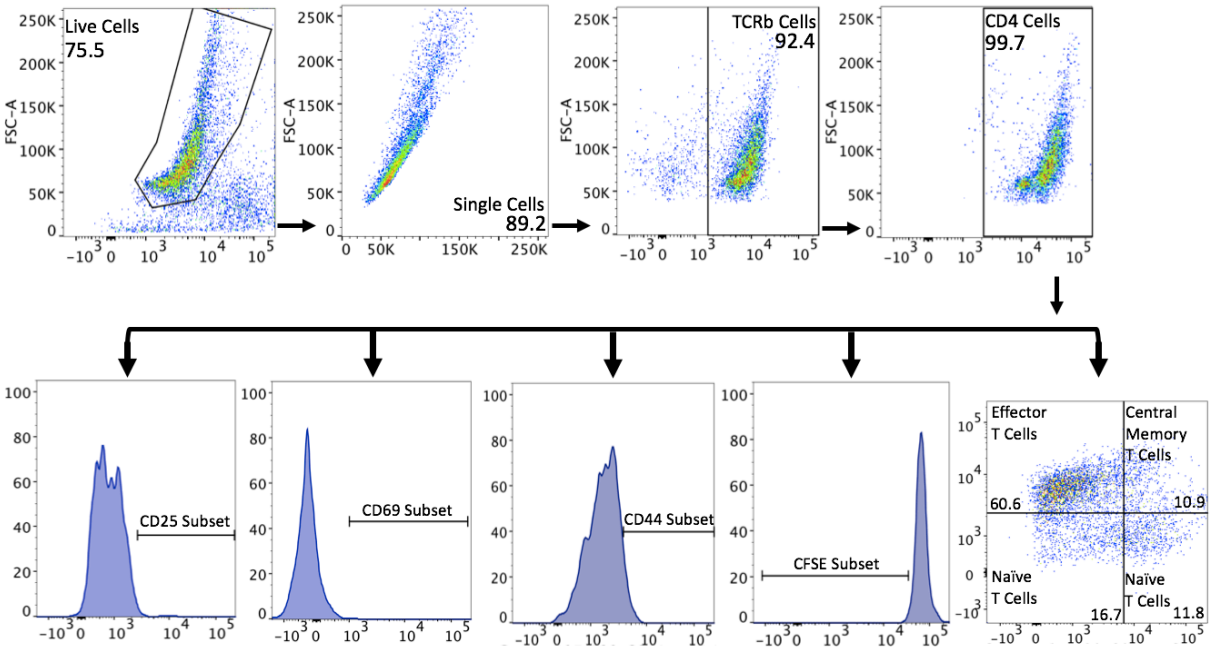

Figure 6-5. OT-II CD4 T Cell flow cytometry gating strategy. The live cells were first selected followed by the single cells. The T cell receptor beta (TCRb) and CD4 markers were used to Identify the T cell population. A CFSE control ascertained the proliferating CD4 T cell population and cells were further gated to identify the CD25, CD44 and CD69 subsets. Finally, an analysis of the CD44 and CD62L markers allowed the identification of the separate T cell populations within the CD4 T cell samples.

6.3.2 Analysis of CD4 T cell proliferation in response to Fc-OVA uptake

To establish if the method of Fc-OVA presentation to the dendritic cells affected the amount of CD4 T cell proliferation, the percentage of CFSE positive cells was compared between the Fc-OVA conjugations using flow cytometry. There was a significant increase in T cell proliferation when Fc-OVA was conjugated to either the HBc-VLP or I3-01-PA compared to when it was presented alone ($p<0.0001$). There was also no significant difference between which of the platforms are selected to present the Fc-OVA antigen ($p=0.9996$) (Figure 6.6). This suggests that the ability to stimulate a CD4 T cell response to the Fc-OVA antigen is enhanced by the HBc-PA VLP and that the synthetic I3-01-PA assembly can produce the same effect equally as successfully. The Fc-OVA only conjugation stimulated a significant increase in CD4 T cells in comparison to the unmodified ovalbumin ($p<0.0001$). The reason for this could be explained by binding of Fc-OVA to the Fcγ receptors on the cell surface (Figure 6.2). The I3-01-PA platform appears to be just as capable at proliferating T cells in response to coupled Fc-OVA antigen as the established HBc-PA VLP- a key finding of this work.

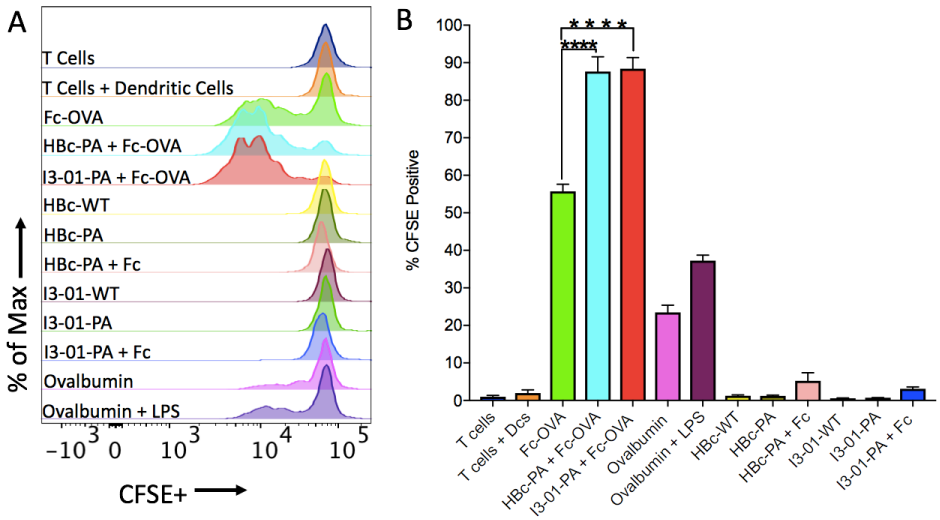

Figure 6-6. Analysis of CD4 OT-II T cell proliferation. (A) Histogram of the CFSE labelled T cells at day 3 in different conditions analysed by flow cytometry. (B) The percentage of CFSE positive T cells in different conditions for triplicate samples in a single experiment. A one-way ANOVA with Tukey's multiple comparison tests was used to analyse the statistical significance. ****$p<0.0001$, ***$p<0.001$, **$p<0.01$, *$p<0.05$. $p>0.05$ defines no significant difference.

6.3.3 Analysis of CD4 T cell activation in response to Fc-OVA uptake

6.3.3.1 CD25

It is clear that there was an increase in CD4 T cells when the Fc-OVA antigen was presented on both the HBc-PA VLP or I3-01-PA platforms. It was important to analyse the level of activation of these proliferated T cells: the cell surface markers CD25, CD69 and CD44 were used to assess this. CD25 is the receptor for the cytokine IL-2: production of IL-2 in response to antigen stimulation of the dendritic cells would lead to an increase expression of this marker [285]. There was a parallel increase in the expression of CD25 when the dendritic cells are stimulated by Fc-OVA when the antigen is conjugated to either the HBc-PA VLP or I3-01-PA assembly, compared to when it is presented alone ($p<0.0001$) (Figure 6.7). This suggests that the T cells which are proliferated are activated further with the addition of the HBc-PA VLP or I3-01-PA assemblies and that the synthetic assembly is as effective as the VLP ($p=0.9997$). The Fc-OVA antigen alone led to an increase in CD25 expression compared to the ovalbumin positive control ($p=0.0045$). This can be attributed, as previously, to the increased uptake of Fc-OVA due to the expression of the Fcγ receptors on the dendritic cells.

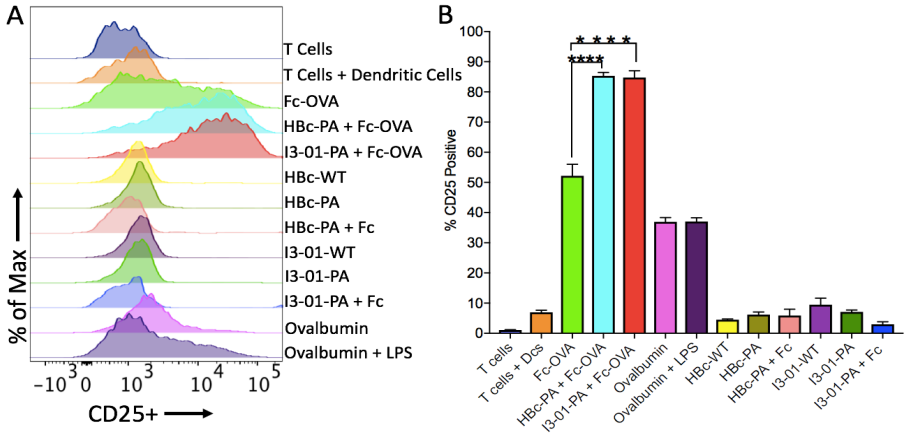

Figure 6-7. Analysis of CD4 OT-II T cell CD25 expression. (A) Histogram of the CD25 expression from the OT-II T cells at day 3 in different conditions analysed by flow cytometry. (B) The percentage of CD25 positive T cells in different conditions for triplicate samples in a single experiment. A one-way ANOVA with Tukey's multiple comparison tests was used to analyse the statistical significance. ****$p<0.0001$, ***$p<0.001$, **$p<0.01$, *$p<0.05$. $p>0.05$ defines no significant difference.

6.3.3.2 CD69

The second marker assessed was CD69: this is marker of CD4 T cell activation which is expressed early on in the adaptive immune response. It is stimulated by multiple mechanisms, including the IL-2 interaction with CD25 mentioned above [285]. Much like CD25, there was a significant increase in the expression of CD69 when Fc-OVA stimulated dendritic cells when conjugated to either the HBc-PA VLP or I3-01-PA in comparison to the presentation of Fc-OVA alone ($p<0.0001$) (Figure 6.8). There was also a significant difference between expression of CD69 when the Fc-OVA was conjugated to the HBc-PA VLP, compared to the I3-01-PA assembly. Finally, there was no significant difference in the expression of CD69 when Fc-OVA was presented to dendritic cells alone in comparison to the ovalbumin control, showing no effect of the Fcγ receptor here ($p=0.9854$).

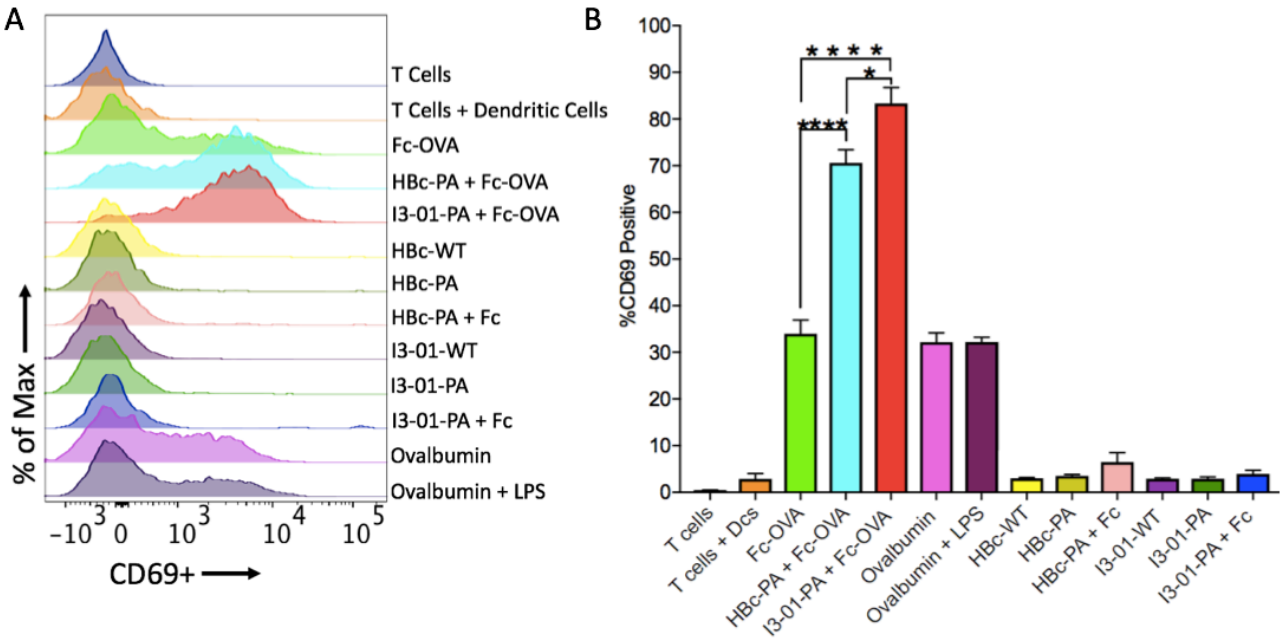

Figure 6-8. Analysis of CD4 OT-II T cell CD69 expression. (A) Histogram of the CD69 expression from the OT-II T cells at day 3 in different conditions analysed by flow cytometry. (B) The percentage of CD69 positive T cells in different conditions for triplicate samples in a single experiment. A one-way ANOVA with Tukey's multiple comparison tests was used to analyse the statistical significance. ****$p<0.0001$, ***$p<0.001$, **$p<0.01$, *$p<0.05$.

6.3.3.3 CD44

CD44 is a marker which is involved in early T cell signalling events and can be used to distinguish between different CD4 T cell subtypes [286]. There is a significant increase in CD44 expression when Fc-OVA is presented to the dendritic cells on the HBc-PA VLP in comparison to when it is unconjugated (p=0.0078) (Figure 6.9). However, there was no significant difference when the Fc-OVA antigen was conjugated to the I3-01-PA platform, suggesting the HBc-PA VLP has some advantageous method of activating the CD4 T cells which I3-01-PA does not (p=0.1117). Finally, there was no significant difference in the expression of CD44 when Fc-OVA was presented to dendritic cells alone in comparison to the ovalbumin control (p=0.3578), suggesting that the T cell subtype is unaffected by the presence of the Fcγ receptor.

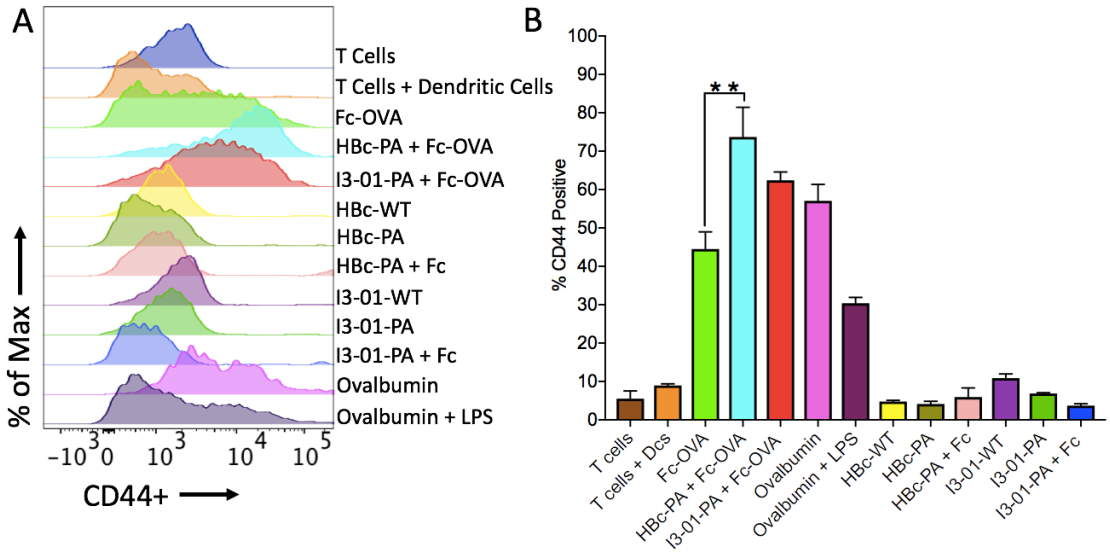

Figure 6-9. Analysis of CD4 OT-II T cell CD44 expression. (A) Histogram of the CD44 expression from the OT-II T cells at day 3 in different conditions analysed by flow cytometry. (B) The percentage of CD44 positive T cells in different conditions for triplicate samples in a single experiment. A one-way ANOVA with Tukey's multiple comparison tests was used to analyse the statistical significance. ****p<0.0001, ***p<0.001, **p<0.01, *p<0.05. p>0.05 defines no significant difference.

6.3.4 Analysis of the memory T cell populations induced through Fc-OVA stimulation

The markers assessed in section 6.3.3 allowed the analysis of the effector T cell population of the CD4 cells. However this is only one subset of the CD4 T cells and it was important to examine a second population, the memory cell subsets, within the T cells that have proliferated in response to antigen [16]. Two subsets were to be examined; the effector memory T (T_{EM}) cells and the central memory (T_{CM}) cells. The T_{EM} subset can be defined as having high expression of CD44 and low expression of CD26L whereas the T_{CM} cells have high expression of both CD44 and CD62L [287].

The percentages of the T_{EM} and T_{CM} populations were analysed by flow cytometry using the same protein conjugations as in section 6.3.3. There was a significant increase in the percentage T_{EM} cells when Fc-OVA was conjugated with the HBc-PA VLP and I3-01-PA in comparison to when Fc-OVA was presented to the dendritic cells alone (p=0.0003) (Figure 6.10A). There was no difference in the choice of platform: each assembly is as effective as producing this response (p=0.9989). These results reflect the results from the marker expression profiles discussed in section 6.3.3 and therefore confirm the importance of the antigen scaffolds in the ability to stimulate a T cell response and that both the assemblies work equally well.

There was no significant increase in the percentage of T_{CM} cells when Fc-OVA was conjugated with the HBc-PA VLP and I3-01-PA in comparison to when Fc-OVA was presented to the dendritic cells alone (p=0.2269 and p=0.9328) (Figure 6.10B). This suggests that the T_{CM} CD4 population is unaffected by the method of antigen presentation contrasting with the effect observed in the T_{EM} CD4 population.

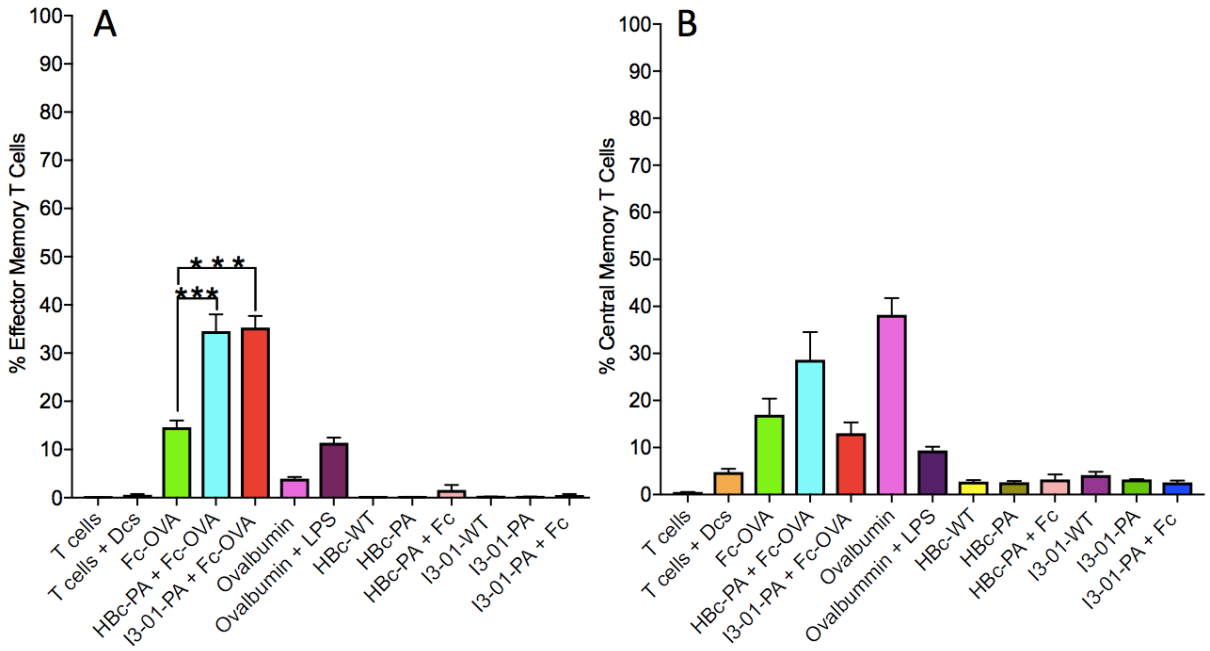

Figure 6-10. Effect of the method of antigen presentation on the CD4 OT-II effector and central memory T cell populations. (A) The percentage of effector memory cells from the OT-II T cell population at day 3 in different conditions analysed by flow cytometry. (B) The percentage of central memory cells from the OT-II T cell population at day 3 in different conditions analysed by flow cytometry. For (A) and (B) samples were in triplicate from a single experiment. A one-way ANOVA with Tukey's multiple comparison tests was used to analyse the statistical significance. ****$p<0.0001$, ***$p<0.001$, **$p<0.01$, *$p<0.05$. $p>0.05$ defines no significant difference.

6.3.5 Analysis of the CD4 T cell lineage transcription factors produced in response to Fc-OVA uptake by dendritic cells

6.3.5.1 T-bet

It was important to investigate the nature of the proliferated, activated CD4 T cells further to analyse if the method of antigen presentation to dendritic cells plays a role in skewing the immune response. In order to do this the expression of three T cell lineage transcription factors were analysed; T-bet, RORγt, and FoxP3. T box transcription factor (T-bet) is a transcriptional factor that determines the fate of a naïve T cell to a Th1 lineage through the control of the IFN-γ cytokine. The expression of T-bet correlates with the expression of IFN-γ, therefore an expression of this intracellular marker would suggest a Th1 T cell response is induced [21]. It is clear that there is expression of T-bet in all samples but that there is no significant difference in the amount of expression of this transcription factor related to the nature of the Fc-OVA antigen display (Figure 6.11).

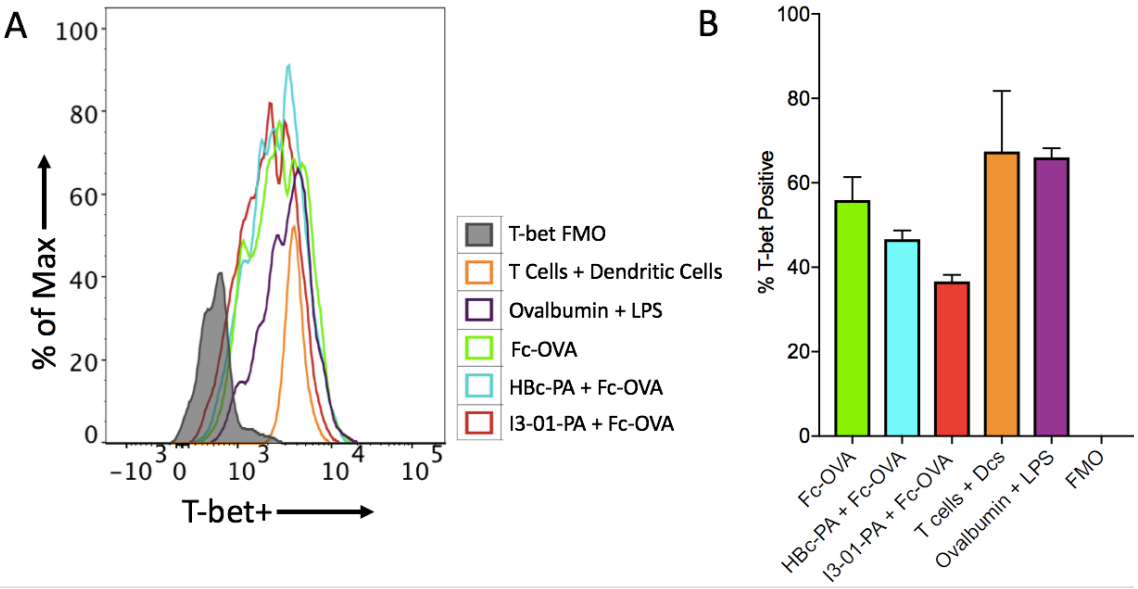

Figure 6-11. Analysis of production of CD4 OT-II transcription factor T-bet. (A) Histogram of the T-bet expression from the OT-II T cells at day 3 in different conditions analysed by flow cytometry. (B) The percentage of T-bet positive T cells in different conditions for triplicate samples in a single experiment. A one-way ANOVA with Tukey's multiple comparison tests was used to analyse the statistical significance. $p>0.05$ defines no significant difference.

6.3.5.2 RORγt

RORγt is a transcription factor that is involved in determining the fate of naïve T cells to the Th17 lineage. The nature of a Th17 response can lead to autoimmune diseases through the production of inflammatory cytokines such as IL-17 [27]. There is a production of RORγt in the T cells which were co-cultured with unstimulated dendritic cells (Figure 6.12). However, there is a significant decrease in this level in the T cells co-cultured with the Fc-OVA alone (p=0.0279), conjugated to the HBC-PA VLP (p=0.0262) and conjugated to I3-01-PA (p=0.0254). This suggests that the differentiation of naïve T cells into a Th17 lineage is an effect lost upon dendritic cell stimulation with Fc-OVA, independent of the method of display.

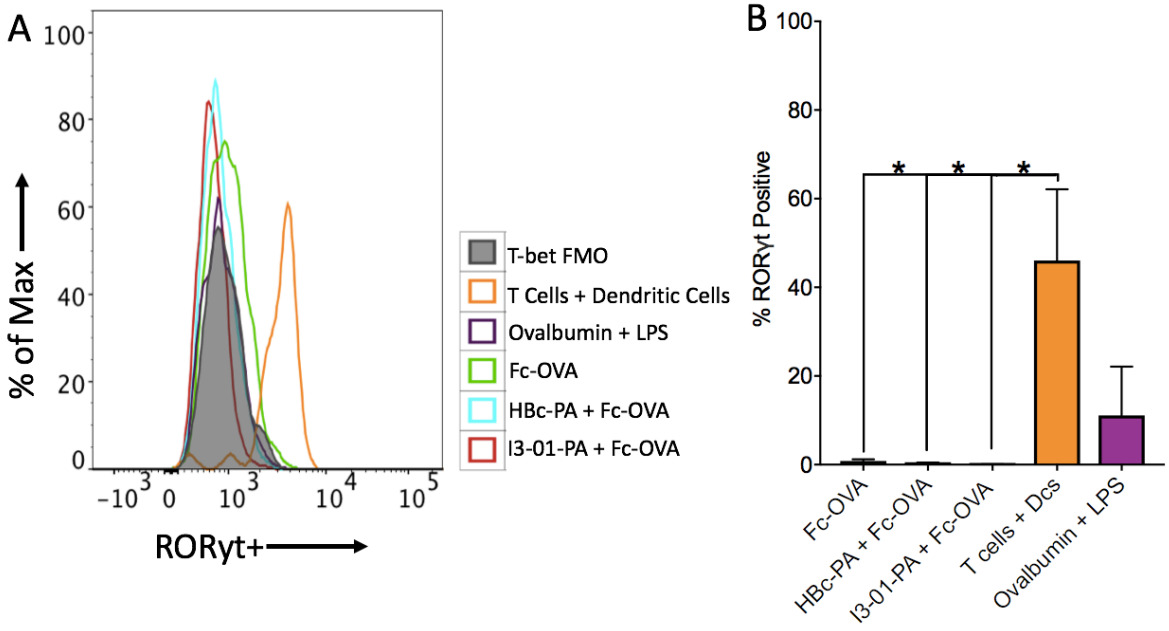

Figure 6-12. Analysis of production of CD4 OT-II transcription factor RORγt. (A) Histogram of the RORγt expression from the OT-II T cells at day 3 in different conditions analysed by flow cytometry. (B) The percentage of RORγt positive T cells in different conditions for triplicate samples in a single experiment. A one-way ANOVA with Tukey's multiple comparison tests was used to analyse the statistical significance. ****p<0.0001, ***p<0.001, **p<0.01, *p<0.05. p>0.05 defines no significant difference.

6.3.5.3 FoxP3

The final transcription factor investigated was Forkhead Box P3 (FoxP3), a determiner of a Treg population. These cells supress the immune response through the secretion of IL-10 and TGF-β and it is reported FoxP3 has the biggest role in stimulating this process [27]. There was no expression of this intracellular marker in any of the cells as analysed by flow cytometry (data not shown). This suggests that stimulation of dendritic cells by this antigen does not lead to a Treg response.

Based on the advice from colleagues and from an initial experiment looking into transcription factor lineages, it was decided not to look into Th2 cells as expression of these transcription factors, specifically GATA-3, was found to be very low. To conclude, the above data suggests that the activation of dendritic cells with Fc-OVA stimulates the T cells to differentiate into the Th1 lineage rather than a Th17 or Treg class, as T-bet is the only intracellular marker with significant expression. It also suggests the fact that the nature of antigen presentation makes no difference to the eventual lineage of proliferated T cells.

6.3.6 The cytokine profiles produced from CD4 OT-II T cells primed with dendritic cells stimulated by different Fc-OVA conjugations

Much like the transcription factors previously analysed, the production of cytokines by CD4 T cells can give information into the skewing of the T cell responses produced by different Fc-OVA conjugations. This also provides an insight as to whether the choice of antigen presentation platform alters the samples' individual cytokine profiles and hence the overall CD4 T cell response. The levels of IFN-γ, IL-4, IL-10, IL-2 and Granzyme B produced by the CD4 T cells primed by stimulated dendritic cells was assessed by ELISA.

The OT-II T cells primed with dendritic cells stimulated by Fc-OVA alone secreted a high amount of IFN-γ but low amounts of the other cytokines analysed. The HBc-PA + Fc-OVA conjugation produced a large amount of all of the cytokines apart from IL-10 and the I3-01-PA + Fc-OVA

conjugation led to the secretion of a high amount of IL-4, IFN-γ and Granzyme B and a low amount of IL-2 and IL-10 (Table 6.3).

There was no significant difference between when Fc-OVA was presented alone, with the HBc-PA platform or with the I3-01-PA platform on the amount of IFN-γ produced (Figure 6.13A and Table 6.4). There was a significant difference in the amount of IL-4 produced by the OT-II T cells when they were primed with dendritic cells stimulated by Fc-OVA conjugated to either the HBc-PA VLP or the I3-01-PA assembly compared to Fc-OVA alone ($p<0.0001$ in both cases, Figure 6.13B). There was also a significant difference between the HBC-PA + Fc-OVA and I3-01-PA + Fc-OVA samples ($p<0.001$). The levels of IL-10 produced were low in all samples, with a small significant difference between only the Fc-OVA alone and HBc-PA + Fc-OVA conjugation ($p=0.0191$, Figure 13C).

IFN-γ is produced by Th1 effector T cells and has a role in proliferating these cells to promote a specific response further. This cytokine also works to reduce the Th2 response through the inhibition of IL-4 [288]. IL-10 and IL-4 are markers for the Th2 subset of CD4 T cells and IL-4 specifically also works to supress the Th1 CD4 T cell population through inhibition of IFN-γ [289] [290]. Taken together, these results suggest that the response is skewed towards a Th1 subtype due to the high amounts of IFN-γ and low amounts of IL-10 produced across all samples. This is safe to conclude, despite the increase in volume of IL-4 in the Fc-OVA conjugation samples, as the amount produced is significantly smaller than the amount of IFN-γ [291].

IL-2 is produced mainly by activated T cells, is very important for promoting proliferation of T cells and is essential for the production and expansion of Treg cells [292]. This role of stimulating proliferation extends to effector T cells, suggesting this function is present in both pro- and anti-inflammatory T cells [293]. There was a significant increase in IL-2 production between the Fc-OVA sample, compared to the HBc-PA + Fc-OVA and I3-01-PA + Fc-OVA samples ($p=0.0007$ and $p<0.0001$ respectively, Figure 6.13D). The I3-01-PA + Fc-OVA sample stimulated a significantly greater increase in IL-2 cytokine production in comparison to the HBc-PA + Fc-OVA sample

(p=0.0007). This would suggest that presenting the Fc-OVA antigen on either platform led to a larger expansion of effector T cells than when it was presented alone, with the I3-01-PA assembly producing the greatest effect.

The final T cell cytokine analysed was Granzyme B. This is a serine protease which is produced by a range of T cell populations including; CD4 memory T cells, Tregs, Th17 and Th1 cells [294]. Granzyme B has the function of inducing cell death following the activation of the T cell receptor [294]. There was a significant increase in the production of Granzyme B when Fc-OVA was conjugated to both the HBc-PA VLP and I3-01-PA assembly compared to Fc-OVA alone (p=0.0019 and p=0.0023, Figure 6.13E). This increase was no different between the HBc-PA + Fc-OVA and I3-01-PA + Fc-OVA conditions. Presenting Fc-OVA on either platform increases the production of Granzyme B in comparison to the antigen alone. This is presumably down to the clonal expansion of T cells which enable more production of this cytokine due to the increase in IL-2 also found in these conditions.

To summarise, the CD4 T cells were polarised to a Th1 subtype, independent of the method of antigen presentation, as high amounts of IFN-γ and low amounts of IL-4 and IL-10 were found in all samples. However, the number of these CD4 T cells and their ability to kill infected cells, through the secretion of IL-2 and Granzyme B respectively, is increased by the presentation of the Fc-OVA antigen on a platform. The specific platform that appears to perform this most effectively is the I3-01-PA assembly.

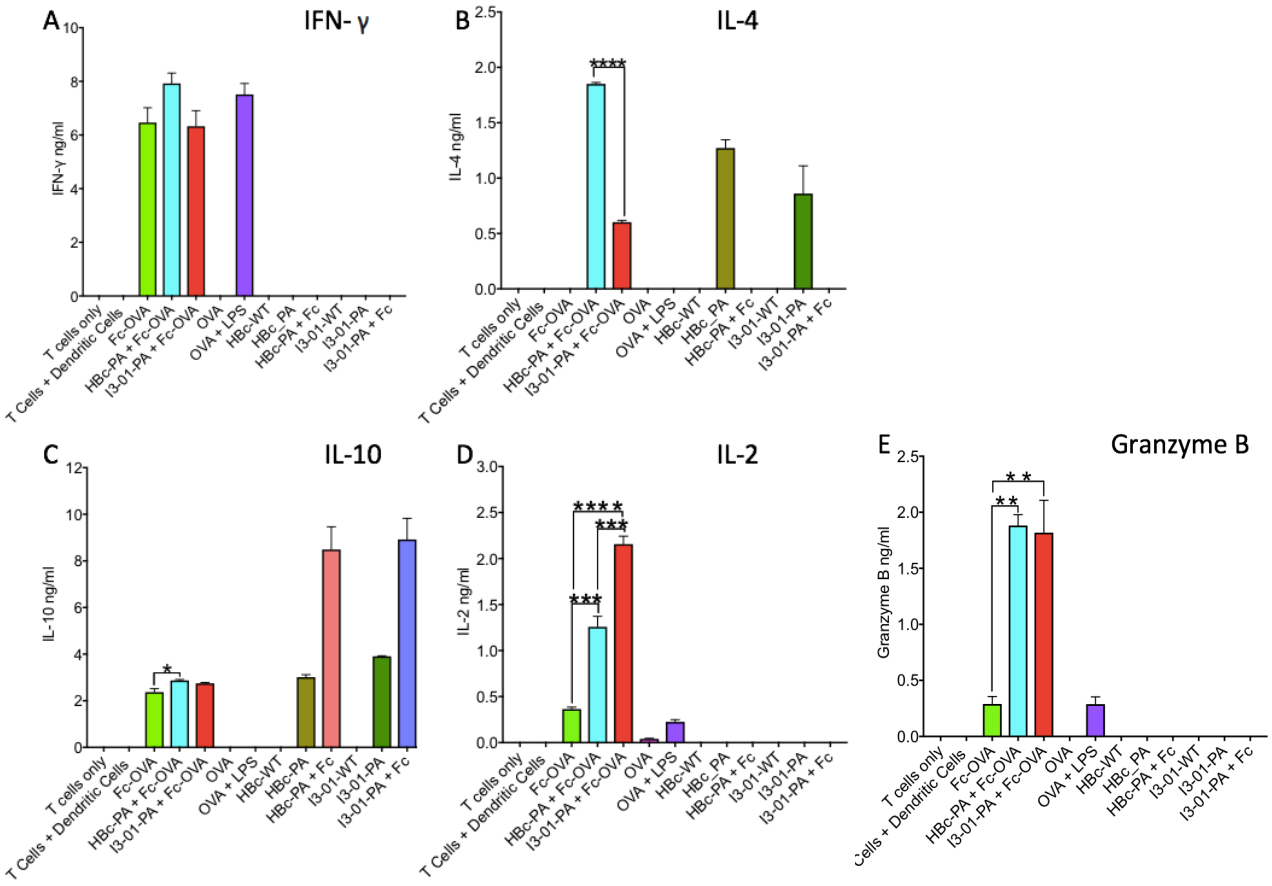

Figure 6-13. CD4 T cell cytokine secretion following priming with dendritic cells stimulated by various Fc-OVA conjugations. The dendritic cells and T cells were co-cultured and the supernatant was collected on day 3 before analysis for cytokine production by ELISA. (A-E) The secretion of IFNγ, IL-4, IL-10, IL-2 and Granzyme B was analysed. Each bar represents mean and SEM of triplicate biological sample from a single experiment. A one-way ANOVA with Tukey's multiple comparison tests was used to analyse the statistical significance. ****p<0.0001, ***p<0.001, **p<0.01, *p<0.05. p>0.05 defines no significant difference.

6.3.7 Summary of T cell proliferation and activation

Experiments		Fc-OVA	HBc-PA + Fc-OVA	I3-01-PA + Fc-OVA
CD4 T cell proliferation	% CFSE Positive Cells	Low	High	High
CD4 T-cell activation	% CD25 Positive Cells	Low	High	High
	% CD69 Positive Cells	Low	High	High
	% CD44 Positive Cells	Low	High	Low
CD4 T Cell Memory Cells	% Effector Memory Cells	Low	High	High
	% Central Memory Cells	Low	Low	Low
CD4 T cell Transcription Factors	T-bet	High	High	High
	RORγt	Low	Low	Low
CD4 T Cell Cytokine Production	IL-2	Low	High	High
	IL-4	Low	High	Low
	IL-10	Low	Low	Low
	IFN-y	High	High	High
	Granzyme B	Low	High	High

Table 6-3. Summary of the proliferation and activation of CD4 T cells following the stimulation of dendritic cells by different Fc-OVA conjugations.

Experiments		Fc-OVA v HBc-PA + Fc-OVA	Fc-OVA v I3-01-PA + Fc-OVA	HBc-PA + Fc-OVA v I3-01-PA + Fc-OVA
CD4 T cell proliferation	% CFSE Positive Cells	p<0.0001	p<0.0001	NSD
CD4 T-cell activation	% CD25 Positive Cells	p<0.0001	p<0.0001	NSD
	% CD69 Positive Cells	p<0.0001	p<0.0001	p=0.0378
	% CD44 Positive Cells	p=0.0078	NSD	NSD
CD4 T Cell Memory Cells	% Effector Memory Cells	p=0.0003	p=0.0003	NSD
	% Central Memory Cells	NSD	NSD	NSD
CD4 T cell Transcription Factors	T-bet	NSD	NSD	NSD
	RORγt	NSD	NSD	NSD
CD4 T Cell Cytokine Production	IL-2	p= 0.0007	p<0.0001	p=0.0007
	IL-4	p<0.0001	p<0.0001	p<0.0001
	IL-10	p=0.0191	NSD	NSD
	IFN-y	NSD	NSD	NSD
	Granzyme B	p=0.0019	p=0.0023	NSD

Table 6-4. Comparison of the proliferation and activation of CD4 T cells following the stimulation of dendritic cells by different Fc-OVA conjugations. NSD= No significant difference, a one-way ANOVA with Tukey's multiple comparison tests was used to analyse the statistical significance. ****p<0.0001, ***p<0.001, **p<0.01, *p<0.05.

6.4 Discussion

The first aim of this chapter was to investigate if I3-01-PA was an equally successful antigen presentation platform as the HBc-PA VLP. This was assessed by the level of uptake and activation of BMDCs in response to the Fc-OVA antigen alone compared to when it was conjugated to the HBc-PA VLP and I3-01-PA assembly. Secondly, the ability to produce a proliferation of CD4 T cells was also evaluated using these Fc-OVA conjugations. This would enable the nature of the T cell response to the Fc-OVA antigen when displayed on different platforms to be established.

6.4.1 BMDC uptake and activation when Fc-OVA is presented on alternative platforms

There was no difference in the amount of uptake of Fc-OVA into BMDCs over the 5-hour time period, independent of the method of presentation. This is the effect seen previously with the uptake into THP-1 macrophages in Chapter 5. Antigen uptake is only the initial stage forming the immune response and the level of activation of these BMDCs in response to this uptake is important to analyse. The four common dendritic cell activation markers were used to assess the level of activation CD40, CD80, CD86 and MHC-II [295]. These markers have been shown in multiple studies to be upregulated in response to dendritic cell maturation following antigen uptake [296, 297]. The dendritic cells were highly activated in response to all of the Fc-OVA conjugations and there was no difference in the expression of these markers between the three conditions. The I3-01-PA + Fc-OVA and HBc-PA + Fc-OVA conjugations are taken up by the same percentage of cells and activate these cells to the same level as each other. This suggests that, in terms of dendritic cell uptake and activation, the I3-01-PA platform behaves in the same way as the model VLP. This is unsurprising as they are a similar size and there is much evidence for size-dependent uptake into APCs [298] [299]. Differences between the conditions become clear when analysing the dendritic cell cytokine production. There is an increase in a range of pro-inflammatory and anti-inflammatory cytokine secretion from the activated dendritic cells when the Fc-OVA antigen is conjugated to the HBc-PA VLP. Interestingly, this is not seen when the I3-01-PA assembly is used, despite the same level of activation being measured in both conditions.

This is potentially due to the origins of HBc-PA as a VLP in comparison to a thermophilic enzyme being used to create, synthetically, a biological assembly and the differing level of intrinsic T cell epitopes present. It is important to consider these differences as they may become important in terms of the ability of both assemblies to prime and proliferate the resulting T cell response.

6.4.2 CD4 T cell proliferation and activation in response to Fc-OVA

It was important to understand to what extent the activation of dendritic cells following antigen uptake promoted the priming and proliferation of T cells. This would enable any differences in the way the Fc-OVA antigen was presented had on this stage of the immune response to be understood by allowing a comparison of a model VLP with the synthetic I3-01-PA assembly. The T cell response was specific to the antigen, ovalbumin, through the use of the OT-II strain of transgenic mice that contain T cell receptors specifically for an ovalbumin epitope [201].

A significant increase in specific T cell proliferation was seen when Fc-OVA was presented on either the HBc-PA VLP or I3-01-PA platform compared to Fc-OVA alone. This indicates that it is at this point in the immune response that the antigen presentation platform has the effect of an adjuvant on the Fc-OVA antigen and that the I3-01-PA platform is as effective at this as the HBc-PA VLP. This method has been used previously to establish that the use of the adjuvant type II heat-labile enterotoxin LT-IIa of *E. coli* led to a significant ovalbumin specific proliferation of OT-II T cells [300].

The expression of two common T cell activation markers, CD25 and CD69, was assessed: this showed the same effect as the T cell proliferation [285]. In previous studies, an increase in CD25 and CD69 expression was associated with activated proliferating OT-II CD4 cells in response to different antigen presentation methods [301]. The expression pattern reported here suggests that the increased number of T cells produced in response to Fc-OVA conjugated to either platform are T cells that are activated. A third activation marker, CD44, is also a marker of memory so is key to investigate in terms of exploring potential vaccine candidates [286]. As there was no significant increase in expression of CD44 in when I3-01-PA was conjugated to Fc-

OVA in comparison to the antigen alone, the effector and central memory T cell populations were examined. In terms of the effector T cell population, many of the T cells that proliferated were effector T cells and either platform was as effective as the other at producing this response. The second population, the memory T cells, increased in size when Fc-OVA was conjugated to the HBc-PA VLP in comparison to Fc-OVA alone but a decrease was observed when the I3-01-PA platform used. As there is little known about the mechanisms of CD4 memory T cells generation, it is difficult to draw conclusions as to why this difference is present. However, it is clear that the platforms do not perform in the same way as each other, supporting the effect seen previously in the CD44 expression levels.

In order to understand the nature of the T cell responses, the expression of intracellular transcription factors and cytokines was examined across the Fc-OVA conjugations. The expression of T-bet, RORγt and FoxP3 were used to assess the polarisation of the proliferated T cells to either the Th1, TH17 and Treg populations respectively. As it is known that the cytokine production from activated dendritic cells can skew the T cell response the earlier results could inform the results seen here. A large amount of IL-12 and IL-6 produced suggested a Th1/Th17 response was induced rather than a Th2 response [282]. Taken as a whole these results imply a Th1 response is most likely induced when the Fc-OVA is presented to dendritic cells either alone, or conjugated to each platform.

Previous studies using ovalbumin to analyse cytokine production have found these are only secreted in the presence of the costimulatory molecules CD80 and CD86 [302]. We have seen here that these molecules are highly expressed amongst dendritic cells stimulated by Fc-OVA so it is logical that an increase in T cell cytokines follows. This is further supported by the OT-II cytokine responses measured as high amounts of IFN-γ and low amounts of IL-4 and IL-10 present in all Fc-OVA conjugations, independent of the platform choice. The production of these cytokines have been analysed previously using ovalbumin to stimulate OT-II T cells under different conditions and a skewing towards either a Th1 or Th2 response has been reported [303] [304]. Here, antigen presentation appears to effect the amount of IL-2 produced which is

important as this cytokine is known to be required for the CD8 memory T cell response, key in vaccination development [305, 306].

6.4.3 Summary

The work described here suggests that the I3-01-PA assembly can function as a successful antigen presentation platform in a similar fashion to the HBc-PA VLP. On the whole, the two assemblies behave in a very similar manner but the subtler differences observed need to be investigated further both *in vitro* and *in vivo.*

Chapter 7

General Discussion

Chapter 7 -General Discussion

The field of vaccine design is rapidly developing and, given the current global situation, is at the forefront of biomedical research. An estimated 2-3 million deaths are prevented annually due to the availability of vaccines, showing that they are successful at reducing deaths from infectious diseases [307]. There has been a shift from using live attenuated vaccines to designing protein-based formulations and utilising assemblies to display heterologous antigens. This has mainly been achieved through chemical conjugation and, with a lower success rate, genetic fusion [138-142, 144]. The aim of this work was to study the novel I3-01 protein assembly and its application as an antigen presentation platform.

To better understand the context of the progress made in this work it is important to consider the challenges faced in the design of a vaccine. Many hurdles need to be overcome to produce an effective vaccine, including the ability to stimulate the adaptive immune system following processing by antigen presenting cells (APCs). To achieve this the antigen must first reach the APCs, with the two main classes being macrophages and dendritic cells. Dendritic cells have the primary function of antigen presentation, so are the key APCs to target in the process of vaccine design [308]. These cells differentiate from bone marrow-derived precursors, a process that is completed once the dendritic cells reach peripheral tissues [308]. Dendritic cells move through the blood and lymph nodes until they're met by signals of inflammation and their distribution is unique in comparison to macrophages and B cells [308, 309]. Differentiated dendritic cells receive danger signals which cause the cells to mature and internalise antigens, at this point they are effective APCs [308]. The second class of professional APCs to consider is macrophages. These cells are particularly noted for their ability to internalise antigen either non-specially or via a range of receptors, following migration to tissues where there is an infection [308]. The work here analysed the process of antigen uptake into both these classes of APC.

Once an antigen is taken up by an APC, the adaptive immune response is engaged and T cells are appropriately activated. The role of dendritic cells is to bind and internalise antigen, process it and to present it to T cells to engage the adaptive immune response through priming T cells [15]. In order to achieve this, the activated dendritic cells migrate to the lymph nodes [310]. A key element of this work was to investigate any differences in this process that were dependent on how antigens were presented to dendritic cells and macrophages. There is evidence that the shape, size and charge of an antigen can affect the process of antigen uptake and internalisation. When studying antigen uptake by macrophages, it is important to consider evidence which supports the theory that different geometries of antigen have different attachment tendencies to the APC cell surface [311]. This suggests that the surface features of the macrophage determine when the antigen is bound to the cell surface for internalisation and highlights the importance of this initial stage of antigen recognition. As the I3-01-PA assembly and HBc-PA VLP are similar in shape and size, it is unsurprising that we found similar rates of uptake of the Fc-OVA antigen when presented on the two assemblies. Once bound to the cell surface, it has been shown that the shape of the antigen can modulate the process of phagocytosis and that a change in shape can lead to a decrease in rate of this process [312]. The impact of shape and size of the antigen has also been shown to affect the APC internalisation rates separately [313]. There is evidence that shape and size of the antigen can modulate the immune response in dendritic cells, in terms of both IgG antibody titre and the T helper cell subtype skewing [314]. Considering the T cell response specifically, smaller, spherical, particles generated a stronger response than larger rod shaped platforms [314]. The optimal diameter of a particle to be taken up by dendritic cells was found to be 0.5µm and below, however the rate of internalisation by these cells could be increased if the particles were given a positive charge [315]. The I3-01-PA assembly has a diameter of 35nm, as measured by DLS, which explains the high uptake rates measured here in both macrophages and dendritic cells.

Hydrophobicity has also been a variable investigated for its relative effects on antigen internalisation. Microparticles with similar shape, size and charge were shown to be taken up

more efficiently by dendritic cells following an increase in hydrophobic chemistry [316]. There were big increases in the dendritic cell activation markers MHC-II and CD86 *in vitro* and also in the secretion of T cell cytokines *in vivo* [316]. This suggests that not only internalisation rates into dendritic cells are effected by particle hydrophobicity but the level of activation and downstream antigen processing is also increased. This highlights that there are many factors to consider when trying to increase uptake into and activation of APCs.

Another important consideration in the development of many modern vaccines is the use of adjuvants. An adjuvant is defined as an entity that can increase the immunogenicity of antigens when added to a vaccine formulation through activation of the innate and adaptive arms of the immune system [317]. There is a renewed focus on novel adjuvants which can achieve this effect without leading to an increase in side effects. The innate immune system is activated when an adjuvant binds to pattern recognition receptors on the host immune cells [317]. Examples of adjuvants in current vaccines include aluminium salts for Hepatitis A and B, oil-water emulsions for seasonal influenza and water-oil emulsions for malaria [318]. Aluminium salts have been used in vaccines as adjuvants more many years and have been associated with slow, continuous release after injection and an increase of antigen uptake by APCs [318]. There has been more recent evidence that the addition of aluminium salts leads to the antigens being presented in a multivalent form, hence increasing internalisation by APCs [319]. The two current Hepatitis vaccines licensed in the USA, Engerix-B™ and Recombivax™, include aluminium salts as an adjuvant and they both induce high protective responses, especially in children [320]. Emulsions both water-oil and oil-water have been used as adjuvants in vaccine development [318]. Water-in-oil emulsions are generally used in therapeutic vaccines having initially being discontinued due to safety concerns [318]. A montanide emulsion was found to be a safe adjuvant in a trial for a human prostate cancer vaccine [321]. Oil-in-water emulsions have reduced reactogenicity compared with water-in-oil emulsions but their mode of action is unclear [318]. It is thought that APC recruitment, activation and cytokine secretion, along with other innate inflammatory responses, are involved in the increase in immunogenicity [322].

MF59 is an example of an oil-in-water adjuvant that has been used in in the licensed seasonal influenza vaccine, stimulating an adaptive Th2 response [323].

A more recent development has been the use of VLPs as adjuvants in vaccine design. These assemblies have the ability to induce strong B-cell responses by cross-linking specific receptors on B cells without the need for adjuvants [204]. They have also been used to display antigens to APCs in a more natural form and orientation than the adjuvants mentioned previously [324]. A novel vaccine against Anthrax has been successfully produced using VLPs from Flock House virus without the need for an additional adjuvant [325]. These VLPs have also been used in the design of an Influenza vaccine displaying 180 copies of the Hemagglutinin antigen [326]. Upon inoculation into mice, cross reactive antibodies were produced without the need for an adjuvant; however, they were not found to be neutralising [326]. A second influenza vaccine was designed without adjuvant using VLPs generated from the M2 antigen, this provided protective long lasting immunity [327]. However, many of the current licensed VLP based vaccines require adjuvants, including the use of aluminium in the human papilloma virus Gardasil and all hepatitis B virus vaccines [328-331]. It is clear that, even though vaccines containing only VLPs are highly immunogenic, an adjuvant is often required to ensure that the immunity induced is sufficient and long lasting [332]. Finally, a range of nanoparticles, including lipid-based nanoparticles and synthetic assemblies, have been found to have the effect of an adjuvant [333, 334]. Lipid-based nanoparticles, including a recombinant protein antigen, were investigated as a possible novel malaria vaccine [333]. There was found to be an increase in the responses measured, including the level of the specific T cell proliferation and the avidity of the antibodies elicited. These effects were found to occur relative to adjuvant use, highlighting the effect of displaying antigen on a nanoparticle [333]. Here, we found that the I3-01-PA assembly induced comparable responses to the HBc-PA VLP, suggesting this synthetic assembly may have the effect of an adjuvant. Nanoparticles have also been designed to have increased immunogenicity through the addition of adjuvants such as the TLR-4 and TLR-7 ligands [334]. These ligands have been engineered into a synthetic biodegradable polymer to resemble a virus in size and composition. This led to a production of specific neutralising antibodies and the long

term presence of T cells, suggesting it is possible to increase the immunogenicity of a nanoparticle for use in a vaccine. This suggests that the I3-01 assembly could be genetically modified further using TLR ligands to enhance the immunogenicity of this platform, removing the need for addition adjuvants.

In the design of any vaccine, initial *in vitro* experiments can be carried out using murine or human dendritic cells. In order to understand and interpret the responses measured, it is important to have a grasp on the complications surrounding dendritic cell subsets. There is more understood about murine dendritic cells and their differentiation in comparison to their human counterparts and it is important to consider this fact when translating results between these two classes of cells [335]. Human dendritic cells can be classified into two main subtypes-classical (cDC) and plasmacytoid (pDC)-with the latter having more limited ability to phagocytose, process and present antigen [336, 337].

The cDCs can be split into two further subtypes: cDC1 (type 1) and cDC2 (type 2) [338]. The cDC1 subtype of dendritic cells are identified by the expression of CD8a, XCR1, CLEC9A or CD103 on their cell surface in comparison to the expression of CD11b and CD172a markers on the cDC2 class [339]. cDC1s have the ability to cross-present antigens from intracellular pathogens and stimulate a $CD8^+$ T cell responses [339]. It has been found that the differentiation of this subclass is due to the transcription factors interferon regulatory factor 8 (IRF8) and basic leucine zipper transcriptional factor ATF-like 3 (BATF-3) [340, 341]. The function and differentiation process of cDC1's is fairly well understood and based on initial transcriptomic studies cDC1s they can be defined as forming a fairly homogenous population [339, 342]. The cDC2 subclass is far less understood and they appear to form a much more heterogeneous population [339]. It has been recently discovered that this heterogeneity is on a transcriptional level in both murine and human dendritic cells. The transcription factors RORyt and T-bet are differentially expressed in the two major cDC2 subsets which can be defined by the expression of distinct sets of transcription factors [339]. The cDC1 subset have been found to represent the human counterpart of mouse $CD8^+$ DCs, both having the ability to capture and cross present

endogenous antigens [335]. These mouse and human subtypes are capable of generating CD8 T cell immunity and provides an opportunity to translate murine data into humans [335]. This highlights that the murine data collected in this work can potentially be translated into specific human dendritic cell subtypes. However, there is clearly a large amount of complexity in the human subtypes and the extent that the data can be compared is largely unknown.

Aside from cDCs, another class of cells, pDCs, also circulate in human blood and are identified through the expression of the marker CD303 [343]. These cells have a unique capacity to produce a large amount of IFN-1 in response to viruses and therefore are associated with antiviral immunity [344]. pDCs use their TLR-7 and TLR-9 receptors to recognise viral components and can therefore respond extremely rapidly [345]. It has been hypothesised that this rapid innate response is possible due to the utilisation of pre-synthesized stores of MHC-I and MHC-II [346]. These dendritic cells are also involved in the adaptive arm of the immune response and have been shown to expand the viral antigen-specific CD8+ T effector cell population [346, 347]. Finally, it has been suggested that pDCs could promote the maturation of other dendritic cell subsets, due to their production of large amount of IFN-1, and priming these cells could form the basis of future antiviral vaccines [346].

This additional understanding of the different dendritic subtypes and their role in the immune response has provided the opportunity to target specific subtypes in vaccination [348]. Initial work focused on targeting all subtypes by focusing on the CD11c receptor but more recently studies have targeted a specific dendritic cell subtype [349, 350]. Murine pDCs have been targeted through the bone marrow stromal antigen 2 (BST2) receptor, in combination with TLR agonists [351]. This vaccination strategy was found to elicit strong cellular and humoral responses, including a high titre of broad ranging IgG isotype antibody [351]. There have also been less successful examples of targeting pDCs reported. When Clec9A was targeted on pDCs there was no expansion of the OT-II cell population, suggesting that this dendritic cell subtype has a little role in the immune response when targeted in this way [350, 352]. More success has been found with the classical dendritic cells subtype. When the Dectin-1 receptor was targeted

in vivo with antigen, both $CD4^+$ and $CD8^-$ T cell responses, alongside antibody responses which were much larger than without the receptor targeting [353]. In $CD8^-$ mice targeting the c-type lectin receptor increased antibody production to the same extent as a CpG adjuvant (100-1000 fold) but when the CD205 receptor was targeted this effect was not achieved without adjuvant [354]. As CD205 is more commonly expressed on the $CD8^-$ this suggests a difference in immune responses depending on the involvement of different dendritic cell subtypes [354, 355]. This provides evidence that the preliminary work presented here could be built upon to target certain receptors on specific dendritic cell subtypes to enhance antigen uptake and direct the processing pathway.

Evidently, there are multiple challenges faced during the process of developing a vaccine. The work here presents an alternative platform technology that can be used to present antigens and boost the specific T cell response *in vitro*. This offers the potential of increased immunogenicity coupled with thermal stability. Future work should be focussed on using this technique of antigen insertion as opposed to genetic fusion. This has proven here to be a big success and overcomes one of the major problems in this project; inserting large antigens whilst maintaining assembly. The fact that multiple antigens were displayed successfully on I3-01-PA suggests this technology is applicable to a range of antigens and therefore range of diseases and also heterologous antigen display. Finally, BMDCs have been shown here to be the best *in vitro* method at investigating the uptake and downstream processing of antigens by APCs and future work should look at using this system.

It is important to remember how this work began, looking for a novel vaccine technology that could be applied to Meningitis vaccine development. This protein A technology could be exploited to display an array of meningococcal antigens (such as NadA and NHBA which were investigated here by genetic fusion) at the same time. This would allow the antigens in the current Bexsero MenB vaccine to be displayed in a more optimal way for antigen uptake and downstream processing with the I3-01-PA assembly acting as the antigen presenting platform.

Further work should be prioritised to investigate the potential of the I3-01 assembly being used in part of a vaccine formulation against meningitis and other infectious emerging diseases.

7.1 Future Work

This project could be extended in several ways. The work would aim to establish if the I3-01-PA assembly is a viable antigen presentation platform for use as a vaccine and would include:

- To demonstrate that the I3-01-PA-Fc-OVA construct produces the same responses *in vivo* as shown here *in vitro.*

- To compare the I3-01-PA-Fc-OVA and HBc-PA-Fc-OVA constructs as antigen presentation platforms, including investigating the ability to specifically target dendritic cells using antibodies to specific receptors to try to increase and direct antigen uptake through both of these platforms.

- To scale up the production of the I3-01-PA protein assembly and remove the issue of endotoxin contamination from the current method. This would be carried out through the testing the expression of the I3-01 protein in different systems, to confirm a good yield is produced and that it is assembled. Examples of these systems include the use of mammalian cells lines and insect cells, similar to the method for the production of the Fc-OVA antigen in this work.

- To evaluate the versatility of this platform and its ability to display heterologous antigen by the Protein A fusion method, a number of alternative Fc antigen fusion proteins should be purified and tested. This would allow an assessment of the versatility of the technology as this would be the most appropriate use of the scaffold as a vaccine candidate.

References

1. WHO, *Immunisation Coverage* www.who.int/news-room/fact-sheets/detail/immunization-coverage, 2016.
2. Zepp, F., *Principles of Vaccination.* Methods Mol Biol, 2016. **1403**: p. 57-84.
3. Karch, C.P. and P. Burkhard, *Vaccine technologies: From whole organisms to rationally designed protein assemblies.* Biochem Pharmacol, 2016.
4. Plotkin, S.A. and S.L. Plotkin, *The development of vaccines: how the past led to the future.* Nat Rev Microbiol, 2011. **9**(12): p. 889-93.
5. Ericsson, C.D.a.S., R., *Cholera Vaccines* Clinical Infectious Diseases, 2000. **31**: p. 561-5.
6. Broder, K.R., et al., *Preventing tetanus, diphtheria, and pertussis among adolescents: use of tetanus toxoid, reduced diphtheria toxoid and acellular pertussis vaccines recommendations of the Advisory Committee on Immunization Practices (ACIP).* MMWR Recomm Rep, 2006. **55**(RR-3): p. 1-34.
7. MacKay, P., et al., *Production of immunologically active surface antigens of hepatitis B virus by Escherichia coli.* Proc Natl Acad Sci U S A, 1981. **78**(7): p. 4510-14.
8. Valenzuela, P., Medina, A. and Rutter, W.J., *Synthesis and assembly of hepatitis B virus surface antigen particles in yeast* Nature, 1982. **298**: p. 347-50.
9. Dandolos, E., et al., *Safety and immunogenicity of a recombinant hepatitis B vaccine.* Journal of medical virology, 1985. **17**(1): p. 57-62.
10. FDA, *Recombivax HB.* www.fda.gov/vaccines-blood-biologics/vaccines, 2019.
11. FDA, *Engerix-B.* www.fda.gov/vaccines-blood-biologics/vaccines, 2019.
12. Kelly, D.F., E.R. Moxon, and A.J. Pollard, *Haemophilus influenzae type b conjugate vaccines.* Immunology, 2004. **113**(2): p. 163-74.
13. Janeway, C.A., Travers, P., Walport M., AL,. E. , *Principles of innate and adaptive immunity*, in *The Immune System in Helath and Disease* 2001, Garland Science p. 1-9.
14. Pasare, C. and R. Medzhitov, *Toll-like receptors: linking innate and adaptive immunity.* Microbes Infect, 2004. **6**(15): p. 1382-7.
15. Walsh, K.P. and K.H. Mills, *Dendritic cells and other innate determinants of T helper cell polarisation.* Trends Immunol, 2013. **34**(11): p. 521-30.
16. Pennock, N.D., et al., *T cell responses: naive to memory and everything in between.* Adv Physiol Educ, 2013. **37**(4): p. 273-83.
17. Barnden, M.J., et al., *Defective TCR expression in transgenic mice constructed using cDNA-based alpha- and beta-chain genes under the control of heterologous regulatory elements.* Immunol Cell Biol, 1998. **76**(1): p. 34-40.
18. Paul, W.E. and R.A. Seder, *Lymphocyte responses and cytokines.* Cell, 1994. **76**(2): p. 241-51.
19. Yang, D.D., et al., *Differentiation of CD4+ T cells to Th1 cells requires MAP kinase JNK2.* Immunity, 1998. **9**(4): p. 575-85.
20. Abad, R., et al., *A large portion of meningococcal antigen typing system-negative meningococcal strains from spain is killed by sera from adolescents and infants immunized with 4CMenB.* Clin Vaccine Immunol, 2015. **22**(4): p. 357-60.

21. Szabo, S.J., et al., *A novel transcription factor, T-bet, directs Th1 lineage commitment.* Cell, 2000. **100**(6): p. 655-69.
22. Adorini, L., *Interleukin-12, a key cytokine in Th1-mediated autoimmune diseases.* Cell Mol Life Sci, 1999. **55**(12): p. 1610-25.
23. Walker, J.A. and A.N.J. McKenzie, *TH2 cell development and function.* Nat Rev Immunol, 2018. **18**(2): p. 121-133.
24. Paul, W.E., *Interleukin 4: signalling mechanisms and control of T cell differentiation.* Ciba Found Symp, 1997. **204**: p. 208-16; discussion 216-9.
25. O'Garra, A., *Cytokines induce the development of functionally heterogeneous T helper cell subsets.* Immunity, 1998. **8**(3): p. 275-83.
26. Deo, S.S., et al., *Role played by Th2 type cytokines in IgE mediated allergy and asthma.* Lung India, 2010. **27**(2): p. 66-71.
27. Chen, Z., et al., *FOXP3 and RORgammat: transcriptional regulation of Treg and Th17.* Int Immunopharmacol, 2011. **11**(5): p. 536-42.
28. Korn, T., et al., *IL-17 and Th17 Cells.* Annu Rev Immunol, 2009. **27**: p. 485-517.
29. Komiyama, Y., et al., *IL-17 plays an important role in the development of experimental autoimmune encephalomyelitis.* J Immunol, 2006. **177**(1): p. 566-73.
30. Schwartz, S., J.F. Beaulieu, and F.M. Ruemmele, *Interleukin-17 is a potent immuno-modulator and regulator of normal human intestinal epithelial cell growth.* Biochem Biophys Res Commun, 2005. **337**(2): p. 505-9.
31. Edinger, M. and P. Hoffmann, *Regulatory T cells in stem cell transplantation: strategies and first clinical experiences.* Curr Opin Immunol, 2011. **23**(5): p. 679-84.
32. Kohm, A.P., et al., *Cutting edge: CD4+CD25+ regulatory T cells suppress antigen-specific autoreactive immune responses and central nervous system inflammation during active experimental autoimmune encephalomyelitis.* J Immunol, 2002. **169**(9): p. 4712-6.
33. Sagoo, P., et al., *Human regulatory T cells with alloantigen specificity are more potent inhibitors of alloimmune skin graft damage than polyclonal regulatory T cells.* Sci Transl Med, 2011. **3**(83): p. 83ra42.
34. Bachmann, M.F. and G.T. Jennings, *Vaccine delivery: a matter of size, geometry, kinetics and molecular patterns.* Nat Rev Immunol, 2010. **10**(11): p. 787-96.
35. Lechner, F., et al., *Virus-Like Particles as a Modular System for Novel Vaccines.* Intervirology, 2003. **45**(4-6): p. 212-217.
36. Grgacic, E.V. and D.A. Anderson, *Virus-like particles: passport to immune recognition.* Methods, 2006. **40**(1): p. 60-5.
37. Vietheer, P., *Immunizations with chimeric hepatitis B virus- like particles to induce potential anti-hepatitis C virus neutralizing antibodies Immunizations with chimeric hepatitis B virus-like particles to induce potential anti-hepatitis C virus neutralizing antibodies.* Antiviral Therapy, 2007. **12**: p. 477-487.
38. Schodel, F., Moriaty A.M., Peterson,D.L., Heng, J., Hughes J.L., Will, H., Lecturq, D.J., McGee, J.S., And Milich, D.R., *The Position of Heterologous Epitopes Inserted in Hepatitis B Virus Core Particles Determines Their Immunogenicity.* Journal of Virology, 1992. **66**(1): p. 106-114.

39. Schödel, F., et al., *Hybrid hepatitis B virus core antigen as a vaccine carrier moiety. II. Expression in avirulent Salmonella spp. for mucosal immunization.* Advances in experimental medicine and biology, 1996. **397**: p. 15-21.
40. Nardin, E.H., et al., *Phase I testing of a malaria vaccine composed of hepatitis B virus core particles expressing Plasmodium falciparum circumsporozoite epitopes.* Infect Immun, 2004. **72**(11): p. 6519-27.
41. Tsybalova, L.M., et al., *Development of a candidate influenza vaccine based on virus-like particles displaying influenza M2e peptide into the immunodominant region of hepatitis B core antigen: Broad protective efficacy of particles carrying four copies of M2e.* Vaccine, 2015. **33**(29): p. 3398-3406.
42. Lu, Y., et al., *Assessing sequence plasticity of a virus-like nanoparticle by evolution toward a versatile scaffold for vaccines and drug delivery.* Proc Natl Acad Sci U S A, 2015. **112**(40): p. 12360-5.
43. Zhu, F.C., Zhang, J., Zhang, X.F., Zhou, C., Wang, Z-Z, Huang, S-J.,Wang, H.,Yang, C-L., Jiang, H-M., Cai, J-P., Wang, Y-J.,Ai, X.,Hu, Y-M., Tang, Q., Yao, X., Yan, Q., Xian, Y-L., Wu, T., Li, Y-M., Miao, J.,Ng, M-N., Shih, J.W-Y., Xia, N.S, *Efficacy and safety of a recombinant hepatitis E vaccine in healthy adults: a large-scale, randomised, double-blind placebo-controlled, phase 3 trial.* Lancet, 2010. **376**: p. 895-902.
44. Zhang, J., et al., *Long-term efficacy of a hepatitis E vaccine.* N Engl J Med, 2015. **372**(10): p. 914-22.
45. Qi, Y., et al., *Expression and characterization of hepatitis E virus-like particles and non-virus-like particles from insect cells.* Biotechnol Appl Biochem, 2016. **63**(3): p. 362-70.
46. Liu, W.J., et al., *Papillomavirus virus-like particles for the delivery of multiple cytotoxic T cell epitopes.* Virology, 2000. **273**(2): p. 374-82.
47. Zhang, L.F., et al., *HPV6b virus like particles are potent immunogens without adjuvant in man.* Vaccine, 2000. **18**(11-12): p. 1051-1058.
48. Garland, S.M., et al., *Supplement to: Quadrivalent vaccine against human papillomavirus to prevent anogenital diseases.* The New England Journal of Medicine, 2007. **356**(19): p. 1928-1943.
49. Joshi, H., et al., *A molecular dynamics study of loop fluctuation in human papillomavirus type 16 virus-like particles: a possible indicator of immunogenicity.* Vaccine, 2011. **29**(51): p. 9423-30.
50. Galarza, J.M., T. Latham, and A. Cupo, *Protection against a Lethal Influenza Virus Challenge.* Viral Immunology, 2005. **18**(1): p. 244-251.
51. Quan, F.S., et al., *Virus-like particle vaccine induces protective immunity against homologous and heterologous strains of influenza virus.* J Virol, 2007. **81**(7): p. 3514-24.
52. Pushko, P., et al., *Influenza virus-like particle can accommodate multiple subtypes of hemagglutinin and protect from multiple influenza types and subtypes.* Vaccine, 2011. **29**(35): p. 5911-8.
53. Liu, Y.V., et al., *Recombinant virus-like particles elicit protective immunity against avian influenza A(H7N9) virus infection in ferrets.* Vaccine, 2015. **33**(18): p. 2152-8.
54. Schwartzman, L.M., et al., *An Intranasal Virus-Like Particle Vaccine Broadly Protects Mice from Multiple Subtypes of Influenza A Virus.* mBio, 2015. **6**(4): p. e01044.

55. Freivalds, J., et al., *Assembly of bacteriophage Qbeta virus-like particles in yeast Saccharomyces cerevisiae and Pichia pastoris.* J Biotechnol, 2006. **123**(3): p. 297-303.
56. Patel, K.G. and J.R. Swartz, *Surface functionalization of virus-like particles by direct conjugation using azide-alkyne click chemistry.* Bioconjug Chem, 2011. **22**(3): p. 376-87.
57. Fiedler, J.D., et al., *Engineered mutations change the structure and stability of a virus-like particle.* Biomacromolecules, 2012. **13**(8): p. 2339-48.
58. Tissot, A.C., et al., *Effect of immunisation against angiotensin II with CYT006-AngQb on ambulatory blood pressure: a double-blind, randomised, placebo-controlled phase IIa study.* Lancet, 2008. **371**(9615): p. 821-7.
59. Klimek, L., et al., *Assessment of clinical efficacy of CYT003-QbG10 in patients with allergic rhinoconjunctivitis: a phase IIb study.* Clin Exp Allergy, 2011. **41**(9): p. 1305-12.
60. Goldinger, S.M., et al., *Nano-particle vaccination combined with TLR-7 and -9 ligands triggers memory and effector CD8(+) T-cell responses in melanoma patients.* Eur J Immunol, 2012. **42**(11): p. 3049-61.
61. Spohn, G., et al., *Preclinical efficacy and safety of an anti-IL-1beta vaccine for the treatment of type 2 diabetes.* Mol Ther Methods Clin Dev, 2014. **1**: p. 14048.
62. Peabody, D.S., et al., *Immunogenic display of diverse peptides on virus-like particles of RNA phage MS2.* J Mol Biol, 2008. **380**(1): p. 252-63.
63. Plevka, P., K. Tars, and L. Liljas, *Structure and stability of icosahedral particles of a covalent coat protein dimer of bacteriophage MS2.* Protein Sci, 2009. **18**(8): p. 1653-61.
64. Caldeira, J.C. and D.S. Peabody, *Thermal stability of RNA phage virus-like particles displaying foreign peptides.* Journal of nanobiotechnology 2011. **9**(1): p. 22.
65. Ord, R.L., et al., *A malaria vaccine candidate based on an epitope of the Plasmodium falciparum RH5 protein.* Malaria Journal, 2014. **13**(1): p. 326.
66. Crossey, E., et al., *Identification of an Immunogenic Mimic of a Conserved Epitope on the Plasmodium falciparum Blood Stage Antigen AMA1 Using Virus-Like Particle (VLP) Peptide Display.* PLoS One, 2015. **10**(7): p. e0132560.
67. Brune, K.D., et al., *Plug-and-Display: decoration of Virus-Like Particles via isopeptide bonds for modular immunization.* Sci Rep, 2016. **6**: p. 19234.
68. Tumban, E., et al., *A universal virus-like particle-based vaccine for human papillomavirus: longevity of protection and role of endogenous and exogenous adjuvants.* Vaccine, 2013. **31**(41): p. 4647-54.
69. Caldeira, J., et al., *Epitope-Specific Anti-hCG Vaccines on a Virus Like Particle Platform.* PLoS One, 2015. **10**(10): p. e0141407.
70. Atmar, R.L., et al., *Norovirus Vaccine against Experimental Human Norwalk Virus Illness.* New England Journal of Medicine, 2011. **365**(23): p. 2178-2187.
71. Tamminen, K., et al., *A comparison of immunogenicity of norovirus GII-4 virus-like particles and P-particles.* Immunology, 2012. **135**(1): p. 89-99.
72. Tomé-Amat, J., et al., *Secreted production of assembled Norovirus virus-like particles from Pichia pastoris.* Microbial Cell Factories, 2014. **13**(1): p. 134.
73. Koho, T., et al., *His-tagged norovirus-like particles: A versatile platform for cellular delivery and surface display.* Eur J Pharm Biopharm, 2015. **96**: p. 22-31.

74. Brown, C.S., et al., *Assembly of empty capsids by using baculovirus recombinants expressing human parvovirus B19 structural proteins.* Journal of virology, 1991. **65**(5): p. 2702-2706.
75. Amexis, G. and N.S. Young, *Parvovirus B19 empty capsids as antigen carriers for presentation of antigenic determinants of dengue 2 virus.* The Journal of infectious disease, 2006. **194**(6): p. 790-794.
76. Sanchez-Rodriguez, S.P., et al., *Human parvovirus B19 virus-like particles: In vitro assembly and stability.* Biochimie, 2012. **94**(3): p. 870-8.
77. Chandramouli, S., et al., *Generation of a parvovirus B19 vaccine candidate.* Vaccine, 2013. **31**(37): p. 3872-8.
78. Gromadzka, B., et al., *Recombinant VP60 in the form of virion-like particles as a potential vaccine against rabbit hemorrhagic disease virus.* Acta Biochimica Polonica, 2006. **53**(2): p. 371-376.
79. Jemon, K., et al., *An enhanced heterologous virus-like particle for human papillomavirus type 16 tumour immunotherapy.* PLoS One, 2013. **8**(6): p. e66866.
80. Speir, J.A., et al., *Structures of the native and swollen forms of cowpea chlorotic mottle virus determined by X-ray crystallography and cryo-electron microscopy.* Structure 1995. **3**(1): p. 63-78.
81. Schoonen, L., et al., *Sortase A-Mediated N-Terminal Modification of Cowpea Chlorotic Mottle Virus for Highly Efficient Cargo Loading.* Bioconjug Chem, 2015. **26**(12): p. 2429-34.
82. Chatterji, A., et al., *New addresses on an addressable virus nanoblock; uniquely reactive Lys residues on cowpea mosaic virus.* Chem Biol, 2004. **11**(6): p. 855-63.
83. Venter, P.A., et al., *Multivalent display of proteins on viral nanoparticles using molecular recognition and chemical ligation strategies.* Biomacromolecules, 2011. **12**(6): p. 2293-301.
84. Munro, H.N. and M.C. Linder, *Ferritin: structure, biosynthesis, and role in iron metabolism.* Physiol Rev, 1978. **58**(2): p. 317-396.
85. Lawson, D.M., et al., *Solving the structure of human H ferritin by genetically engineering intermolecular crystal contacts.* Nature, 1991. **349**(6309): p. 541-544.
86. Kim, M., et al., *pH-dependent structures of ferritin and apoferritin in solution: disassembly and reassembly.* Biomacromolecules, 2011. **12**(5): p. 1629-40.
87. Li, C.Q., Soistman, E. and Carter, D.C. , *Ferritin nanoparticle technology.* Industrial Biotechnology, 2006. **2**(2): p. 143-47.
88. Han, J.A., et al., *Ferritin protein cage nanoparticles as versatile antigen delivery nanoplatforms for dendritic cell (DC)-based vaccine development.* Nanomedicine, 2014. **10**(3): p. 561-9.
89. Kanekiyo, M., et al., *Self-assembling influenza nanoparticle vaccines elicit broadly neutralizing H1N1 antibodies.* Nature, 2013. **499**(7456): p. 102-6.
90. Yassine, H.M., et al., *Hemagglutinin-stem nanoparticles generate heterosubtypic influenza protection.* Nat Med, 2015. **21**(9): p. 1065-70.
91. He, L., et al., *Approaching rational epitope vaccine design for hepatitis C virus with meta-server and multivalent scaffolding.* Sci Rep, 2015. **5**: p. 12501.

92. Kanekiyo, M., et al., *Rational Design of an Epstein-Barr Virus Vaccine Targeting the Receptor-Binding Site.* Cell, 2015. **162**(5): p. 1090-100.
93. Schott, K., *Synthase Complex of Bacillus subtilis.* 1990, 1990. **265**(21): p. 12686-12689.
94. Ra, J.S., et al., *Lumazine synthase protein cage nanoparticles as antigen delivery nanoplatforms for dendritic cell-based vaccine development.* Clin Exp Vaccine Res, 2014. **3**(2): p. 227-34.
95. Lopez-Sagaseta, J., et al., *Self-assembling protein nanoparticles in the design of vaccines.* Comput Struct Biotechnol J, 2016. **14**: p. 58-68.
96. Kim, K.K., R. Kim, and S.H. Kim, *Crystal structure of a small heat-shock protein.* Nature, 1998. **1998**(6693): p. 595-9.
97. Kim, K.K., et al., *Purification, crystallization, and preliminary x-ray crystallographic data analysis of small heat shock protein homolog from Methanococcus jannaschii, a hyperthermophile.* Jouurnal of Structural Biology, 1998. **121**(1): p. 76-80.
98. Haley, D.A., et al., *Small heat-shock protein structures reveal a continuum from symmetric to variable assemblies.* J Mol Biol, 2000. **298**(2): p. 261-72.
99. Bova, M.P., et al., *Subunit exchange, conformational stability, and chaperone-like function of the small heat shock protein 16.5 from Methanococcus jannaschii.* J Biol Chem, 2002. **277**(41): p. 38468-75.
100. Wang, X.Y., et al., *Current ideas about applications of heat shock proteins in vaccine design and immunotherapy.* Int J Hyperthermia, 2005. **21**(8): p. 717-22.
101. Flenniken, M.L., et al., *Melanoma and lymphocyte cell-specific targeting incorporated into a heat shock protein cage architecture.* Chem Biol, 2006. **13**(2): p. 161-70.
102. Strbo, N., et al., *Secreted heat shock protein gp96-Ig: next-generation vaccines for cancer and infectious diseases.* Immunol Res, 2013. **57**(1-3): p. 311-25.
103. Sutter, M., et al., *Structural basis of enzyme encapsulation into a bacterial nanocompartment.* Nat Struct Mol Biol, 2008. **15**(9): p. 939-47.
104. Rahmanpour, R. and T.D. Bugg, *Assembly in vitro of Rhodococcus jostii RHA1 encapsulin and peroxidase DypB to form a nanocompartment.* FEBS J, 2013. **280**(9): p. 2097-104.
105. Dalmau, M., et al., *Thermostability and molecular encapsulation within an engineered caged protein scaffold.* Biotechnol Bioeng, 2008. **101**(4): p. 654-64.
106. Molino, N.M., et al., *Biomimetic protein nanoparticles facilitate enhanced dendritic cell activation and cross-presentation.* ACS Nano, 2013. **7**(11): p. 9743-9752.
107. Esfandiary, R., et al., *Structural stability of vault particles.* J Pharm Sci, 2009. **98**(4): p. 1376-86.
108. Champion, C.I., et al., *A vault nanoparticle vaccine induces protective mucosal immunity.* PLoS One, 2009. **4**(4): p. e5409.
109. Kar, U.K., et al., *Vault nanocapsules as adjuvants favor cell-mediated over antibody-mediated immune responses following immunization of mice.* PLoS One, 2012. **7**(7): p. e38553.
110. Lovejoy, B., et al., *rystal structure of a synthetic triple-stranded alpha-helical bundle.* Science (New York, N.Y.), 1993. **259**(5099): p. 1288-93.
111. Nautiyal, S., et al., *A designed heterotrimeric coiled coil.* Biochemistry, 1995. **34**(37): p. 11645-51.

112. Ogihara, N.L., et al., *The crystal structure of the designed trimeric coiled coil coil-VaLd: implications for engineering crystals and supramolecular assemblies.* Protein Science : a publication of the Protein Society, 1997. **6**(1): p. 80-8.
113. Burkhard, P., S. Ivaninskii, and A. Lustig, *Improving Coiled-coil Stability by Optimizing Ionic Interactions.* Journal of Molecular Biology, 2002. **318**(3): p. 901-910.
114. Burkhard, P., J. Stetefeld, and S.V. Strelkov, *Coiled coils: a highly versatile protein folding motif.* Trend in Cell Biology, 2001. **11**(2): p. 82-86.
115. Pimentel, T.A., et al., *Peptide nanoparticles as novel immunogens: design and analysis of a prototypic severe acute respiratory syndrome vaccine.* Chem Biol Drug Des, 2009. **73**(1): p. 53-61.
116. Yang, Y., et al., *Optimizing the refolding conditions of self-assembling polypeptide nanoparticles that serve as repetitive antigen display systems.* J Struct Biol, 2012. **177**(1): p. 168-76.
117. Yang, Y., et al., *The biodistribution of self-assembling protein nanoparticles shows they are promising vaccine platforms.* Journal of Nanobiotechnology, 2013. **11**(1): p. 36.
118. Babapoor, S., et al., *A Novel Vaccine Using Nanoparticle Platform to Present Immunogenic M2e against Avian Influenza Infection.* Influenza Res Treat, 2011. **2011**: p. 126794.
119. Ghasparian, A., et al., *Engineered synthetic virus-like particles and their use in vaccine delivery.* Chembiochem, 2011. **12**(1): p. 100-9.
120. Wahome, N., et al., *Conformation-specific display of 4E10 and 2F5 epitopes on self-assembling protein nanoparticles as a potential HIV vaccine.* Chem Biol Drug Des, 2012. **80**(3): p. 349-57.
121. Kaba, S.A., et al., *Protective antibody and CD8+ T-cell responses to the Plasmodium falciparum circumsporozoite protein induced by a nanoparticle vaccine.* PLoS One, 2012. **7**(10): p. e48304.
122. McCoy, M.E., et al., *Mechanisms of protective immune responses induced by the Plasmodium falciparum circumsporozoite protein-based, self-assembling protein nanoparticle vaccine.* Malaria Journal 2013. **12**(1): p. 136.
123. Burkhard, P. and D.E. Lanar, *Malaria vaccine based on self-assembling protein nanoparticles.* Expert Rev Vaccines, 2015. **14**(12): p. 1525-7.
124. Tamborrini, M., et al., *A Synthetic Virus-Like Particle Streptococcal Vaccine Candidate Using B-Cell Epitopes from the Proline-Rich Region of Pneumococcal Surface Protein A.* Vaccines (Basel), 2015. **3**(4): p. 850-74.
125. Stranges, P.B., et al., *Computational design of a symmetric homodimer using beta-strand assembly.* Proc Natl Acad Sci U S A, 2011. **108**(51): p. 20562-7.
126. Rudra, J.S., et al., *Self-assembled peptide nanofibers raising durable antibody responses against a malaria epitope.* Biomaterials, 2012. **33**(27): p. 6476-84.
127. Powell, T.J., et al., *Synthetic nanoparticle vaccines produced by layer-by-layer assembly of artificial biofilms induce potent protective T-cell and antibody responses in vivo.* Vaccine, 2011. **29**(3): p. 558-69.
128. Powell, T.J., et al., *Plasmodium falciparum synthetic LbL microparticle vaccine elicits protective neutralizing antibody and parasite-specific cellular immune responses.* Vaccine, 2013. **31**(15): p. 1898-904.

129. Jorquera, P.A., et al., *Layer-By-Layer Nanoparticle Vaccines Carrying the G Protein CX3C Motif Protect against RSV Infection and Disease.* Vaccines (Basel), 2015. **3**(4): p. 829-49.
130. King, N.P., et al., *Computational Design of Self-Assembling Protein Nnomaterials with Atomic Level Accuracy* Science 2012. **828**(June): p. 1171-1175.
131. Lai, Y.T., et al., *Structure and flexibility of nanoscale protein cages designed by symmetric self-assembly.* J Am Chem Soc, 2013. **135**(20): p. 7738-43.
132. Lai, Y.T., et al., *Structure of a designed protein cage that self-assembles into a highly porous cube.* Nat Chem, 2014. **6**(12): p. 1065-71.
133. Bale, J.B., et al., *Structure of a designed tetrahedral protein assembly variant engineered to have improved soluble expression.* Protein Sci, 2015. **24**(10): p. 1695-701.
134. Hsia, Y., et al., *Design of a hyperstable 60-subunit protein icosahedron.* Nature, 2016. **535**(7610): p. 136-138.
135. Butterfield, G.L., et al., *Evolution of a designed protein assembly encapsulating its own RNA genome.* Nature, 2017. **552**(7685): p. 415-420.
136. Li, H., G. Zheng, and S. Zhu, *Construction of an organelle-like nanodevice via supramolecular self-assembly for robust biocatalysts.* Microb Cell Fact, 2018. **17**(1): p. 26.
137. He, L., et al., *HIV-1 vaccine design through minimizing envelope metastability.* Sci Adv, 2018. **4**(11): p. eaau6769.
138. Gomes, A.C., M. Mohsen, and M.F. Bachmann, *Harnessing Nanoparticles for Immunomodulation and Vaccines.* Vaccines (Basel), 2017. **5**(1).
139. Leneghan, D.B., et al., *Nanoassembly routes stimulate conflicting antibody quantity and quality for transmission-blocking malaria vaccines.* Sci Rep, 2017. **7**(1): p. 3811.
140. Charlton Hume, H.K. and L.H.L. Lua, *Platform technologies for modern vaccine manufacturing.* Vaccine, 2017. **35**(35 Pt A): p. 4480-4485.
141. Walker, A., C. Skamel, and M. Nassal, *SplitCore: an exceptionally versatile viral nanoparticle for native whole protein display regardless of 3D structure.* Sci Rep, 2011. **1**: p. 5.
142. Billaud, J.N., et al., *Combinatorial approach to hepadnavirus-like particle vaccine design.* J Virol, 2005. **79**(21): p. 13656-66.
143. Caldeira, J.C. and D.S. Peabody, *Thermal stability of RNA phage virus-like particles displaying foreign peptides.* J Nanobiotechnology, 2011. **9**: p. 22.
144. Janssens, M.E., et al., *Folding properties of the hepatitis B core as a carrier protein for vaccination research.* Amino Acids, 2010. **38**(5): p. 1617-26.
145. Thrane, S., et al., *Bacterial superglue enables easy development of efficient virus-like particle based vaccines.* J Nanobiotechnology, 2016. **14**: p. 30.
146. Palladini, A., et al., *Virus-like particle display of HER2 induces potent anti-cancer responses.* Oncoimmunology, 2018. **7**(3): p. e1408749.
147. Bruun, T.U.J., et al., *Engineering a Rugged Nanoscaffold To Enhance Plug-and-Display Vaccination.* ACS Nano, 2018. **12**(9): p. 8855-8866.

148. Okba, N.M.A., et al., *Particulate multivalent presentation of the receptor binding domain induces protective immune responses against MERS-CoV.* Emerg Microbes Infect, 2020. **9**(1): p. 1080-1091.
149. Jafri, R.Z., et al., *Global epidemiology of invasive meningococcal disease.* Population Health Metrics, 2013. **11**(1): p. 17.
150. Plant, L., et al., *Lipooligosaccharide structure contributes to multiple steps in the virulence of Neisseria meningitidis.* Infect Immun, 2006. **74**(2): p. 1360-7.
151. Harrison, L.H., *Vaccines for Prevention of Group B Meningococcal Disease: Not Your Father's Vaccines.* Am J Prev Med, 2015. **49**(6 Suppl 4): p. S345-54.
152. Takada, S., et al., *Meningococcemia in Adults: A Review of the Literature.* Intern Med, 2016. **55**(6): p. 567-72.
153. Bosis, S., A. Mayer, and S. Esposito, *Meningococcal disease in childhood: Epidemiology, clinical features and prevention.* Journal of Preventive Medicine and Hygiene, 2015. **56**(3): p. E121-E124.
154. Hill, D.J., et al., *Cellular and molecular biology of Neisseria meningitidis colonization and invasive disease.* Clin Sci (Lond), 2010. **118**(9): p. 547-64.
155. Rouphael, N.G. and D.S. Stephens, *Neisseria meningitidis: biology, microbiology, and epidemiology.* Methods Mol Biol, 2012. **799**: p. 1-20.
156. Harrison, L.H., *Prospects for vaccine prevention of meningococcal infection.* Clin Microbiol Rev, 2006. **19**(1): p. 142-64.
157. Virji, M., *Pathogenic neisseriae: surface modulation, pathogenesis and infection control.* Nat Rev Microbiol, 2009. **7**(4): p. 274-86.
158. Renauld-Mongenie, G., et al., *Role of transferrin receptor from a Neisseria meningitidis tbpB isotype II strain in human transferrin binding and virulence.* Infect Immun, 2004. **72**(6): p. 3461-70.
159. Stork, M., et al., *An outer membrane receptor of Neisseria meningitidis involved in zinc acquisition with vaccine potential.* PLoS Pathog, 2010. **6**: p. e1000969.
160. Vipond, C., R. Care, and I.M. Feavers, *History of meningococcal vaccines and their serological correlates of protection.* Vaccine, 2012. **30 Suppl 2**: p. B10-7.
161. Harrison, L.H., *Epidemiological profile of meningococcal disease in the United States.* Clin Infect Dis, 2010. **50 Suppl 2**: p. S37-44.
162. Carter, N.J., *Multicomponent meningococcal serogroup B vaccine (4CMenB; Bexsero((R))): a review of its use in primary and booster vaccination.* BioDrugs, 2013. **27**(3): p. 263-74.
163. Aston-Deaville, S., et al., *An assessment of the use of Hepatitis B Virus core protein virus-like particles to display heterologous antigens from Neisseria meningitidis.* Vaccine, 2020.
164. Xie, O., et al., *Emergence of serogroup X meningococcal disease in Africa: need for a vaccine.* Vaccine, 2013. **31**(27): p. 2852-61.
165. Mamat, U., et al., *Detoxifying Escherichia coli for endotoxin-free production of recombinant proteins.* Microb Cell Fact, 2015. **14**: p. 57.
166. Tsuchiya, S., et al., *Establishment and characterization of a human acute monocytic leukemia cell line (THP-1).* Int J Cancer, 1980. **26**(2): p. 171-6.

167. Pettersen, E.F., et al., *UCSF Chimera--a visualization system for exploratory research and analysis.* J Comput Chem, 2004. **25**(13): p. 1605-12.
168. Rohl, C.A., et al., *Protein structure prediction using Rosetta.* Methods Enzymol, 2004. **383**: p. 66-93.
169. Kellogg, E.H., A. Leaver-Fay, and D. Baker, *Role of conformational sampling in computing mutation-induced changes in protein structure and stability.* Proteins, 2011. **79**(3): p. 830-8.
170. Gasteiger, E., et al., *ExPASy: The proteomics server for in-depth protein knowledge and analysis.* Nucleic Acids Res, 2003. **31**(13): p. 3784-8.
171. Altschul, S.F., et al., *Basic local alignment search tool.* J Mol Biol, 1990. **215**(3): p. 403-10.
172. Scheres, S.H., *Semi-automated selection of cryo-EM particles in RELION-1.3.* J Struct Biol, 2015. **189**(2): p. 114-22.
173. GraphPad, *GraphPad Prism version 7.00 Software for Windows, Graphs produced.* La Jolia California USA, www.graphpad.com 2019
174. FlowJo™, *Software for Mac Version 10- Macrophage Gating and Geometric Mean Intensity.* Ashland, 2019.
175. FlowJo™, *Software for Mac Version 10- Dendritic Cell gating and Geometric Mean Analysis* Ashland, 2019.
176. GraphPad, *GraphPad Prism version 7.00 Software for Windows, Transform of Non-linear fit of standard curve following production of a standard curve.* La Jolia California USA, www.graphpad.com, 2019.
177. FlowJo™, *Software for Mac Version 10- T cell gating and Geomertic Mean Intensity* Ashland, 2019.
178. Schneider, C.A., W.S. Rasband, and K.W. Eliceiri, *NIH Image to ImageJ: 25 years of image analysis.* Nat Methods, 2012. **9**(7): p. 671-5.
179. GraphPad, *GraphPad Prism version 7.00 Software for Windows, One-way ANOVA followed by Tukeys muliple comparisons test and performed* La Jolia Claifornia USA, www.graphpad,com, 2019.
180. Lechner, F., et al., *Virus-like particles as a modular system for novel vaccines.* Intervirology, 2002. **45**(4-6): p. 212-217.
181. Smith, D.M., J.K. Simon, and J.R. Baker, Jr., *Applications of nanotechnology for immunology.* Nat Rev Immunol, 2013. **13**(8): p. 592-605.
182. Smith, J.D., L.D. Morton, and B.D. Ulery, *Nanoparticles as synthetic vaccines.* Current Opinion in Biotechnology, 2015. **34**: p. 217-224.
183. Noad, R. and P. Roy, *Virus-like particles as immunogens.* Trends in Microbiology, 2003. **11**(9): p. 438-444.
184. Grgacic, E.V.L. and D.A. Anderson, *Virus-like particles: Passport to immune recognition.* Methods, 2006. **40**(1): p. 60-65.
185. Vietheer, P.T., et al., *Immunizations with chimeric hepatitis B virus-like particles to induce potential anti-hepatitis C virus neutralizing antibodies.* Antivir Ther, 2007. **12**(4): p. 477-87.
186. Schodel, F., et al., *Hybrid hepatitis B virus core antigen as a vaccine carrier moiety .1. Presentation of foreign epitopes.* Journal of Biotechnology, 1996. **44**(1-3): p. 91-96.

187. Nardin, E.H., et al., *Phase I testing of a malaria vaccine composed of hepatitis B virus core particles expressing Plasmodium falciparum circumsporozoite epitopes.* Infection and Immunity, 2004. **72**(11): p. 6519-6527.
188. Crowther, R.A., et al., *Three-dimensional structure of hepatitis B virus core particles determined by electron cryomicroscopy.* Cell, 1994. **77**(6): p. 943-50.
189. Dishlers, A., et al., *The Hepatitis B Virus Core Variants that Expose Foreign C-Terminal Insertions on the Outer Surface of Virus-Like Particles.* Molecular Biotechnology, 2015. **57**(11-12): p. 1038-1049.
190. Pumpens, P. and E. Grens, *HBV core particles as a carrier for B cell/T cell epitopes.* Intervirology, 2001. **44**(2-3): p. 98-114.
191. Wynne, S.A., R.A. Crowther, and A.G.W. Leslie, *The crystal structure of the human hepatitis B virus capsid.* Molecular Cell, 1999. **3**(6): p. 771-780.
192. Malito, E., et al., *Structure of the meningococcal vaccine antigen NadA and epitope mapping of a bactericidal antibody.* Proc Natl Acad Sci U S A, 2014. **111**(48): p. 17128-33.
193. King, N.P., et al., *Computational Design of Self-Assembling Protein Nanomaterials with Atomic Level Accuracy.* Science, 2012. **336**(6085): p. 1171-1174.
194. King, N.P., et al., *Accurate design of co-assembling multi-component protein nanomaterials.* Nature, 2014. **510**(7503): p. 103-8.
195. Ito, K. and N. Matsudomi, *Structural characteristics of hen egg ovalbumin expressed in yeast Pichia pastoris.* Biosci Biotechnol Biochem, 2005. **69**(4): p. 755-61.
196. Brito, L.A. and M. Singh, *Acceptable Levels of Endotoxin in Vaccine Formulations During Preclinical Research.* Journal of Pharmaceutical Sciences, 2011. **100**(1): p. 34-37.
197. Fleri, W., et al., *The immune Epitope Database and Analysis Resource in Epitope Discovery and Synthetic Vaccine Design.* Frontiers in Immunology, 2017. **8**.
198. Zhang, Q., et al., *Immune epitope database analysis resource (IEDB-AR).* Nucleic Acids Res, 2008. **36**(Web Server issue): p. W513-8.
199. Fahmy, T.M., et al., *Design opportunities for actively targeted nanoparticle vaccines.* Nanomedicine, 2008. **3**(3): p. 343-355.
200. Maecker, H.T., et al., *Cytotoxic T cell responses to DNA vaccination: Dependence on antigen presentation via class II MHC.* Journal of Immunology, 1998. **161**(12): p. 6532-6536.
201. Robertson, J.M., P.E. Jensen, and B.D. Evavold, *DO11.10 and OT-II T cells recognize a C-terminal ovalbumin 323-339 epitope.* Journal of Immunology, 2000. **164**(9): p. 4706-4712.
202. Esposito, V., et al., *Structure of the C-terminal Domain of Neisseria Heparin Binding Antigen (NHBA), One of the Main Antigens of a Novel Vaccine against Neisseria meningitidis.* Journal of Biological Chemistry, 2011. **286**(48): p. 41767-41775.
203. Cai, X.D., et al., *A virus-like particle of the hepatitis B virus preS antigen elicits robust neutralizing antibodies and T cell responses in mice.* Antiviral Research, 2018. **149**: p. 48-57.
204. Roldao, A., et al., *Virus-like particles in vaccine development.* Expert Review of Vaccines, 2010. **9**(10): p. 1149-1176.

205. Huynh, K. and C.L. Partch, *Analysis of protein stability and ligand interactions by thermal shift assay.* Curr Protoc Protein Sci, 2015. **79**: p. 28 9 1-28 9 14.
206. Vita, R., et al., *The Immune Epitope Database (IEDB): 2018 update.* Nucleic Acids Research, 2019. **47**(D1): p. D339-D343.
207. Rodriguez-Limas, W.A., K. Sekar, and K.E.J. Tyo, *Virus-like particles: the future of microbial factories and cell-free systems as platforms for vaccine development.* Current Opinion in Biotechnology, 2013. **24**(6): p. 1089-1093.
208. Yu, Y. and S. Lutz, *Circular permutation: a different way to engineer enzyme structure and function.* Trends Biotechnol, 2011. **29**(1): p. 18-25.
209. Heinemann, U. and M. Hahn, *Circular permutation of polypeptide chains: Implications for protein folding and stability.* Progress in Biophysics & Molecular Biology, 1995. **64**(2-3): p. 121-143.
210. Qian, Z. and S. Lutz, *Improving the catalytic activity of Candida antarctica lipase B by circular permutation.* Journal of the American Chemical Society, 2005. **127**(39): p. 13466-13467.
211. Reitinger, S., et al., *Circular permutation of Bacillus circulans xylanase: a kinetic and structural study.* Biochemistry, 2010. **49**(11): p. 2464-74.
212. Jia, J., et al., *Crystal structure of transaldolase B from Escherichia coli suggests a circular permutation of the alpha/beta barrel within the class I aldolase family.* Structure, 1996. **4**(6): p. 715-24.
213. Moffat, J.M., et al., *Hepatitis B virus-like particles access major histocompatibility class I and II antigen presentation pathways in primary dendritic cells.* Vaccine, 2013. **31**(18): p. 2310-6.
214. Teunissen, E.A., M. de Raad, and E. Mastrobattista, *Production and biomedical applications of virus-like particles derived from polyomaviruses.* J Control Release, 2013. **172**(1): p. 305-321.
215. Chen, M.M., et al., *Immunogenicity of different recombinant rabbit hemorrhagic disease virus-like particles carrying CD8+T cell epitope from chicken ovalbumin (OVA).* Virus Research, 2014. **183**: p. 15-22.
216. Matthias, D.M., et al., *Freezing temperatures in the vaccine cold chain: A systematic literature review.* Vaccine, 2007. **25**(20): p. 3980-3986.
217. Lopez-Sagaseta, J., et al., *Self-assembling protein nanoparticles in the design of vaccines.* Computational and Structural Biotechnology Journal, 2016. **14**: p. 58-68.
218. Brune, K.D., et al., *Plug-and-Display: decoration of Virus-Like Particles via isopeptide bonds for modular immunization.* Scientific Reports, 2016. **6**.
219. Sivakumar, S.M., et al., *Vaccine adjuvants - Current status and prospects on controlled release adjuvancity.* Saudi Pharmaceutical Journal, 2011. **19**(4): p. 197-206.
220. Sjoquist, J., B. Meloun, and H. Hjelm, *Protein A isolated from Staphylococcus aureus after digestion with lysostaphin.* Eur J Biochem, 1972. **29**(3): p. 572-8.
221. Rigi, G., S. Ghaedmohammadi, and G. Ahmadian, *A comprehensive review on staphylococcal protein A (SpA): Its production and applications.* Biotechnol Appl Biochem, 2019. **66**(3): p. 454-464.
222. Sjodahl, J., *Structural studies on the four repetitive Fc-binding regions in protein A from Staphylococcus aureus.* Eur J Biochem, 1977. **78**(2): p. 471-90.

223. Moks, T., et al., *Staphylococcal protein A consists of five IgG-binding domains.* Eur J Biochem, 1986. **156**(3): p. 637-43.
224. Deisenhofer, J., *Crystallographic refinement and atomic models of a human Fc fragment and its complex with fragment B of protein A from Staphylococcus aureus at 2.9- and 2.8-A resolution.* Biochemistry, 1981. **20**(9): p. 2361-70.
225. Myers, J.K. and T.G. Oas, *Mechanism of fast protein folding.* Annu Rev Biochem, 2002. **71**: p. 783-815.
226. Czajkowsky, D.M., et al., *Fc-fusion proteins: new developments and future perspectives.* EMBO Mol Med, 2012. **4**(10): p. 1015-28.
227. Vincenti, F., A. Dritselis, and P. Kirkpatrick, *Belatacept.* Nat Rev Drug Discov, 2011. **10**(9): p. 655-6.
228. Moreland, L., G. Bate, and P. Kirkpatrick, *Abatacept.* Nat Rev Drug Discov, 2006. **5**(3): p. 185-6.
229. Roopenian, D.C. and S. Akilesh, *FcRn: the neonatal Fc receptor comes of age.* Nature Reviews Immunology, 2007. **7**(9): p. 715-725.
230. Nimmerjahn, F. and J.V. Ravetch, *Fc gamma receptors as regulators of immune responses.* Nature Reviews Immunology, 2008. **8**(1): p. 34-47.
231. Huntington, J.A. and P.E. Stein, *Structure and properties of ovalbumin.* J Chromatogr B Biomed Sci Appl, 2001. **756**(1-2): p. 189-98.
232. Kalkanidis, M., et al., *Methods for nano-particle based vaccine formulation and evaluation of their immunogenicity.* Methods, 2006. **40**(1): p. 20-29.
233. Rudra, J.S., et al., *A self-assembling peptide acting as an immune adjuvant.* Proceedings of the National Academy of Sciences of the United States of America, 2010. **107**(2): p. 622-627.
234. Didierlaurent, A.M., et al., *Enhancement of adaptive immunity by the human vaccine adjuvant AS01 depends on activated dendritic cells.* J Immunol, 2014. **193**(4): p. 1920-30.
235. Petersen, R.L., *Strategies Using Bio-Layer Interferometry Biosensor Technology for Vaccine Research and Development.* Biosensors-Basel, 2017. **7**(4).
236. McKenzie, E.A. and W.M. Abbott, *Expression of recombinant proteins in insect and mammalian cells.* Methods, 2018. **147**: p. 40-49.
237. Pechtner V, K.C., Garcia-Perez LE, Glaesner W, *A New Approach to Drug Therapy: Fc-Fusion Technology* Primary Health Care 2017. **7**(1).
238. Moreland, L.W., et al., *Etanercept therapy in rheumatoid arthritis. A randomized, controlled trial.* Ann Intern Med, 1999. **130**(6): p. 478-86.
239. Kangwa, M., et al., *An engineered Staphylococcal Protein A based ligand: Production, characterization and potential application for the capture of Immunoglobulin and Fc-fusion proteins.* Protein Expr Purif, 2019. **155**: p. 27-34.
240. Chanput, W., J.J. Mes, and H.J. Wichers, *THP-1 cell line: an in vitro cell model for immune modulation approach.* Int Immunopharmacol, 2014. **23**(1): p. 37-45.
241. Daigneault, M., et al., *The identification of markers of macrophage differentiation in PMA-stimulated THP-1 cells and monocyte-derived macrophages.* PLoS One, 2010. **5**(1): p. e8668.

242. Huang, X.C., D.P.' Townley, H.E. , *Macrophage-like THP-1 cells show effective uptake of silica nanoparticles carrying inactivated diphtheria toxoid for vaccination.* Journal of Nanoparticle Research 2020. **22**(23).
243. Gustafson, H.H., et al., *Nanoparticle Uptake: The Phagocyte Problem.* Nano Today, 2015. **10**(4): p. 487-510.
244. East, L. and C.M. Isacke, *The mannose receptor family.* Biochim Biophys Acta, 2002. **1572**(2-3): p. 364-86.
245. Kato, M., et al., *Expression of human DEC-205 (CD205) multilectin receptor on leukocytes.* Int Immunol, 2006. **18**(6): p. 857-69.
246. Forrester, M.A., et al., *Similarities and differences in surface receptor expression by THP-1 monocytes and differentiated macrophages polarized using seven different conditioning regimens.* Cell Immunol, 2018. **332**: p. 58-76.
247. Cruz, L.J., et al., *Targeting nanoparticles to CD40, DEC-205 or CD11c molecules on dendritic cells for efficient CD8(+) T cell response: a comparative study.* J Control Release, 2014. **192**: p. 209-18.
248. Curtis, B.M., S. Scharnowske, and A.J. Watson, *Sequence and expression of a membrane-associated C-type lectin that exhibits CD4-independent binding of human immunodeficiency virus envelope glycoprotein gp120.* Proc Natl Acad Sci U S A, 1992. **89**(17): p. 8356-60.
249. Rappocciolo, G., et al., *DC-SIGN is a receptor for human herpesvirus 8 on dendritic cells and macrophages.* J Immunol, 2006. **176**(3): p. 1741-9.
250. Li, R.E., et al., *Systematic Dual Targeting of Dendritic Cell C-Type Lectin Receptor DC-SIGN and TLR7 Using a Trifunctional Mannosylated Antigen.* Front Chem, 2019. **7**: p. 650.
251. Mortezai, N., et al., *Tumor-associated Neu5Ac-Tn and Neu5Gc-Tn antigens bind to C-type lectin CLEC10A (CD301, MGL).* Glycobiology, 2013. **23**(7): p. 844-52.
252. van Vliet, S.J., E. Saeland, and Y. van Kooyk, *Sweet preferences of MGL: carbohydrate specificity and function.* Trends Immunol, 2008. **29**(2): p. 83-90.
253. Napoletano, C., et al., *Targeting of macrophage galactose-type C-type lectin (MGL) induces DC signaling and activation.* Eur J Immunol, 2012. **42**(4): p. 936-45.
254. Villasenor-Cardoso, M.I., D.A. Frausto-Del-Rio, and E. Ortega, *Aminopeptidase N (CD13) is involved in phagocytic processes in human dendritic cells and macrophages.* Biomed Res Int, 2013. **2013**: p. 562984.
255. Licona-Limon, I., et al., *CD13 mediates phagocytosis in human monocytic cells.* J Leukoc Biol, 2015. **98**(1): p. 85-98.
256. Ghosh, M., et al., *CD13 regulates dendritic cell cross-presentation and T cell responses by inhibiting receptor-mediated antigen uptake.* J Immunol, 2012. **188**(11): p. 5489-99.
257. Hayashi, N., et al., *A novel photodynamic therapy targeting cancer cells and tumor-associated macrophages.* Mol Cancer Ther, 2015. **14**(2): p. 452-60.
258. Heijnen, I.A., et al., *Antigen targeting to myeloid-specific human Fc gamma RI/CD64 triggers enhanced antibody responses in transgenic mice.* J Clin Invest, 1996. **97**(2): p. 331-8.
259. Hatami, E., et al., *Mannose-decorated hybrid nanoparticles for enhanced macrophage targeting.* Biochem Biophys Rep, 2019. **17**: p. 197-207.

260. Raiber, E.A., et al., *Targeted delivery of antigen processing inhibitors to antigen presenting cells via mannose receptors.* ACS Chem Biol, 2010. **5**(5): p. 461-476.
261. Georgoudaki, A.M., et al., *Reprogramming Tumor-Associated Macrophages by Antibody Targeting Inhibits Cancer Progression and Metastasis.* Cell Rep, 2016. **15**(9): p. 2000-11.
262. Lunov, O., et al., *Differential uptake of functionalized polystyrene nanoparticles by human macrophages and a monocytic cell line.* ACS Nano, 2011. **5**(3): p. 1657-69.
263. Hoppstadter, J., et al., *M2 polarization enhances silica nanoparticle uptake by macrophages.* Front Pharmacol, 2015. **6**: p. 55.
264. Yu, S.S., et al., *Size- and charge-dependent non-specific uptake of PEGylated nanoparticles by macrophages.* Int J Nanomedicine, 2012. **7**: p. 799-813.
265. Kettler, K., et al., *Uptake of silver nanoparticles by monocytic THP-1 cells depends on particle size and presence of serum proteins.* J Nanopart Res, 2016. **18**(9): p. 286.
266. Lanone, S., et al., *Comparative toxicity of 24 manufactured nanoparticles in human alveolar epithelial and macrophage cell lines.* Part Fibre Toxicol, 2009. **6**: p. 14.
267. Jiang, Q., et al., *Combined effects of low levels of palmitate on toxicity of ZnO nanoparticles to THP-1 macrophages.* Environ Toxicol Pharmacol, 2016. **48**: p. 103-109.
268. Krystek, P.K., K.: van der Wagt, B.; de Jong, W.H., *Exploring influences on the cellular uptake of medium-sized silver nanoparticles into THP-1 cells.* Microchemical Journal 2015. **120**.
269. Zhu, Z.J., et al., *The interplay of monolayer structure and serum protein interactions on the cellular uptake of gold nanoparticles.* Small, 2012. **8**(17): p. 2659-63.
270. Steinman, R.M., *The dendritic cell system and its role in immunogenicity.* Annu Rev Immunol, 1991. **9**: p. 271-96.
271. Inaba, K., et al., *Generation of large numbers of dendritic cells from mouse bone marrow cultures supplemented with granulocyte/macrophage colony-stimulating factor.* J Exp Med, 1992. **176**(6): p. 1693-702.
272. Wang, W., et al., *Culture and Identification of Mouse Bone Marrow-Derived Dendritic Cells and Their Capability to Induce T Lymphocyte Proliferation.* Med Sci Monit, 2016. **22**: p. 244-50.
273. Singh-Jasuja, H., et al., *The mouse dendritic cell marker CD11c is down-regulated upon cell activation through Toll-like receptor triggering.* Immunobiology, 2013. **218**(1): p. 28-39.
274. ten Broeke, T., R. Wubbolts, and W. Stoorvogel, *MHC class II antigen presentation by dendritic cells regulated through endosomal sorting.* Cold Spring Harb Perspect Biol, 2013. **5**(12): p. a016873.
275. Murthy, N., et al., *A macromolecular delivery vehicle for protein-based vaccines: acid-degradable protein-loaded microgels.* Proc Natl Acad Sci U S A, 2003. **100**(9): p. 4995-5000.
276. Nembrini, C., et al., *Nanoparticle conjugation of antigen enhances cytotoxic T-cell responses in pulmonary vaccination.* Proc Natl Acad Sci U S A, 2011. **108**(44): p. E989-97.
277. Hamdy, S., et al., *Activation of antigen-specific T cell-responses by mannan-decorated PLGA nanoparticles.* Pharm Res, 2011. **28**(9): p. 2288-301.

278. Maji, M., et al., *A Lipid Based Antigen Delivery System Efficiently Facilitates MHC Class-I Antigen Presentation in Dendritic Cells to Stimulate CD8(+) T Cells.* Sci Rep, 2016. **6**: p. 27206.
279. Dixon, G.L., et al., *Dendritic cell activation and cytokine production induced by group B Neisseria meningitidis: interleukin-12 production depends on lipopolysaccharide expression in intact bacteria.* Infect Immun, 2001. **69**(7): p. 4351-7.
280. Dienz, O. and M. Rincon, *The effects of IL-6 on CD4 T cell responses.* Clin Immunol, 2009. **130**(1): p. 27-33.
281. Mehta, A.K., D.T. Gracias, and M. Croft, *TNF activity and T cells.* Cytokine, 2018. **101**: p. 14-18.
282. Blanco, P., et al., *Dendritic cells and cytokines in human inflammatory and autoimmune diseases.* Cytokine Growth Factor Rev, 2008. **19**(1): p. 41-52.
283. Moore, K.W., et al., *Interleukin-10 and the interleukin-10 receptor.* Annu Rev Immunol, 2001. **19**: p. 683-765.
284. Luckheeram, R.V., et al., *CD4(+)T cells: differentiation and functions.* Clin Dev Immunol, 2012. **2012**: p. 925135.
285. Hosono, M., et al., *Increased expression of T cell activation markers (CD25, CD26, CD40L and CD69) in atherectomy specimens of patients with unstable angina and acute myocardial infarction.* Atherosclerosis, 2003. **168**(1): p. 73-80.
286. Schumann, J., et al., *Differences in CD44 Surface Expression Levels and Function Discriminates IL-17 and IFN-gamma Producing Helper T Cells.* PLoS One, 2015. **10**(7): p. e0132479.
287. Willinger, T., et al., *Molecular signatures distinguish human central memory from effector memory CD8 T cell subsets.* J Immunol, 2005. **175**(9): p. 5895-903.
288. Schroder, K., et al., *Interferon-gamma: an overview of signals, mechanisms and functions.* J Leukoc Biol, 2004. **75**(2): p. 163-89.
289. Wong, C.K., et al., *Proinflammatory cytokines (IL-17, IL-6, IL-18 and IL-12) and Th cytokines (IFN-gamma, IL-4, IL-10 and IL-13) in patients with allergic asthma.* Clin Exp Immunol, 2001. **125**(2): p. 177-83.
290. Nelms, K., et al., *The IL-4 receptor: signaling mechanisms and biologic functions.* Annu Rev Immunol, 1999. **17**: p. 701-38.
291. de Waal Malefyt, R., et al., *Interleukin 10 (IL-10) and viral IL-10 strongly reduce antigen-specific human T cell proliferation by diminishing the antigen-presenting capacity of monocytes via downregulation of class II major histocompatibility complex expression.* J Exp Med, 1991. **174**(4): p. 915-24.
292. Malek, T.R., *The main function of IL-2 is to promote the development of T regulatory cells.* J Leukoc Biol, 2003. **74**(6): p. 961-5.
293. Ross, S.H. and D.A. Cantrell, *Signaling and Function of Interleukin-2 in T Lymphocytes.* Annu Rev Immunol, 2018. **36**: p. 411-433.
294. Lin, L., et al., *Granzyme B secretion by human memory CD4 T cells is less strictly regulated compared to memory CD8 T cells.* BMC Immunol, 2014. **15**: p. 36.
295. Tai, Y., et al., *Molecular Mechanisms of T Cells Activation by Dendritic Cells in Autoimmune Diseases.* Front Pharmacol, 2018. **9**: p. 642.

296. Eriksson, K., et al., *Cholera toxin and its B subunit promote dendritic cell vaccination with different influences on Th1 and Th2 development.* Infect Immun, 2003. **71**(4): p. 1740-7.
297. Rathinam, V.A., K.A. Hoag, and L.S. Mansfield, *Dendritic cells from C57BL/6 mice undergo activation and induce Th1-effector cell responses against Campylobacter jejuni.* Microbes Infect, 2008. **10**(12-13): p. 1316-24.
298. Blank, F., et al., *Size-dependent uptake of particles by pulmonary antigen-presenting cell populations and trafficking to regional lymph nodes.* Am J Respir Cell Mol Biol, 2013. **49**(1): p. 67-77.
299. Pan, R., et al., *Size-dependent endocytosis and a dynamic-release model of nanoparticles.* Nanoscale, 2018. **10**(17): p. 8269-8274.
300. Lee, C.H., et al., *Enhanced antigen uptake by dendritic cells induced by the B pentamer of the type II heat-labile enterotoxin LT-IIa requires engagement of TLR2.* Vaccine, 2010. **28**(21): p. 3696-705.
301. Moldenhauer, L.M., et al., *Cross-presentation of male seminal fluid antigens elicits T cell activation to initiate the female immune response to pregnancy.* J Immunol, 2009. **182**(12): p. 8080-93.
302. Maj, T., A. Slawek, and A. Chelmonska-Soyta, *CD80 and CD86 costimulatory molecules differentially regulate OT-II CD4(+) T lymphocyte proliferation and cytokine response in cocultures with antigen-presenting cells derived from pregnant and pseudopregnant mice.* Mediators Inflamm, 2014. **2014**: p. 769239.
303. Jeon, S.G., et al., *Impaired Memory in OT-II Transgenic Mice Is Associated with Decreased Adult Hippocampal Neurogenesis Possibly Induced by Alteration in Th2 Cytokine Levels.* Mol Cells, 2016. **39**(8): p. 603-10.
304. Chang, T.T., et al., *Spaceflight impairs antigen-specific tolerance induction in vivo and increases inflammatory cytokines.* FASEB J, 2015. **29**(10): p. 4122-32.
305. Feau, S., et al., *Autocrine IL-2 is required for secondary population expansion of CD8(+) memory T cells.* Nat Immunol, 2011. **12**(9): p. 908-13.
306. Wilson, E.B. and A.M. Livingstone, *Cutting edge: CD4+ T cell-derived IL-2 is essential for help-dependent primary CD8+ T cell responses.* J Immunol, 2008. **181**(11): p. 7445-8.
307. Rappuoli, R., et al., *Vaccines, new opportunities for a new society.* Proc Natl Acad Sci U S A, 2014. **111**(34): p. 12288-93.
308. Trombetta, E.S. and I. Mellman, *Cell biology of antigen processing in vitro and in vivo.* Annu Rev Immunol, 2005. **23**: p. 975-1028.
309. Guermonprez, P., et al., *Antigen presentation and T cell stimulation by dendritic cells.* Annu Rev Immunol, 2002. **20**: p. 621-67.
310. Swartz, M.A., J.A. Hubbell, and S.T. Reddy, *Lymphatic drainage function and its immunological implications: from dendritic cell homing to vaccine design.* Semin Immunol, 2008. **20**(2): p. 147-56.
311. Doshi, N. and S. Mitragotri, *Macrophages recognize size and shape of their targets.* PLoS One, 2010. **5**(4): p. e10051.
312. Champion, J.A. and S. Mitragotri, *Shape induced inhibition of phagocytosis of polymer particles.* Pharm Res, 2009. **26**(1): p. 244-9.

313. Sharma, G., et al., *Polymer particle shape independently influences binding and internalization by macrophages.* J Control Release, 2010. **147**(3): p. 408-12.
314. Kumar, S., et al., *Shape and size-dependent immune response to antigen-carrying nanoparticles.* J Control Release, 2015. **220**(Pt A): p. 141-148.
315. Foged, C., et al., *Particle size and surface charge affect particle uptake by human dendritic cells in an in vitro model.* Int J Pharm, 2005. **298**(2): p. 315-22.
316. Liu, Y., et al., *Surface hydrophobicity of microparticles modulates adjuvanticity.* J Mater Chem B, 2013. **1**(32): p. 3888-3896.
317. Bastola, R., et al., *Vaccine adjuvants: smart components to boost the immune system.* Arch Pharm Res, 2017. **40**(11): p. 1238-1248.
318. Leroux-Roels, G., *Unmet needs in modern vaccinology: adjuvants to improve the immune response.* Vaccine, 2010. **28 Suppl 3**: p. C25-36.
319. Morefield, G.L., et al., *Role of aluminum-containing adjuvants in antigen internalization by dendritic cells in vitro.* Vaccine, 2005. **23**(13): p. 1588-95.
320. Coates, T., et al., *Hepatitis B vaccines: assessment of the seroprotective efficacy of two recombinant DNA vaccines.* Clin Ther, 2001. **23**(3): p. 392-403.
321. Aucouturier, J., et al., *Montanide ISA 720 and 51: a new generation of water in oil emulsions as adjuvants for human vaccines.* Expert Rev Vaccines, 2002. **1**(1): p. 111-8.
322. Garcon, N., P. Chomez, and M. Van Mechelen, *GlaxoSmithKline Adjuvant Systems in vaccines: concepts, achievements and perspectives.* Expert Rev Vaccines, 2007. **6**(5): p. 723-39.
323. Podda, A., *The adjuvanted influenza vaccines with novel adjuvants: experience with the MF59-adjuvanted vaccine.* Vaccine, 2001. **19**(17-19): p. 2673-80.
324. Grimm, S.K. and M.E. Ackerman, *Vaccine design: emerging concepts and renewed optimism.* Curr Opin Biotechnol, 2013. **24**(6): p. 1078-88.
325. Manayani, D.J., et al., *A viral nanoparticle with dual function as an anthrax antitoxin and vaccine.* PLoS Pathog, 2007. **3**(10): p. 1422-31.
326. Schneemann, A., et al., *A virus-like particle that elicits cross-reactive antibodies to the conserved stem of influenza virus hemagglutinin.* J Virol, 2012. **86**(21): p. 11686-97.
327. Song, J.M., et al., *Influenza virus-like particles containing M2 induce broadly cross protective immunity.* PLoS One, 2011. **6**(1): p. e14538.
328. Munoz, N., et al., *Safety, immunogenicity, and efficacy of quadrivalent human papillomavirus (types 6, 11, 16, 18) recombinant vaccine in women aged 24-45 years: a randomised, double-blind trial.* Lancet, 2009. **373**(9679): p. 1949-57.
329. Keating, G.M. and S. Noble, *Recombinant hepatitis B vaccine (Engerix-B): a review of its immunogenicity and protective efficacy against hepatitis B.* Drugs, 2003. **63**(10): p. 1021-51.
330. Van Damme, P., et al., *Safety, tolerability and immunogenicity of a recombinant hepatitis B vaccine manufactured by a modified process in healthy young adults.* Hum Vaccin, 2009. **5**(2): p. 92-7.
331. Soulie, J.C., et al., *Immunogenicity and safety in newborns of a new recombinant hepatitis B vaccine containing the S and pre-S2 antigens.* Vaccine, 1991. **9**(8): p. 545-8.
332. Cimica, V. and J.M. Galarza, *Adjuvant formulations for virus-like particle (VLP) based vaccines.* Clin Immunol, 2017. **183**: p. 99-108.

333. Moon, J.J., et al., *Enhancing humoral responses to a malaria antigen with nanoparticle vaccines that expand Tfh cells and promote germinal center induction.* Proc Natl Acad Sci U S A, 2012. **109**(4): p. 1080-5.
334. Kasturi, S.P., et al., *Programming the magnitude and persistence of antibody responses with innate immunity.* Nature, 2011. **470**(7335): p. 543-7.
335. Palucka, K. and J. Banchereau, *Human dendritic cell subsets in vaccination.* Curr Opin Immunol, 2013. **25**(3): p. 396-402.
336. Hashimoto, D., J. Miller, and M. Merad, *Dendritic cell and macrophage heterogeneity in vivo.* Immunity, 2011. **35**(3): p. 323-35.
337. Villadangos, J.A. and L. Young, *Antigen-presentation properties of plasmacytoid dendritic cells.* Immunity, 2008. **29**(3): p. 352-61.
338. Guilliams, M., et al., *Dendritic cells, monocytes and macrophages: a unified nomenclature based on ontogeny.* Nat Rev Immunol, 2014. **14**(8): p. 571-8.
339. Brown, C.C., et al., *Transcriptional Basis of Mouse and Human Dendritic Cell Heterogeneity.* Cell, 2019. **179**(4): p. 846-863 e24.
340. Aliberti, J., et al., *Essential role for ICSBP in the in vivo development of murine CD8alpha + dendritic cells.* Blood, 2003. **101**(1): p. 305-10.
341. Hildner, K., et al., *Batf3 deficiency reveals a critical role for CD8alpha+ dendritic cells in cytotoxic T cell immunity.* Science, 2008. **322**(5904): p. 1097-100.
342. Villani, A.C., et al., *Single-cell RNA-seq reveals new types of human blood dendritic cells, monocytes, and progenitors.* Science, 2017. **356**(6335).
343. Dzionek, A., et al., *BDCA-2, BDCA-3, and BDCA-4: three markers for distinct subsets of dendritic cells in human peripheral blood.* J Immunol, 2000. **165**(11): p. 6037-46.
344. Siegal, F.P., et al., *The nature of the principal type 1 interferon-producing cells in human blood.* Science, 1999. **284**(5421): p. 1835-7.
345. Liu, Y.J., *IPC: professional type 1 interferon-producing cells and plasmacytoid dendritic cell precursors.* Annu Rev Immunol, 2005. **23**: p. 275-306.
346. Palucka, K., J. Banchereau, and I. Mellman, *Designing vaccines based on biology of human dendritic cell subsets.* Immunity, 2010. **33**(4): p. 464-78.
347. Di Pucchio, T., et al., *Direct proteasome-independent cross-presentation of viral antigen by plasmacytoid dendritic cells on major histocompatibility complex class I.* Nat Immunol, 2008. **9**(5): p. 551-7.
348. Tacken, P.J. and C.G. Figdor, *Targeted antigen delivery and activation of dendritic cells in vivo: steps towards cost effective vaccines.* Semin Immunol, 2011. **23**(1): p. 12-20.
349. Castro, F.V., et al., *CD11c provides an effective immunotarget for the generation of both CD4 and CD8 T cell responses.* Eur J Immunol, 2008. **38**(8): p. 2263-73.
350. Caminschi, I. and K. Shortman, *Boosting antibody responses by targeting antigens to dendritic cells.* Trends Immunol, 2012. **33**(2): p. 71-7.
351. Loschko, J., et al., *Antigen delivery to plasmacytoid dendritic cells via BST2 induces protective T cell-mediated immunity.* J Immunol, 2011. **186**(12): p. 6718-25.
352. Lahoud, M.H., et al., *Targeting antigen to mouse dendritic cells via Clec9A induces potent CD4 T cell responses biased toward a follicular helper phenotype.* J Immunol, 2011. **187**(2): p. 842-50.

353. Carter, R.W., et al., *Preferential induction of CD4+ T cell responses through in vivo targeting of antigen to dendritic cell-associated C-type lectin-1.* J Immunol, 2006. **177**(4): p. 2276-84.
354. Corbett, A.J., et al., *Antigen delivery via two molecules on the CD8- dendritic cell subset induces humoral immunity in the absence of conventional "danger".* Eur J Immunol, 2005. **35**(10): p. 2815-25.
355. Dudziak, D., et al., *Differential antigen processing by dendritic cell subsets in vivo.* Science, 2007. **315**(5808): p. 107-11.

Appendices

Appendix 1 : DNA Sequences

Protein	DNA/ Protein Sequence
I3-01 672bp XhoI/NdeI	CATATGATGCACCATCATCATCACCATGGCGGTAGCGGTGGTAGTGGTGGTTCAGGTGGTAGCATGGAAGAACTGTTCAAAAAGCACAAAATTGTTGCAGTTCT GCGTGCCAATAGCGTTGAAGAAGCAAAAAAGAAAGCACTGGCCGTTTTTTTAGGTGGTGTTCATCTGATTGAAATCACCTTTACCGTTCCGGATGCAGATACCGT TATTAAAGAACTGAGCTTTCTGAAAGAAATGGGTGCAATTATTGGTGCAGGCACCGTTACCAGCGTTGAACAGTGTCGTAAAGCAGTTGAAAGCGGTGCAGAA TTTATTGTTAGTCCGCATCTGGATGAAGAAATCAGCCAGTTTTGTAAAGAAAAGGGCGTGTTTTATATGCCTGGTGTTATGACCCCGACCGAACTGGTTAAAGCA ATGAAACTGGGTCATACCATCCTGAAACTGTTTCCGGGTGAAGTTGTTGGTCCGCAGTTTGTGAAAGCCATGAAAGGTCCGTTTCCGAATGTTAAATTTGTTCCG ACCGGTGGTGTGAATCTGGATAATGTTTGTGAATGGTTTAAAGCCGGTGTTCTGGCAGTTGGTGTTGGTAGCGCACTGGTGAAAGGTACACCGGTTGAAGTTG CAGAAAAAGCAAAAGCCTTTGTGGAAAAAATTCGTGGTTGTACCGAATGACTCGAG
I3-01-T40S 672bp XhoI/NdeI	CATATGATGCACCATCATCATCACCATGGCGGTAGCGGTGGTAGTGGTGGTTCAGGTGGTAGCATGGAAGAACTGTTCAAAAAGCACAAAATTGTTGCAGTTCT GCGTGCCAATAGCGTTGAAGAAGCAAAAAAGAAAGCACTGGCCGTTTTTTTAGGTGGTGTTCATCTGATTGAAATCACCTTTACCGGTTCCGGATGCAGATACCGT TATTAAAGAACTGAGCTTTCTGAAAGAAATGGGTGCAATTATTGGTGCAGGCACCGTTACCAGCGTTGAACAGTGTCGTAAAGCAGTTGAAAGCGGTGCAGAA TTTATTGTTAGTCCGCATCTGGATGAAGAAATCAGCCAGTTTTGTAAAGAAAAGGGCGTGTTTTATATGCCTGGTGTTATGACCCCGACCGAACTGGTTAAAGCA ATGAAACTGGGTCATACCATCCTGAAACTGTTTCCGGGTGAAGTTGTTGGTCCGCAGTTTGTGAAAGCCATGAAAGGTCCGTTTCCGAATGTTAAATTTGTTCCG ACCGGTGGTGTGAATCTGGATAATGTTTGTGAATGGTTTAAAGCCGGTGTTCTGGCAGTTGGTGTTGGTAGCGCACTGGTGAAAGGTACACCGGTTGAAGTTG CAGAAAAAGCAAAAGCCTTTGTGGAAAAAATTCGTGGTTGTACCGAATGACTCGAG
I3-01-OVA 265bp XhoI/NdeI	CATATGATGCACCATCATCATCACCATGGCGGTAGCGGTGGTAGTGGTGGTTCAGGTGGTAGCATGAAAATGGAAGAACTGTTCAAAAAGCACAAAATTGTTG CAGTTCTGCGTGCCAATAGCGTTGAAGAAGCAAAAAAGAAAGCACTGGCCGTTTTTTTAGGTGGTGTTCATCTGATTGAAATCACCTTTACCGTTCCGGATGCAG ATACCGTTATTAAAGAACTGAGCTTTCTGAAAGAAATGGGTGCAATTATTGGTGCAGGCACCGTTACCAGCGTTGAACAGTGTCGTAAAGCAGTTGAAAGCGGT GCAGAATTTATTGTTAGTCCGCATCTGGATGAAGAAATCAGCCAGTTTTGTAAAGAAAAGGGCGTGTTTTATATGCCTGGTGTTATGACCCCGACCGAACTGGTT AAAGCAATGAAACTGGGTCATACCATCCTGAAACTGTTTCCGGGTGAAGTTGTTGGTCCGCAGTTTGTGAAAGCCATGAAAGGTCCGTTTCCGGGCGGTGGCG GTAGCGGCGGTGGCGGATCCAGCCTGAAGATATCTCAAGCTGTCCATGCAGCACATGCAGAAATCAATGAAGCAGGCAGAGAGGTGGAATTCGGCGGTGGCG GTAGCGGCGGTGGCGGTAATGTTAAATTTGTTCCGACCGGTGGTGTGAATCTGGATAATGTTTGTGAATGGTTTAAAGCCGGTGTTCTGGCAGTTGGTGTTGGT AGCGCACTGGTGAAAGGTACACCGGTTGAAGTTGCAGAAAAAGCAAAAGCCTTTGTGGAAAAAATTCGTGGTTGTACCGAATAACTCGAG
I3-01-OVA11 256bp XhoI/NdeI	CATATGATGCACCATCATCATCACCATGGCGGTAGCGGTGGTAGTGGTGGTTCAGGTGGTAGCATGAAAATGGAAGAACTGTTCAAAAAGCACAAAATTGTTG CAGTTCTGCGTGCCAATAGCGTTGAAGAAGCAAAAAAGAAAGCACTGGCCGTTTTTTTAGGTGGTGTTCATCTGATTGAAATCACCTTTACCGTTCCGGATGCAG ATACCGTTATTAAAGAACTGAGCTTTCTGAAAGAAATGGGTGCAATTATTGGTGCAGGCACCGTTACCAGCGTTGAACAGTGTCGTAAAGCAGTTGAAAGCGGT GCAGAATTTATTGTTAGTCCGCATCTGGATGAAGAAATCAGCCAGTTTTGTAAAGAAAAGGGCGTGTTTTATATGCCTGGTGTTATGACCCCGACCGAACTGGTT AAAGCAATGAAACTGGGTCATACCATCCTGAAACTGTTTCCGGGTGAAGTTGTTGGTCCGCAGTTTGTGAAAGCCATGAAAGGTCCGTTTCCGGGCGGTGGCG GTAGCGGCGGTGGCGGATCCCAGCTTGAGAGTATAATCAACTTTGAAAAACTGACTGAAGAATTCGGCGGTGGCGGTAGCGGCGGTGGCGGTAATGTTAAATT TGTTCCGACCGGTGGTGTGAATCTGGATAATGTTTGTGAATGGTTTAAAGCCGGTGTTCTGGCAGTTGGTGTTGGTAGCGCACTGGTGAAAGGTACACCGGTTG AAGTTGCAGAAAAAGCAAAAGCCTTTGTGGAAAAAATTCGTGGTTGTACCGAATAACTCGAG
I3-01-CP-G60 717bp XhoI/NdeI	CATATGATGCACCATCATCATCACCATGGCGGTAGCGGTGGTAGTGGTGGTTCAGGTGGTAGCATGGCAATTATTGGTGCAGGCACCGTTACCAGCGTTGAACA GTGTCGTAAAGCAGTTGAAAGCGGTGCAGAATTTATTGTTAGTCCGCATCTGGATGAAGAAATCAGCCAGTTTTGTAAAGAAAAGGGCGTGTTTTATATGCCTG GTGTTATGACCCCGACCGAACTGGTTAAAGCAATGAAACTGGGTCATACCATCCTGAAACTGTTTCCGGGTGAAGTTGTTGGTCCGCAGTTTGTGAAAGCCATG AAAGGTCCGTTTCCGAATGTTAAATTTGTTCCGACCGGTGGTGTGAATCTGGATAATGTTTGTGAATGGTTTAAAGCCGGTGTTCTGGCAGTTGGTGTTGGTAGC GCACTGGTGAAAGGTACACCGGTTGAAGTTGCAGAAAAAGCAAAAGCCTTTGTGGAAAAAATTCGTGGTTGTACCGAAGGCGGTAGCGGTGGTAGTGGTGGT TCAGGTGGTAGCATGAAAATGGAAGAACTGTTCAAAAAGCACAAAATTGTTGCAGTTCTGCGTGCCAATAGCGTTGAAGAAGCAAAAAAGAAAGCACTGGCCG TTTTTTTAGGTGGTGTTCATCTGATTGAAATCACCTTTACCGTTCCGGATGCAGATACCGTTATTAAAGAACTGAGCTTTCTGAAAGAAATGTGACTCGAG
I3-01-CP-N148 705bp XhoI/NdeI	CATATGATGCACCATCATCATCACCATGGCGGTAGCGGTGGTAGTGGTGGTTCAGGTGGTAGCATGGTTAAATTTGTTCCGACCGGTGGTGTGAATCTGGATAA TGTTTGTGAATGGTTTAAAGCCGGTGTTCTGGCAGTTGGTGTTGGTAGCGCACTGGTGAAAGGTACACCGGTTGAAGTTGCAGAAAAAGCAAAAGCCTTTGTG GAAAAAATTCGTGGTTGTACCGAAGGCGGTAGCGGTGGTAGTGGTGGTTCAGGTGGTAGCATGAAAATGGAAGAACTGTTCAAAAAGCACAAAATTGTTGCA GTTCTGCGTGCCAATAGCGTTGAAGAAGCAAAAAAGAAAGCACTGGCCGTTTTTTTAGGTGGTGTTCATCTGATTGAAATCACCTTTACCGTTCCGGATGCAGAT ACCGTTATTAAAGAACTGAGCTTTCTGAAAGAAATGGGTGCAATTATTGGTGCAGGCACCGTTACCAGCGTTGAACAGTGTCGTAAAGCAGTTGAAAGCGGTGC AGAATTTATTGTTAGTCCGCATCTGGATGAAGAAATCAGCCAGTTTTGTAAAGAAAAGGGCGTGTTTTATATGCCTGGTGTTATGACCCCGACCGAACTGGTTAA AGCAATGAAACTGGGTCATACCATCCTGAAACTGTTTCCGGGTGAAGTTGTTGGTCCGCAGTTTGTGAAAGCCATGAAAGGTCCGTTTCCGTGACTCGAG
I3-01-PA 861bp XhoI/NdeI	CATATGATGCACCATCATCATCACCATGGCGGTAGCGGTGGTAGTGGTGGTTCAGGTGGTAGCATGAAAATGGAAGAACTGTTCAAAAAGCACAAAATTGTTG CAGTTCTGCGTGCCAATAGCGTTGAAGAAGCAAAAAAGAAAGCACTGGCCGTTTTTTTAGGTGGTGTTCATCTGATTGAAATCACCTTTACCGTTCCGGATGCAG ATACCGTTATTAAAGAACTGAGCTTTCTGAAAGAAATGGGTGCAATTATTGGTGCAGGCACCGTTACCAGCGTTGAACAGTGTCGTAAAGCAGTTGAAAGCGGT GCAGAATTTATTGTTAGTCCGCATCTGGATGAAGAAATCAGCCAGTTTTGTAAAGAAAAGGGCGTGTTTTATATGCCTGGTGTTATGACCCCGACCGAACTGGTT AAAGCAATGAAACTGGGTCATACCATCCTGAAACTGTTTCCGGGTGAAGTTGTTGGTCCGCAGTTTGTGAAAGCCATGAAAGGTCCGTTTCCGAATGTTAAATTT GTTCCGACCGGTGGTGTGAATCTGGATAATGTTTGTGAATGGTTTAAAGCCGGTGTTCTGGCAGTTGGTGTTGGTAGCGCACTGGTGAAAGGTACACCGGTTGA AGTTGCAGAAAAAGCAAAAGCCTTTGTGGAAAAAATTCGTGGTTGTACCGAAGGCGGTAGCATGGCCGACAACAAATTCAATAAAGAACAGCAGAACGCCTTC TACGAAATTCTGCATCTGCCGAATCTGACCGAAGAACAGCGTAATGGTTTTATTCAGAGCCTGAAAGATGATCCGAGCGTGAGCAAAGAAATTCTGGCCGAAGC AAAAAAACTGAATGATGCACAGGCACCGAAATGACTCGA
NadA 489bp XhoI/NdeI	ATATGATGCACCATCATCATCACCATGGCGGTAGCGGTGGTAGTGGTGGTTCAGGTGGTAGCATGGCCACAAGCGACGACGATGTTAAAAAAGCTGCCACTGT GGCCATTGTTGCTGCCTACAACAATGGCCAAGAAATCAACGGTTTCAAAGCTGGAGAGACCATCTACGACATTGGTGAAGACGGCACAATTACCCAAAAAGAC GCAACTGCAGCCGATGTTGAAGCCGACGACTTTAAAGGTCTGGGTCTGAAAAAAGTCGTGACTAACCTGACCAAAACCGTCAATGAAAACAAACAAAACGTCG ATGCCAAAGTAAAAGCTGCAGAATCTGAAATAGAAAAGTTAACAACCAAGTTAGCAGACACTGATGCCGCTTTAGCAGATACTGATGCCGCTCTGGATGAAACC ACCAACGCCTTGAATAAATTGGGAGAAAATATAACGACATTTGCTGAAGAGACTAAGACAAATATCGTAAAAATTGATGAAAAATTAGAAGCCGTGGCTGATAC CGTCGACAAGCATGCCGAAGCATTCAACGATATCGCCGATTCATTGGATGAAACCAACACTAAGGCAGACGAAGCCGTCAAAACCGCCAATGAAGCCAAACAG ACGGCCGAAGAAACCAAACAAAACGTCGATGCCAAAGTAAAAGCTGCAGAAACTGCAGCAGGCAAAGCCGAAGCTGCCGCTGGCACAGCTAATACTGCAGCC GACAAGGCCGAAGCTGTCGCTGCAAAAGTTACCGACATCAAAGCTGATATCGCTACGAACAAAGCTGATATTGCTAAAAACTCAGCACGCATCGACAGCTTGGA CAAAAACGTAGCTAATCTGCGCAAAGAAACCCGCCAAGGCCTTGCAGAACAAGCCGCGCTCTCCGGCCTGTTCCAACCTTACAACGTGGGTTGACTCGAG

I3-01- CP-NHBA 1116bp XhoI/NdeI	CATATGATGCACCATCATCATCACCATGGCGGTAGCGGTGGTAGTGGTGGTTCAGGTGGTAGCATGGTTAAATTTGTTCCGACC GGTGGTGTGAATCTGGATAATGTTTGTGAATGGTTTAAAGCCGGTGTTCTGGCAGTTGGTGTTGGTAGCGCACTGGTGAAAGGTACACCGGTTGAAGTTGCA GAAAAAGCAAAAGCCTTTGTGGAAAAAATTCGTGGTTGTACCGAAGGCGGTAGCGGTGGTAGTGGTGGTTCAGGTGGTAGCATGAAAATGGAAGAACTGTTC AAAAAGCACAAAATTGTTGCAGTTCTGCGTGCCAATAGCGTTGAAGAAGCAAAAAAGAAAGCACTGGCCGTTTTTTTAGGTGGTGTTCATCTGATTGAAATCAC CTTTACCGTTCCGGATGCAGATACCGTTATTAAAGAACTGAGCTTTCTGAAAGAAATGGGTGCAATTATTGGTGCAGGCACCGTTACCAGCGTTGAACAGTGTC GTAAAGCAGTTGAAAGCGGTGCAGAATTTATTGTTAGTCCGCATCTGGATGAAGAAATCAGCCAGTTTTGTAAAGAAAAGGGCGTGTTTTATATGCCTGGTGTT ATGACCCCGACCGAACTGGTTAAAGCAATGAAACTGGGTCATACCATCCTGAAACTGTTTCCGGGTGAAGTTGTTGGTCCGCAGTTTGTGAAAGCCATGAAAGG TCCGTTTCCGGGTGGAGGTGGATCTGGAGGTGGAGGTTCTGGTGGAGGTGGAAGTATGCTTGCGGGCGCGGCCGTGTACAACGGCGAAGTACTGCATTTCCA TACGGAAAACGGCCGTCCGTACCCGACCAGGGGCAGGTTTGCCGCAAAAGTCGATTTCGGCAGCAAATCTGTGGACGGCATTATCGACAGCGGCGATGATTTG CATATGGGTACGCAAAAATTCAAAGCCGCCATCGATGGAAACGGCTTTAAGGGGACTTGGACGGAAAATGGCAGCGGGGATGTTTCCGGAAAGTTTTACGGCC CGGCCGGCGAGGAAGTGGCGGGAAAATACAGCTATCGCCCGACAGATGCGGAAAAGGGCGGATTCGGCGTGTTTGCCGGCAAAAAAGAGCAGGATTAATAA CTCGAG
Ovalbumin 1158bp XhoI/NdeI	GGCAGCATTGGCGCGGCGAGCATGGAATTTTGCTTTGATGTGTTTAAAGAACTGAAAGTGCATCATGCGAACGAAAACATTTTTTATTGCCCGATTGCGATTAT GAGCGCGCTGGCGATGGTGTATCTGGGCGCGAAAGATAGCACCCGCACCCAGATTAACAAAGTGGTGCGCTTTGATAAACTGCCGGGCTTTGGCGATAGCATT GAAGCGCAGTGCGGCACCAGCGTGAACGTGCATAGCAGCCTGCGCGATATTCTGAACCAGATTACCAAACCGAACGATGTGTATAGCTTTAGCCTGGCGAGCC GCCTGTATGCGGAAGAACGCTATCCGATTCTGCCGGAATATCTGCAGTGCGTGAAAGAACTGTATCGCGGCGGCCTGGAACCGATTAACTTTCAGACCGCGGC GGATCAGGCGCGCGAACTGATTAACAGCTGGGTGGAAAGCCAGACCAACGGCATTATTCGCAACGTGCTGCAGCCGAGCAGCGTGGATAGCCAGACCGCGAT GGTGCTGGTGAACGCGATTGTGTTTAAAGGCCTGTGGGAAAAAGCGTTTAAAGATGAAGATACCCAGGCGATGCCGTTTCGCGTGACCGAACAGGAAAGCAA ACCGGTGCAGATGATGTATCAGATTGGCCTGTTTCGCGTGGCGAGCATGGCGAGCGAAAAATGAAAATTCTGGAACTGCCGTTTGCGAGCGGCACCATGAGC ATGCTGGTGCTGCTGCCGGATGAAGTGAGCGGCCTGGAACAGCTGGAAAGCATTATTAACTTTGAAAAACTGACCGAATGGACCAGCAGCAACGTGATGGAA GAACGCAAAATTAAAGTGTATCTGCCGCGCATGAAAATGGAAGAAAAATATAACCTGACCAGCGTGCTGATGGCGATGGGCATTACCGATGTGTTTAGCAGCA GCGCGAACCTGAGCGGCATTAGCAGCGCGGAAAGCCTGAAAATTAGCCAGGCGGTGCATGCGGCGCATGCGGAAATTAACGAAGCGGGCCGCGAAGTGGTG GGCAGCGCGGAAGCGGGCGTGGATGCGGCGAGCGTGAGCGAAGAATTTCGCGCGGATCATCCGTTTCTGTTTTGCATTAAACATATTGCGACCAACGCGGTGC TGTTTTTTGGCCGCTGCGTGAGCCCG
NadA-I3-01 MW= 54.2kDa 1542bp XhoI/NdeI	CATATGATGCACCATCATCATCACCATGGCGGTAGCGGTGGTAGTGGTGGTTCAGGTGGTAGCATGGCCACAAGCGACGACGATGTTAAAAAAGCTGCCACTG TGGCCATTGTTGCTGCCTACAACAATGGCCAAGAAATCAACGGTTTCAAAGCTGGAGAGACCATCTACGACATTGGTGAAGACGGCACAATTACCCAAAAAGAC GCAACTGCAGCCGATGTTGAAGCCGACGACTTTAAAGGTCTGGGTCTGAAAAAAGTCGTGACTAACCTGACCAAAACCGTCAATGAAAACAAACAAAACGTCG ATGCCAAAGTAAAAGCTGCAGAATCTGAAATAGAAAAGTTAACAACCAAGTTAGCAGACACTGATGCCGCTTTAGCAGATACTGATGCCGCTCTGGATGAAACC ACCAACGCCTTGAATAAATTGGGAGAAAATATAACGACATTTGCTGAAGAGACTAAGACAAATATCGTAAAAATTGATGAAAAATTAGAAGCCGTGGCTGATAC CGTCGACAAGCATGCCGAAGCATTCAACGATATCGCCGATTCATTGGATGAAACCAACACTAAGGCAGACGAAGCCGTCAAAACCGCCAATGAAGCCAAACAG ACGGCCGAAGAAACCAAACAAAACGTCGATGCCAAAGTAAAAGCTGCAGAAACTGCAGCAGGCAAAGCCGAAGCTGCCGCTGGCACAGCTAATACTGCAGCC GACAAGGCCGAAGCTGTCGCTGCAAAAGTTACCGACATCAAAGCTGATATCGCTACGAACAAAGCTGATATTGCTAAAAACTCAGCACGCATCGACAGCTTGGA CAAAAACGTAGCTAATCTGCGCAAAGAAACCCGCCAAGGCCTTGCAGAACAAGCCGCGCTCTCCGGCCTGTTCCAACCTTACAACGTGGGTGGTGGAGGTGGA TCTGGAGGTGGAGGTTCTGGTGGAGGTGGAAGTATGAAAATGGAAGAACTGTTCAAAAAGCACAAAATTGTTGCAGTTCTGCGTGCCAATAGCGTTGAAGAA GCAAAAAAGAAAGCACTGGCCGTTTTTTTAGGTGGTGTTCATCTGATTGAAATCACCTTTACCGTTCCGGATGCAGATACCGTTATTAAAGAACTGAGCTTTCTG AAAGAAATGGGTGCAATTATTGGTGCAGGCACCGTTACCAGCGTTGAACAGTGTCGTAAAGCAGTTGAAAGCGGTGCAGAATTTATTGTTAGTCCGCATCTGGA TGAAGAAATCAGCCAGTTTTGTAAAGAAAAGGGCGTGTTTTATATGCCTGGTGTTATGACCCCGACCGAACTGGTTAAAGCAATGAAACTGGGTCATACCATCC TGAAACTGTTTCCGGGTGAAGTTGTTGGTCCGCAGTTTGTGAAAGCCATGAAAGGTCCGTTTCCGAATGTTAAATTTGTTCCGACCGGTGGTGTGAATCTGGATA ATGTTTGTGAATGGTTTAAAGCCGGTGTTCTGGCAGTTGGTGTTGGTAGCTGACTCGAG
I3-01-NadA MW= 53.8kDa 1533bp XhoI/NdeI	CATATGATGCACCATCATCATCACCATGGCGGTAGCGGTGGTAGTGGTGGTTCAGGTGGTAGCATGAAAATGGAAGAACTGTTCAAAAAGCACAAAATTGTTG CAGTTCTGCGTGCCAATAGCGTTGAAGAAGCAAAAAAGAAAGCACTGGCCGTTTTTTTAGGTGGTGTTCATCTGATTGAAATCACCTTTACCGTTCCGGATGCAG ATACCGTTATTAAAGAACTGAGCTTTCTGAAAGAAATGGGTGCAATTATTGGTGCAGGCACCGTTACCAGCGTTGAACAGTGTCGTAAAGCAGTTGAAAGCGGT GCAGAATTTATTGTTAGTCCGCATCTGGATGAAGAAATCAGCCAGTTTTGTAAAGAAAAGGGCGTGTTTTATATGCCTGGTGTTATGACCCCGACCGAACTGGTT AAAGCAATGAAACTGGGTCATACCATCCTGAAACTGTTTCCGGGTGAAGTTGTTGGTCCGCAGTTTGTGAAAGCCATGAAAGGTCCGTTTCCGAATGTTAAATTT GTTCCGACCGGTGGTGTGAATCTGGATAATGTTTGTGAATGGTTTAAAGCCGGTGTTCTGGCAGTTGGTGTTGGTAGCGCACTGGTGAAAGGTACACCGGTTGA AGTTGCAGAAAAAGCAAAAGCCTTTGTGGAAAAAATTCGTGGTTGTACCGAAGGTGGAGGTGGATCTGGAGGTGGAGGTTCTGGTGGAGGTGGAAGTATGGC CACAAGCGACGACGATGTTAAAAAAGCTGCCACTGTGGCCATTGTTGCTGCCTACAACAATGGCCAAGAAATCAACGGTTTCAAAGCTGGAGAGACCATCTACG ACATTGGTGAAGACGGCACAATTACCCAAAAAGACGCAACTGCAGCCGATGTTGAAGCCGACGACTTTAAAGGTCTGGGTCTGAAAAAAGTCGTGACTAACCT GACCAAAACCGTCAATGAAAACAAACAAAACGTCGATGCCAAAGTAAAAGCTGCAGAATCTGAAATAGAAAAGTTAACAACCAAGTTAGCAGACACTGATGCC GCTTTAGCAGATACTGATGCCGCTCTGGATGAAACCACCAACGCCTTGAATAAATTGGGAGAAAATATAACGACATTTGCTGAAGAGACTAAGACAAATATCGT AAAAATTGATGAAAAATTAGAAGCCGTGGCTGATACCGTCGACAAGCATGCCGAAGCATTCAACGATATCGCCGATTCATTGGATGAAACCAACACTAAGGCA GACGAAGCCGTCAAAACCGCCAATGAAGCCAAACAGACGGCCGAAGAAACCAAACAAAACGTCGATGCCAAAGTAAAAGCTGCAGAAACTGCAGCAGGCAAA GCCGAAGCTGCCGCTGGCACAGCTAATACTGCAGCCGACAAGGCCGAAGCTGTCGCTGCAAAAGTTACCGACATCAAAGCTGATATCGCTACGAACAAAGCTG ATATTGCTAAAAACTCAGCACGCATCGACAGCTTGGACAAAAACGTAGCTAATCTGCGCAAAGAAACCCGCCAAGGCCTTGCAGAACAAGCCGCGCTCTCCGGC CTGTTCCAACCTTACAACGTGGGTTGACTCGAG
NadA-I3-01-CP MW= 40.8kDa 1182bp XhoI/NdeI	CATATGATGCACCATCATCATCACCATGGCGGTAGCGGTGGTAGTGGTGGTTCAGGTGGTAGCATGGCCACAAGCGACGACGATGTTAAAAAAGCTGCCACTG TGGCCATTGTTGCTGCCTACAACAATGGCCAAGAAATCAACGGTTTCAAAGCTGGAGAGACCATCTACGACATTGGTGAAGACGGCACAATTACCCAAAAAGAC GCAACTGCAGCCGATGTTGAAGCCGACGACTTTAAAGGTCTGGGTCTGAAAAAAGTCGTGACTAACCTGACCAAAACCGTCAATGAAAACAAACAAAACGTCG ATGCCAAAGTAAAAGCTGCAGAATCTGAAATAGAAAAGTTAACAACCAAGTTAGCAGACACTGATGCCGCTTTAGCAGATACTGATGCCGCTCTGGATGAAACC ACCAACGCCTTGAATAAATTGGGAGAAAATATAACGACATTTGCTGAAGAGACTAAGACAAATATCGTAAAAATTGATGAAAAAGGTGGAGGTGGATCTGGAG GTGGAGGTTCTGGTGGAGGTGGAAGTATGGTTAAATTTGTTCCGACCGGTGGTGTGAATCTGGATAATGTTTGTGAATGGTTTAAAGCCGGTGTTCTGGCAGTT GGTGTTGGTAGCGCACTGGTGAAAGGTACACCGGTTGAAGTTGCAGAAAAAGCAAAAGCCTTTGTGGAAAAAATTCGTGGTTGTACCGAAGGCGGTAGCGGT GGTAGTGGTGGTTCAGGTGGTAGCATGAAAATGGAAGAACTGTTCAAAAAGCACAAAATTGTTGCAGTTCTGCGTGCCAATAGCGTTGAAGAAGCAAAAAAGA AAGCACTGGCCGTTTTTTTAGGTGGTGTTCATCTGATTGAAATCACCTTTACCGTTCCGGATGCAGATACCGTTATTAAAGAACTGAGCTTTCTGAAAGAAATGG GTGCAATTATTGGTGCAGGCACCGTTACCAGCGTTGAACAGTGTCGTAAAGCAGTTGAAAGCGGTGCAGAATTTATTGTTAGTCCGCATCTGGATGAAGAAATC AGCCAGTTTTGTAAAGAAAAGGGCGTGTTTTATATGCCTGGTGTTATGACCCCGACCGAACTGGTTAAAGCAATGAAACTGGGTCATACCATCCTGAAACTGTTT CCGGGTGAAGTTGTTGGTCCGCAGTTTGTGAAAGCCATGAAAGGTCCGTTTCCGTGATGACTCGAG
Mouse IgG Fc 654bp XhoI/NdeI	GCGTGCGATGAATTTGGCCATATTAAACTGATGAACCCGCAGCGCAGCACCGTGTGGTATTAACCGGCGCCGAACCTGCTGGGCGGCCCGAGCGTGTTTATTTT TCCGCCGAAAATTAAAGATGTGCTGATGATTAGCCTGAGCCCGATTGTGACCTGCGTGGTGGTGGATGTGAGCGAAGATGATCCGGATGTGCAGATTAGCTGG TTTGTGAACAACGTGGAAGTGCATACCGCGCAGACCCAGACCCATCGCGAAGATTATAACAGCACCCTGCGCGTGGTGAGCGCGCTGCCGATTCAGCATCAGG ATTGGATGAGCGGCAAAGAATTTAAATGCAAAGTGAACAACAAAGATCTGCCGGCGCCGATTGAACGCACCATTAGCAAACCGAAAGGCAGCGTGCGCGCGC CGCAGGTGTATGTGCTGCCGCCGCCGGAAGAAGAAATGACCAAAAAACAGGTGACCCTGACCTGCATGGTGACCGATTTTATGCCGGAAGATATTTATGTGGA ATGGACCAACAACGGCAAAACCGAACTGAACTATAAAAACACCGAACCGGTGCTGGATAGCGATGGCAGCTATTTTATGTATAGCAAACTGCGCGTGGAAAAA AAAAACTGGGTGGAACGCAACAGCTATAGCTGCAGCGTGGTGCATGAAGGCCTGCATAACCATCATACCACCAAAAGCTTTAGCCGCACCCCGGGCAAA
	PAPNLLGGPSVFIFPPKIKDVLMISLSPIVTCVVVDVSEDDPDVQISWFVNNVEVHTAQTQTHREDYNSTLRVVSALPIQHQDWMSGK EFKCKVNNKDLPAPIERTISKPKGSVRAPQVYVLPPPEEEMTKKQVTLTCMVTDFMPEDIYVEWTNNGKTELNYKNTEPVLDSDGSYF MYSKLRVEKKNWVERNSYSCSVVHEGLHNHHTTKSFSRTPGK

Fc- OVA 1833bp XhoI/NdeI	GCGTGCGATGAATTTGGCCATATTAAACTGATGAACCCGCAGCGCAGCACCGTGTGGTATTAAGGCAGCATTGGCGCGGCGAGCATGGAATTTTGCTTTGATGT GTTTAAAGAACTGAAAGTGCATCATGCGAACGAAAACATTTTTTATTGCCCGATTGCGATTATGAGCGCGCTGGCGATGGTGTATCTGGGCGCGAAAGATAGCA CCCGCACCCAGATTAACAAAGTGGTGCGCTTTGATAAACTGCCGGGCTTTGGCGATAGCATTGAAGCGCAGTGCGGCACCAGCGTGAACGTGCATAGCAGCCT GCGCGATATTCTGAACCAGATTACCAAACCGAACGATGTGTATAGCTTTAGCCTGGCGAGCCGCCTGTATGCGGAAGAACGCTATCCGATTCTGCCGGAATATC TGCAGTGCGTGAAAGAACTGTATCGCGGCGGCCTGGAACCGATTAACTTTCAGACCGCGGCGGATCAGGCGCGCGAACTGATTAACAGCTGGGTGGAAAGCC AGACCAACGGCATTATTCGCAACGTGCTGCAGCCGAGCAGCGTGGATAGCCAGACCGCGATGGTGCTGGTGAACGCGATTGTGTTTAAAGGCCTGTGGGAAAA AGCGTTTAAAGATGAAGATACCCAGGCGATGCCGTTTCGCGTGACCGAACAGGAAAGCAAACCGGTGCAGATGATGTATCAGATTGGCCTGTTTCGCGTGGCG AGCATGGCGAGCGAAAAAATGAAAATTCTGGAACTGCCGTTTGCGAGCGGCACCATGAGCATGCTGGTGCTGCTGCCGGATGAAGTGAGCGGCCTGGAACAG CTGGAAAGCATTATTAACTTTGAAAAACTGACCGAATGGACCAGCAGCAACGTGATGGAAGAACGCAAAATTAAAGTGTATCTGCCGCGCATGAAAATGGAAG AAAAATATAACCTGACCAGCGTGCTGATGGCGATGGGCATTACCGATGTGTTTAGCAGCAGCGCGAACCTGAGCGGCATTAGCAGCGCGGAAAGCCTGAAAAT TAGCCAGGCGGTGCATGCGGCGCATGCGGAAATTAACGAAGCGGGCCGCGAAGTGGTGGGCAGCGCGGAAGCGGGCGTGGATGCGGCGAGCGTGAGCGAA GAATTTCGCGCGGATCATCCGTTTCTGTTTTGCATTAAACATATTGCGACCAACGCGGTGCTGTTTTTTGGCCGCTGCGTGAGCCCGGGCGGCAGCGGCGGCGG CAGCGGCCCGGCGCCGAACCTGCTGGGCGGCCCGAGCGTGTTTATTTTTCCGCCGAAAATTAAAGATGTGCTGATGATTAGCCTGAGCCCGATTGTGACCTGCG TGGTGGTGGATGTGAGCGAAGATGATCCGGATGTGCAGATTAGCTGGTTTGTGAACAACGTGGAAGTGCATACCGCGCAGACCCAGACCCATCGCGAAGATTA TAACAGCACCCTGCGCGTGGTGAGCGCGCTGCCGATTCAGCATCAGGATTGGATGAGCGGCAAAGAATTTAAATGCAAAGTGAACAACAAAGATCTGCCGGCG CCGATTGAACGCACCATTAGCAAACCGAAAGGCAGCGTGCGCGCGCCGCAGGTGTATGTGCTGCCGCCGCCGGAAGAAGAAATGACCAAAAAACAGGTGACC CTGACCTGCATGGTGACCGATTTTATGCCGGAAGATATTTATGTGGAATGGACCAACAACGGCAAAACCGAACTGAACTATAAAAACACCGAACCGGTGCTGG ATAGCGATGGCAGCTATTTTATGTATAGCAAACTGCGCGTGGAAAAAAAAAACTGGGTGGAACGCAACAGCTATAGCTGCAGCGTGGCATGAAGGCCTGCATA ACCATCATACCACCAAAAGCTTTAGCCGCACCCCGGGCAAA
HBc WT 570bp XhoI/NdeI BamHI/Eco RI	CATATGATGGACATTGACCCTTACAAAGAATTTGGCGCGACAGTGGAACTGTTGAGCTTCCTTCCCTCTGATTTTTTCCCCTCCGTGCGCGATCTGCTGGATACGG CCTCCGCCCTTTATCGCGAAGCGTTGGAGAGTCCAGAACATTGTTCACCGCATCATACTGCTCTGCGCCAGGCAATCCTGTGTTGGGGTGAGTTAATGACTCTGG CAACGTGGGTGGGGAATAACCTTGAGGACGGCGGTGGCGGTAGCGGCGGTGGCGGATCCTTGGCTATGGTAAGCGCTATAGAATTCGGCGGTGGCGGTAGC GGCGGTGGCGGTTCGCGCGATCTGGTGGTAAACTATGTGAACACGAATATGGGCTTAAAAATTCGGCAGCTGCTCTGGTTTCACATTAGCTGTCTGACCTTTGG TCGGGAAACGGTCCTGGAGTACCTGGTTAGCTTCGGGGTCTGGATTCGGACACCGCCAGCTTACCGGCCCCCAAACGCTCCGATCTTAAGTACGCTGCCGGAAA CCACCGTGGTTGGTAGCGGCGGTGGTACCGGTAAGCTTGGCGGTGGCTGGAGCCATCCGCAGTTTGAAAAATAACTCGAG
HBc-PA 1020bp XhoI/NdeI BamHI/Eco RI	CATATGATGGACATTGACCCTTACAAAGAATTTGGCGCGACAGTGGAACTGTTGAGCTTCCTTCCCTCTGATTTTTTCCCCTCCGTGCGCGATCTGCTGGATACGG CCTCCGCCCTTTATCGCGAAGCGTTGGAGAGTCCAGAACATTGTTCACCGCATCATACTGCTCTGCGCCAGGCAATCCTGTGTTGGGGTGAGTTAATGACTCTGG CAACGTGGGTGGGGAATAACCTTGAGGACGGCGGTGGCGGTAGCGGCGGTGGCGGATCCAGAACAGCAGAACGCCTTCTACGAAATTCTGCATCTGCCGAAT CTGACCGAAGAACAGCGTAATGGTTTTATTCAGAGCCTGAAAGATGATCCGAGCGTGAGCAAAGAAATTCTGGCCGAAGCAAAAAAACTGAATGATGCACAGG CACCGAAGGTGGTGGTTCAGGTGGCGGTGGTTCACATATGAAATTCAATAAAGAGCAACAAAACGCGTTCTATGAGATCCTGCATTTACCGAACCTGAATGAG GAACAGCGCAACGCATTTATTCAGTCACTGAAAGACGACCCGTCACAGAGCGCAAATCTGCTGGCAGAGGCCAAAAAGCTGAACGAACAGCAGGCAGCATTTT ATGAAATCCTGAGCTTAGGCGGTGGCGGTAGTGGCGGAGGTGGTAGTGAATTCGGCGGTGGCGGTAGCGGCGGTGGCGGTTCGCGCGATCTGGTGGTAAAC TATGTGAACACGAATATGGGCTTAAAAATTCGGCAGCTGCTCTGGTTTCACATTAGCTGTCTGACCTTTGGTCGGGAAACGGTCCTGGAGTACCTGGTTAGCTTC GGGGTCTGGATTCGGACACCGCCAGCTTACCGGCCCCCAAACGCTCCGATCTTAAGTACGCTGCCGGAAACCACCGTGGTTGGTAGCGGCGGTGGTACCGGTA AGCTTGGCGGTGGCTGGAGCCATCCGCAGTTTGAAAAATA ACTCGAG

Table 8-1. Construct DNA Sequences

Appendix 2: Rosetta-3.5 Computational Scripts

Idealise

/home/mjfssjpd/rosetta_bin_linux_2014.52.57520_bundle/main/source/bin/idealize_jd2.linuxgccrelease \-database
/home/mjfssjpd/rosetta_bin_linux_2014.52.57520_bundle/main/database \
-in::file::s i301A.pdb -nstruct 5 -ignore_unrecognized_res -ignore_waters >log.file

Relax

/home/mjfssjpd/rosetta_bin_linux_2014.52.57520_bundle/main/source/bin/relax.linuxgccrelease \
-database /home/mjfssjpd/rosetta_bin_linux_2014.52.57520_bundle/main/database \
-in::file::s i301a_0005.txt -in:file:fullatom -relax:fast -nstruct 10 -ignore_unrecognized_res -ignore_waters

Point Mutation Scan- Single Mutations

/home/mjfssjpd/rosetta_bin_linux_2014.52.57520_bundle/main/source/bin/pmut_scan_parallel.linuxgccrelease \-database
/home/mjfssjpd/rosetta_bin_linux_2014.52.57520_bundle/main/database \-s i301a_0005_0001.pdb -output_mutant_structures -ex1 -ex2 -extrachi_cutoff 1 -use_input_sc -ignore_unrecognized_res -no_his_his_pairE -multi_cool_annealer 10 -mute basic core > pmsaoutput.txt

Point Mutation Scan – Double Mutations

/home/mjfssjpd/rosetta_bin_linux_2014.52.57520_bundle/main/source/bin/pmut_scan_parallel.linuxgccrelease \-database
/home/mjfssjpd/rosetta_bin_linux_2014.52.57520_bundle/main/database \-s i301a_0005_0001.pdb -double_mutant_structures -output_mutant_structures -ex1 -ex2 -extrachi_cutoff 1 -use_input_sc -ignore_unrecognized_res -no_his_his_pairE -multi_cool_annealer 10 -mute basic core > pmsaoutput.txt